frontiers | Research Topics

Mechanisms and advances in respiratory allergic diseases

Edited by
Bao-Hui Cheng, Xiaojun Xiao, Jing Li and Yu Jin

Published in
Frontiers in Immunology

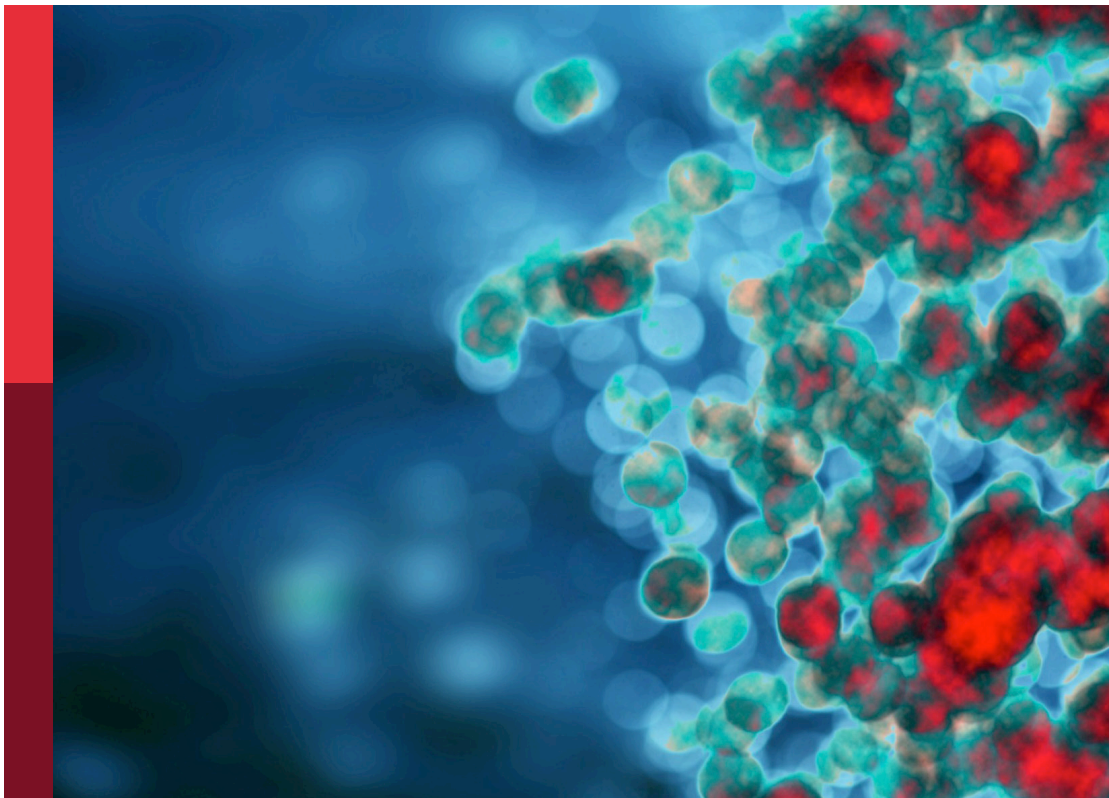

ISSN 1664-8714
ISBN 978-2-83252-143-4
DOI 10.3389/978-2-83252-143-4

About Frontiers

Frontiers is more than just an open access publisher of scholarly articles: it is a pioneering approach to the world of academia, radically improving the way scholarly research is managed. The grand vision of Frontiers is a world where all people have an equal opportunity to seek, share and generate knowledge. Frontiers provides immediate and permanent online open access to all its publications, but this alone is not enough to realize our grand goals.

Frontiers journal series

The Frontiers journal series is a multi-tier and interdisciplinary set of open-access, online journals, promising a paradigm shift from the current review, selection and dissemination processes in academic publishing. All Frontiers journals are driven by researchers for researchers; therefore, they constitute a service to the scholarly community. At the same time, the *Frontiers journal series* operates on a revolutionary invention, the tiered publishing system, initially addressing specific communities of scholars, and gradually climbing up to broader public understanding, thus serving the interests of the lay society, too.

Dedication to quality

Each Frontiers article is a landmark of the highest quality, thanks to genuinely collaborative interactions between authors and review editors, who include some of the world's best academicians. Research must be certified by peers before entering a stream of knowledge that may eventually reach the public - and shape society; therefore, Frontiers only applies the most rigorous and unbiased reviews. Frontiers revolutionizes research publishing by freely delivering the most outstanding research, evaluated with no bias from both the academic and social point of view. By applying the most advanced information technologies, Frontiers is catapulting scholarly publishing into a new generation.

What are Frontiers Research Topics?

Frontiers Research Topics are very popular trademarks of the *Frontiers journals series*: they are collections of at least ten articles, all centered on a particular subject. With their unique mix of varied contributions from Original Research to Review Articles, Frontiers Research Topics unify the most influential researchers, the latest key findings and historical advances in a hot research area.

Find out more on how to host your own Frontiers Research Topic or contribute to one as an author by contacting the Frontiers editorial office: frontiersin.org/about/contact

Mechanisms and advances in respiratory allergic diseases

Topic editors

Bao-Hui Cheng — Longgang ENT Hospital, Institute of ENT and Shenzhen Key Laboratory of ENT, China

Xiaojun Xiao — Shenzhen University, China

Jing Li — First Affiliated Hospital of Guangzhou Medical University, China

Yu Jin — Yale University, United States

Citation

Cheng, B.-H., Xiao, X., Li, J., Jin, Y., eds. (2023). *Mechanisms and advances in respiratory allergic diseases*. Lausanne: Frontiers Media SA.

doi: 10.3389/978-2-83252-143-4

The authors declare that the research was conducted in the absence of any commercial or financial relationships that could be construed as a potential conflict of interest.

Table of contents

frontiers | Frontiers in Immunology

TYPE Editorial
PUBLISHED 28 March 2023
DOI 10.3389/fimmu.2023.1186301

OPEN ACCESS

EDITED AND REVIEWED BY
Lucienne Chatenoud,
Université Paris Cité, France

*CORRESPONDENCE
Bao-Hui Cheng
chengbaohui@sina.com

SPECIALTY SECTION
This article was submitted to Immunological Tolerance and Regulation, a section of the journal Frontiers in Immunology

RECEIVED 14 March 2023
ACCEPTED 22 March 2023
PUBLISHED 28 March 2023

CITATION
Cheng B-H, Xiao X, Jin Y and Li J (2023) Editorial: Mechanisms and advances in respiratory allergic diseases. *Front. Immunol.* 14:1186301. doi: 10.3389/fimmu.2023.1186301

Editorial: Mechanisms and advances in respiratory allergic diseases

Bao-Hui Cheng[1]*, Xiaojun Xiao[2], Yu Jin[3] and Jing Li[4]

[1]Department of Otolaryngology, Longgang E.N.T Hospital & Shenzhen Key Laboratory of E.N.T, Institute of Ear Nose Throat (E.N.T), Shenzhen, China, [2]Institute of Allergy and Immunology, Health Science Center, Shenzhen University, Shenzhen, China, [3]Department of Pathology, Yale University, New Haven, CT, United States, [4]Department of Allergy and Clinical Immunology, State Key Laboratory of Respiratory Disease, Guangzhou Institute of Respiratory Health, The First Affiliated Hospital of Guangzhou Medical University, Guangzhou, China

KEYWORDS

allergic asthma, epithelial barrier dysfunction, inorganic particles, Aspergillus fumigatus, microbial dysbiosis

Editorial on the Research Topic
Mechanisms and advances in respiratory allergic diseases

Allergic respiratory diseases (ARD), including asthma, chronic rhinosinusitis and allergic rhinitis, are amongst the most common allergies worldwide and constitute major public health and economic problem for their morbidity and impact on quality of life(1). A substantial documented study has been attributed to unraveling the mechanisms of respiratory allergic and inflammatory diseases, but still, a lot of questions are elusive. New findings in the pathogenesis of ARD which may provide new targets for diagnosis or treatment for ARD.

The lung epithelial barrier serves as a guardian towards environmental insults and responds to allergen encounter with a cascade of immune reactions that can possibly lead to inflammation(2). Epithelial barrier dysfunction is fascinating research area in the initial of allergic inflammation. Alessandrini et al. revealed that CYP1B1 deficiency leads to enhanced expression and activity of CYP1A1 in lung epithelial cells and to an increased availability of the AhR ligand kynurenic acid following allergen challenge. Thus, differential CYP1 family member expression and signaling *via* the AhR in epithelial cells represents an immunoregulatory layer protecting the lung from exacerbation of allergic airway inflammation. Wang et al. suggested a functional axis of AhR-TGF-β1 that is critical in driving allergic airway inflammation through regulating allergen-induced cellular autophagy. In addition, RNA-seq analysis suggests that autophagy is one of the major pathways and that CALCOCO2/NDP52 and S1009 are major autophagy-associated genes in AT2 cells that may contribute to the AhR-mediated cockroach allergen–induced airway inflammation and, subsequently, ARD.

Allergic respiratory diseases have increased dramatically due to air pollution over the past few decades. However, studies are limited on the effects of inorganic components and particulate matter with different particle sizes in smog on allergic diseases, and the possible molecular mechanism of inducing allergies has not been thoroughly studied. Yang et al. screened four common inorganic mineral elements (Al_2O_3, TiO_2, Fe_2O_3, and SiO_2) smog particles, and only 20 nm SiO_2 particles significantly increased β-hexosaminidase release,

based on dinitrophenol (DNP)-human serum albumin (HSA) stimulation, from IgE-sensitized mast cells. Yang et al. indicated that nano-SiO_2 particles stimulation might synergistically activate IgE-sensitized mast cells by enhancing the MAPK signaling pathway and that nano-SiO_2 particles exposure could exacerbate allergic inflammation.

As a common airborne allergen that contributes to allergic asthma, *Aspergillus fumigatus* (*A.f*) can colonize in the airway and lead to allergic bronchopulmonary aspergillosis (ABPA)(3). The pathogenesis of *A.f*-sensitized asthma and ABPA remains inadequate. Chen et al. suggested the distinct humoral and cell immunological responses in *A.f*-sensitized asthma and ABPA patients. ABPA patients have more severe eosinophilic inflammation and enhanced Th1 responses compared with *A.f*-sensitized asthma patients. Wang et al. supported the notion that miR-365-3p, which was diminished by IL-17 in murine and human asthmatic pathogenesis, functioned as an essential negative mediator in IL-17-stimuated inflammatory response by targeting ARRB2, which would shed new light to the understanding and therapeutics thereof of asthmatic inflammation.

Changes in microbiome (dysbiosis) contribute to severity of allergic asthma(4). Preexisting epidemiological studies in humans correlate perinatal dysbiosis with increased long-term asthma severity(5). However, these studies cannot discriminate between prenatal and postnatal effects of dysbiosis and suffer from a high variability of dysbiotic causes ranging from antibiotic treatment, delivery by caesarian section to early-life breastfeeding practices. Given that maternal antibiotic exposure in mice increases the risk of newborn bacterial pneumonia in offspring, Lingel et al. revealed that prenatally induced dysbiosis in mice led to an increase in pulmonary $Th17^+$ non-conventional T cells with limited functional effect on airway resistance, pro-asthmatic Th2/Th17 cytokine production, pulmonary localization and cell-cell contacts. These data indicate that dysbiosis-related immune-modulation with long-term effects on asthma development occurs to a lesser extent prenatally and will allow to focus future studies on more decisive postnatal timeframes.

Pyroptosis and its mediated immune phenotype are crucial in the occurrence, development, and prognosis of asthma. Yang et al. demonstrated that BNIP3 was identified as a diagnostic marker and associated with immune cell infiltration such as, M2 macrophages. Small molecules obtained from the cMAP database that may have therapeutic effects on asthma are mainly DPP4 inhibitors. Yu et al. uncovered a previously uncharacterized role for the *de novo* creatine biosynthesis enzyme GATM in M2 macrophage polarization, which may be involved in the pathogenesis of related inflammatory diseases such as an T helper 2 (Th2)-associated allergic asthma. Kardas et al. summarized recent data on existing and potential monoclonal antibodies in asthma. Recent advances have resulted in the registration of a new antibody targeting TSLP (tezepelumab), with others being under development. In addition, as available monoclonal antibody treatments have shown little benefit among patients with T2-low asthma, research continues in this area, with several antibodies in development.

Author contributions

BC drafted the initial draft. All authors carefully reviewed and approved the manuscript.

Funding

The present study was supported in part by the National Natural Science Foundation of China (81973915 and 81773978); Guangdong Basic and Applied Basic Research Foundation (2023A1515012207); Shenzhen Innovation of Science and Technology Commission (No. JCYJ20220531091602005 and JCYJ20200109144625016); Shenzhen Key Medical Discipline Construction Fund (No. SZXK039); Longgang Innovation of Science and Technology Commission (LGKCYLWS2022010 and LGKCYLWS2020092).

Conflict of interest

The authors declare that the research was conducted in the absence of any commercial or financial relationships that could be construed as a potential conflict of interest.

Publisher's note

References

1. Porsbjerg C, Melén E, Lehtimäki L, Shaw D. Asthma. *Lancet* (2023) 401 (10379):858–73. doi: 10.1016/S0140-6736(22)02125-0

2. Carlier FM, de Fays C, Pilette C. (2021). doi: 10.3389/fphys.2021.691227

3. Agarwal R, Muthu V, Sehgal IS, Dhooria S, Prasad KT, Aggarwal AN. Allergic bronchopulmonary aspergillosis. *Clin Chest Med* (2022) 43(1):99–125. doi: 10.1016/j.ccm.2021.12.002

4. Attar N. Early life dysbiosis increases asthma risk. *Nat Rev Microbiol* (2015) 13 (11):660–0. doi: 10.1038/nrmicro3574

5. Wasserman E, Worgall S. Perinatal origins of chronic lung disease: mechanisms–prevention–therapy—sphingolipid metabolism and the genetic and perinatal origins of childhood asthma. *Mol Cell Pediatr* (2021) 8(1):22. doi: 10.1186/s40348-021-00130-y

frontiers | Frontiers in Immunology

ORIGINAL RESEARCH
published: 06 June 2022
doi: 10.3389/fimmu.2022.901194

Lung Epithelial CYP1 Activity Regulates Aryl Hydrocarbon Receptor Dependent Allergic Airway Inflammation

Francesca Alessandrini[1†], Renske de Jong[1†], Maria Wimmer[1], Ann-Marie Maier[1], Isis Fernandez[2,3,4], Miriam Hils[5], Jeroen T. Buters[1], Tilo Biedermann[5,6], Ulrich M. Zissler[1,2], Christian Hoffmann[1,7], Julia Esser-von-Bieren[1], Carsten B. Schmidt-Weber[1,2] and Caspar Ohnmacht[1]*

[1] Center of Allergy and Environment (ZAUM), Technical University and Helmholtz Center Munich, Munich, Germany, [2] Member of the German Center of Lung Research (DZL), Partner Site, Munich, Germany, [3] Department of Internal Medicine V, Ludwig-Maximilians-University of Munich (LMU), Munich, Germany, [4] Comprehensive Pneumology Centre, Helmholtz Center Munich, Munich, Germany, [5] Department of Dermatology and Allergology Biederstein, School of Medicine, Technical University of Munich, Munich, Germany, [6] Clinical Unit Allergology, Helmholtz Center Munich, Munich, Germany, [7] Food Research Center (FoRC), Department of Food Science and Experimental Nutrition, School of Pharmaceutical Sciences, University of São Paulo, São Paulo, Brazil

The lung epithelial barrier serves as a guardian towards environmental insults and responds to allergen encounter with a cascade of immune reactions that can possibly lead to inflammation. Whether the environmental sensor aryl hydrocarbon receptor (AhR) together with its downstream targets cytochrome P450 (CYP1) family members contribute to the regulation of allergic airway inflammation remains unexplored. By employing knockout mice for AhR and for single CYP1 family members, we found that AhR$^{-/-}$ and CYP1B1$^{-/-}$ but not CYP1A1$^{-/-}$ or CYP1A2$^{-/-}$ animals display enhanced allergic airway inflammation compared to WT. Expression analysis, immunofluorescence staining of murine and human lung sections and bone marrow chimeras suggest an important role of CYP1B1 in non-hematopoietic lung epithelial cells to prevent exacerbation of allergic airway inflammation. Transcriptional analysis of murine and human lung epithelial cells indicates a functional link of AhR to barrier protection/inflammatory mediator signaling upon allergen challenge. In contrast, CYP1B1 deficiency leads to enhanced expression and activity of CYP1A1 in lung epithelial cells and to an increased availability of the AhR ligand kynurenic acid following allergen challenge. Thus, differential CYP1 family member expression and signaling *via* the AhR in epithelial cells represents an immunoregulatory layer protecting the lung from exacerbation of allergic airway inflammation.

Keywords: aryl hydrocarbon receptor, cytochrome P450 enzyme, CYP1B1, eosinophilia, airway epithelial cells, lung allergy

OPEN ACCESS

Edited by:
Bao-Hui Cheng, Longgang ENT Hospital, Institute of ENT and Shenzhen Key Laboratory of ENT, China

Reviewed by:
Maria Salagianni, Biomedical Research Foundation of the Academy of Athens (BRFAA), Greece
Marco Gargaro, University of Perugia, Italy

****Correspondence:***
Caspar Ohnmacht
caspar.ohnmacht@helmholtz-muenchen.de

[†]These authors have contributed equally to this work

Specialty section:
This article was submitted to Immunological Tolerance and Regulation, a section of the journal Frontiers in Immunology

Received: *21 March 2022*
Accepted: *04 May 2022*
Published: *06 June 2022*

Citation:
Alessandrini F, de Jong R, Wimmer M, Maier A-M, Fernandez I, Hils M, Buters JT, Biedermann T, Zissler UM, Hoffmann C, Esser-von-Bieren J, Schmidt-Weber CB and Ohnmacht C (2022) Lung Epithelial CYP1 Activity Regulates Aryl Hydrocarbon Receptor Dependent Allergic Airway Inflammation. Front. Immunol. 13:901194. doi: 10.3389/fimmu.2022.901194

INTRODUCTION

The aryl hydrocarbon receptor (AhR) is a ligand-activated transcription factor used by immune cells and non-hematopoietic cells to sense the environment and adapt to physiological processes particularly at and within barrier sites such as the skin, the gut or the lung (1). Upon ligand binding, cytoplasmic AhR translocates to the nucleus to regulate gene transcription either alone or in a complex with other transcription factors. The AhR thereby acts as an intracellular sensor, which is able to respond to a variety of organic compounds including xenobiotics and tryptophane metabolites both from the host and from microbial/dietary sources. Interestingly, knockout of the AhR or deprivation of AhR ligands has been shown to alter the proper function of the immune system, particularly intestinal type 3 immunity including Th17 cells, innate lymphoid cells type (ILC)3 and a subset of intraepithelial cells (2–5).

In the context of allergic diseases, ablation of the AhR has been shown to increase the severity of allergic inflammation, indicating a rather protective role of the AhR in these settings (6–11). In fact, the AhR agonist Tranilast has been successfully employed as anti-allergic drug (12–14). Noteworthy, the AhR also regulates ILC2 activity (15), immunogenicity of dendritic cells (16), macrophage polarization towards a M2 phenotype *via* mesenchymal cells (17) and class-switch recombination as well as IL-10 expression in B cells (18, 19). Mechanistically, activation of the AhR typically results in upregulation of the cytochrome P450 (CYP1) members *cyp1a1*, *cyp1a2* and *cyp1b1* (1). CYP enzymes are monooxygenases that catalyze various reactions involved in drug metabolism, synthesis of cholesterol, steroids and other lipids. Importantly, a polymorphism in the *CYP1B1* gene has been linked to enhanced risk of bronchial asthma (20). However, whether and how AhR activity and particularly individual cytochrome P450 members play a role in allergic airway inflammation (AAI) has not been addressed so far.

Therefore, we investigated whether knockout of AhR and individual CYP1 family members differentially impact AAI in murine model systems using clinically-relevant, naturally occurring aeroallergens. We show that AhR and CYP1B1 but not CYP1A1 or CYP1A2 deficiency leads to disease exacerbation in preclinical models of AAI. We further show that airway epithelial cells (ECs) express high levels of CYP1B1 and CY1B1 expression in non-hematopoietic cells is required for protection from exacerbated AAI. AhR deficiency results in alteration of gene expression profiles in primary airway ECs at steady state and even more following AAI, but CYP1B1 deficiency did not. We identified enhanced CYP1A1 activity in $CYP1B1^{-/-}$ ECs and altered tryptophane (Trp) metabolite levels as a possible mechanism responsible for the AAI-potentiating effects observed in $CYP1B1^{-/-}$ animals. This work reveals a novel protective role of AhR signaling in airway ECs, which may have the potential to serve as a novel target for therapy of allergic asthma.

RESULTS

AhR and CYP1B1 Deficiency Aggravates Ragweed-Induced Allergic Airway Inflammation

To assess the role of AhR signaling and cytochrome P450 enzymes in AAI, we sensitized $AhR^{-/-}$, $CYP1A1^{-/-}$, $CYP1A2^{-/-}$ and $CYP1B1^{-/-}$ mice to ragweed extract as depicted in **Figure 1A**. Although the overall detection of serum immunoglobulins was very modest, $CYP1B1^{-/-}$ animals showed a significant increase at the endpoint in total IgE compared to WT (**Figure 1B**; left panel) and Amb a 1-specific IgG1 level compared to PBS, WT and $CYP1A2^{-/-}$ (**Figure 1B**; right panel). A tendency towards increased IgE and Amb a 1-specific IgG1 levels was observed also for $AhR^{-/-}$ mice albeit not reaching significance (**Figure 1B**). Enhanced BAL cell infiltration could be observed in $AhR^{-/-}$ and $CYP1B1^{-/-}$ compared to PBS and WT but not to $CYP1A1^{-/-}$ and $CYP1A2^{-/-}$ animals (**Figure 1C**). Differential cell counts revealed that this effect was predominantly due to enhanced infiltration of eosinophils, lymphocytes and macrophages into the bronchoalveolar space (**Figure 1C**). Additionally, $CYP1B1^{-/-}$ animals revealed enhanced frequencies of $Gata3^{+}Foxp3^{-}$ T helper (Th2) cells in lung tissue compared to PBS, WT, $AhR^{-/-}$ and $CYP1A1^{-/-}$ (**Figure 1D**). Gene expression analysis of key Th1/Th2-associated cytokines and CCL11 in lung tissue revealed a tendency for increased IL-4 expression in $AhR^{-/-}$ and $CYP1B1^{-/-}$ animals, but overall, no significant differences were detected between the investigated genotypes (**Figure 1E**). Histological analysis of lung tissue showed strongest inflammatory infiltration and mucus hypersecretion in $AhR^{-/-}$ - and $CYP1B1^{-/-}$ animals, although significantly only compared to PBS and not to WT or to other genotypes (**Figure 1F**). Altogether, these results demonstrate that $AhR^{-/-}$ and $CYP1B1^{-/-}$ animals suffer from a stronger AAI upon chronic exposure to ragweed extract compared to WT and to the other investigated genotypes.

AhR and CYP1B1 Deficiency Aggravates House Dust Mite-Induced Allergic Airway Inflammation

In order to assess the allergen specificity of our finding in the ragweed model, we next exposed WT, $AhR^{-/-}$ and $CYP1B1^{-/-}$ animals to HDM-induced AAI (**Figure 2A**). Here, a more pronounced increase of total serum IgE and a significant increase of Der f specific IgG1 was found both in $AhR^{-/-}$ and $CYP1B1^{-/-}$ compared to WT mice (**Figures 2B, G**). Further, we found enhanced lung cellular infiltration in the BALF of $AhR^{-/-}$ and $CYP1B1^{-/-}$ animals predominantly due to eosinophils and lymphocytes and macrophages (**Figures 2C, H**). No difference in BALF neutrophils was detected (data not shown). In contrast, increased frequencies of Th2 cells could be observed in lung tissue of both genotypes compared to WT (**Figures 2D, I**). $AhR^{-/-}$ mice showed three- to fourfold higher levels of IL-4 and IL-13 as well as of CCL11 in lung tissue and a slight increase of

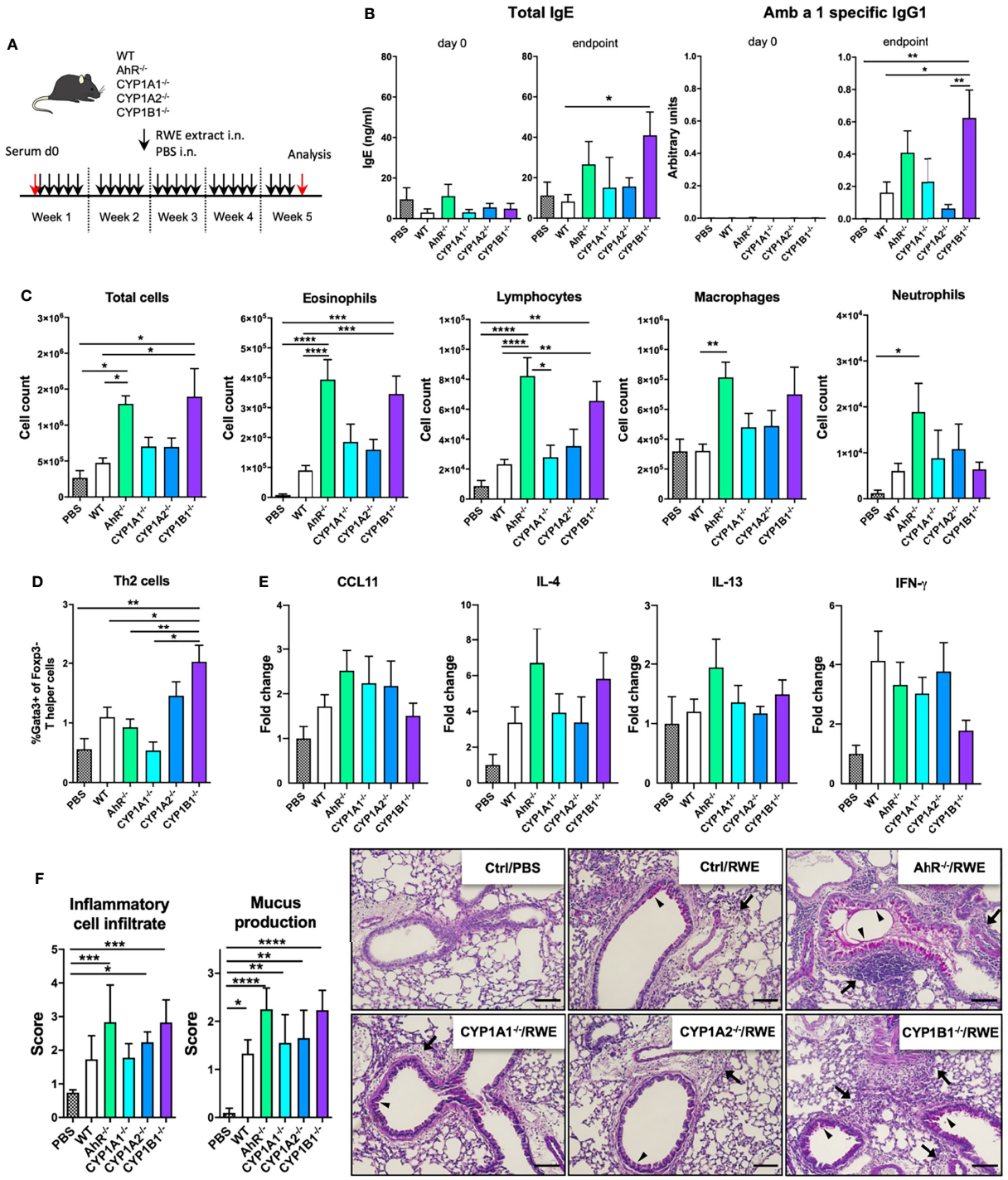

FIGURE 1 | AhR and CYP1B1 deficiency aggravates pollen-induced allergic airway inflammation. **(A)** Experimental setup. Mice of indicated genotypes were exposed for five weeks to RWE extract. Wildtype mice exposed to PBS served as negative controls (PBS). **(B)** Total IgE (left) and Amb a 1-specific IgG1 (right) at day 0 and endpoint. **(C)** Total and differential BAL cell counts, **(D)** Th2 cell frequency, **(E)** CCL11, IL-4, IL-13, IFN-γ expression in whole lung tissue and **(F)** histological scores (left) and representative lung sections (right). Arrows: inflammatory infiltrate; arrowheads: mucus hypersecretion; scale bar: 100µm. Mean ± SEM, n=6-21 mice/group from up to 3 independent experiments. Histological scores: mean ± SD, (n=5). ANOVA with Tukey's multiple comparisons. *p < 0.05, **p < 0.01, ***p < 0.001, ****p < 0.0001.

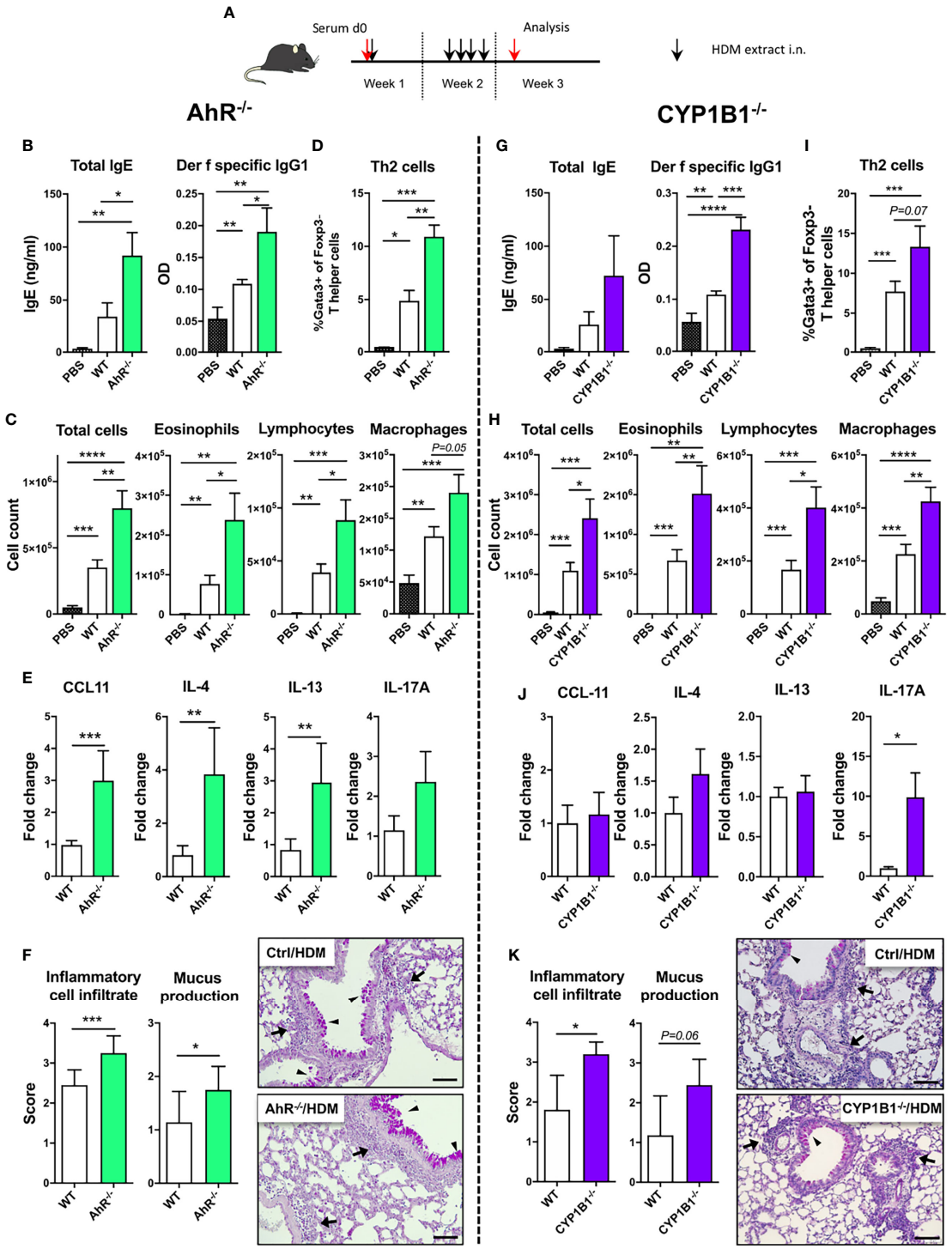

FIGURE 2 | AhR and CYP1B1 deficiency aggravates HDM-induced allergic airway inflammation. **(A)** Experimental setup. AhR$^{-/-}$ (left) and CYP1B1$^{-/-}$ (right) were exposed to house dust mite (HDM) as indicated. **(B, G)** Total IgE (left) and *Der f*-specific IgG1 (right) at endpoint. **(C, H)** Total and differential BAL cell counts, **(D, I)** Th2 cell frequency, **(E, J)** CCL11, IL-4, IL-13, IL-17A mRNA levels in whole lung tissue, **(F, K)** histological scores (left) and representative lung sections (right) at endpoint in AhR$^{-/-}$ and CYP1B1$^{-/-}$, respectively. Arrows: inflammatory infiltrate; arrowheads: mucus hypersecretion; scale bar: 100µm. Mean ± SEM, n=5-10 mice/group/experiment from 2 independent experiments. Histological scores: mean ± SD, (n=5). Student's unpaired two-tailed t-test. *p < 0.05, **p < 0.01, ***p < 0.001, ****p < 0.0001.

IL-17A, whereas CYP1B1$^{-/-}$ mice showed only slightly elevated expression of IL-4, a strong increase of IL-17A and no variations in CCL11 and IL-13 compared to WT (**Figures 2E, J**). Importantly, HDM has been shown to elicit a mixed Th2/Th17 response (21) and elevated IL-17A underline enhanced inflammation. IFN-γ levels were not affected in either genotype (data not shown). Lastly, histological analysis of HDM-exposed lungs revealed enhanced peribronchiolar and perivascular infiltration and mucus hypersecretion in both AhR$^{-/-}$ and CYP1B1$^{-/-}$ animals compared to WT (**Figures 2F, K**).

Altogether our *in vivo* data from two different adjuvant-free AAI models indicate that both AhR and its downstream target CYP1B1 are essential to prevent excessive AAI in a non-allergen-specific manner.

CYP1B1 Is Primarily Expressed in Airway Epithelial Cells

Given the selective effect of CYP1B1expression on the allergic inflammatory response, we then aimed to identify the cell type(s) that primarily express CYP1B1 in the lung and to evaluate if our results can be translated to human. Therefore, we first separated hematopoietic (CD45^{+}) and non-hematopoietic (CD45^{-} cells) from the lungs of naïve WT, AhR$^{-/-}$ and CYP1B1$^{-/-}$ animals. Strikingly, non-hematopoietic WT lung cells expressed roughly 100-200 times higher levels of CYP1B1 compared to hematopoietic cells at baseline (**Figure 3A**). Interestingly, CYP1B1 expression was not affected by the absence of AhR (**Figure 3A**) suggesting a basal CYP1B1 expression independent of AhR activity. Immunofluorescence staining of murine lung tissue showed that CYP1B1 stained within bronchial epithelial cells (EC), similarly in control and allergic animals (**Figure 3B**). Also, in human lung sections, CYP1B1 stained bronchial ECs (**Figure 3C**). In contrast, CYP1B1 did not stain alveolar ECs in mouse or human lung sections (**Figures 3B, C**). These data are in line with single cell expression data demonstrating CYP1B1 but not CYP1A1 or CYP1A2 expression across different subsets of human lung epithelial and fibroblastic cells (**Supplementary Figure S1**). By contrast, AhR expression was found in both epithelial and hematopoietic human lung cells irrespective of an asthma background (**Supplementary Figure S2**).

To assess whether human lung ECs are directly regulated by AhR signaling, normal human bronchial epithelial cells (NHBE) were stimulated for 24 h with HDM in the presence of IL-4 (to mimic an 'allergic' status), an AhR inhibitor or the combination of both. As expected, microarray analysis revealed a strong effect of HDM exposure compared to non-exposed cells (not shown). Whereas IL-4 strongly stimulated the expression of typical pro-allergic genes such as *CCL26* or *IL13R2* and interestingly also *AHR* (**Figure 3D** and **Supplementary Table S3**), AhR inhibition led to a more drastic change in differentially expressed genes (DEGs) compared to IL-4 (**Supplementary Table S3**). We then focused the analysis on the DEGs mostly altered solely by the inhibition of AhR during HDM exposure. As expected, inhibition of AhR led to downregulation of the AhR target genes *CYP1A1* and *CYP1B1* irrespective of whether IL-4 was present or not. Noteworthy, the inhibition of AhR lead to a strong upregulation of genes critical for allergic tissue inflammation, e.g. cell recruitment (*CX3CL1*), barrier integrity/protection (*ITGB3, PIGR*), antigen presentation (*HLA-DRA, HLA-DMB*), Th2 differentiation (*IL19*) and lipid mediator synthesis (*ALOX15*) (**Figure 3D** and **Supplementary Table S3**).

Thus, bronchial ECs seem to be the major CYP1B1-expressing cell type in murine and human lung. Furthermore, AhR activity in allergen-exposed NHBEs regulates a number of genes associated to AAI.

Non-Hematopoietic Expression of CYP1B1 Protects From Exacerbation of HDM-Induced Allergic Airway Inflammation

Given the predominant expression of CYP1B1 in mouse and human bronchial ECs, we then investigated whether non-hematopoietic expression of CYP1B1 is sufficient to prevent exacerbation of AAI. To this end, we generated CYP1B1$^{-/-}$ and WT bone marrow chimeras (**Figure 4A**) and sensitized them to HDM, as depicted in **Figure 2A**. Strikingly, only CYP1B1$^{-/-}$ chimeras with WT hematopoietic cells mirrored previously detected parameters of elevated AAI in full CYP1B1$^{-/-}$ mice, including serum immunoglobulin response (**Figure 4B**), BAL total cell numbers, particularly eosinophils and lymphocytes (**Figure 4C**), lung-resident Th2 cells (**Figure 4D**), IL-4 and IL-17A in BALF (**Figure 4E**) and histological scores in lung sections (**Figure 4F**). Conversely, WT chimeras with CYP1B1$^{-/-}$ hematopoietic cells showed much milder symptoms of AAI. Thus, CYP1B1 expression in non-hematopoietic cells is primarily responsible to prevent exaggerated AAI after exposure to HDM.

Transcriptional Comparison Indicates AhR- but Not CYP1B1-Dependent Regulation of Bronchial Epithelial Cells

To get a deeper insight into the molecular mechanism responsible for AhR- and CYP1B1-dependent effects, we performed RNA sequencing of sort-purified primary lung ECs (CD45^{-}CD31^{-}EpCAM^{+}live^{+}) at steady state and after HDM-elicited-AAI. The analysis of the number of DEGs in AhR$^{-/-}$ and CYP1B1$^{-/-}$ relatively to WT showed a stronger impact of the deficiency of AhR compared to CYP1B1 in gene regulation, especially following HDM exposure (**Figure 5A**). In fact, at steady state, we detected only few DEGs between WT and AhR-deficient ECs. Interestingly, some of these genes have been linked to regulation of circadian clock (*Nr1d1*, *Nr1d2*, *Cry1*) (**Figure 5B**). Following HDM-induced allergy, ECs from AhR$^{-/-}$ showed a strongly altered gene expression profile, contrarily to CYP1B1$^{-/-}$, which showed only low DEGs compared to WT with and none without allergy (**Figure 5B** and **Supplementary Table S4**). KEGG pathway analysis revealed an overall upregulation of genes involved in cell-to-cell contact and TGF-β signaling whereas genes associated to pattern recognition (TLR-like and NOD-like receptor signaling), chemokine receptor signaling and JAK-STAT signaling pathway were overall downregulated (**Figure 5C** and **Supplementary Table S5**). Overall, these data indicate that

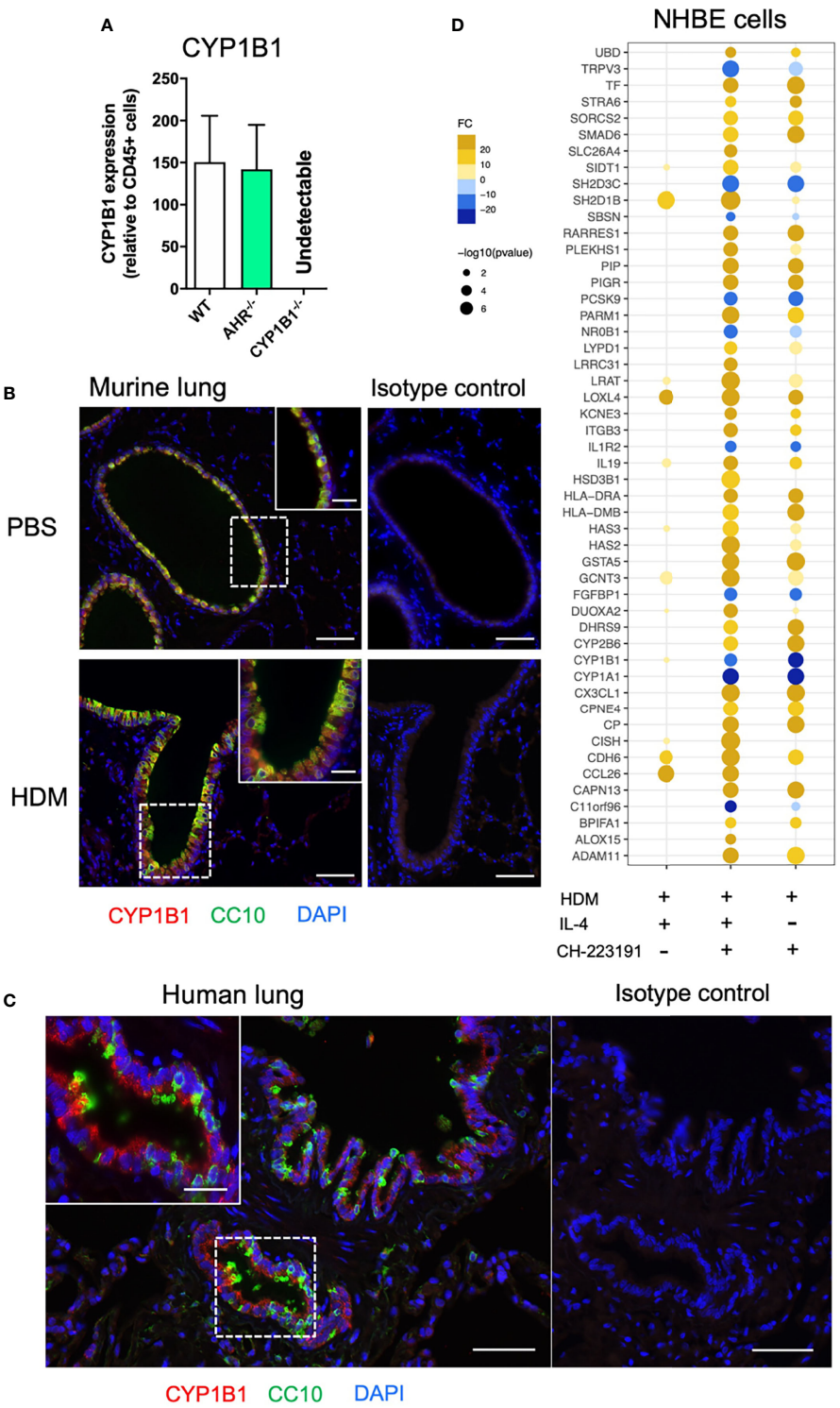

FIGURE 3 | Non-hematopoietic lung cells express CYP1B1. **(A)** CYP1B1 expression in $CD45^{-}$ relative to $CD45^{+}$ lung cells from WT, $AhR^{-/-}$ and $CYP1B1^{-/-}$ mice. Mean ± SEM of 2-6 mice/group. **(B)** Immune fluorescence staining of PBS- and HDM-challenged WT lungs or **(C)** human lung sections. Red: CYP1B1, Green: CC10, Blue: DAPI. Scale bar: 50µm or 20µm (insets). **(D)** NHBEs were stimulated for 6h with HDM extract (40µg/mL) in the presence of the AhR inhibitor CH-223191 (1µM/mL), IL-4 (50 ng/mL) or a combination of both. Results display top 25 upregulated and top 10 downregulated DEGs identified in the IL-4- and CH-223191-treated group relative to HDM only (center). These DEGs are also shown in NHBEs treated solely with IL-4 (left) or CH-223191 (right), respectively. Mean fold change of 4 independent donors NHBE, normal human bronchial epithelial cell.

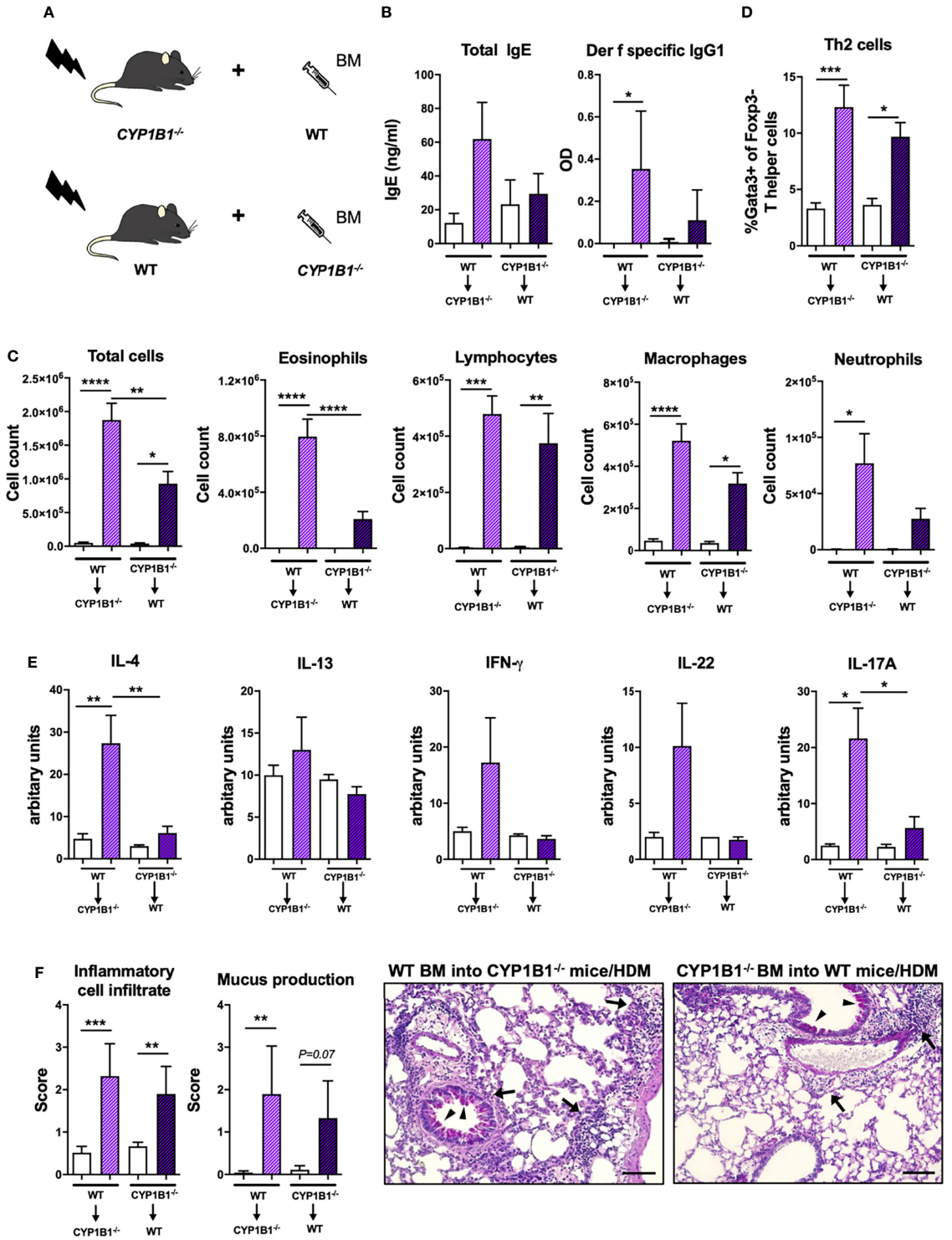

FIGURE 4 | Non-hematopoietic CYP1B1 expression prevents exacerbation of HDM-induced allergic airway inflammation. **(A)** Schematic representation of the generation of WT and CYP1B1$^{-/-}$ bone marrow chimeras, which were subsequently treated with HDM or PBS (setup **Figure 2A**). **(B)** Total IgE (left) and *Der f*-specific IgG1 (right) at endpoint. **(C)** Total and differential BAL cell counts, **(D)** Th2 cell frequency, **(E)** IL-4, IL-13, IFN-γ, IL-22, IL-17A protein levels in whole lung tissue, **(F)** histological scores (left) and representative lung sections (right). Arrows: inflammatory infiltrate; arrowheads: mucus hypersecretion; scale bar: 100μm. Mean ± SEM, n=4-13 mice/group from 2 independent experiments. Histological scores: mean ± SD, (n=5). ANOVA with Tukey's multiple comparisons. *p < 0.05, **p < 0.01, ***p < 0.001, ****p < 0.0001.

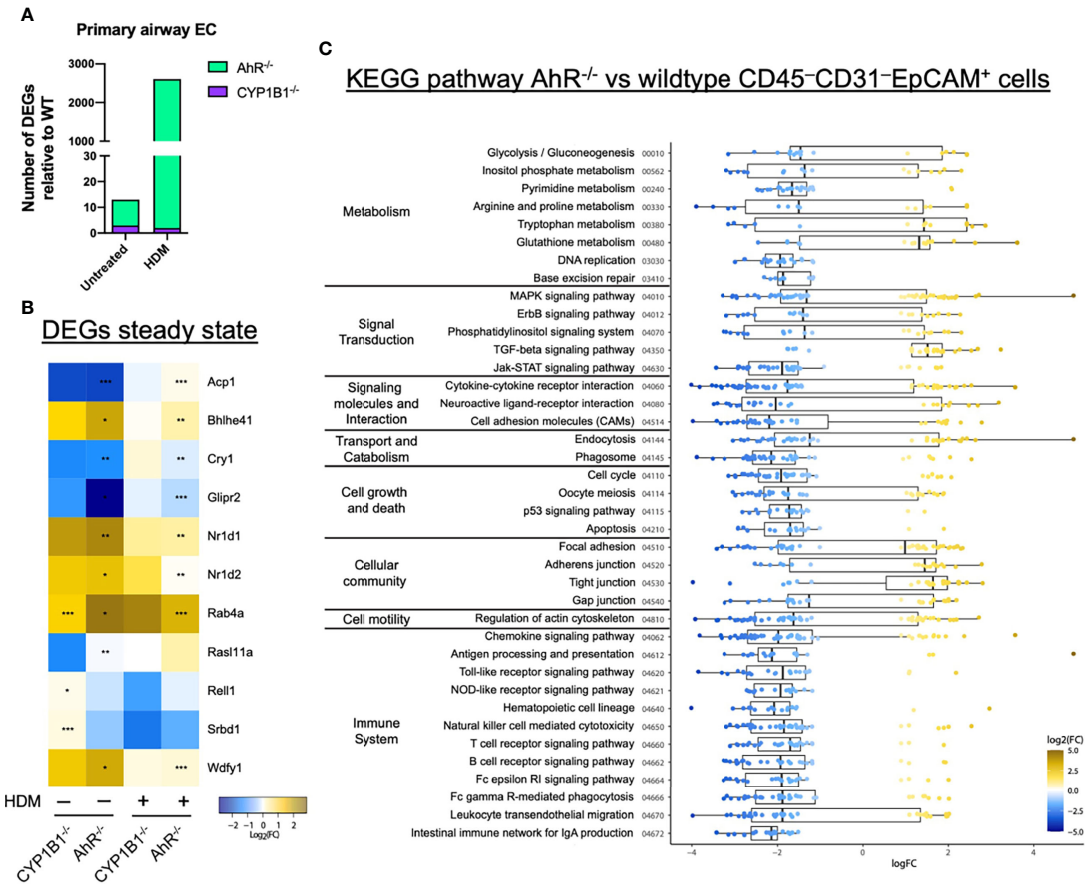

FIGURE 5 | AhR regulates gene expression in airway epithelial cells of sensitized mice. **(A)** Total DEGs in AhR$^{-/-}$ and CYP1B1$^{-/-}$ epithelial cells (EC) relatively to WT from untreated or allergic (HDM) mice. **(B, C)** RNAseq analysis of sort-purified EC (CD45^{-}CD31^{-}EpCAM^{+}live^{+}) of AhR$^{-/-}$ and CYP1B1$^{-/-}$ mice **(B)** Heatmap of all genes differently expressed in AhR$^{-/-}$ or CYP1B1$^{-/-}$ versus WT EC at steady state and their expression in HDM-exposed animals. *p < 0.05, **p < 0.01, ***p < 0.001. **(C)** KEGG pathway analysis of DEGs between AhR and WT EC of HDM-exposed animals. Only pathways with at least 5 DEGs are shown.

AhR, but not CYP1B1, is a major transcriptional regulator of ECs function, particularly after exposure to aeroallergens.

Absence of CYP1B1 Leads to Enhanced Transcription and Activity of CYP1A1 and to Altered Tryptophane Metabolites Levels

Our results indicating a non-transcriptional effect of CYP1B1 deficiency in ECs prompted us to investigate underlying mechanisms responsible for the enhanced allergic phenotype in CYP1B1$^{-/-}$ mice. Since artificial overexpression of CYP1A1 is known to limit availability of AhR agonists *in vivo* (5), we measured the expression of CYP1A1 in the absence of CYP1B1. Interestingly, lung tissue of CYP1B1$^{-/-}$ animals showed higher CYP1A1 expression levels compared to WT both at steady state and in tendency also following RWE-induced AAI, whereas CYP1A1 was not detected in AhR$^{-/-}$ or CYP1A1$^{-/-}$ lung tissue (**Figures 6A, B**). Similarly, higher CYP1A1 expression compared to WT could be observed in CYP1B1$^{-/-}$ lung tissue following HDM-induced AAI (**Figure 6C**). Notably, this effect was even more pronounced in purified non-hematopoietic (CD45^{-}) cells from HDM-allergic lungs with a roughly 20-fold higher CYP1A1 expression in the absence of CYP1B1 (**Figure 6D**).

To assess whether the HDM extract used for sensitization directly activates the AhR in ECs, we stimulated lung homogenates from all investigated genotypes with HDM extract or with the prototypical AhR ligand FICZ and compared the resulting EROD activity. HDM induced a slight, yet non-significant increase of EROD activity only in CYP1B1$^{-/-}$ animals compared to WT (**Figure 6E**). In contrast, FICZ induced EROD activity indistinctively in WT and CYP1B1$^{-/-}$ but not in all other genotypes (**Figure 6F**). As CYP1B1 was predominantly expressed in ECs (**Figure 3**), we measured EROD activity in primary murine tracheobronchial ECs (MTECs). Here, HDM did not elicit EROD activity in any background, whereas FICZ induced highest EROD activity in CYP1B1$^{-/-}$ compared to WT, but not in AhR$^{-/-}$ MTECs (**Figure 6G**). As expected, baseline CYP1A1 expression was higher in CYP1B1$^{-/-}$ MTEC cultures compared to WT and further increased following FICZ stimulation (**Figure 6H**). Since the HDM extract used for sensitization lacked AhR activation properties, we investigated whether endogenously

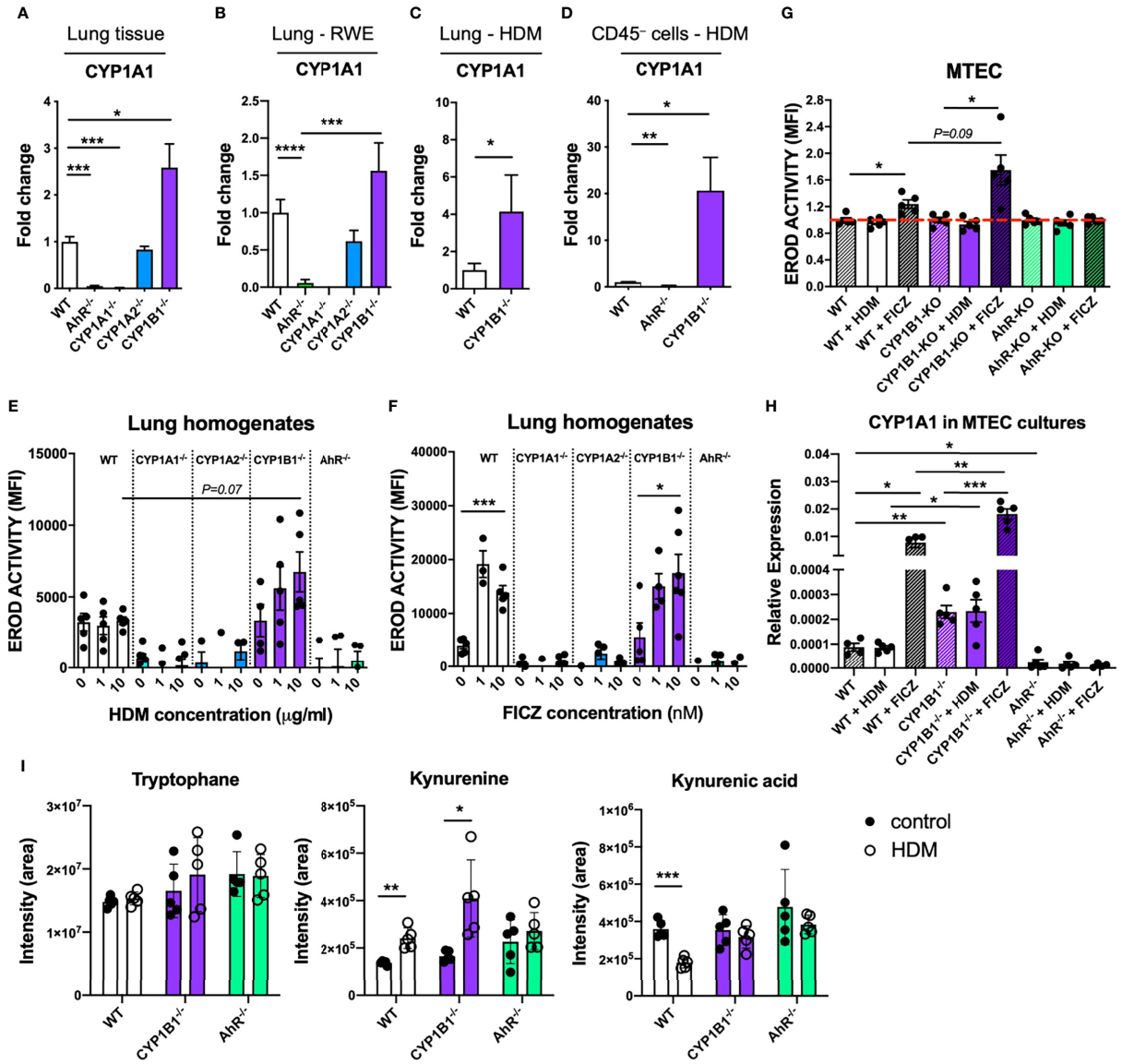

FIGURE 6 | Functional consequences of CYP1B1 deficiency in airway epithelial cells. CYP1A1 expression in total lung tissue from mice either **(A)** untreated, **(B)** sensitized to RWE, or **(C)** sensitized to HDM. **(D)** CYP1A1 expression in $CD45^-$ cells isolated from HDM-sensitized mice of indicated genotypes. **(E, F)** EROD assay in total lung homogenates of indicated genotypes after 24 hour stimulation with HDM (10μg/ml) **(E)** or FICZ (10nM) **(F)**. **(G)** EROD assay and **(H)** CYP1A1 expression of murine MTEC of the indicated genotypes after 24 hour stimulation with HDM (10μg/ml) or FICZ (10nM). Mean ± SEM of 4-20/group/condition [n=2 for $CYP1A1^{-/-}$ and $CYP1A2^{-/-}$, **(A)**]. **(I)** Targeted LC-MS/MS measurement of tryptophane, kynurenine and kynurenic acid in lung homogenates of the indicated genotype with or without AAI. Mean ± SD; n=5/group/treatment. MTEC, mouse tracheobronchial epithelial cells. Student's unpaired two-tailed t-test with Welch's correction. *p < 0.05, **p < 0.01, ***p < 0.001, ****p < 0.0001.

produced AhR ligands would be affected by a disrupted AhR-CYP1 axis. Therefore, the endogenous AhR ligands of the Trp pathway kynurenine (Kyn) and kynurenine acid (KynA) (22, 23) were measured in lung homogenates at steady state and following AAI. Interestingly, Kyn levels increased in WT and $CYP1B1^{-/-}$ lung cells after AAI while this did not reach significance for $AhR^{-/-}$ (**Figure 6I**). In contrast, KynA levels decreased after AAI in lungs of WT mice, but not in $AhR^{-/-}$ nor in $CYP1B1^{-/-}$ lungs (**Figure 6I**). In summary, these results point towards a cross-regulation of different CYP1 family members in bronchial ECs and to the employment of selective endogenous AhR ligands in regulating AhR activity in lung tissue following HDM-induced AAI.

DISCUSSION

Here, we provide evidence of an important role of the AhR-CYP1 axes in preventing exacerbation of AAI using two adjuvant-free

murine models with clinically-relevant aeroallergens. In fact, ablation of the AhR as well as of the immediate AhR response-gene CYP1B1 resulted both in enhanced AAI upon exposure to both RWE and HDM, as characterized by serum immunoglobulins, lung inflammatory cell infiltration and mucus hypersecretion. Our results confirm a recent study showing enhanced AAI and remodeling in an ovalbumin-induced chronic asthma model using $AhR^{-/-}$ compared to WT mice (10) and complete the picture adding the role of the CYP1 gene family. Whether a similar mechanism is present in humans remains to be elucidated. Still, CYP1B1 expression was clearly confined to bronchial and bronchiolar ECs in mouse and human, in line with early reports showing upregulation of CYP1B1 expression upon exposure to AhR ligands within club cells of peripheral airways (24, 25). Besides the well-known upregulation of CYP1B1 in an AhR-dependent manner, we also found basal CYP1B1 expression independent of AhR (**Figure 3A**) which has also been reported earlier in different settings (26, 27). Thus, we suggest that CYP1B1 is most likely active in steady state conditions but inflammation may potentiate CYP1B1 (and CYP1A1) expression and activity in an AhR-dependent manner.

Functionally, we demonstrate that a well-balanced AhR-CYP1 activity in non-hematopoietic cells is decisive in the protection from disease exacerbation, as only $CYP1B1^{-/-}$ chimeras with WT hematopoietic cells reproduced the previously detected parameters of elevated AAI in full $CYP1B1^{-/-}$ mice. As opposed to CYP1B1, we did not observe any consistent effect of CYP1A1 nor CYP1A2 deficiency in AAI, conforming to their low expression in bronchial ECs (**Figure S1**). Noteworthy, previous studies have already suggested a protective role of AhR in skin and intestinal inflammatory disorders (6, 8, 28). Interestingly, immune regulation in the skin has been associated to AhR activity in non-hematopoietic cells, presumably keratinocytes (6), confirming the critical role of AhR in epithelium as an interface between environment and mucosal immunity.

What is the consequence of the paucity of AhR signaling in lung epithelial cells?

Our transcriptional analysis of primary lung epithelial cells from non-allergic mice revealed only relatively few differentially expressed genes in the absence of AhR signaling and almost none in the absence of CYP1B1. Surprisingly, the majority of these AhR-dependent genes indicates a deregulation of the peripheral circadian clock. Interestingly, some key effector cells in allergy, such as mast cells, show circadian regulation patterns (29) and ablation of circadian clock genes in lung ECs has been shown to aggravate inflammation (30, 31). Whether disruption of peripheral circadian clock networks has a functional impact in our model should be matter of future investigations. In contrast to the relatively few DEGs found in airway ECs from $AhR^{-/-}$ mice at steady-state, we identified strong differences in gene expression of airway ECs from $AhR^{-/-}$ but not $CYP1B1^{-/-}$ animals following HDM exposure. Pathway analysis of these DEGs revealed a role for AhR to ensure epithelial barrier function, limit TGF-β receptor signaling and regulate a number of pathways associated to pattern recognition receptor or cytokine/chemokine signaling (32, 33). Some of these pathways may not be regulated directly by the AhR, but are rather a consequence of the enhanced AAI observed in $AhR^{-/-}$ mice. As this analysis did not detect differential expression of typical cytokines associated with epithelial cell activation (e.g. *Il33 or IL1B*, **Supplementary Table S4**) future work aiming to investigate the role of the AhR for barrier integrity of epithelial cells (34) should focus on earlier time points and employ conditional knockout approaches. On the other hand, the lack of DEGs in ECs from healthy and allergic $CYP1B1^{-/-}$ animals, despite the enhanced AAI similar to $AhR^{-/-}$, suggests that CYP1B1 deficiency in airway ECs affects hematopoietic cell types by other means. To investigate the mechanism responsible for the key role of CYP1B1 in airway ECs, we first assessed the expression of CYP1A1 in the absence of CYP1B1. As our results indicate enhanced activity of CYP1A1 in lung epithelial cells in the absence of CYP1B1, they point towards a cross regulation of CYP1 family members in lung ECs. This finding is in line with earlier studies showing that lungs and livers of $CYP1B1^{-/-}$ animals stimulated with carcinogenic agents had elevated levels of CYP1A1 expression (35, 36).

As aeroallergens typically interact with the epithelium as particles containing multiple molecules, we also tested whether HDM extracts were able to activate the AhR pathway directly, but did not find functionally relevant quantities of AhR ligands in HDM extracts able to activate WT cells. This suggests that naturally occurring activating ligands of AhR, e.g. of the Trp pathway generated through either Ido1 or IL4i1 activity (37, 38), may be sufficient for AhR-dependent regulation of AAI. To test this hypothesis, we conducted a targeted metabolomics approach to quantify key endogenous AhR ligands of the Trp pathway in lung tissue of WT compared to AhR- and CYP1B1-deficient mice at steady state and following HDM-driven AAI. Interestingly, in WT and $CYP1B1^{-/-}$ lungs, but not in $AhR^{-/-}$, levels of the AhR ligand Kyn increased after AAI. As AhR expression in lung ECs is directly induced by IL-4 signaling [**Supplementary Table S3** and (39, 40)], enhanced AhR activity during AAI, fueled with endogenous ligands, may serve as a feedback loop to protect airway ECs from excessive inflammation (16, 41).

Moreover, contrarily to Kyn, the levels of the acid form KynA decreased in WT after AAI. A plausible explanation for this observation could be the preferential use of KynA for AhR-dependent regulation of AAI *in vivo*, as KynA has a higher affinity to AhR compared to Kyn (22). Interestingly, KynA levels remained high in lungs of $CYP1B1^{-/-}$ and $AhR^{-/-}$ mice after AAI. In our study we focused on the two most relevant AhR ligands but further studies should assess the role of additional host-intrinsic AhR ligands. Degradation of AhR ligands by excessive CYP1A1 activity has already been identified previously as an important feedback mechanism to negatively regulate activity and duration of AhR signaling and can therefore functionally mimic AhR deficiency in the intestinal tract (5). Thus, enhanced CYP1A1 activity in the absence of CYP1B1 may explain a comparable defect of immune regulation in $AhR^{-/-}$ and $CYP1B1^{-/-}$ animals upon repetitive contact with aeroallergens.

Indeed, the activity of individual CYP1 members are able to differentially modulate the availability of local AhR ligands thereby regulating AhR activity in hematopoietic cells (see **Supplementary Figure S2**) such as ILC2s or macrophages, known players in AAI expressing AhR (15), in analogy to a similar scenario recently proposed for intestinal ECs and skin keratinocytes (5, 42).

In summary, this work extends a role of the AhR in the regulation of lung non-hematopoietic cells. Moreover, it suggests that balanced AhR/CYP1 activity within ECs represents an important layer of immune regulation necessary to prevent exacerbation of allergic responses in the lung and offers novel possibilities for tailor-made strategies in immune regulation at barrier sites.

METHODS

Mice and Human Samples

The following genotypes were used: C57BL/6 wildtype (WT), and $AhR^{-/-}$ (43), $CYP1A1^{-/-}$ (44), $CYP1A2^{-/-}$ (45) and $CYP1B1^{-/-}$ (35), all backcrossed to C57BL/6. All mice were bred and kept under specific pathogen-free conditions in individually ventilated cages at the central animal facility of Helmholtz Center Munich. Mice were kept in autoclaved, individually ventilated cages (501 cm^2, IVCs) with stocking density according to the EU guideline 2010/63 with a 12 hour dark/light cycle. Each cage was supplied with autoclaved bedding, bite sticks, nestles and mouse houses. Standard diet (Altromin Spezialfutter GmbH & Co. KG, Lage, Germany) and water were provided *ad libitum*. Cage manipulation took place in laminar flow hoods. Air temperature was 22 ± 2°C and humidity 55 ± 10% with daily control and record. Occasionally, C57BL/6 wildtype animals were bought from Charles River (Sulzfeld, Germany). In this case, mice were allowed to acclimatize for at least one week before sensitization. Both male and female mice over the age of 7 weeks were used.

For the generation of bone marrow chimeras, recipient mice were lethally irradiated by a Co-60 source with two doses of 6 Gray 4 h apart. Irradiated mice were reconstituted with 8×10^6 purified bone marrow cells of respective donors by i.v. injection. After reconstitution, mice received 0.25 mg/ml Enrofloxacin (Baytril; Bayer Vital GmbH) in drinking water for 3 weeks. Mice were maintained for 10-12 weeks to allow replacement of the hematopoietic system before allergen sensitization protocols were applied.

Experiments were performed on age- and sex-matched animals kept in the same rack, according to the European Convention for Animal Care and Use of Laboratory Animals and were approved by local ethics committee and government authorities (ROB-55-2-2532.Vet_02-18-94 and 55.2-1-54-2532-156-12). Human samples were obtained from the BioArchive of the Comprehensive Pneumology Center Munich. All patients gave written informed consent and the study was approved by local ethics committee of the Ludwig-Maximilians University of Munich, Germany (number 19-630).

Preparation of Ragweed and House Dust Mite Extracts

Aqueous ragweed pollen extracts (RWE) were prepared as previously described (46). Briefly, ragweed pollen were suspended in PBS (2.5 mg/ml), incubated for 30 min at 37°C and then centrifuged for 10 min at 4000 rpm by 4°C. The supernatants were sterile filtered through a 0.22 µm syringe filter (Merck KGaA, Darmstadt, Germany) and frozen at -80°C. House dust mite extracts from *Dermatophagoides farinae* (Stallergene Greer Laboratories, Kamp-Lintfort, Germany and Citeq BV, Groningen, NL) were suspended in 9% NaCl (1 mg/ml) and stored at -20°C until use. The final solution for intranasal instillation was prepared in PBS.

Mouse Models of Allergic Airway Inflammation

For the ragweed model, a sensitization protocol previously established in BALB/c mice (46) was adapted to C57BL/6. In short, mice received bilateral intranasal (i.n.) instillations of ragweed pollen extract (RWE) (20 mg/ml; 10 µl/nostril) once a day for a total of 23 days in 5 consecutive weeks. For the HDM model, mice were sensitized once by bilateral i.n. instillations of house dust mite extract of *Dermatophagoides farinae* (HDM) (50 µg/ml; 10 µl/nostril) (Stallergene Greer Laboratories, Kamp-Lintfort, Germany and Citeq BV, Groningen, NL). After eight days, mice were challenged with HDM (500 µg/ml; 10 µl/nostril) for 4 consecutive days. Control animals of both protocols received same amounts of PBS. Weight was monitored throughout the whole experiment. Mice were sacrificed either 24 or 72 h after the last instillation for the RWE or HDM protocol, respectively. After recovery of serum and bronchoalveolar lavage fluid (BALF) (46), lung tissue was prepared for histology, immunofluorescence, real-time PCR or FACS analysis. Non-lavaged lungs were used for characterization of non-hematopoietic cells by immunomagnetic- or flow cytometry-based cell separation, real-time PCR and metabolite analysis.

Analysis of Plasma Immunoglobulins

Plasma samples were prepared from blood taken prior to sensitization (day 0) and at sacrifice (endpoint). Total IgE and RWE-specific IgG1 were measured as previously described (46). For the detection of Dermatophagoides farinae (Der-f)-specific IgG1, 96-well plated were coated with goat anti-mouse IgG1 (CITEQ Biologics, Groningen, Netherlands) and mouse plasma was added. Subsequently, samples were incubated with biotinylated Der-f (CITEQ), avidin-horseradish peroxidase (Biolegend, San Diego, CA, USA), tetramethylbenzidine (ThermoFisher Scientific, Rockford, IL, USA) and read at 450 nm according to the manufacturer's instructions.

Analysis of Bronchoalveolar Lavage and Lung Histology

BAL and evaluation of inflammatory cell infiltration were performed as described previously (46). Aliquots of cell-free BAL fluid were used to measure cytokines using a Multiplex-bead-array (Mouse ProcartaPlex, Thermo Fisher Scientific,

Waltham, MA, USA) according to manufacturer's instructions. For lung histology, after BAL, the lungs were excised and the left lobe fixed in 4% buffered formalin and embedded in paraffin. Sections of 4µm thickness were stained with hematoxylin-eosin (H&E) and periodic acid Schiff (PAS). Mucus hypersecretion and inflammatory cell infiltration were graded in a blinded fashion on a scale from 0 to 4 (0=none, 1=mild, 2=moderate, 3=marked, 4=severe), reflecting the degree of the pathological alteration (47).

Immunofluorescence

Immunofluorescence staining was performed on mouse and human lung tissue embedded in paraffin. Slides were deparaffinized overnight at 60°C and rehydrated in a graded series of ethanol and distilled water. For antigen retrieval the slides were immersed in citrate buffer solution (pH 6.0) and placed into a Decloaking Chamber heated up to 125°C (30 seconds), 90°C (10 seconds), and cooled down to room temperature. Following a washing step in Tris buffer, blocking with 5% BSA in Tris buffer, the slides were double-stained with CYP1B1 rabbit polyclonal (aa400-450) antibody (LS-B1790, LifeSpan BioSciences, Inc., Seattle, WA, USA) and CC10 mouse monoclonal antibody (E-11) (sc-365992, Santa Cruz Biotechnology, Inc., Dallas, TX, USA). The primary antibodies were diluted in antibody diluent (Zytomed Systems, Berlin, Germany), CYP1B1 (1:50) and CC10 (1:100). For isotype control, rabbit IgG (sc-3888, Santa Cruz Biotechnology, Inc.) and mouse IgG1 kappa isotype control (16-4714-82, Invitrogen, Carlsbad, CA, USA) were used. The staining with the primary antibody occurred overnight in a wet chamber at 4°C. After rinsing in Tris buffer, a 1:250 dilution of each secondary antibody (Alexa Fluor 488 donkey anti-mouse and Alexa Fluor 568 donkey anti-rabbit, respectively for CYP1B1 and CC10 antibodies, Thermo Fisher Scientific), as well as DAPI (Sigma-Aldrich; St Louis, MO, USA, 1:2000) was applied to the slides and incubated 1 hour at room temperature in the dark. After rinsing again in Tris buffer, the slides were mounted in Fluorescence Mounting Medium (Dako, Hamburg, Germany). Images of the sections were obtained using Axiovert II (Carl Zeiss) and processed using the ZEN 3.2 software (blue edition, Carl Zeiss).

Flow Cytometry of Murine Lungs

After sacrifice, lungs were perfused with PBS, minced and digested in RPMI 1640 (Gibco, Life Technologies GmbH, Darmstadt, Germany) containing 1 mg/ml collagenase A (Sigma-Aldrich) and 100 µg/ml DNase I (Sigma-Aldrich) at 37°C for 30 minutes. Digested lungs were meshed and filtered through a 70-µm cell strainer and centrifuged at 500 × g for 10 min. Cell pellets were resuspended in a 40% Percoll (GE Healthcare, South Logan, USA) solution and layered onto an 80% Percoll layer. The Percoll gradient was run at 1500 × g at room temperature for 15 min. The interlayer containing mononuclear cells was collected, washed and incubated with Fc block (BD) and stained with the corresponding antibodies for 30 minutes on ice. Intracellular staining was performed using a Foxp3 fixation/permeabilization kit (eBiosciences, San Diego, CA, USA) according to the manufacturer's instructions. Live/Dead exclusion was routinely performed using a kit from Life Technologies. Antibodies used for flow cytometry are listed in **Supplementary Table S1** and the gating strategy employed for the identification of lung Th2 cells is depicted in **Supplementary Figure S3A**.

Measurement of Tryptophane Metabolites in Lung Tissue

Lungs were excised, weighted, cut into small pieces and snap frozen in liquid nitrogen. All solvents used for metabolite analysis were from Sigma Aldrich, LC-MS grade. For the extraction, a mixture of ice-cold methanol:acetonitrile:water (3:2:1, v/v, 600 µl) was added to 100-150 mg frozen tissue. The tissue was lysed using a tissue Lyser (Qiagen), vortex for 1 min at 4–8°C and incubated for 4 h at -20°C. After 10 minutes centrifugation at 14,000g at 4–8°C, the supernatant was collected. Methanol 80% (vol/vol, – 20°C, 400 µl) was added to the precipitate, each sample was vortexed for 1 minute at 4–8°C, and incubated for 30 minutes at -20°C. After centrifugation at 14,000g for 10 minutes at 4–8°C, the supernatant was collected and combined to the supernatant of the first extraction step from the same sample. After a final centrifugation step at 14,000g for 10 minutes at 4–8°C, the supernatant was collected and stored at – 80°C until LC-MS/MS analysis by targeted metabolomics. Before mass spectrometric analysis, 200 µl of the extracts were dried down in a vacuum centrifuge and resolubilized in 100 µl of 5 mM ammonium bicarbonate in water. Reversed phase liquid chromatography-tandem mass spectrometry (LC-MS/MS) was used for the quantification of metabolites by directly injecting 1 ul of the resolubilized mixture onto an Atlantis PREMIER BEH C18 AX VanGuard FIT Column, (2.5 µm, 2.1 x 100 mm; Waters). A RSLC ultimate 3000 (Thermo Fisher Scientific) HPLC system was used, directly coupled to a TSQ Quantiva mass spectrometer (Thermo Fisher Scientific) *via* electrospray ionization. A 8-minute-long linear gradient was used, beginning with 99% A (5 mM ammonium bicarbonate in water) linearly rising up to 70% B (95% Methanol and 5% 5 mM ammonium bicarbonate in water) employing a flow rate of 100 µl/min. LC-MS/MS was performed by employing the selected reaction monitoring (SRM) mode of the instrument using the transitions (quantifiers) 205.1 $m/z \rightarrow$ 188.1 m/z (tryptophan); 209.1 $m/z \rightarrow$ 192.1 m/z (kynurenine); 190.1 $m/z \rightarrow$ 144.1 m/z (kynurenic acid) in the positive ion mode. Authentic metabolite standards (Merck) were used for determining the optimal collision energies for LC-MS/MS and for validating experimental retention times. Ion chromatograms were interpreted manually using Xcalibur (Thermo Fisher Scientific).

Immunomagnetic Cell Isolation of Non-Hematopoietic Cells From Murine Lungs

For the isolation of CD45– and CD45+ cells lungs were flushed with PBS and digested as described above. CD45– cells were separated by negative selection from CD45+ cells using CD45 MicroBeads and LC separation columns (all Miltenyi Biotech GmbH, Bergisch Gladbach, Germany), according to the manufacturer's protocol. After controlling for cell purity by

flow cytometry, cell pellets were lysed in RNA-lysis buffer (Zymo Research, Freiburg, Germany) and further processed for real-time PCR analysis.

RNA Extraction and Real-Time PCR

RNA extraction of whole lung pieces or purified cells was performed using the Quick-RNA Miniprep or Quick-RNA Microprep (Zymo Research), respectively, according to the manufacturer's instructions and RNA was reversed transcribed with a cDNA synthesis kit (Fermentas, Thermo Fisher Scientific). For qPCR, a SYBR green-containing master mix (Roche, Basel, Switzerland) was used. Genes were run in triplicates in a 384well format using a light cycler (Roche) and normalized to two housekeeping genes. The relative expression was calculated with the $2^{-\Delta CT}$ method and typically fold change above control or wildtype are shown as indicated. Primer sequences are listed in **Supplementary Table S2**.

Normal Human Bronchial Epithelial Cell Cell Culture

NHBE culture was performed as previously described (40). Briefly, primary NHBEs (Lonza, Basel, Switzerland) of four genetically independent donors were grown as monolayers in 100% humidity and 5% CO_2 at 37 °C in serum-free defined growth media (BEGM, Lonza). NHBEs (passage 3) were used at ~80% confluence in 6-well plates. To avoid gene expression changes or influences by growth factors in the BEGM medium, cells were rested in basal medium (BEBM, Lonza) for 12 h, then stimulated with HDM extract at a final concentration of 40µg/mL (CITEQ), recombinant human IL-4 at 50 ng/ml (R&D Systems, Minneapolis, MN, USA) for 6 h. When indicated, cells were pretreated for two h prior to stimulation with the AhR inhibitor CH-223191 (Sigma-Aldrich) at a concentration of 1µM/mL. For RNA analysis, harvested cells were lysed in RLT buffer (Qiagen, Hilden, Germany) containing 1% β-mercaptoethanol (Roth, Karlsruhe, Germany) directly in the cell culture well.

RNA Extraction, Quantification and Microarray Analysis of Human NHBE

Total RNA was extracted using RNeasy Mini Kit (Qiagen, Hilden, Germany). RNA quantification and quality assessments were performed by ultraviolet–visible spectrophotometry (Nanodrop Technologies, Wilmington, DE) and the RNA 6000 Nano Chip Kit with the Agilent 2100 Bioanalyzer (Agilent Technologies, Santa Clara, CA, USA). RNA quality of all samples reached a RNA integrity number (Agilent Technologies) of >8.5. Total RNA was amplified and Cy3 labeled by using the one-color Low Input Quick Amp Labeling Kit (Agilent Technologies) according to the manufacturer's protocol. Hybridization to SurePrint G3 Human Gene Expression 8x60K Microarrays (Agilent Technologies) was performed with the Gene Expression Hybridization Kit (Agilent Technologies).

Data Analysis Strategy for Microarray

For microarray, data analysis was performed using the Genespring Software GX 14.9.1 (Agilent Technologies) under minimal data reduction constraints (1.5-fold change and $P \leq 0.05$ cutoff). Upon data import a standard baseline transformation to the median of all values was performed, including log transformation and computation of fold changes (log2(A/B) = log2(A)–log2(B)). Subsequently, a principle component analysis was conducted and revealed a homogenous component distribution. Compromised array signals (array spot non uniform due to pixel noise of feature exceeding threshold or above saturation) were excluded from further analysis. Genes regulated more than 1.5-fold were further analyzed by using the paired Student's t-test and filtered for P-value of <0.05). The significantly regulated genes were summarized in entity lists (see **Supplementary Table S3**). Only differentially expressed probes annotated with a Gene Symbol were considered for further analysis. Probe intensities were averaged in cases where more than one probe per genes was considered differentially expressed, and the lowest p value among these probes was considered for plotting. Genes annotated as protein coding, using the Bioconductor's AnnotationHub package (Ensemble Human Genome version 99) were used as input for a KEGG map enrichment test as described for RNA-seq data. Microarray data have been deposited in NCBI's Gene Expression Omnibus (GEO) and are accessible through GEO Series accession number GSE196949.

Generation of Mouse Tracheobronchial Epithelial Cells Cultures

Mouse tracheobronchial epithelial cells (MTEC) were isolated and differentiated as described previously (48). Briefly, mouse tracheas were surgically removed and placed in 10 ml 0.15% pronase solution (Roche, Basel, CH) and incubated overnight at 4°C. On the second day, a single cell suspension was generated by gently rocking the digested trachea. To remove fibroblasts, a native selection step was performed by incubating the cell suspension at 37°C in an atmosphere of 95% air, 5% CO_2 for 5 h in MTEC basic medium containing 10% FCS (48). Subsequently, supernatants were collected, cells were counted and plated in a 12 well plate (7.5 x 10 (4)-1.0 x 10 (5) cells/well) coated with collagen (Thermo Fisher Scientific). Submerged MTEC cultures were incubated at 37°C in a humidified incubator containing 95% air, 5% CO_2 for 7-10 days in MTEC proliferation medium containing retinoic acid (48).

EROD-Assay

To determine CYP1A1 enzyme activity an EROD Assay was performed. When indicated, cells were stimulated with HDM or the known AhR agonist FICZ (5,11-Dihydroindolo[3,2-b] carbazole-6-carboxaldehyde, Tocris Bioscience, Bristol, UK or Sigma-Aldrich) to activate the AhR and induce CYP1A1 transcription. Prior to the start of the assay, cells seeded in round-bottom cell culture plates (96 well) were washed twice with pre-warmed PBS (37°C). After aspirating the PBS, the desired volume of EROD reaction mixture [(5 µM Ethoxyresorufin (7-ER, Sigma-Aldrich), 0.5 mM NADPH (Sigma-Aldrich), 1.0 mg/ml BSA (Sigma-Aldrich), 50 mM Tris (pH 7.4)] was pipetted into the plate and subsequently incubated for 20 minutes at 37°C. To terminate the reaction 2M glycine

(Sigma-Aldrich, pH 10.3-10.4) was added in a ~1:1.5 ratio of glycine:EROD mixture volume. Supernatants were spun down at RT for 1-2 minutes to pellet any cellular debris. Subsequently, a fixed fraction of the supernatant was pipetted into a new plate. The plate was read at 535-550nm excitation and 570-590nm emission with a spectrophotometer (InfiniteM200pro, TECAN).

Isolation of Primary Mouse Alveolar Epithelial Cells

Mouse primary alveolar epithelial cells were isolated as described previously (49). Briefly, cardiac perfusion was performed using DPBS (Life Technologies). Subsequently, a cannula was placed in the trachea to infuse, first, dispase (50 U/ml, Roche) for ~45 seconds to allow the enzyme to distribute throughout the lungs without allowing it to spill back out. Next, 1 ml of 1% low-melt agarose (Sigma Aldrich) was gently infused. Lungs were covered with crushed ice for 2 minutes to allow for the agarose to solidify. Individual intact lung lobes were cut away and additionally kept in a dispase solution (50 U/ml, Roche) for 45 min at room temperature on a rocker at 150 rpm. After 45 minutes digested lungs were decanted in complete DMEM/F-12 (Gibco, Life Technologies) with DNase I (Qiagen) for 10 minutes to avoid clumping of cells. Single cell preparations were serially strained though a 100 µm, 70 µm and 40 µm strainers. Primary epithelial cells (singlets, alive, CD45-, EpCAM+ cells) were isolated with a FACSAria III cell sorter (BD) with a cell purity typically around 96%. The gating strategy is depicted in **Supplementary Figure S3B**.

RNA-Sequencing Analysis of Primary Lung Epithelial Cells

Total RNA was extracted from sort-purified lung epithelial cells from wildtype, $AhR^{-/-}$ and $CYP1B1^{-/-}$ mice using a RNeasy Micro Kit (Qiagen) and eluted in nuclease-free water. RNA was desiccated to 3 µl and denatured for 3 minutes at 72 °C in the presence of 2.4 mM dNTP (Invitrogen Carlsbad, USA), 240 nM dT-primer* (Metabion, Planegg, Germany) and 4 U RNase Inhibitor (New England Biolabs, Frankfurt, Germany). Reverse transcription and addition of the template switch oligo was performed at 42°C for 90 min after filling up to 10 µl with RT buffer mix for a final concentration of 1x superscript II buffer (Invitrogen), 1 M betaine (Themo Scientific), 5 mM DTT (Invitrogen), 6 mM $MgCl_2$ (Ambion), 1 µM TSO-primer* (Metabion), 9 U RNase Inhibitor (NEB) and 90 U Superscript II (Invitrogen). The reverse transcriptase was inactivated at 70°C for 15 min and single stranded cDNA was subsequently amplified using Kapa HiFi HotStart Readymix (Roche) at a 1x concentration together with 250 nM UP-primer* (Metabion) under following cycling conditions: initial denaturation at 98°C for 3 min, 10 cycles [98°C 20 sec, 67°C 15 sec, 72°C 6 min] and final elongation at 72°C for 5 min. The amplified cDNA was purified using 1x volume of Sera-Mag SpeedBeads (GE Healthcare, South Logan, USA) resuspended in a buffer consisting of 10 mM Tris (Applichem, Darmstadt, Germany), 20 mM EDTA (AppliChem), 18.5 % (w/v) PEG 8000 (Sigma Aldrich) and 2 M sodium chloride solution (Invitrogen). The cDNA quality and concentration was determined with the Fragment Analyzer (Agilent). For library preparation, 1.5 ng cDNA was tagmented using 0.5 µl TruePrep Tagment Enzyme V50 and 1x TruePrep Tagment Buffer L (TruePrep DNA Library Prep Kit V2 for Illumina, Vazyme), followed by an incubation step at 55°C for 10 min. Next, Illumina indices were added during PCR (72°C 3 min, 98°C 30 sec, 12 cycles [98°C 10 sec, 63°C 20 sec, 72°C 1 min], 72°C 5 min) with 1x concentrated KAPA Hifi HotStart Ready Mix and 300 nM dual indexing primers. After PCR, libraries were purified twice with 1x volume Sera-Mag SpeedBeads (GE Healthcare) and quantified with the Fragment Analyzer (Agilent Technologies), followed by Illumina sequencing on a Nextseq500 with a sample sequencing depth of 30 mio reads on average.

*dT-primer: C6-aminolinker-AAGCAGTGGTATCAACGCAGAGTCGAC TTTTTTTTTTTTTTTTTTTTTTTTTTTTTTVN, where N represents a random base and V any base beside thymidine;

TSO-primer: AAGCAGTGGTATCAACGCAGAGTACATrGrGrG, where G stands for ribo-guanosine;

UP-primer: AAGCAGTGGTATCAACGCAGAGT

Sequencing reads were pre-processed with bbduk [https://sourceforge.net/projects/bbmap/ (50)] to remove adapters still present in the raw reads and for quality trimming. Pre-processed reads were mapped to the mouse genome mm10 using GSNAP version 2020-03-12 (51). RNA sequencing quality was accessed using RNA-SeQC version 2.3.5 (52). Read counts were obtained using featureCounts version 2.0.0 (53). Splice site support and gene annotations were made using the Ensemble mm10 genome release version 99. Gene counts were filtered using the Bioconductor's AnnotationHub package (R package version 2.18.0) to contain only protein coding genes. The protein coding genes were used for a differential expression analysis using the Bioconductor package edgeR (54). Genes were considered as differentially expressed when FDR corrected p-values were <= 0.05. Differentially expressed genes were used as input on a gene ontology enrichment analysis using the R package topGO (R package version 2.38.1). Only nodes containing at least 10 genes were considered in the analysis, using the classic algorithm with the Fisher's exact test, and the p values were corrected using False Discovery Rate (FDR). Additionally, a Fisher's exact test was used to detect KEGG metabolic maps (55) that were enriched for differentially expressed genes. This enrichment test was performed in an automated fashion using all available maps, and the resulting p values were also adjusted using FDR correction. Annotations from maps under "Human Disease" and "Drug Discovery" were ignored for the interpretation of the results, and only "Immune System" was used from heading "Organismal systems". All RNA-seq related calculations were performed using the R environment for statistical computing. The raw data is available at the National Center for Biotechnology Information's Gene Expression Omnibus database and are accessible through GEO Series accession number GSE158715 (https://www.ncbi.nlm.nih.gov/geo/query/acc.cgi?acc=GSE158715).

Statistics

Mouse data is displayed as mean ± SEM, histological and metabolite analysis as mean ± SD. Statistical significance was

determined by ANOVA with Tukey's multiple comparisons or by Student's unpaired two-tailed t-test with or without Welch's correction. The analysis was performed by GraphPad Prism software (version 7.0 and 8.0). Statistical analysis of RNAseq and microarray datasets was performed using R language for statistical computing.

DATA AVAILABILITY STATEMENT

Microarray and sequencing data sets are publicly available in NCBI's GEO, accession GSE158715 and GSE196949.

ETHICS STATEMENT

The studies involving human participants were reviewed and approved by Local ethics committee of the Ludwig-Maximilians University of Munich, Germany (number 19-630). The patients/participants provided their written informed consent to participate in this study. The animal study was reviewed and approved by Local ethics committee and government authorities (ROB-55-2-2532.Vet_02-18-94 and 55.2-1-54-2532-156-12).

AUTHOR CONTRIBUTIONS

Study design: JB, CS-W and CO Design and conduction of experiments FA, RJ, MW, A-MM, IF, MH and CO Data analysis: FA, RJ, MW, A-MM. and IF Bioinformatic analyses: CH, UZ. Supervision: FA, JB, TB, JE-v-B, CS-W, CO Writing original draft: FA, RJ and CO Review & Editing: All Authors. Funding Acquisition: CO. All authors contributed to the article and approved the submitted version.

FUNDING

This work was supported by grants from the European Research Council (ERC Starting grant project number 716718 to CO) and the Deutsche Forschungsgemeinschaft (grant number OH 282/1-1 and OH 282/1-2 within FOR2599 to CO and project P07 within SFB1371 to CO). RJ was supported by a fellowship from the Humboldt foundation (grant number 1200905 - HFST-P). MW was supported by the Christine-Kühne Center (CK-Care). CH is supported by a fellowship grant #2019/14245-1, and by grant #2013/07914-8 from the São Paulo Research Foundation (FAPESP). The VBCF Metabolomics Facility is supported by the City of Vienna through the Vienna Business Agency.

ACKNOWLEDGMENTS

The authors wish to thank the animal caretakers of the Helmholtz Center Munich and Benjamin Schnautz, Johanna Grosch and Anela Arifovic for excellent technical assistance.

SUPPLEMENTARY MATERIAL

The Supplementary Material for this article can be found online at: https://www.frontiersin.org/articles/10.3389/fimmu.2022.901194/full#supplementary-material

REFERENCES

1. Stockinger B, Di Meglio P, Gialitakis M, Duarte JH. The Aryl Hydrocarbon Receptor: Multitasking in the Immune System. *Annu Rev Immunol* (2014) 32:403–32. doi: 10.1146/annurev-immunol-032713-120245
2. Veldhoen M, Hirota K, Christensen J, O'Garra A, Stockinger B. Natural Agonists for Aryl Hydrocarbon Receptor in Culture Medium are Essential for Optimal Differentiation of Th17 T Cells. *J Exp Med* (2009) 206(1):43–9. doi: 10.1084/jem.20081438
3. Kiss EA, Vonarbourg C, Kopfmann S, Hobeika E, Finke D, Esser C, et al. Natural Aryl Hydrocarbon Receptor Ligands Control Organogenesis of Intestinal Lymphoid Follicles. *Science* (2011) 334(6062):1561–5. doi: 10.1126/science.1214914
4. Gilles S, Fekete A, Zhang X, Beck I, Blume C, Ring J, et al. Pollen Metabolome Analysis Reveals Adenosine as a Major Regulator of Dendritic Cell-Primed T (H) Cell Responses. *J Allergy Clin Immunol* (2011) 127(2):454–461.e451-459. doi: 10.1016/j.jaci.2010.12.1082
5. Schiering C, Wincent E, Metidji A, Iseppon A, Li Y, Potocnik AJ, et al. Feedback Control of AHR Signalling Regulates Intestinal Immunity. *Nature* (2017) 542(7640):242–5. doi: 10.1038/nature21080
6. Di Meglio P, Duarte JH, Ahlfors H, Owens ND, Li Y, Villanova F, et al. Activation of the Aryl Hydrocarbon Receptor Dampens the Severity of Inflammatory Skin Conditions. *Immunity* (2014) 40(6):989–1001. doi: 10.1016/j.immuni.2014.04.019
7. Schulz VJ, Smit JJ, Willemsen KJ, Fiechter D, Hassing I, Bleumink R, et al. Activation of the Aryl Hydrocarbon Receptor Suppresses Sensitization in a Mouse Peanut Allergy Model. *Toxicol Sci* (2011) 123(2):491–500. doi: 10.1093/toxsci/kfr175
8. van den Bogaard EH, Bergboer JG, Vonk-Bergers M, van Vlijmen-Willems IM, Hato SV, van der Valk PG, et al. Coal Tar Induces AHR-Dependent Skin Barrier Repair in Atopic Dermatitis. *J Clin Invest* (2013) 123(2):917–27. doi: 10.1172/JCI65642
9. Xu T, Zhou Y, Qiu L, Do DC, Zhao Y, Cui Z, et al. Aryl Hydrocarbon Receptor Protects Lungs From Cockroach Allergen-Induced Inflammation by Modulating Mesenchymal Stem Cells. *J Immunol* (2015) 195(12):5539–50. doi: 10.4049/jimmunol.1501198
10. Chang YD, Li CH, Tsai CH, Cheng YW, Kang JJ, Lee CC. Aryl Hydrocarbon Receptor Deficiency Enhanced Airway Inflammation and Remodeling in a Murine Chronic Asthma Model. *FASEB J* (2020) 34(11):15300–13. doi: 10.1096/fj.202001529R
11. Negishi T, Kato Y, Ooneda O, Mimura J, Takada T, Mochizuki H, et al. Effects of Aryl Hydrocarbon Receptor Signaling on the Modulation of TH1/TH2 Balance. *J Immunol* (2005) 175(11):7348–56. doi: 10.4049/jimmunol.175.11.7348
12. Kawabata Y, Aoki Y, Matsui T, Yamamoto K, Sato H, Onoue S, et al. Stable Dry Powder Inhaler Formulation of Tranilast Attenuated Antigen-Evoked Airway Inflammation in Rats. *Eur J Pharm Biopharm* (2011) 77(1):178–81. doi: 10.1016/j.ejpb.2010.11.005
13. Hu W, Zhao J, Pei G. Activation of Aryl Hydrocarbon Receptor (Ahr) by Tranilast, an Anti-Allergy Drug, Promotes miR-302 Expression and Cell Reprogramming. *J Biol Chem* (2013) 288(32):22972–84. doi: 10.1074/jbc.M113.475624

14. Darakhshan S, Pour AB. Tranilast: A Review of its Therapeutic Applications. *Pharmacol Res* (2015) 91:15–28. doi: 10.1016/j.phrs.2014.10.009
15. Li S, Bostick JW, Ye J, Qiu J, Zhang B, Urban JF Jr, et al. Aryl Hydrocarbon Receptor Signaling Cell Intrinsically Inhibits Intestinal Group 2 Innate Lymphoid Cell Function. *Immunity* (2018) 49(5):915–28.e915. doi: 10.1016/j.immuni.2018.09.015
16. Nguyen NT, Kimura A, Nakahama T, Chinen I, Masuda K, Nohara K, et al. Aryl Hydrocarbon Receptor Negatively Regulates Dendritic Cell Immunogenicity *via* a Kynurenine-Dependent Mechanism. *Proc Natl Acad Sci U S A* (2010) 107(46):19961–6. doi: 10.1073/pnas.1014465107
17. Cui Z, Feng Y, Li D, Li T, Gao P, Xu T. Activation of Aryl Hydrocarbon Receptor (AhR) in Mesenchymal Stem Cells Modulates Macrophage Polarization in Asthma. *J Immunotoxicol* (2020) 17(1):21–30. doi: 10.1080/1547691X.2019.1706671
18. Piper CJM, Rosser EC, Oleinika K, Nistala K, Krausgruber T, Rendeiro AF, et al. Aryl Hydrocarbon Receptor Contributes to the Transcriptional Program of IL-10-Producing Regulatory B Cells. *Cell Rep* (2019) 29(7):1878–1892.e1877. doi: 10.1016/j.celrep.2019.10.018
19. Vaidyanathan B, Chaudhry A, Yewdell WT, Angeletti D, Yen WF, Wheatley AK, et al. The Aryl Hydrocarbon Receptor Controls Cell-Fate Decisions in B Cells. *J Exp Med* (2017) 214(1):197–208. doi: 10.1084/jem.20160789
20. Polonikov AV, Ivanov VP, Solodilova MA. Genetic Variation of Genes for Xenobiotic-Metabolizing Enzymes and Risk of Bronchial Asthma: The Importance of Gene-Gene and Gene-Environment Interactions for Disease Susceptibility. *J Hum Genet* (2009) 54(8):440–9. doi: 10.1038/jhg.2009.58
21. Chesne J, Braza F, Chadeuf G, Mahay G, Cheminant MA, Loy J, et al. Prime Role of IL-17A in Neutrophilia and Airway Smooth Muscle Contraction in a House Dust Mite-Induced Allergic Asthma Model. *J Allergy Clin Immunol* (2015) 135(6):1643–1643.e1643. doi: 10.1016/j.jaci.2014.12.1872
22. DiNatale BC, Murray IA, Schroeder JC, Flaveny CA, Lahoti TS, Laurenzana EM, et al. Kynurenic Acid is a Potent Endogenous Aryl Hydrocarbon Receptor Ligand That Synergistically Induces Interleukin-6 in the Presence of Inflammatory Signaling. *Toxicol Sci* (2010) 115(1):89–97. doi: 10.1093/toxsci/kfq024
23. Hubbard TD, Murray IA, Perdew GH. Indole and Tryptophan Metabolism: Endogenous and Dietary Routes to Ah Receptor Activation. *Drug Metab Dispos* (2015) 43(10):1522–35. doi: 10.1124/dmd.115.064246
24. Boyd MR. Evidence for the Clara Cell as a Site of Cytochrome P450-Dependent Mixed-Function Oxidase Activity in Lung. *Nature* (1977) 269 (5630):713–5. doi: 10.1038/269713a0
25. Chang H, Chang LW, Cheng YH, Tsai WT, Tsai MX, Lin P. Preferential Induction of CYP1A1 and CYP1B1 in CCSP-Positive Cells. *Toxicol Sci* (2006) 89(1):205–13. doi: 10.1093/toxsci/kfj025
26. Kerzee JK, Ramos KS. Constitutive and Inducible Expression of Cyp1a1 and Cyp1b1 in Vascular Smooth Muscle Cells: Role of the Ahr bHLH/PAS Transcription Factor. *Circ Res* (2001) 89(7):573–82. doi: 10.1161/hh1901.097083
27. Smerdova L, Smerdova J, Kabatkova M, Kohoutek J, Blazek D, Machala M, et al. Upregulation of CYP1B1 Expression by Inflammatory Cytokines is Mediated by the P38 MAP Kinase Signal Transduction Pathway. *Carcinogenesis* (2014) 35(11):2534–43. doi: 10.1093/carcin/bgu190
28. Metidji A, Omenetti S, Crotta S, Li Y, Nye E, Ross E, et al. The Environmental Sensor AHR Protects From Inflammatory Damage by Maintaining Intestinal Stem Cell Homeostasis and Barrier Integrity. *Immunity* (2018) 49(2):353–62.e355. doi: 10.1016/j.immuni.2018.07.010
29. Nakao A. Clockwork Allergy: How the Circadian Clock Underpins Allergic Reactions. *J Allergy Clin Immunol* (2018) 142(4):1021–31. doi: 10.1016/j.jaci.2018.08.007
30. Pariollaud M, Gibbs JE, Hopwood TW, Brown S, Begley N, Vonslow R, et al. Circadian Clock Component REV-ERBalpha Controls Homeostatic Regulation of Pulmonary Inflammation. *J Clin Invest* (2018) 128(6):2281–96. doi: 10.1172/JCI93910
31. Gibbs J, Ince L, Matthews L, Mei J, Bell T, Yang N, et al. An Epithelial Circadian Clock Controls Pulmonary Inflammation and Glucocorticoid Action. *Nat Med* (2014) 20(8):919–26. doi: 10.1038/nm.3599
32. Halwani R, Al-Muhsen S, Al-Jahdali H, Hamid Q. Role of Transforming Growth Factor-Beta in Airway Remodeling in Asthma. *Am J Respir Cell Mol Biol* (2011) 44(2):127–33. doi: 10.1165/rcmb.2010-0027TR
33. Frischmeyer-Guerrerio PA, Guerrerio AL, Oswald G, Chichester K, Myers L, Halushka MK, et al. TGFbeta Receptor Mutations Impose a Strong Predisposition for Human Allergic Disease. *Sci Transl Med* (2013) 5 (195):195ra194. doi: 10.1126/scitranslmed.3006448
34. Akdis CA. Does the Epithelial Barrier Hypothesis Explain the Increase in Allergy, Autoimmunity and Other Chronic Conditions? *Nat Rev Immunol* (2021) 21(11):739–51. doi: 10.1038/s41577-021-00538-7
35. Buters JT, Sakai S, Richter T, Pineau T, Alexander DL, Savas U, et al. Cytochrome P450 CYP1B1 Determines Susceptibility to 7, 12-Dimethylbenz [a]Anthracene-Induced Lymphomas. *Proc Natl Acad Sci U S A* (1999) 96 (5):1977–82. doi: 10.1073/pnas.96.5.1977
36. Bansal S, Leu AN, Gonzalez FJ, Guengerich FP, Chowdhury AR, Anandatheerthavarada HK, et al. Mitochondrial Targeting of Cytochrome P450 (CYP) 1B1 and its Role in Polycyclic Aromatic Hydrocarbon-Induced Mitochondrial Dysfunction. *J Biol Chem* (2014) 289(14):9936–51. doi: 10.1074/jbc.M113.525659
37. Bessede A, Gargaro M, Pallotta MT, Matino D, Servillo G, Brunacci C, et al. Aryl Hydrocarbon Receptor Control of a Disease Tolerance Defence Pathway. *Nature* (2014) 511(7508):184–90. doi: 10.1038/nature13323
38. Sadik A, Somarribas Patterson LF, Ozturk S, Mohapatra SR, Panitz V, Secker PF, et al. IL4I1 Is a Metabolic Immune Checkpoint That Activates the AHR and Promotes Tumor Progression. *Cell* (2020) 182(5):1252–70.e1234. doi: 10.1016/j.cell.2020.07.038
39. Tanaka G, Kanaji S, Hirano A, Arima K, Shinagawa A, Goda C, et al. Induction and Activation of the Aryl Hydrocarbon Receptor by IL-4 in B Cells. *Int Immunol* (2005) 17(6):797–805. doi: 10.1093/intimm/dxh260
40. Zissler UM, Chaker AM, Effner R, Ulrich M, Guerth F, Piontek G, et al. Interleukin-4 and Interferon-Gamma Orchestrate an Epithelial Polarization in the Airways. *Mucosal Immunol* (2016) 9(4):917–26. doi: 10.1038/mi.2015.110
41. Mezrich JD, Fechner JH, Zhang X, Johnson BP, Burlingham WJ, Bradfield CA. An Interaction Between Kynurenine and the Aryl Hydrocarbon Receptor can Generate Regulatory T Cells. *J Immunol* (2010) 185(6):3190–8. doi: 10.4049/jimmunol.0903670
42. Kyoreva M, Li Y, Hoosenally M, Hardman-Smart J, Morrison K, Tosi I, et al. CYP1A1 Enzymatic Activity Influences Skin Inflammation Via Regulation of the AHR Pathway. *J Invest Dermatol* (2020) 141(6):1553–63. doi: 10.1016/j.jid.2020.11.024
43. Schmidt JV, Su GH, Reddy JK, Simon MC, Bradfield CA. Characterization of a Murine Ahr Null Allele: Involvement of the Ah Receptor in Hepatic Growth and Development. *Proc Natl Acad Sci U S A* (1996) 93(13):6731–6. doi: 10.1073/pnas.93.13.6731
44. Dalton TP, Dieter MZ, Matlib RS, Childs NL, Shertzer HG, Genter MB, et al. Targeted Knockout of Cyp1a1 Gene Does Not Alter Hepatic Constitutive Expression of Other Genes in the Mouse [Ah] Battery. *Biochem Biophys Res Commun* (2000) 267(1):184–9. doi: 10.1006/bbrc.1999.1913
45. Pineau T, Fernandez-Salguero P, Lee SS, McPhail T, Ward JM, Gonzalez FJ. Neonatal Lethality Associated With Respiratory Distress in Mice Lacking Cytochrome P450 1a2. *Proc Natl Acad Sci U S A* (1995) 92(11):5134–8. doi: 10.1073/pnas.92.11.5134
46. Wimmer M, Alessandrini F, Gilles S, Frank U, Oeder S, Hauser M, et al. Pollen-Derived Adenosine is a Necessary Cofactor for Ragweed Allergy. *Allergy* (2015) 70(8):944–54. doi: 10.1111/all.12642
47. Alessandrini F, Schulz H, Takenaka S, Lentner B, Karg E, Behrendt H, et al. Effects of Ultrafine Carbon Particle Inhalation on Allergic Inflammation of the Lung. *J Allergy Clin Immunol* (2006) 117(4):824–30. doi: 10.1016/j.jaci.2005.11.046
48. Lam HC, Choi AM, Ryter SW. Isolation of Mouse Respiratory Epithelial Cells and Exposure to Experimental Cigarette Smoke at Air Liquid Interface. *J Vis Exp* (2011) (48):2513. doi: 10.3791/2513
49. Sinha M, Lowell CA. Isolation of Highly Pure Primary Mouse Alveolar Epithelial Type II Cells by Flow Cytometric Cell Sorting. *Bio Protoc* (2016) 6(22):e2013. doi: 10.21769/BioProtoc.2013
50. Bushnell B, Rood J, Singer E. BBMerge - Accurate Paired Shotgun Read Merging *via* Overlap. *PloS One* (2017) 12(10):e0185056. doi: 10.1371/journal.pone.0185056
51. Wu TD, Nacu S. Fast and SNP-Tolerant Detection of Complex Variants and Splicing in Short Reads. *Bioinformatics* (2010) 26(7):873–81. doi: 10.1093/bioinformatics/btq057
52. DeLuca DS, Levin JZ, Sivachenko A, Fennell T, Nazaire MD, Williams C, et al. RNA-SeQC: RNA-Seq Metrics for Quality Control and Process

Optimization. *Bioinformatics* (2012) 28(11):1530–2. doi: 10.1093/bioinformatics/bts196
53. Liao Y, Smyth GK, Shi W. Featurecounts: An Efficient General Purpose Program for Assigning Sequence Reads to Genomic Features. *Bioinformatics* (2014) 30(7):923–30. doi: 10.1093/bioinformatics/btt656
54. Robinson MD, McCarthy DJ, Smyth GK. Edger: A Bioconductor Package for Differential Expression Analysis of Digital Gene Expression Data. *Bioinformatics* (2010) 26(1):139–40. doi: 10.1093/bioinformatics/btp616
55. Kanehisa M, Goto S. KEGG: Kyoto Encyclopedia of Genes and Genomes. *Nucleic Acids Res* (2000) 28(1):27–30. doi: 10.1093/nar/28.1.27

Conflict of Interest: The authors declare that the research was conducted in the absence of any commercial or financial relationships that could be construed as a potential conflict of interest.

Publisher's Note: All claims expressed in this article are solely those of the authors and do not necessarily represent those of their affiliated organizations, or those of the publisher, the editors and the reviewers. Any product that may be evaluated in this article, or claim that may be made by its manufacturer, is not guaranteed or endorsed by the publisher.

frontiers | Frontiers in Immunology

TYPE Original Research
PUBLISHED 22 July 2022
DOI 10.3389/fimmu.2022.964575

OPEN ACCESS

EDITED BY
Bao-Hui Cheng,
Institute of ENT and Shenzhen Key Laboratory of ENT, China

REVIEWED BY
Devendra K. Agrawal,
Western University of Health Sciences, United States
Erwin William Gelfand,
University of Colorado Anschutz Medical Campus, United States

*CORRESPONDENCE
Peisong Gao
pgao1@jhmi.edu

†These authors have contributed equally to this work

SPECIALTY SECTION
This article was submitted to Immunological Tolerance and Regulation, a section of the journal Frontiers in Immunology

RECEIVED 08 June 2022
ACCEPTED 28 June 2022
PUBLISHED 22 July 2022

CITATION
Wang J, Zhao Y, Zhang X, Tu W, Wan R, Shen Y, Zhang Y, Trivedi R and Gao P (2022) Type II alveolar epithelial cell aryl hydrocarbon receptor protects against allergic airway inflammation through controlling cell autophagy.
Front. Immunol. 13:964575.
doi: 10.3389/fimmu.2022.964575

Type II alveolar epithelial cell aryl hydrocarbon receptor protects against allergic airway inflammation through controlling cell autophagy

Ji Wang[1,2,3†], Yilin Zhao[1,4†], Xin Zhang[1,5†], Wei Tu[1,6], Rongjun Wan[1,7], Yingchun Shen[1], Yan Zhang[1,7], Ruchik Trivedi[1] and Peisong Gao[1*]

[1]Division of Allergy and Clinical Immunology, Johns Hopkins School of Medicine, Baltimore, MD, United States, [2]Department of Respiratory and Critical Care Medicine, West China Hospital, Sichuan University, Chengdu, China, [3]Laboratory of Pulmonary Immunology and Inflammation, Frontiers Science Center for Disease-related Molecular Network, Sichuan University, Chengdu, China, [4]Department of Respiratory Medicine, Xijing Hospital, The Fourth Military Medical University, Xi'an, China, [5]Department of Integrated Traditional Chinese and Western Medicine, West China Hospital, Sichuan University, Chengdu, China, [6]Department of Respirology and Allergy, Third Affiliated Hospital of Shenzhen University, Shenzhen, China, [7]Department of Respiratory Medicine, Xiangya Hospital, Central South University, Changsha, China

Rationale: Aryl hydrocarbon receptor (AhR), a ligand-activated transcription factor, has been considered as an important regulator for immune diseases. We have previously shown that AhR protects against allergic airway inflammation. The underlying mechanism, however, remains undetermined.

Objectives: We sought to determine whether AhR specifically in type II alveolar epithelial cells (AT2) modulates allergic airway inflammation and its underlying mechanisms.

Methods: The role of AhR in AT2 cells in airway inflammation was investigated in a mouse model of asthma with AhR conditional knockout mice in AT2 cells (*Sftpc-Cre;AhR$^{f/f}$*). The effect of AhR on allergen-induced autophagy was examined by both *in vivo* and *in vitro* analyses. The involvement of autophagy in airway inflammation was analyzed by using autophagy inhibitor chloroquine. The AhR-regulated gene profiling in AT2 cells was also investigated by RNA sequencing (RNA-seq) analysis.

Results: *Sftpc-Cre;AhR$^{f/f}$* mice showed exacerbation of allergen-induced airway hyperresponsiveness and airway inflammation with elevated Th2 cytokines in bronchoalveolar lavage fluid (BALF). Notably, an increased allergen-induced autophagy was observed in the lung tissues of *Sftpc-Cre;AhR$^{f/f}$* mice when compared with wild-type mice. Further analyses suggested a functional axis of AhR-TGF-β1 that is critical in driving allergic airway inflammation through regulating allergen-induced cellular autophagy. Furthermore, inhibition of autophagy with autophagy inhibitor chloroquine

10.3389/fimmu.2022.964575

significantly suppressed cockroach allergen–induced airway inflammation, Th2 cytokines in BALFs, and expression of autophagy-related genes LC3 and Atg5 in the lung tissues. In addition, RNA-seq analysis suggests that autophagy is one of the major pathways and that *CALCOCO2/NDP52* and *S1009* are major autophagy-associated genes in AT2 cells that may contribute to the AhR-mediated cockroach allergen–induced airway inflammation and, subsequently, allergic asthma.

Conclusion: These results suggest that AhR in AT2 cells functions as a protective mechanism against allergic airway inflammation through controlling cell autophagy.

KEYWORDS

asthma, cockroach allergen, aryl hydrocarbon receptor, autophagy, AT2 cells

Introduction

Asthma is a leading serious chronic illness of children and adults worldwide, and its prevalence has reached unprecedented levels over the past few decades (1). Environmental allergen exposure has been considered to be one of the major risk factors for asthma (2). Of these, cockroach allergen is one of the major sources of indoor allergens and can give rise to Immunoglobulin E (IgE) sensitization and, subsequently, development of asthma (3–5). Furthermore, a recent study suggested that serum IgE levels specific to cockroach allergen were correlated with Th2 polarization (6). However, it remains unclear about the biological mechanisms underlying the cockroach allergen exposure-induced Th2-associated airway inflammation in asthma. Airway epithelium is the first line of defense against inhaled allergens. Interaction of airway epithelium with allergens leads to the release of inflammatory mediators, resulting in inappropriate recruitment of immune cells and skewing of downstream immune responses. However, the mechanisms underlying the allergen-induced mediator release from epithelial cells are still not completely understood.

The aryl hydrocarbon receptor (AhR) is a ligand-activated transcription factor widely expressed in barrier organs, such as airway, gut, and skin (7, 8), and in different cell types [e.g., DCs, Th17 and Treg cells, ILCs, and mesenchymal stem cells (MSCs)] (9–12). AhR is originally characterized for its function in the metabolism of environmental toxicants such as dioxins and many other polycyclic aromatic hydrocarbons (PAHs) (13–16). Recent studies have suggested a central role for AhR as an environmental sensing molecule in cell growth, cell differentiation, cell immune responses, and respiratory function (17–21). Not surprisingly, AhR has emerged as an attractive therapeutic target for different diseases including asthma (14–16, 22). Indeed, AhR has been associated with environmental pollutant–induced allergic airway inflammation (18, 23–25) and reactive oxygen species (ROS)-dependent mast cell degranulation and activation (26, 27). Our previous findings have suggested that benzo(a)pyrene (BaP, a ubiquitous air pollutant) co-exposure with Der f 1 (a common allergen to human) exacerbated AhR signaling pathway that regulates the co-exposure–induced airway epithelial cell oxidative stress and cytokine release (28, 29). Furthermore, our recent study demonstrated that epithelial AhR is essential in protecting against cockroach allergen–induced ROS generation, NLRP3 inflammasome activation, and Muc5ac expression (30). However, the specific role of AhR signaling in regulating allergic airway inflammation and its precise mechanisms has not been fully elucidated.

Autophagy is an the endogenous housekeeping process in maintaining cell homeostatic process by delivering damaged proteins and redundant cellular organelles to lysosomes for degradation during cellular stress (2). Evidence shows that autophagy is critical in shaping cellular immune responses and progression of inflammatory diseases. It was found that autophagy was increased in peripheral blood cells and sputum granulocytes from severe asthmatic patients (31). The increased autophagy has also been associated with asthma pathological processes such as extracellular matrix deposition, airway remodeling, and immune dysregulation

Abbreviations: CRE, cockroach extract; AhR, aryl hydrocarbon receptor; WT, wild-type; BALF, bronchoalveolar lavage fluid; PAS, Alcian Blue periodic acid–Schiff; RT-PCR, quantitative real-time PCR; AHR, airway hyperresponsiveness; BSA, bovine serum albumin; FBS, fetal bovine serum; H&E, hematoxylin and eosin; AT2, type II alveolar epithelial cells; HBEC, human bronchial epithelial cell; CLQ, chloroquine; GO, Gene Ontology; NLRP3, nucleotide-binding oligomerization domain (NOD)–like receptor family pyrin domain-containing 3.

(32–35). Previously, we found that inhibition of autophagy led to attenuated cockroach allergen–induced airway epithelial ROS generation, cytokine release, and subsequent allergic airway inflammation, suggesting a role for autophagy in promoting asthma development (36). However, it remains unclear how cellular autophagy is regulated in the pathogenesis of asthma.

In the present study, we focused on type II alveolar epithelial cells (AT2) to determine whether AhR, specifically in AT2 cells, is involved in regulating cellular autophagy and, subsequently, allergic airway inflammation. In particular, we generated AhR conditional knockout mice in AT2 cells (*Sftpc-Cre;AhR$^{f/f}$*) and investigated the role of AhR specifically in AT2 cells in cockroach allergen–induced airway inflammation. We then uncovered a unique role for AhR in regulating allergen-induced cellular autophagy by both *in vivo* and *in vitro* analyses. We further elucidated an overexpression of autophagy in the lung tissues of asthma mouse model and inhibition of autophagy suppressed allergic airway inflammation. Most importantly, RNA sequencing (RNA-seq) analysis identified autophagy to be one of the most AhR-regulated biological processes in AT2 cells. Further analyses suggest that *CALCOCO2* and *S100a9* are the major AhR-regulated autophagy-associated genes. Overall, this study provides evidence that AhR regulates allergen-induced autophagy that may contribute to the protective mechanism of AhR signaling against allergic airway inflammation.

Methods

Mice

Sftpc-Cre;AhR$^{f/f}$ mice on the C57BL/6 background were generated by cross-breeding *Sftpc-cre* with *AhR$^{f/f}$* mice in this study. *Sftpc-cre* mice were provided by Michael A. O'Reilly at the University of Rochester Medical Center (Rochester, NY, USA), and *AhR$^{f/f}$* mice were purchased from the Jackson Laboratory (Bar Harbor, ME, USA). All mice were maintained under specific pathogen–free conditions at the animal facility of the Johns Hopkins University School of Medicine. The animal care and experiments were performed in compliance with the institutional and US National Institutes of Health guidelines and were reviewed and approved by the Johns Hopkins University Animal Care and Use Committee. All mice were used at 6–8 weeks of age, and all experiments used age- and sex-matched controls.

Cockroach allergen–induced asthma mouse model

The cockroach allergen–induced asthma mouse model was established with the protocol as illustrated in Figure 1A. Briefly, mice were sensitized by intra-tracheal (i.t.) inhalation of 20 μg of cockroach extract (CRE, B46, GREER Laboratories) per mouse in

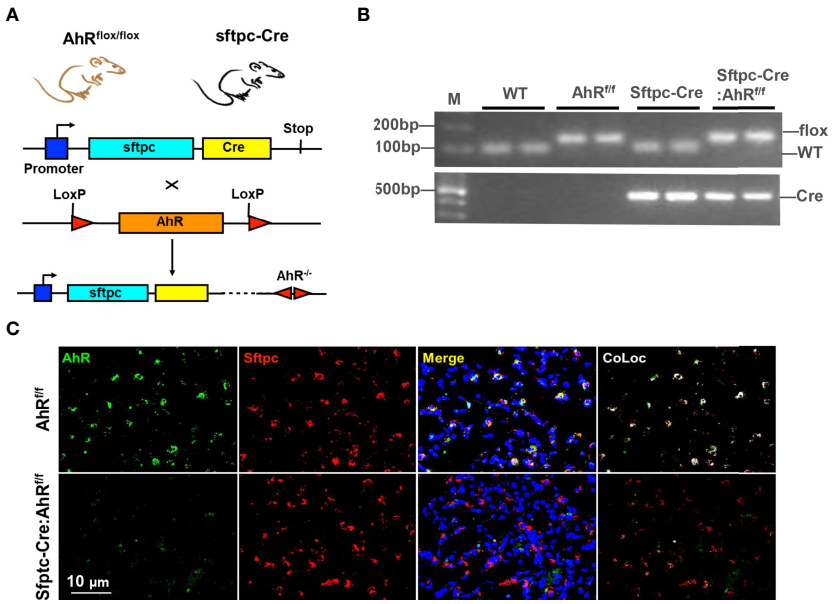

FIGURE 1
Generation of type II alveolar epithelial cell–specific AhR knockout mice. **(A)** Schematic representation of the crossbreeding of a floxed AhR mouse (*AhR$^{f/f}$*) with a Sftpc-cre mouse. **(B)** Confirmation of *Sftpc-cre: AhR$^{f/f}$* mice by genotyping. **(C)** AhR deletion in AT2 cells of *Sftpc-cre: AhR$^{f/f}$* mice was confirmed by co-immunostaining with Sftpc and AhR in the lung tissues.

50 µl of Phosphate-Buffered Saline (PBS) under light anesthesia with isoflurane and challenged with the same amount of CRE. Control mice were treated with PBS. Mice were sacrificed, and samples [lung tissues, bronchoalveolar lavage fluid (BALF), and blood] were collected on the next day after the last allergen challenge (30). In particular, BALF was harvested by two consecutive flushes of the lung with 1.0 ml of ice-cold PBS. Blood was taken to screen for serum antibodies against cockroach allergen. In some cases, mice were pre-treated with autophagy inhibitor chloroquine (CLQ; C6628, 60 mg/kg, Sigma-Aldrich, St. Louis, MO, USA) or saline vehicle control by intraperitoneal administration 1 h before every single allergen challenge.

Airway hyperresponsiveness

Mice were anesthetized with a ketamine (90 mg/kg)/xylazine (18 mg/kg) mixture, and a tracheotomy tube was inserted. Ventilation was initiated with a volume-cycled ventilator (Flexivent; SCIREQ Scientific) with a positive-end expiratory pressure of 2 cmH2O). Airway responsiveness was monitored by challenging mice with a dose-dependent aerosolized methacholine (0–30 mg/ml). The airway resistance was measured with the Flexivent software and exported to Pulmodyn data-acquisition software (Hugo Sachs Electronic) for data analysis (37).

Histological analysis

Mouse lungs were perfused with 10 ml of ice-cold PBS injected into the right ventricle followed by excision, fixed with 4% formalin, and embedded in paraffin. Sections (4 µm) were then prepared from these paraffin-embedded lungs and subjected to hematoxylin and eosin (H&E) and periodic acid–Schiff (PAS) staining to evaluate general morphology and mucus production as previously described (30).

Flow cytometry analysis

Single-cell suspensions were prepared from BALFs, and total cells in BALFs were counted by Countless II (ThermoFisher). Cellular differential percentages in BALFs were measured by flow cytometry on an Accuri C6 Plus Flow Cytometer (BD Biosystems), and the data were analyzed with FlowJo software (Tree Star Inc.) as previously described (38).

Immunofluorescence staining

Immunofluorescence staining was performed as previously reported (37). Briefly, sectioned lung tissues were first blocked using 5% w/v BSA at room temperature for 1 h, followed by incubation with the primary antibodies as listed in the online repository (Supplementary Table 1) overnight at 4°C. The sample sections were then incubated with secondary antibodies conjugated with fluorescence at room temperature for 1 h. Isotype-matched negative control antibodies were used under the same conditions. The sections were mounted with the Fluoromount Mounting medium (Sigma) with DAPI (4′,6-diamidino-2-phenylindole) (ThermoFisher) and then observed by a NIKON ECLIPSE Ti-U microscope equipped with DS-Fi2 camera (NIKON, USA).

Enzyme-linked immunosorbent assay

Interleukin-4 (IL-4), IL-5, Interferon-gamma (IFN-γ), IL-17A, IL-25, and Transforming growth factor-beta 1 (TGF-β1) in cell-free BALF or supernatant were quantified by using the Ready-Set-Go! ELISA (ThermoFisher) according to the manufacturer's instructions. Serum levels of cockroach allergen–specific IgE and IgG1 were analyzed by Enzyme-linked immunosorbent assay (ELISA) as previously described (36).

Cell culture and treatment

Human bronchial epithelial cells (HBEC3-KT, ATCC CRL-4051) were cultured in Ham's F-12K (Kaighn's) medium supplemented with 10% v/v FBS and 1% penicillin-streptomycin. The cells were maintained at 37°C in a humidified atmosphere at 5% CO_2. HBECs were treated with cockroach extract (CRE, Greer Laboratory) alone or pre-treated with AhR agonist TCDD (Sigma, 45899; 1.0 µM) or antagonist CH-223191 (Sigma, C8124; 10 µM) or vehicle controls 1 h before CRE treatment.

Isolation of mouse alveolar type 2 cells

Mouse AT2 cells were isolated from $AhR^{fl/fl}$ mice and *Sftpc-Cre;* $AhR^{flox/flox}$ mice as previously reported (38). Briefly, mice were euthanized with ketamine and xylazine intraperitoneally. Lung tissues from these mice were digested with Dispase (50 units/ml, Gibco) at room temperature for 45 min and then incubated with AT2 isolation medium consisting of a 1:1 mixture of Dulbecco's modified Eagle's medium (DMEM) and Ham's F-12 (DMEM/F-12; Sigma) supplemented with 0.01% DNase I (Sigma), sodium penicillin G (100 U/ml), and streptomycin (100 µg/ml). The mixed cells were filtered through cell strainers; stained with biotinylated anti-CD16/32, anti-CD45, anti-Ter119, and anti-Sca-1 (BioLegend); and incubated at 37°C shaking incubator for 30 min. These cells were further negatively selected with streptavidin-conjugated magnetic beads for 30 min at room temperature. Cells

were centrifuged for 10 min at 300*g* at 4°C and incubated on dishes pre-coated with mouse IgG. After incubation for 2 h, non-adherent cells were collected, centrifuged, and re-suspended with AT2 isolation medium.

RNA-seq analysis

RNA-seq libraries were prepared for sequencing using an Illumina TruSeq stranded mRNA sample preparation kit following the manufacturer's recommended procedure. Briefly, total RNA was extracted using the RNeasy Mini Kit (QIAGEN). mRNA was enriched using oligo dT beads and then fragmented chemically by incubating at 94°C for 8 min. cDNA was synthesized with SuperScript II. After purification using AMPure XP beads, the double-stranded cDNA was ligated to TruSeq RNA adapters followed by 15 cycles of amplification and library purification. Sequencing was performed on an Illumina NextSeq6000. RNA-seq reads were aligned to the mouse reference genome GRCm38 using STAR aligner version 2.7.2b. BAM file outputs from STAR were annotated using Partek Genomic Suite (v6.6) and the RefSeq database. The gene expression levels were defined as counts by Salmon (39) and then normalized by $\log_2$-transformed counts per million (CPM, edgeR version 3.34.1) (40). Different expression analyses were performed with multiple linear regression models and empirical Bayes moderation embedded in the limma-trend approach (limma version 3.48.3) (40). Genes with absolute $\log_2$ fold change [abs($\log_2$FC)] > 0.5 and $p < 0.05$ were defined as differentially expressed genes (DEGs). Gene set enrichment analyses was performed by the clusterProfiler 4.0 version 4.0.5 (41). Up- or downregulated DEGs were visualized by ComplexHeatmap (version 2.8.0) and ggplot2 (version 3.3.5) (42). All RNA-seq–based downstream analyses and visualizations were performed in R version 4.1.2. (see RNA-seq data used for analysis in Supplementary Materials).

Transfection of siRNA

AhR knockdown in HBECs was accomplished by using a pre-designed MISSION siRNA small interfering RNA pair (Sigma-Aldrich, SASI_Hs01_00140198). siRNA transfection was performed with Lipofectamine™ RNAiMAX (ThermoFisher) following the manufacturer's instruction, whereas control cells received negative control siRNA. Cells were cultured for 48 h, and transfection efficiency was evaluated by quantitative real-time PCR and Western blot.

RNA isolation and quantitative real-time PCR analysis

Total RNA from lung tissues or HBECs was isolated using the Monarch Total RNA Miniprep Kit (New England Biolabs), and cDNAs were synthesized with the High-Capacity cDNA Reverse Transcription Kit (ThermoFisher). Quantitative real-time PCR analysis was performed using the Power SYBR Green PCR Master Mix (ThermoFisher) on an ABI Prism 7300 detection system. Data were analyzed using the $2^{-\Delta\Delta CT}$ method relative to the housekeeping gene Actin (43). Primer sequences are provided in the Online Repository (see **Table E1**).

Western blotting

Tissues or cells were lysed with an radioimmunoprecipitation assay (RIPA) buffer containing protease and phosphatase inhibitor cocktails (Sigma-Aldrich). Protein concentrations were measured by using a BCA kit (Thermo Fisher). An equal amount of total protein (20–50 μg) was loaded onto a 4%–12% Tris-Glycine Gel in NuPAGE MOPS SDS Running Buffer (Thermo Fisher Scientific) and then transferred using the iBlot2 NC Stack System (ThermoFisher). The membranes were blocked in 5% non-fat milk in Tris buffered saline with Tween® 20 (TBST) for 1 h at room temperature and then probed with primary antibodies overnight at 4°C. Species-appropriate secondary antibodies conjugated to IRDye 680RD or IRdye 800CW (LI-COR Biosciences) were used according to the manufacturer's instructions. Detection was performed using iBright 1500 Imaging Systems, and fluorescent intensity was quantified using the system built in IBright Analysis Software (Thermo Fisher Scientific).

Statistical analysis

All statistical analyses were carried out using GraphPad Prism version 8.2.1 (GraphPad Software, La Jolla, CA, USA). All data are presented as means ± SEM. Comparison of two groups was performed by student's two-tailed unpaired t-test. Comparison of more than two groups was performed by ordinary one-way ANOVA followed by Tukey's *post hoc* test. $P < 0.05$ was considered statistically significant.

Results

Generation of type II alveolar epithelial cell–specific AhR knockout mice

Airway epithelial cells are the first line of defense against inhaled particulate antigens, and epithelial activation is one of the characteristics of asthma (44). We have found that expression of AhR was significantly increased in the airways of asthmatic patients (45) and the mouse model of asthma (12). To determine the significance of epithelial AhR in cockroach allergen–induced asthma, we deleted AhR selectively from type II alveolar airway epithelium (AT2) by crossing floxed AhR mice

($AhR^{f/f}$) with *Sftpc-cre* mice that express the Cre recombinase in AT2 cells from the endogenous promoter/enhancer elements of the surfactant protein C (Sftpc) locus (*Sftpc-Cre; $AhR^{f/f}$*, Figure 1A). The mice were confirmed by genotyping (Figure 1B). The deletion of AhR in AT2 cells was further confirmed by co-immunostaining with AhR and Sftpc in the lung tissues (Figure 1C). Thus, these mice represent an ideal mouse model to examine the functional role of AhR in AT2 cells in allergic airway inflammation.

Type II alveolar epithelial cell AhR protects against allergic airway inflammation

Next, we used these newly generated *Sftpc-Cre;$AhR^{f/f}$* mice to create an asthma mouse model by using our previous protocol as illustrated in Figure 2A. Histological analysis demonstrated that CRE-treated *Sftpc-Cre;$AhR^{f/f}$* mice had an increased recruitment of inflammatory cells to the lung with dense peribronchial infiltrates (Figure 2B, upper panel) and goblet cell hyperplasia (Figure 2B, lower panel) as compared with *$AhR^{f/f}$* mice. Consistently, these *Sftpc-Cre;$AhR^{f/f}$* mice showed a significant increase in airway resistance (Figure 2C) and decrease in airway compliance (Figure 2D). Compared with *$AhR^{f/f}$* mice, the total inflammatory cells, especially eosinophils, were remarkably increased in the BALFs of *Sftpc-Cre;$AhR^{f/f}$* mice (Figure 2E). Higher levels of cockroach allergen–specific IgE and IgG1 were observed in serum of CRE-treated *Sftpc-Cre;$AhR^{f/f}$* (Figure 2F). Furthermore, *Sftpc-Cre; $AhR^{f/f}$* mice had higher levels of IL-4 and IL-5 in BALFs (Figure 2G). In contrast, no clear change was observed for IFN-γ, IL-17, and IL-25. Collectively, these findings indicate that AhR in AT2 cells protects against cockroach allergen–induced airway hyperresponsiveness and Th2-associated allergic airway inflammation.

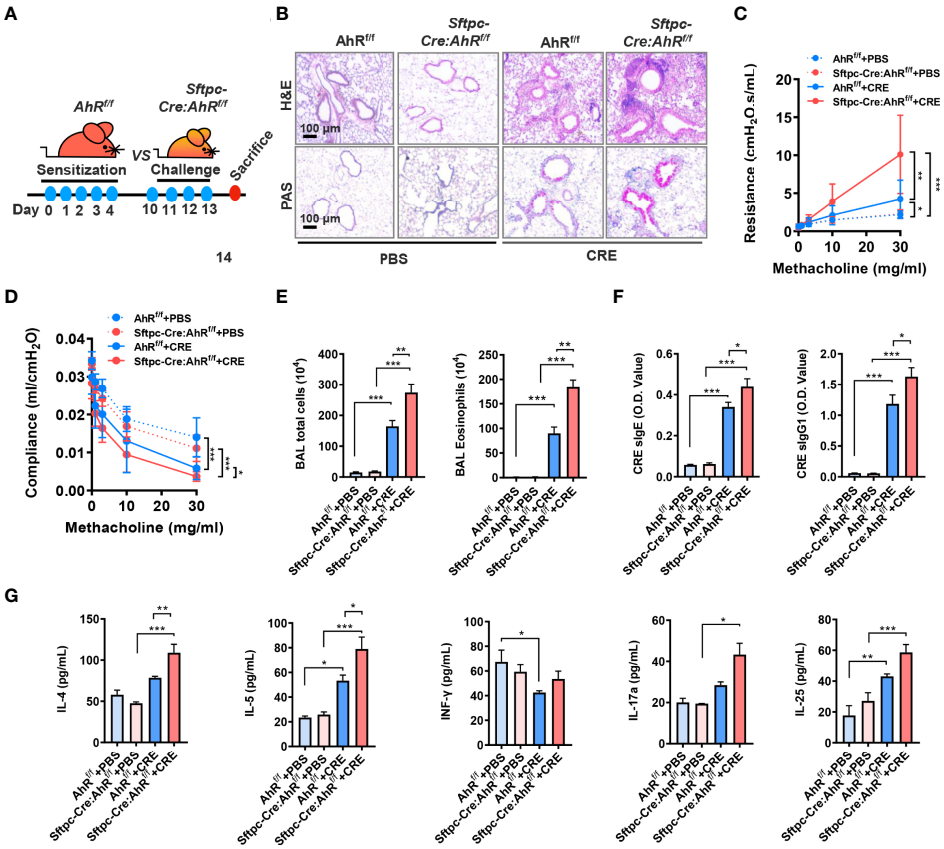

FIGURE 2
Type II alveolar epithelial cell AhR protects against airway hyperresponsiveness and allergic airway inflammation. **(A)** Experimental scheme for cockroach allergen–induced mouse model of asthma. **(B)** Histological examination of mouse paraffin lung sections stained with hematoxylin and eosin (H&E, upper panel) and Alcian Blue periodic acid–Schiff (AB-PAS, lower panel). **(C, D)** Lung resistance **(C)** and compliance **(D)** in response to increasing concentrations of methacholine using the forced oscillation technique (FlexiVent, SCIREQ). **(E)** Bronchoalveolar lavage (BAL) fluid total and eosinophil cell counts as assessed by flow cytometry. **(F)** Serum levels of cockroach allergen–specific IgE and IgG1. **(G)** Levels of cytokines in BALFs. n = 8–10. Data represent means ± SEM. *$p < 0.05$, **$p < 0.01$, and ***$p < 0.001$.

Type II alveolar epithelial cell AhR protects against allergen-induced autophagy in a mouse model of asthma

Previously, we have demonstrated that excessive autophagy is critical in cockroach allergen–induced ROS generation, cytokine release, and subsequent allergic airway inflammation (36). To determine whether epithelial AhR regulates cockroach allergen–induced autophagy, we detected expression of autophagy-related genes in the lung tissues of CRE-induced mouse model with $AhR^{f/f}$ or $Sftpc\text{-}Cre;AhR^{f/f}$ mice. Compared with PBS-treated mice, increased expression of LC3A, Atg5, and p62 was seen in the lung tissues of CRE-sensitized and challenged mice as analyzed by RT-PCR (Figure 3A). Interestingly, compared with $AhR^{f/f}$ mice, the increased expression of ILC3A, LC3B, and Beclin-1 was further enhanced in CRE-treated $Sftpc\text{-}Cre;AhR^{f/f}$ mice. The increased autophagy was specifically confirmed in AT2 cells by co-immunofluorescent staining. The CRE-treated $Sftpc\text{-}Cre;AhR^{f/f}$ mice showed a significantly increased expression of LC3B in AT2 cells compared with $AhR^{f/f}$ mice (Figure 3B). Similar patterns were noted for Beclin-1 and ATG5, indicating that AhR in AT2 cells protects against cockroach allergen–induced autophagy.

Aryl hydrocarbon receptor modulates allergen-induced autophagy in human bronchial epithelial cells

To further confirm the functional significance of AhR in modulating autophagy, we investigated whether AhR knockdown can affect cockroach allergen–induced autophagy by *in vitro* analysis. AhR was knocked down in HBECs by using different doses of siRNA, and siRNA at 100 pmol showed the best deletion of AhR as assessed by RT-PCR (Figure 4A). AhR knockdown was further confirmed by Western blot (Figure 4B). As expected, immunostaining analysis illustrated that CRE exposure induced autophagy in HBECs as assessed by the increased expression of LC3 (Figures 4C, D), ATG5 (Figures 4C, E), and Beclin-1 (Figures 4C, F) but decreased

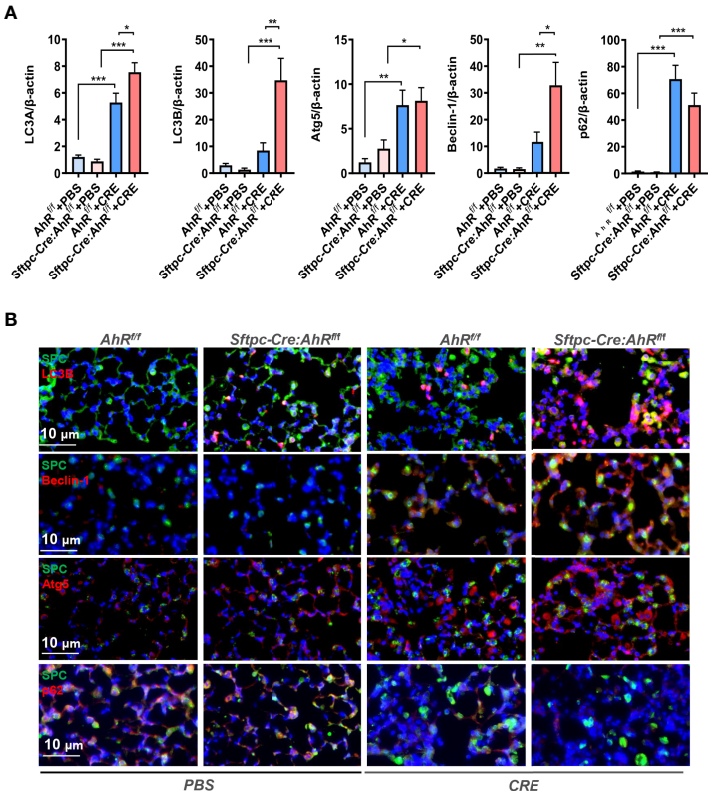

FIGURE 3
Type II alveolar epithelial cell AhR protects against allergen-induced autophagy in a mouse model of asthma. **(A)** RT-PCR analyses of autophagy-related genes in the lung tissues of asthma mouse model. n = 8–12. **(B)** Representative images of co-immunofluorescence staining of autophagy-related genes with AT2 marker SPC. n = 6. Data in **(A)** represent means ± SEM. *$p < 0.05$, **$p < 0.01$, and ***$p < 0.001$.

10.3389/fimmu.2022.964575

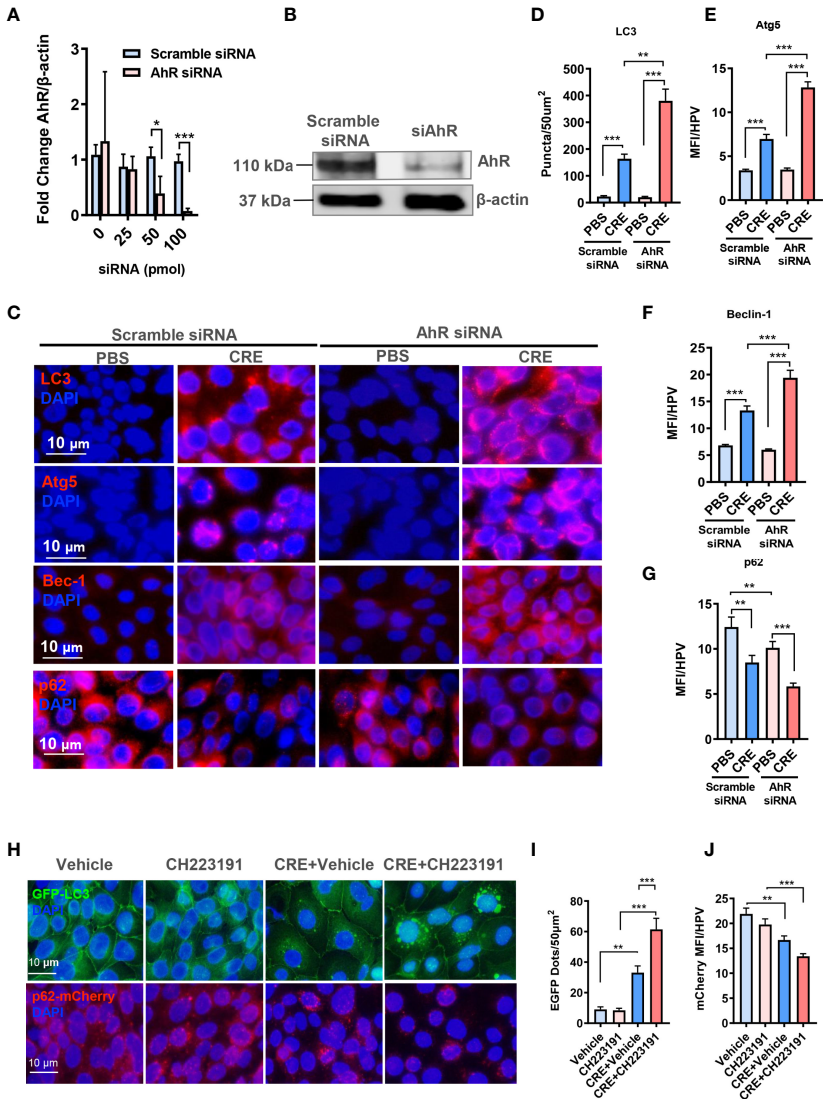

FIGURE 4
Aryl hydrocarbon receptor modulates allergen-induced autophagy in human bronchial epithelial cells (HBECs). **(A)** RT-PCR confirmation of AhR knockdown in HBECs by using different doses of AhR siRNA. **(B)** AhR knockdown in HBECs with 100-pmol AhR siRNA was further confirmed by Western blot. **(C)** Representative images of immunofluorescence staining of autophagy-related genes in HBECs with or without AhR knockdown. n = 6. **(D–G)** Quantification of immunofluorescence staining for autophagy-related genes LC3 **(D)**, Atg5 **(E)**, Beclin-1 **(F)**, and p62 **(G)** in HBECs with or without AhR knockdown. n = 12. **(H)** Representative immunofluorescence images of CRE-treated HBECs expressing GFP-LC3 or p62-mCherry in the presence or absence of AhR antagonist CH223191. **(I)** Quantitative analysis of autophagic flux according to the number of LC3 puncta (GFP dots/50 μm^2). **(J)** Quantitative analysis of p62-mCherry florescent signal in **(H)**. n = 12 [four different high-power fields (hpfs) of three independent experiments]. Data represent means ± SEM. *$p < 0.05$, **$p < 0.01$, and ***$p < 0.001$.

expression of p62 (Figures 4C, G). Of interest, the increased expression of LC3 (Figures 4C, D), ATG5 (Figures 4C, E), and Beclin-1 (Figures 4C, F) was further enhanced in HBECs with AhR knockdown. To visualize the regulation of autophagy by AhR, we transfected either a GFP-LC3 or p62-mCherry construct in HBECs and then treated them with AhR antagonist CH223191. As shown in Figure 4H, the autophagic flux induced by CRE was increased according to the number of LC3 puncta (Figures 4H, I). The increased autophagy was potentiated in HBECs pre-treated with AhR antagonist CH223191. In contrast, expression of p62 was significantly reduced in HBECs treated with CRE in relative to PBS. No statistical difference was observed for HBECs with or without CH223191 pre-treatment (Figures 4H, J). Taken together, our *in vitro* analysis supports that epithelial AhR regulates cockroach allergen–induced autophagy.

Inhibition of autophagy attenuates allergic airway inflammation

Given the significance of autophagy in AT2 cell AhR-modulated allergic airway inflammation, we asked whether inhibition of autophagy can suppress cockroach allergen–induced airway inflammation by using autophagy inhibitor CLQ in our mouse model following the protocol illustrated in (Figure 5A). CLQ is the most widely used classic inhibitor of autophagy that inhibits the last stage of autophagy (46). Consistent with our previous or current findings, CRE exposure induced airway inflammation when compare with PBS treatment. When these CRE-treated mice were pre-exposed to CLQ, the CRE-induced airway inflammation was significantly attenuated. In particular, CLQ pre-treatment inhibited CRE-induced peribronchial inflammation (H&E) (Figure 5B, upper panel) and goblet cell hyperplasia (PAS) (Figure 5B, lower panel). These CLQ-treated mice also showed reduced numbers of total inflammatory cells, particularly eosinophils in BALFs (Figure 5C). Moreover, cockroach allergen specific IgE and IgG1 in serum

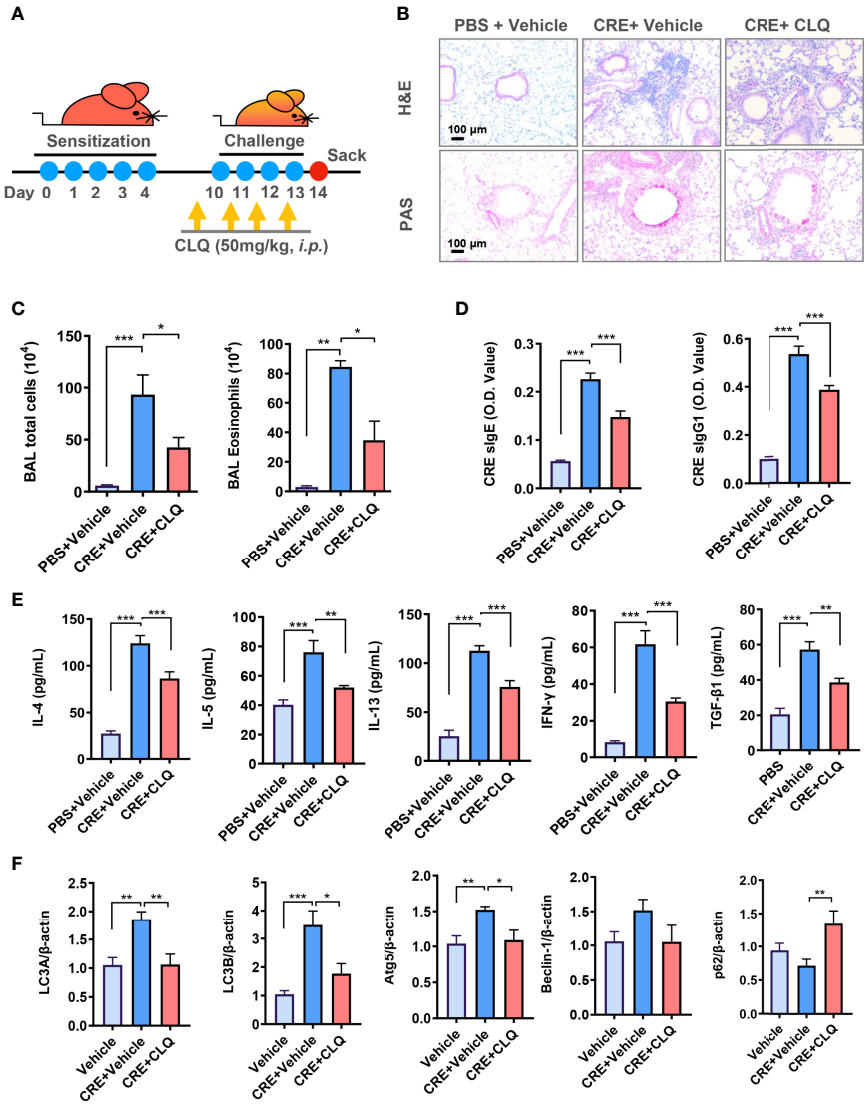

FIGURE 5
Inhibition of autophagy attenuates allergic airway inflammation. **(A)** Experimental scheme for cockroach allergen–induced mouse model of asthma in the presence or absence of autophagy inhibitor chloroquine (CLQ). **(B)** Histological examination of mouse paraffin lung sections stained with hematoxylin and eosin (H&E, upper panel) and periodic acid–Schiff (PAS, lower panel). **(C)** Bronchoalveolar lavage (BAL) fluid total and eosinophil cell counts as assessed by flow cytometry. **(D)** Serum levels of cockroach allergen–specific IgE and IgG1. **(E)** Levels of cytokines in BALFs. **(F)** RT-PCR analyses of autophagy-related genes in the lung tissues of asthma mouse model. n = 10. Data represent means ± SEM. $*p < 0.05$, $**p < 0.01$, and $***p < 0.001$.

(sIgE and sIgG1) were reduced in mice treated with CLQ (Figure 5D). Furthermore, CLQ treatment led to the significant reduction in the levels of IL-4, IL-5, IL13, IFNγ, and TGF-β1 in BALFs (Figure 5E). Furthermore, as expected, treatment with CLQ attenuated CRE-induced expression of LC3A, LC3B, and Atg5 but led to the accumulation of p62 (Figure 5F). These results further support that inhibition of autophagy can prevent cockroach allergen–induced Th2-associated airway inflammation.

TGF-β1 is required in AhR-mediated cockroach allergen–induced autophagy

We have previously reported that AhR modulates allergen-induced epithelial TGF-β1 secretion and signaling activation (29). We hypothesized that TGF-β1 may be a key player in AhR-mediated cockroach allergen–induced autophagy. AhR in HEBCs was knocked down by siRNA s illustrated in (Figures 4A, B). These HBECs were exposed to CRE for 24 h, and levels of TGF-β1 in supernatants were measured by ELISA. As noted, cockroach allergen exposure induced significant levels of TGF-β1 release from HBECs (Figure 6A). Of interest, the TGF-β1 release was enhanced in HEBCs with AhR knockdown. These findings provide further evidence that AhR modulates cockroach allergen–induced epithelial TGF-β1 secretion. To determine the role of TGF-β1 in autophagy, HBECs were treated with different doses of recombinant TGF-β1 for 24 h, the expression of autophagy-associated genes was detected by RT-PCR. Significantly increased LC3A and Atg5, but reduced p62 expression was observed in TGF-β1–treated HBECs (Figure 6B). No clear change was noted for Beclin-1. To further investigate whether TGF-β1 is required in cockroach allergen–induced autophagy, TGF-β1 neutralizing antibody (α-TGF-β1) was used to remove TGF-β1 in supernatants of CRE-treated HBECs. Intriguingly, the CRE-induced increased expression of LC3A, LC3B, Atg5, and Beclin-

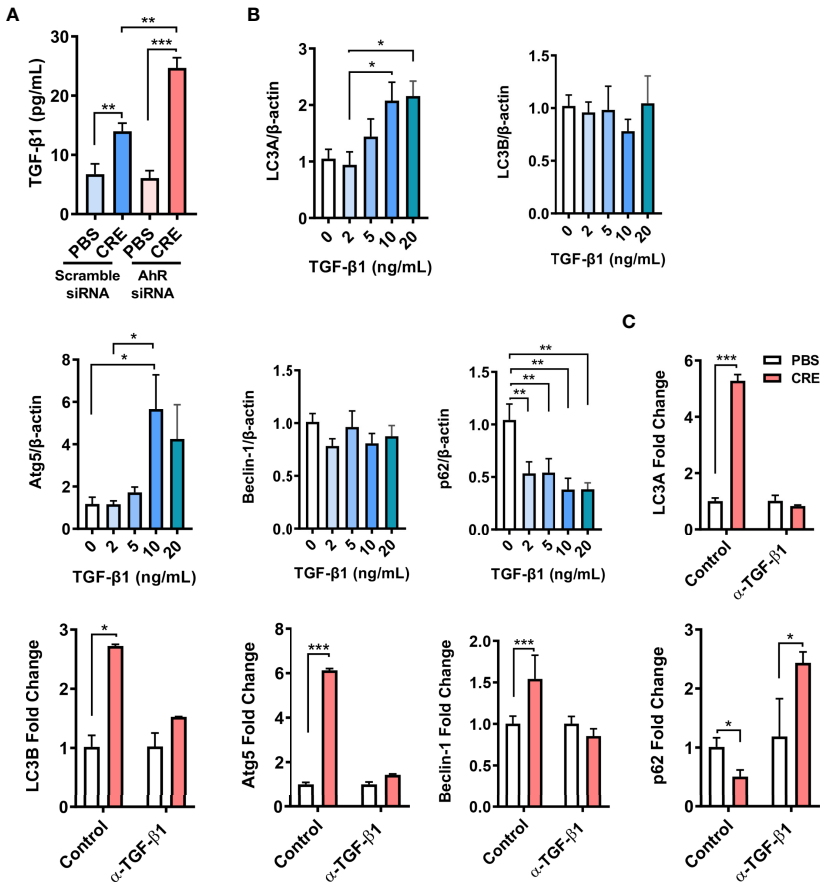

FIGURE 6
TGF-β1 is required in AhR-mediated cockroach allergen–induced autophagy. **(A)** ELISA analysis of TGF-β1 levels in supernatants of cockroach allergen (CRE)–treated HEBCs with or without AhR siRNA knockdown. **(B)** Expression of LC3A, LC3B, Atg5, Beclin-1, and p62 in the recombinant TGF-β1–treated HBECs at different concentrations. **(C)** Expression of LC3A, LC3B, Atg5, Beclin-1, and p62 in cockroach allergen (CRE-treated) HBECs in the presence or absence of TGF-β1 neutralizing antibody (α-TGF-β1). Data represent means ± SEM of at least two independent experiments. *$p < 0.05$, **$p < 0.01$, and ***$p < 0.001$.

1 was almost completely attenuated in α-TGF-β1 pre-treated HBECs (Figure 6C). In contrast, α-TGF-β1 treatment induced increased expression of p62 that was reduced in CRE-treated HBECs. These findings support the hypothesis that TGF-β1 is essential in AhR-mediated cockroach allergen–induced autophagy.

RNA-seq analysis identifies autophagy as one of the major AhR-regulated signaling pathways in AT2 cells

To further examine the underlying mechanisms by which epithelial AhR modulates allergic airway inflammation, we analyzed the transcriptional profiles of AT2 cells isolated from the lungs of $AhR^{f/f}$ and *Sftpc-cre;*$AhR^{f/f}$ mice that were treated with CRE (50 μg/ml) for 24 h. The pattern of the up- and downregulated genes is illustrated by heatmap. First comparisons were made in AT2 cells treated with either PBS or CRE. Results revealed approximately 863 mRNAs that were differentially expressed in AT2 cells from $AhR^{f/f}$ mice, including 357 downregulated (e.g., *Siglec-F*) and 506 upregulated genes [*Ccl20*, *Cxcl2*, *NOXO1*, *Duox2*, and *Slc26a4* (38)] (Figure 7A). Approximately 685 mRNAs were differentially expressed in AT2 cells from *Sftpc-Cre;*$AhR^{f/f}$ mice, including 318 downregulated and 377 upregulated genes (Figure 7B). Next comparisons were made in AT2 cells between $AhR^{f/f}$ and *Sftpc-Cre;*$AhR^{f/f}$ mice. Results showed a total of 845 mRNAs differentially expressed in PBS-treated AT2 cells, including 364 downregulated (e.g., *Cyp1a1* and *Cyp1b1*) and 481 upregulated genes (Figure 7C). Approximately 717 mRNAs were differentially expressed in CRE-treated AT2 cells, including 356 downregulated [e.g., *Ahrr*, *Cyp1b1*, and *Ptgs2* (also called *COX-2*) (47)] and 361 upregulated genes [e.g., *Slc26a4* (38)] (Figure 7D). The DEGs in CRE-treated AT2 cells were further grouped into functional groups using the Gene Ontology (GO) functional enrichment analysis. Of interest, autophagy was identified to be one of the most enriched GO terms (Figure 7E). Several other significant GO terms were also identified, including ubiquitin-protein transferase activity, cell activation, and cilium-related terms (e.g., movement, assembly, organization, and cilium) (Figure 7E). Among all these autophagy-associated genes, *sh3bp4*, *Calcoco2*, *Prkd1*, *Fbxl2*, *Usp10*, and *Trim34b* were significantly upregulated, but *Trim34a*, *Trim12a*, *Trim30d*, *Trim5*, *S100a9*, and *BCL21ll* were downregulated (Figure 7F). These results support our previous findings that autophagy is one of the major AhR-regulated biological processes in AT2 cells.

CALCOCO2 and *S100a9* are the major AhR-regulated autophagy-associated genes in AT2 cells

RT-PCR validation further narrowed down the gene list by focusing on several highly selected genes, including *Calcoco2*, *sh3bp4*, *Prkd1*, *Usp10*, and *S100a9*. AT2 cells were isolated from $AhR^{fl/fl}$ or *Sftpc-Cre;*$AhR^{f/f}$ mice and then confirmed by immunostaining (Figure 8A). AhR deficiency in AT2 cells derived from *Sftpc-Cre;*$AhR^{f/f}$ mice was further confirmed by RT-PCR (Figure 8B). Of these selected genes, *Calcoco2* showed a significant increase in CRE-treated AT2 cells from *Sftpc-cre;*$RhoA^{f/f}$ mice as compared with those from $AhR^{f/f}$ mice (Figure 8C). *Calcoco2* has been shown to initiate selective autophagy through recruiting Unc-51-like kinase (ULK) and TANK-binding kinase 1 (TBK1) kinase complexes (48, 49). Further analysis demonstrated an increased expression of *Calcoco2* in the lung tissues of our asthma mouse model as assessed by immunostaining (Figure 8D). The increased *Calcoco2* was further enhanced in *Sftpc-cre;*$RhoA^{f/f}$ mice as compared with control mice. Notably, the same pattern was observed for *Calcoco2* expression specifically in AT2 cells. In contrast to *Calcoco2*, RT-PCR analysis showed that *S100a9* expression was significantly reduced in AT2 cells from *Sftpc-cre;*$RhoA^{f/f}$ mice compared with those from $AhR^{f/f}$ mice (Figure 8C). S100a9 (S100 calcium binding protein A9) is a pro-inflammatory alarmin associated with inflammation-related diseases. Suppression of S100a9 has been implicated to protect against LPS-induced lung injury (50). Together, these data suggest a possible mechanism that AhR regulates cellular autophagy through modulating *Calcoco2/S100a9* expression.

Discussion

AhR as a receptor for environmental contaminants has been shown to protect against allergic airway information and remodeling in allergic asthma by using global AhR knockout mice (18, 23–25, 51, 52). In the present study, we specially focused on AT2 cells by generating AhR knockout mice in AT2 cells (*Sftpc-Cre;*$AhR^{f/f}$) and provided supporting evidence that AhR in AT2 cells prevents allergen-induced airway hyperresponsiveness and Th2-associated airway inflammation.

AT2 cells are recognized as progenitor cells in response to lung injury and have a unique function in providing pulmonary surfactant and a variety of inflammatory mediators needed for the special microenvironment in the alveolus (53, 54). AT2 cell damage has been implicated in lung fibrosis (55) and inflammation (56). However, the genetic regulation and functional significance of AT2 cells in allergic immune responses to environmental allergens in asthma remain unknown. Here, we generated the *Sftpc-Cre;*$AhR^{f/f}$ mice to determine whether AhR specifically in AT2 cells play an important role in allergic airway inflammation. *Sftpc-Cre;*$AhR^{f/f}$ mice with AhR deletion selectively from AT2 cells were generated by crossing $AhR^{f/f}$ with *Sftpc-cre* mice. We selected *Sftpc-cre* mice for AhR deletion in AT2 cells because Sftpc is highly expressed by AT2 cells and has been widely used as a genetic marker for AT2 cells (57–59). However, we recognize that Sftpc may not be uniquely expressed in AT2 cells (60–62), and future studies are

10.3389/fimmu.2022.964575

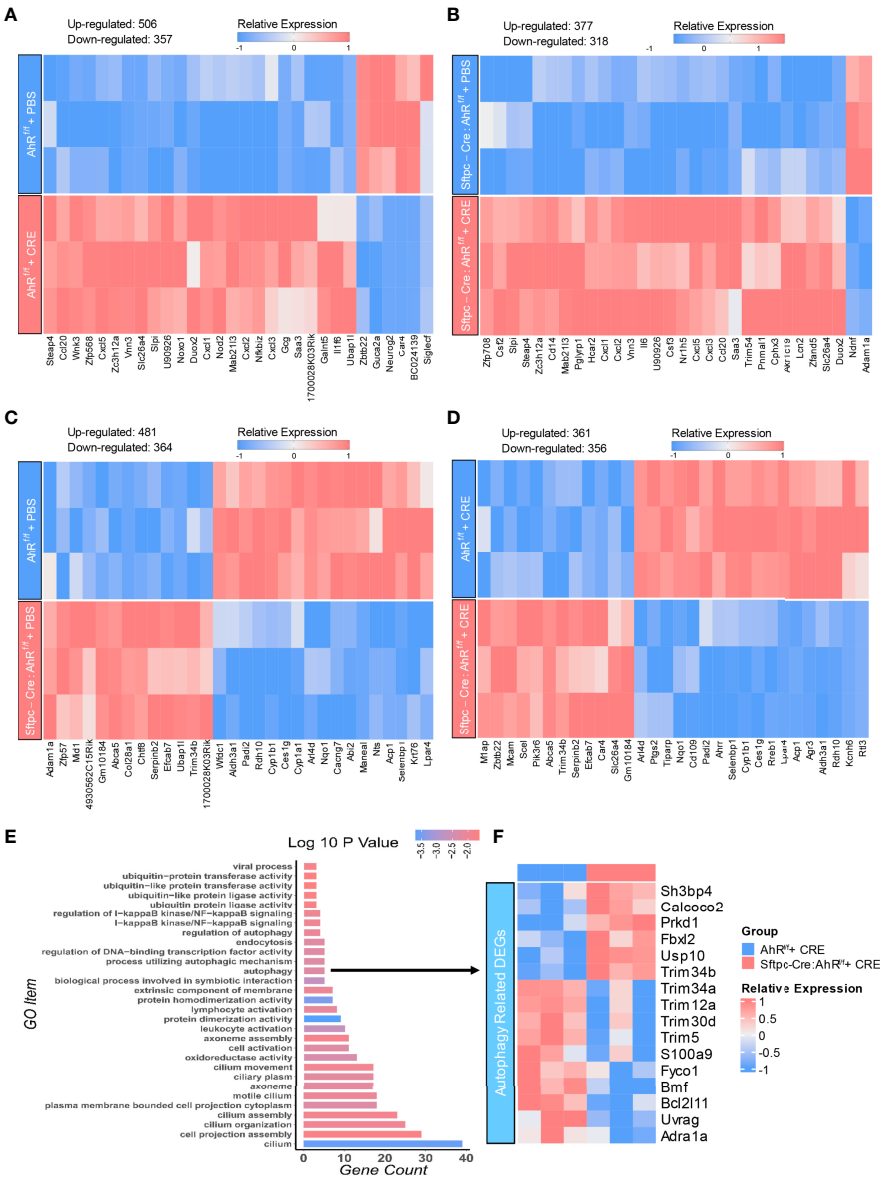

FIGURE 7
AhR-regulated transcriptional profiles in AT2 cells. **(A, B)** Heatmap of differentially expressed mRNAs in AT2 cells of *AhR*$^{f/f}$ **(A)** or *Sftpc-cre;AhR*$^{f/f}$ **(B)** mice treated with PBS verses cockroach allergen (CRE, 50 μg/ml) for 24 h **(C, D)** Heatmap of differentially expressed mRNAs in AT2 cells of *AhR*$^{f/f}$ verses *Sftpc-cre;AhR*$^{f/f}$ mice treated with PBS **(C)** or cockroach allergen CRE, 50 μg/ml) **(D)** for 24 h n = 3 per group **(A–D)**. **(E)** Gene Ontology (GO) functional enrichment analysis of the differentially expressed genes in **(D)**. **(F)** Heatmap of differentially expressed genes (DEG) that are involved in cellular autophagy.

thus needed to identify unique markers to further define the role of AT2 cells in allergic airway inflammation.

Using the newly generated *Sftpc-Cre;AhR*$^{f/f}$ mice, we found that AT2 cell–specific deletion of AhR led to an exacerbation of allergen-induced airway hyperresponsiveness and airway inflammation with elevated eosinophils and Th2 cytokines in BALFs. These results were consistent with our previously report with global AhR knockout mice. Especially, cockroach allergen–treated AhR$^{-/-}$ mice showed exacerbation of airway inflammation when compared with WT mice, which was further supported by using an AhR agonist 2,3,7,8-tetrachlorodibenzo-*p*-dioxin (TCDD) (12). Furthermore, Chang et al. have also reported that AhR$^{-/-}$ mice had exacerbated ovalbumin (OVA)–induced asthma symptoms, including airway inflammation, mucus production, and airway remodeling, and suggested that AhR is required in maintaining normal lung function and mediating disease severity (51). In contrast, Traboulsi et al. found that OVA-induced mouse model

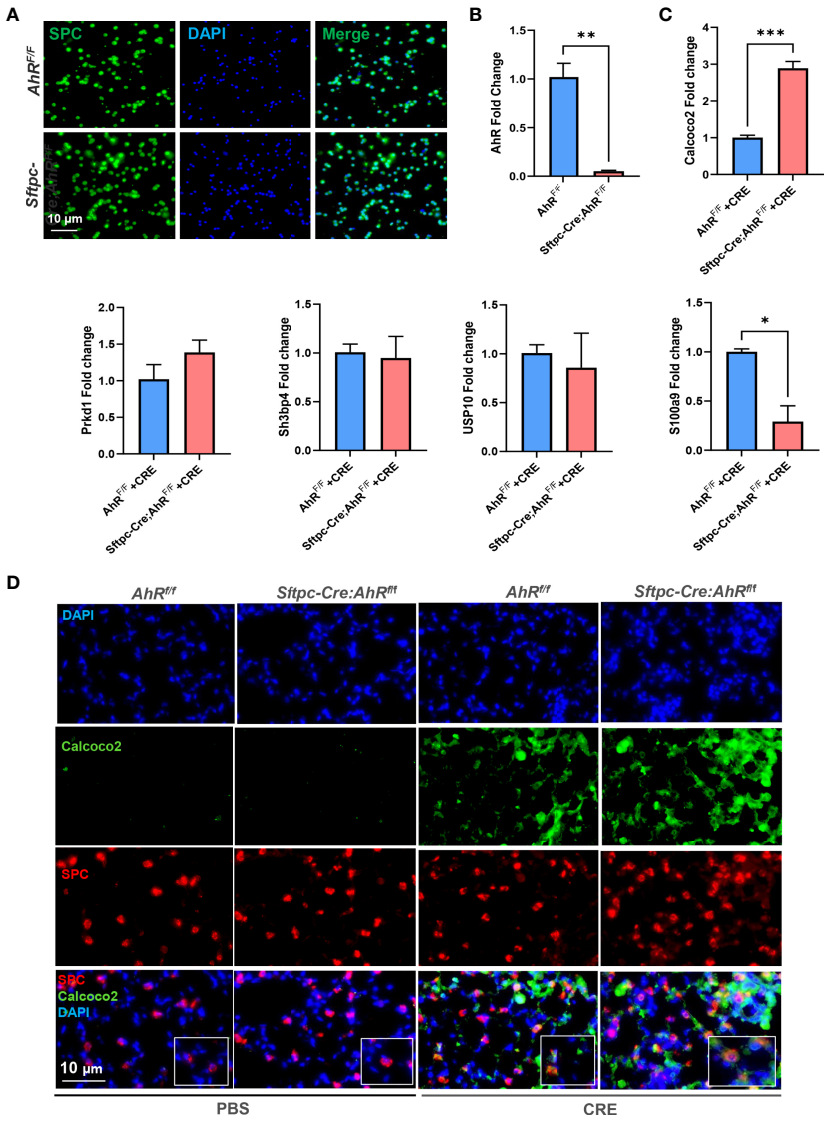

FIGURE 8
Calcoco2 and *S100a9* are the major AhR-regulated autophagy-associated genes in AT2 cells. **(A)** Confirmation of AT2 cells isolated from $AhR^{f/f}$ or *Sftpc-Cre;*$AhR^{f/f}$ mice by immunostaining. **(B)** Confirmation of AhR deficiency in AT2 cells derived from *Sftpc-Cre;*$AhR^{f/f}$ mice by RT-PCR. **(C)** RT-PCR analysis of highly selected differentially expressed autophagy-associated genes of in AT2 cells. **(D)** Representative images of co-immunofluorescence staining of *Calcoco2* with AT2 marker SPC. Data represent means ± SEM of at least two independent experiments. $*p < 0.05$, $**p < 0.01$, and $***p < 0.001$.

with $AhR^{-/-}$ mice showed significantly enhanced eosinophilia and lymphocyte infiltrates into the airways with increased IL-4 and IL-5 in the airways, but no changes were observed for airway hyperresponsiveness (52). These discoveries highlight the complexity of AhR activation and the need for the investigation into how AhR specifically in AT2 cells regulates airway inflammation and airway hyperresponsiveness.

Our studies have suggested several underlying mechanisms as to how AhR regulates airway inflammation. We have provided evidence that AhR protects lungs from allergen-induced inflammation by modulating MSC recruitment and their immune-suppressive activity (12). Further studies suggest that active AhR signaling in MSCs regulates MSC suppressive activity by polarizing macrophages into anti-inflammatory M2 in asthma (63). Our very recent studies uncover a key functional axis of AhR-ROS-NLRP3 inflammasome that plays an important role in the development of allergic airway inflammation (30). In particular, we demonstrated that epithelial AhR plays a role in cockroach allergen–induced ROS generation and NLRP3 inflammasome activation that are

essential in the development of allergic airway inflammation and mucus production. Intriguingly, MCC950, a NLRP3-specifc inhibitor, showed significant inhibition of cockroach allergen–induced airway inflammation and Muc5ac expression. In the current study, we focused on autophagy and demonstrated that AhR regulates allergen-induced cellular autophagy, and, subsequently, allergic airway inflammation. Autophagy is a homeostatic process in which eukaryotic cell encapsulates damaged proteins or organelles for lysosomal degradation and recycling (64). It has also been shown to shape cellular immune responses initiated by environmental pollutants, allergens, and respiratory tract infections (3, 34, 65–71). Abnormality in autophagy has been associated with several major asthma phenotypes, including airway hyperresponsiveness (66), inflammation (72), mucus hyperproduction (73), and remodeling (32). Accumulating evidence suggests that autophagy may be detrimental or beneficial in asthma that depends on the cell types involved (74). We have previously demonstrated that cockroach allergen can induce autophagy in human airway epithelial cells and excessive autophagy may contribute to cockroach allergen–induced airway epithelial ROS generation, cytokine release, and allergic airway inflammation (36). Importantly, autophagy has been shown to regulate NLRP3 inflammasome and secretion of proinflammatory cytokines (75), raising the possibility that autophagy may be a part of the AhR-regulated axis of ROS–inflammasome, which would be of interest to explore in the future.

In this study, we provide a critical but previously unrecognized mechanism that AhR may protect lung from allergic inflammation *via* regulating allergen-induced autophagy in AT2 cells. In particular, we found that *Sftpc-Cre;AhR$^{f/f}$* mice showed an increased cockroach allergen–induced autophagy compared with *AhR$^{f/f}$* mice. The increased autophagy was confirmed in AT2 cells of those mice. Although no human AT2 cells were available, the regulation of AhR in allergen-induced autophagy was further confirmed in HBECs with or without AhR knockdown, suggesting that the AhR regulation on AT2 cell autophagy might also be true for the bronchial airway epithelial cells. Importantly, this finding was further supported by direct monitoring of autophagic flux according to the number of GFP-LC3 puncta under fluorescence microscopy. CRE-treated HBECs showed an increased autophagic flux, which was further enhanced by the treatment with AhR antagonist CH223191. Most importantly, pre-treatment of mice with autophagy inhibitor CLQ abrogated cockroach allergen–induced airway inflammation, Th2-associated cytokines, and autophagy-related gene expression. CLQ is a classic inhibitor of autophagy that blocks the binding of autophagosomes to lysosomes (46). Collectively, these studies highlight a critical role for AhR in AT2 cells in preventing allergen-induced autophagy.

Next, we explored the possible mechanisms underlying the AhR-regulated autophagy. We have previously reported that AhR modulates allergen-induced epithelial TGF-β1 secretion and activation (29, 45). This finding led us to hypothesize that TGF-β1 may be a major player in AhR-mediated autophagy. Indeed, we found increased levels of TGF-β1 in supernatants of cockroach allergen–treated HBECs, which were further enhanced in HBECs with AhR knockdown. Furthermore, we investigated whether the AhR-regulated TGF-β1 can directly induce autophagy. As expected, HBECs showed an increased autophagy after exposed to different doses of recombinant TGF-β1. In contrast, we found that cockroach allergen–induced autophagy was almost completely blocked when TGF-β1 was deleted by using TGF-β1 neutralizing antibody (α-TGF-β1). These studies suggest that TGF-β1 is required in AhR-regulated cockroach allergen–induced autophagy.

In addition to TGF-β1, we expanded our studies to identify novel genes and pathways that are involved in AhR-mediated autophagy and airway inflammation. We analyzed the transcriptional profiles of AT2 cells isolated from the lungs of *AhR$^{f/f}$* and *Sftpc-cre;AhR$^{f/f}$* mice. Although there were different comparisons between groups, the major comparison was between CRE-treated AT2 cells derived from *Sftpc-cre;AhR$^{f/f}$* mice and *AhR$^{f/f}$* mice with a total of 717 differentially expressed mRNAs identified. Of these, both AhR downstream genes Ahrr and Cyp1b1 showed significant reduction in AT2 cells of *Sftpc-cre;AhR$^{f/f}$* mice, supporting the AhR deficiency in AT2 cells and proper experimental approaches we used in this study. In addition, we found our previously identified genes *COX-2* (47) and *Slc26a4* (38) that are associated with allergic airway inflammation. Furthermore, GO functional enrichment analysis based on these DEGs identified autophagy as one of the most enriched GO terms. Among these autophagy-related genes, *Calcoco2*, also named as *NDP52* (nuclear dot protein 52), is an essential selective autophagy adaptor that initiates selective autophagy through recruiting ULK and TBK1 kinase complexes (48). Recruitment of *Calcoco2* has also been suggested to amplify PTEN Induced Kinase 1 (PINK1)/Parkin mitophagy signaling (49). Our study demonstrated that *Calcoco2* was highly expressed in the lung tissues and AT2 cells of our asthma mouse model as determined by immunofluorescence staining. In contrast to *Calcoco2*, *S100a9* is downregulated in AT2 cells of *Sftpc-cre;AhR$^{f/f}$* mice compared with *AhR$^{f/f}$* mice. S100a9 is known as damage-associated molecular pattern, which can be induced in many cells under inflammatory condition (76). Interestingly, studies have highlighted a role for S100a9 in inducing pro-inflammatory cytokine release and in the ROS-dependent activation of the NLRP3 inflammasome (76). However, it remains unclear whether S100a9 is also involved in the allergen-induced and ROS-dependent activation of autophagy. In addition, we have also identified several other significant GO terms, including ubiquitin-protein transferase activity, cell activation, and cilium-related terms (e.g., movement, assembly, organization, and cilium). Those identified biological processes are clearly worth to be

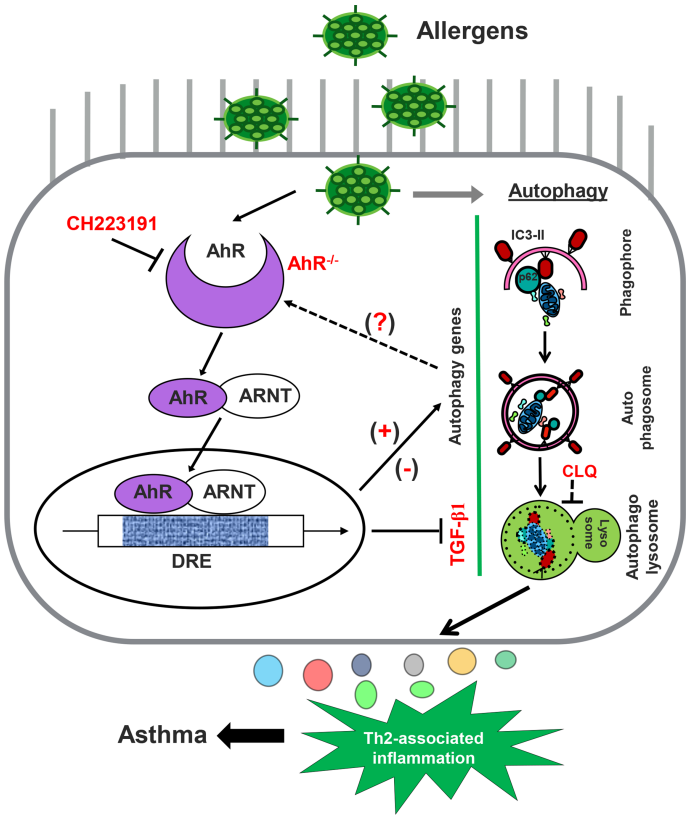

FIGURE 9
Graphic summary. AhR in AT2 cells regulates cockroach allergen–induced autophagy. Cockroach allergen can induce autophagy that is critical in controlling proinflammatory mediator release, Th2-associated airway inflammation, and, subsequently, allergic asthma. AhR in AT2 cells inhibits cockroach allergen–induced autophagy through either controlling TGF-β1 release or AhR-regulated autophagy-associated genes [either upregulated (e.g., *CALCOCO2*) or downregulated (e.g., *S100a9*)].

investigated in the future for their contributions to the AhR-mediated airway inflammation.

Taken together, we used our newly generated *Sftpc-Cre; AhR$^{f/f}$* mice and provided a strong evidence that AhR in AT2 cells protects against cockroach allergen–induced airway hyperresponsiveness and Th2-associated airway inflammation. Further *in vivo* and *in vitro* studies suggest that cockroach allergen can induce autophagy in AT2 cells, and AhR in AT2 cells can prevent cockroach allergen–induced autophagy. Most intriguingly, autophagy inhibition attenuated cockroach allergen–induced airway inflammation and Th2-associated cytokines. Mechanistically, we identified a functional axis of AhR-TGF-β1 that is critical in driving allergen-induced cellular autophagy. Furthermore, our GO functional enrichment analysis on these DEGs from the RNA-seq analysis suggested that autophagy is one of the most enriched GO terms, and the autophagy adaptor *CALCOCO2* and *S100a9* are the major AhR-regulated autophagy genes in cockroach allergen–treated AT2 cells (Figure 9, graphic summary). However, the regulation of AhR on these identified autophagy genes and the exact role of these genes in the pathogenesis of asthma remain unclear, thus warranting further, in-depth investigations. One of the major limitations is the lack of primary human AT2 cells. Instead, we used HBECs, an immortalized cell line under submerged cultures, for *in vitro* studies, which may not truly reflect the real changes seen in AT2 cells. However, our findings in AT2 cells may also apply to the bronchial epithelial cells. Collectively, these findings highlight a critical role for AhR in AT2 cells in preventing allergic airway inflammation through regulating cellular autophagy.

Data availability statement

The datasets presented in this study can be found in online repositories. The name of the repository and accession number can be found below: National Center for Biotechnology Information (NCBI) Gene Expression Omnibus (GEO), https://www.ncbi.nlm.nih.gov/geo/, GSE205818.

Ethics statement

The animal study was reviewed and approved by The Johns Hopkins University Animal Care and Use Committee.

Author contributions

JW, YLZ, XZ, WT, RW, YS, and YZ performed experiments, analyzed data, and review the manuscript. PG designed and supervised the study, and wrote the manuscript. All authors read and approved the final version of the manuscript.

Funding

This work was supported by grants from the US National Institutes of Health (NIH) (1R01AI153331 and R01AI141642 to PG). This study was also supported by grants from the National Natural Science Foundation of China (31900667 to WT) and Shenzhen Scientific Technology Basic Research Project (JCYJ20190812171617278 to WT).

Conflict of interest

The authors declare that the research was conducted in the absence of any commercial or financial relationships that could be construed as a potential conflict of interest.

Publisher's note

All claims expressed in this article are solely those of the authors and do not necessarily represent those of their affiliated organizations, or those of the publisher, the editors and the reviewers. Any product that may be evaluated in this article, or claim that may be made by its manufacturer, is not guaranteed or endorsed by the publisher.

Supplementary material

The Supplementary Material for this article can be found online at: https://www.frontiersin.org/articles/10.3389/fimmu.2022.964575/full#supplementary-material

References

1. Akinbami LJ, Moorman JE, Bailey C, Zahran HS, King M, Johnson CA, et al. Trends in asthma prevalence, health care use, and mortality in the united states, 2001-2010. *NCHS Data Brief* (2012) 94):1–8.

2. Sachdeva K, Do DC, Zhang Y, Hu X, Chen J, Gao P. Environmental exposures and asthma development: Autophagy, mitophagy, and cellular senescence. *Front Immunol* (2019) 10:2787. doi: 10.3389/fimmu.2019.02787

3. Do DC, Zhao Y, Gao P. Cockroach allergen exposure and risk of asthma. *Allergy* (2016) 71(4):463–74. doi: 10.1111/all.12827

4. Glesner J, Filep S, Vailes LD, Wunschmann S, Chapman MD, Birrueta G, et al. Allergen content in German cockroach extracts and sensitization profiles to a new expanded set of cockroach allergens determine *in vitro* extract potency for IgE reactivity. *J Allergy Clin Immunol* (2019) 143(4):1474–81 e8. doi: 10.1016/j.jaci.2018.07.036

5. Pomes A, Glesner J, Calatroni A, Visness CM, Wood RA, O'Connor GT, et al. Cockroach allergen component analysis of children with or without asthma and rhinitis in an inner-city birth cohort. *J Allergy Clin Immunol* (2019) 144(4):935–44. doi: 10.1016/j.jaci.2019.05.036

6. da Silva Antunes R, Sutherland A, Frazier A, Schulten V, Pomes A, Glesner J, et al. Heterogeneity of magnitude, allergen immunodominance, and cytokine polarization of cockroach allergen-specific T cell responses in allergic sensitized children. *Clin Transl Allergy* (2021) 11(8):e12073. doi: 10.1002/clt2.12073

7. Di Meglio P, Duarte JH, Ahlfors H, Owens ND, Li Y, Villanova F, et al. Activation of the aryl hydrocarbon receptor dampens the severity of inflammatory skin conditions. *Immunity* (2014) 40(6):989–1001. doi: 10.1016/j.immuni.2014.04.019

8. Stockinger B, Di Meglio P, Gialitakis M, Duarte JH. The aryl hydrocarbon receptor: multitasking in the immune system. *Annu Rev Immunol* (2014) 32:403–32. doi: 10.1146/annurev-immunol-032713-120245

9. Quintana FJ, Basso AS, Iglesias AH, Korn T, Farez MF, Bettelli E, et al. Control of t(reg) and T(H)17 cell differentiation by the aryl hydrocarbon receptor. *Nature* (2008) 453(7191):65–71. doi: 10.1038/nature06880

10. Nguyen NT, Kimura A, Nakahama T, Chinen I, Masuda K, Nohara K, et al. Aryl hydrocarbon receptor negatively regulates dendritic cell immunogenicity *via* a kynurenine-dependent mechanism. *Proc Natl Acad Sci United States America* (2010) 107(46):19961–6. doi: 10.1073/pnas.1014465107

11. Nguyen NT, Nakahama T, Le DH, Van Son L, Chu HH, Kishimoto T. Aryl hydrocarbon receptor and kynurenine: recent advances in autoimmune disease research. *Front Immunol* (2014) 5:551. doi: 10.3389/fimmu.2014.00551

12. Xu T, Zhou Y, Qiu L, Do DC, Zhao Y, Cui Z, et al. Aryl hydrocarbon receptor protects lungs from cockroach allergen-induced inflammation by modulating mesenchymal stem cells. *J Immunol* (2015) 195(12):5539–50. doi: 10.4049/jimmunol.1501198

13. Nguyen LP, Bradfield CA. The search for endogenous activators of the aryl hydrocarbon receptor. *Chem Res Toxicol* (2008) 21(1):102–16. doi: 10.1021/tx7001965

14. Totlandsdal AI, Cassee FR, Schwarze P, Refsnes M, Lag M. Diesel exhaust particles induce CYP1A1 and pro-inflammatory responses *via* differential pathways in human bronchial epithelial cells. *Particle Fibre Toxicol* (2010) 7:41. doi: 10.1186/1743-8977-7-41

15. Manners S, Alam R, Schwartz DA, Gorska MM. A mouse model links asthma susceptibility to prenatal exposure to diesel exhaust. *J Allergy Clin Immunol* (2014) 134(1):63–72. doi: 10.1016/j.jaci.2013.10.047

16. Stevens EA, Mezrich JD, Bradfield CA. The aryl hydrocarbon receptor: a perspective on potential roles in the immune system. *Immunology* (2009) 127 (3):299–311. doi: 10.1111/j.1365-2567.2009.03054.x

17. Suen JL, Hsu SH, Hung CH, Chao YS, Lee CL, Lin CY, et al. A common environmental pollutant, 4-nonylphenol, promotes allergic lung inflammation in a murine model of asthma. *Allergy* (2013) 68(6):780–7. doi: 10.1111/all.12156

18. Xia M, Viera-Hutchins L, Garcia-Lloret M, Noval Rivas M, Wise P, McGhee SA, et al. Vehicular exhaust particles promote allergic airway inflammation through an aryl hydrocarbon receptor-notch signaling cascade. *J Allergy Clin Immunol* (2015) 136(2):441–53. doi: 10.1016/j.jaci.2015.02.014

19. Huang SK, Zhang Q, Qiu Z, Chung KF. Mechanistic impact of outdoor air pollution on asthma and allergic diseases. *J Thorac Dis* (2015) 7(1):23–33. doi: 10.3978/j.issn.2072-1439.2014.12.13

20. Li X-m, Peng J, Gu W, Guo X-j. TCDD-induced activation of aryl hydrocarbon receptor inhibits Th17 polarization and regulates non-eosinophilic airway inflammation in asthma. *PloS One* (2016) 11(3). 1-12doi: 10.1371/journal.pone.0150551

21. Morales-Rubio R, Amador-Munoz O, Rosas-Perez I, Sanchez-Perez Y, Garcia-Cuellar C, Segura-Medina P, et al. PM2.5 induces airway hyperresponsiveness and inflammation *via* the AhR pathway in a sensitized

Guinea pig asthma-like model. *Toxicology* (2022) 465:153026. doi: 10.1016/j.tox.2021.153026

22. Yang Y, Chan WK. Selective autophagy maintains the aryl hydrocarbon receptor levels in HeLa cells: A mechanism that is dependent on the p23 Co-chaperone. *Int J Mol Sci* (2020) 21(10):3449. doi: 10.3390/ijms21103449

23. Wong TH, Lee CL, Su HH, Lee CL, Wu CC, Wang CC, et al. A prominent air pollutant, Indeno[1,2,3-cd]pyrene, enhances allergic lung inflammation *via* aryl hydrocarbon receptor. *Sci Rep* (2018) 8(1):5198. doi: 10.1038/s41598-018-23542-9

24. Xia M, Harb H, Saffari A, Sioutas C, Chatila TA. A jagged 1-notch 4 molecular switch mediates airway inflammation induced by ultrafine particles. *J Allergy Clin Immunol* (2018) 142(4):1243–56 e17. doi: 10.1016/j.jaci.2018.03.009

25. Vogel CFA, Van Winkle LS, Esser C, Haarmann-Stemmann T. The aryl hydrocarbon receptor as a target of environmental stressors - implications for pollution mediated stress and inflammatory responses. *Redox Biol* (2020) 34:101530. doi: 10.1016/j.redox.2020.101530

26. Zhou Y, Tung HY, Tsai YM, Hsu SC, Chang HW, Kawasaki H, et al. Aryl hydrocarbon receptor controls murine mast cell homeostasis. *Blood* (2013) 121(16):3195–204. doi: 10.1182/blood-2012-08-453597

27. Wang H, Do DC, Liu J, Wang B, Qu J, Ke X, et al. Functional role of kynurenine and aryl hydrocarbon receptor axis in chronic rhinosinusitis with nasal polyps. *J Allergy Clin Immunol* (2018) 141(2):586–600 e6. doi: 10.1016/j.jaci.2017.06.013

28. Wang E, Liu X, Tu W, Do DC, Yu H, Yang L, et al. Benzo(a)pyrene facilitates dermatophagoides group 1 (Der f 1)-induced epithelial cytokine release through aryl hydrocarbon receptor in asthma. *Allergy* (2019) 74(9):1675–90. doi: 10.1111/all.13784

29. Wang E, Tu W, Do DC, Xiao X, Bhatti SB, Yang L, et al. Benzo(a)pyrene enhanced dermatophagoides group 1 (Der f 1)-induced TGFbeta1 signaling activation through the aryl hydrocarbon receptor-RhoA axis in asthma. *Front Immunol* (2021) 12:643260. doi: 10.3389/fimmu.2021.643260

30. Hu X, Shen Y, Zhao Y, Wang J, Zhang X, Tu W, et al. Epithelial aryl hydrocarbon receptor protects from mucus production by inhibiting ROS-triggered NLRP3 inflammasome in asthma. *Front Immunol* (2021) 12:767508:. doi: 10.3389/fimmu.2021.767508

31. Ban GY, Pham DL, Trinh TH, Lee SI, Suh DH, Yang EM, et al. Autophagy mechanisms in sputum and peripheral blood cells of patients with severe asthma: a new therapeutic target. *Clin Exp Allergy* (2016) 46(1):48–59. doi: 10.1111/cea.12585

32. McAlinden KD, Deshpande DA, Ghavami S, Xenaki D, Sohal SS, Oliver BG, et al. Autophagy activation in asthma airways remodeling. *Am J Respir Cell Mol Biol* (2019) 60(5):541–53. doi: 10.1165/rcmb.2018-0169OC

33. Xia F, Deng C, Jiang Y, Qu Y, Deng J, Cai Z, et al. IL4 (interleukin 4) induces autophagy in b cells leading to exacerbated asthma. *Autophagy* (2018) 14(3):450–64. doi: 10.1080/15548627.2017.1421884

34. Poon AH, Chouiali F, Tse SM, Litonjua AA, Hussain SN, Baglole CJ, et al. Genetic and histologic evidence for autophagy in asthma pathogenesis. *J Allergy Clin Immunol* (2012) 129(2):569–71. doi: 10.1016/j.jaci.2011.09.035

35. Martin LJ, Gupta J, Jyothula SS, Butsch Kovacic M, Biagini Myers JM, Patterson TL, et al. Functional variant in the autophagy-related 5 gene promotor is associated with childhood asthma. *PloS One* (2012) 7(4):e33454. doi: 10.1371/journal.pone.0033454

36. Zhang Y, Do DC, Hu X, Wang J, Zhao Y, Mishra S, et al. CaMKII oxidation regulates cockroach allergen-induced mitophagy in asthma. *J Allergy Clin Immunol* (2021) 147(4):1464–77 e11. doi: 10.1016/j.jaci.2020.08.033

37. Do DC, Mu J, Ke X, Sachdeva K, Qin Z, Wan M, et al. miR-511-3p protects against cockroach allergen-induced lung inflammation by antagonizing CCL2. *JCI Insight* (2019) 4(20):e126832. doi: 10.1172/jci.insight.126832

38. Do DC, Zhang Y, Tu W, Hu X, Xiao X, Chen J, et al. Type II alveolar epithelial cell-specific loss of RhoA exacerbates allergic airway inflammation through SLC26A4. *JCI Insight* (2021) 6(14):e148147. doi: 10.1172/jci.insight.148147

39. Patro R, Duggal G, Love MI, Irizarry RA, Kingsford C. Salmon provides fast and bias-aware quantification of transcript expression. *Nat Methods* (2017) 14(4):417–9. doi: 10.1038/nmeth.4197

40. Ritchie ME, Phipson B, Wu D, Hu Y, Law CW, Shi W, et al. Limma powers differential expression analyses for RNA-sequencing and microarray studies. *Nucleic Acids Res* (2015) 43(7):e47. doi: 10.1093/nar/gkv007

41. Wu T, Hu E, Xu S, Chen M, Guo P, Dai Z, et al. clusterProfiler 4.0: A universal enrichment tool for interpreting omics data. *Innovation (N Y)* (2021) 2(3):100141. 10.1016/j.xinn.2021.100141

42. Gu Z, Eils R, Schlesner M. Complex heatmaps reveal patterns and correlations in multidimensional genomic data. *Bioinformatics* (2016) 32(18):2847–9. doi: 10.1093/bioinformatics/btw313

43. Livak KJ, Schmittgen TD. Analysis of relative gene expression data using real-time quantitative PCR and the 2(-delta delta C(T)) method. *Methods* (2001) 25(4):402–8. doi: 10.1006/meth.2001.1262

44. Wang Y, Bai C, Li K, Adler KB, Wang X. Role of airway epithelial cells in development of asthma and allergic rhinitis. *Respir Med* (2008) 102(7):949–55. doi: 10.1016/j.rmed.2008.01.017

45. Zhou Y, Mirza S, Xu T, Tripathi P, Plunkett B, Myers A, et al. Aryl hydrocarbon receptor (AhR) modulates cockroach allergen-induced immune responses through active TGFbeta1 release. *Mediators Inflammation* (2014) 2014:591479. doi: 10.1155/2014/591479

46. Mauthe M, Orhon I, Rocchi C, Zhou X, Luhr M, Hijlkema KJ, et al. Chloroquine inhibits autophagic flux by decreasing autophagosome-lysosome fusion. *Autophagy* (2018) 14(8):1435–55. doi: 10.1080/15548627.2018.1474314

47. Qiu L, Zhang Y, Do DC, Ke X, Zhang S, Lambert K, et al. miR-155 modulates cockroach allergen- and oxidative stress-induced cyclooxygenase-2 in asthma. *J Immunol* (2018) 201(3):916–29. doi: 10.4049/jimmunol.1701167

48. Boyle KB, Ravenhill BJ, Randow F. CALCOCO2/NDP52 initiates selective autophagy through recruitment of ULK and TBK1 kinase complexes. *Autophagy* (2019) 15(9):1655–6. doi: 10.1080/15548627.2019.1628548

49. Padman BS, Nguyen TN, Uoselis L, Skulsuppaisarn M, Nguyen LK, Lazarou M. LC3/GABARAPs drive ubiquitin-independent recruitment of optineurin and NDP52 to amplify mitophagy. *Nat Commun* (2019) 10(1):408. doi: 10.1038/s41467-019-08335-6

50. Zhao B, Lu R, Chen J, Xie M, Zhao X, Kong L. S100A9 blockade prevents lipopolysaccharide-induced lung injury *via* suppressing the NLRP3 pathway. *Respir Res* (2021) 22(1):45. doi: 10.1186/s12931-021-01641-y

51. Chang YD, Li CH, Tsai CH, Cheng YW, Kang JJ, Lee CC. Aryl hydrocarbon receptor deficiency enhanced airway inflammation and remodeling in a murine chronic asthma model. *FASEB J* (2020) 34(11):15300–13. doi: 10.1096/fj.202001529R

52. Traboulsi H, de Souza AR, Allard B, Haidar Z, Sorin M, Moarbes V, et al. Differential regulation of the asthmatic phenotype by the aryl hydrocarbon receptor. *Front Physiol* (2021) 12:720196. doi: 10.3389/fphys.2021.720196

53. Sucre JMS, Jetter CS, Loomans H, Williams J, Plosa EJ, Benjamin JT, et al. Successful establishment of primary type II alveolar epithelium with 3D organotypic coculture. *Am J Respir Cell Mol Biol* (2018) 59(2):158–66. doi: 10.1165/rcmb.2017-0442MA

54. Olajuyin AM, Zhang X, Ji HL. Alveolar type 2 progenitor cells for lung injury repair. *Cell Death Discovery* (2019) 5:63. doi: 10.1038/s41420-019-0147-9

55. Parimon T, Yao C, Stripp BR, Noble PW, Chen P. Alveolar epithelial type II cells as drivers of lung fibrosis in idiopathic pulmonary fibrosis. *Int J Mol Sci* (2020) 21(7):2269. doi: 10.3390/ijms21072269

56. Post S, Heijink IH, Hesse L, Koo HK, Shaheen F, Fouadi M, et al. Characterization of a lung epithelium specific e-cadherin knock-out model: Implications for obstructive lung pathology. *Sci Rep* (2018) 8(1):13275. doi: 10.1038/s41598-018-31500-8

57. Finn J, Sottoriva K, Pajcini KV, Kitajewski JK, Chen C, Zhang W, et al. Dlk1-mediated temporal regulation of notch signaling is required for differentiation of alveolar type II to type I cells during repair. *Cell Rep* (2019) 26(11):2942–54 e5. doi: 10.1016/j.celrep.2019.02.046

58. Wu H, Yu Y, Huang H, Hu Y, Fu S, Wang Z, et al. Progressive pulmonary fibrosis is caused by elevated mechanical tension on alveolar stem cells. *Cell* (2020) 180(1):107–21 e17. doi: 10.1016/j.cell.2019.11.027

59. Choi J, Park JE, Tsagkogeorga G, Yanagita M, Koo BK, Han N, et al. Inflammatory signals induce AT2 cell-derived damage-associated transient progenitors that mediate alveolar regeneration. *Cell Stem Cell* (2020) 27(3):366–82 e7. doi: 10.1016/j.stem.2020.06.020

60. Eblaghie MC, Reedy M, Oliver T, Mishina Y, Hogan BL. Evidence that autocrine signaling through Bmpr1a regulates the proliferation, survival and morphogenetic behavior of distal lung epithelial cells. *Dev Biol* (2006) 291(1):67–82. doi: 10.1016/j.ydbio.2005.12.006

61. Thomas SY, Whitehead GS, Takaku M, Ward JM, Xu X, Nakano K, et al. MyD88-dependent dendritic and epithelial cell crosstalk orchestrates immune responses to allergens. *Mucosal Immunol* (2018) 11(3):796–810. doi: 10.1038/mi.2017.84

62. Jiang M, Roth MG, Chun-On P, Sullivan DI, Alder JK. Phenotypic diversity caused by differential expression of SFTPC-Cre-Transgenic alleles. *Am J Respir Cell Mol Biol* (2020) 62(6):692–8. doi: 10.1165/rcmb.2019-0416MA

63. Cui Z, Feng Y, Li D, Li T, Gao P, Xu T. Activation of aryl hydrocarbon receptor (AhR) in mesenchymal stem cells modulates macrophage polarization in asthma. *J Immunotoxicol* (2020) 17(1):21–30. doi: 10.1080/1547691X.2019.1706671

64. Deretic V, Klionsky DJ. Autophagy and inflammation: A special review issue. *Autophagy* (2018) 14(2):179–80. doi: 10.1080/15548627.2017.1412229

65. Miraglia del Giudice M, Allegorico A, Parisi G, Galdo F, Alterio E, Coronella A, et al. Risk factors for asthma. *Ital J Pediatrics* (2014) 40(Suppl 1):A77–A. doi: 10.1186/1824-7288-40-S1-A77

66. Liu JN, Suh DH, Trinh HK, Chwae YJ, Park HS, Shin YS. The role of autophagy in allergic inflammation: a new target for severe asthma. *Exp Mol Med* (2016) 48(7):e243. doi: 10.1038/emm.2016.38

67. Rowlands DJ. Mitochondria dysfunction: A novel therapeutic target in pathological lung remodeling or bystander? *Pharmacol Ther* (2016) 166:96–105. doi: 10.1016/j.pharmthera.2016.06.019

68. Prakash YS, Pabelick CM, Sieck GC. Mitochondrial dysfunction in airway disease. *Chest* (2017) 152(3):618–26. doi: 10.1016/j.chest.2017.03.020

69. Wu J, Dong F, Wang RA, Wang J, Zhao J, Yang M, et al. Central role of cellular senescence in TSLP-induced airway remodeling in asthma. *PloS One* (2013) 8(10):e77795. doi: 10.1371/journal.pone.0077795

70. Puddicombe SM, Torres-Lozano C, Richter A, Bucchieri F, Lordan JL, Howarth PH, et al. Increased expression of p21(waf) cyclin-dependent kinase inhibitor in asthmatic bronchial epithelium. *Am J Respir Cell Mol Biol* (2003) 28 (1):61–8. doi: 10.1165/rcmb.4715

71. Barnes PJ, Baker J, Donnelly LE. Autophagy in asthma and chronic obstructive pulmonary disease. *Clin Sci (Lond)* (2022) 136(10):733–46. doi: 10.1042/CS20210900

72. Lee J, Kim HS. The role of autophagy in eosinophilic airway inflammation. *Immune Netw* (2019) 19(1):e5. doi: 10.4110/in.2019.19.e5

73. Chen ZH, Wu YF, Wang PL, Wu YP, Li ZY, Zhao Y, et al. Autophagy is essential for ultrafine particle-induced inflammation and mucus hyperproduction in airway epithelium. *Autophagy* (2016) 12(2):297–311:7314. doi: 10.1080/15548627.2015.1124224

74. Theofani E, Xanthou G. Autophagy: A friend or foe in allergic asthma? *Int J Mol Sci* (2021) 22(12). doi: 10.3390/ijms22126314

75. Maneechotesuwan K, Kasetsinsombat K, Wongkajornsilp A, Barnes PJ. Role of autophagy in regulating interleukin-10 and the responses to corticosteroids and statins in asthma. *Clin Exp Allergy: J Br Soc Allergy Clin Immunol* (2021) 51 (12):1553–65. doi: 10.1111/cea.13825

76. Mondet J, Chevalier S, Mossuz P. Pathogenic roles of S100A8 and S100A9 proteins in acute myeloid and lymphoid leukemia: Clinical and therapeutic impacts. *Molecules* (2021) 26(5):1323. doi: 10.3390/molecules26051323

frontiers | Frontiers in Immunology

TYPE Original Research
PUBLISHED 22 July 2022
DOI 10.3389/fimmu.2022.911300

OPEN ACCESS

EDITED BY
Bao-Hui Cheng,
Institute of ENT and Shenzhen Key Laboratory of ENT, China

REVIEWED BY
Ulrich Matthias Zissler,
Technical University of Munich, Germany
Jia-Jie Chen,
Shenzhen University, China

*CORRESPONDENCE
Jin-Lyu Sun
sunjinlv@pumch.cn
Ji-Fu Wei
weijifu@njmu.edu.cn
Dian-Dou Xu
xudd@ihep.ac.cn

†These authors have contributed equally to this work

SPECIALTY SECTION
This article was submitted to Immunological Tolerance and Regulation, a section of the journal Frontiers in Immunology

RECEIVED 02 April 2022
ACCEPTED 27 June 2022
PUBLISHED 22 July 2022

CITATION
Yang Y-S, Cao M-D, Wang A, Liu Q-M, Zhu D-X, Zou Y, Ma L-L, Luo M, Shao Y, Xu D-D, Wei J-F and Sun J-L (2022) Nano-silica particles synergistically ige-mediated mast cell activation exacerbating allergic inflammation in mice.
Front. Immunol. 13:911300.
doi: 10.3389/fimmu.2022.911300

Nano-silica particles synergistically IgE-mediated mast cell activation exacerbating allergic inflammation in mice

Yong-Shi Yang[1†], Meng-Da Cao[2†], An Wang[3†], Qing-Mei Liu[1], Dan-Xuan Zhu[4], Ying Zou[5,6], Ling-Ling Ma[3], Min Luo[3], Yang Shao[3], Dian-Dou Xu[3*], Ji-Fu Wei[2,7*] and Jin-Lyu Sun[1*]

[1]Department of Allergy, State Key Laboratory of Complex Severe and Rare Diseases, Peking Union Medical College Hospital, Chinese Academy of Medical Science and Peking Union Medical College, Beijing, China, [2]Research Division of Clinical Pharmacology, the First Affiliated Hospital of Nanjing Medical University, Nanjing, China, [3]Beijing Engineering Research Center of Radiographic Techniques and Equipment, Institute of High Energy Physics, Chinese Academy of Sciences, Beijing, China, [4]Women and Children Central Laboratory, The First Affiliated Hospital of Nanjing Medical University, Nanjing, China, [5]Shanghai Institute of Applied Physics, Chinese Academy of Sciences, Shanghai, China, [6]Shanghai Advanced Research Institute, Chinese Academy of Sciences, Shanghai, China, [7]Department of Pharmacy, Jiangsu Cancer Hospital, Jiangsu Institute of Cancer Research, The Affiliated Cancer Hospital of Nanjing Medical University, Nanjing, China

Background: Allergic respiratory diseases have increased dramatically due to air pollution over the past few decades. However, studies are limited on the effects of inorganic components and particulate matter with different particle sizes in smog on allergic diseases, and the possible molecular mechanism of inducing allergies has not been thoroughly studied.

Methods: Four common mineral elements with different particle sizes in smog particles were selected, including Al_2O_3, TiO_2, Fe_2O_3, and SiO_2. We studied the relationship and molecular mechanism of smog particle composition, particle size, and allergic reactions using mast cells, immunoglobulin E (IgE)-mediated passive cutaneous anaphylaxis (PCA) model, and an ovalbumin (OVA)-induced asthmatic mouse model *in vitro* and *in vivo*, combined with transmission electron microscopy, scanning transmission X-ray microscopy analysis, and transcriptome sequencing.

Results: Only 20 nm SiO_2 particles significantly increased β-hexosaminidase release, based on dinitrophenol (DNP)-human serum albumin (HSA) stimulation, from IgE-sensitized mast cells, while other particles did not. Meanwhile, the PCA model showed that Evan's blue extravasation in mice was increased after treatment with nano-SiO_2 particles. Nano-SiO_2 particles exposure in the asthmatic mouse model caused an enhancement of allergic airway inflammation as manifested by OVA-specific serum IgE, airway hyperresponsiveness, lung inflammation injury, mucous cell metaplasia, cytokine expression, mast cell activation, and histamine secretion, which

were significantly increased. Nano-SiO_2 particles exposure did not affect the expression of FcεRI or the ability of mast cells to bind IgE but synergistically activated mast cells by enhancing the mitogen-activated protein kinase (MAPK) signaling pathway, especially the phosphorylation levels of the extracellular signal-regulated kinase (ERK)1/2. The ERK inhibitors showed a significant inhibitory effect in reducing β-hexosaminidase release.

Conclusion: Our results indicated that nano-SiO_2 particles stimulation might synergistically activate IgE-sensitized mast cells by enhancing the MAPK signaling pathway and that nano-SiO_2 particles exposure could exacerbate allergic inflammation. Our experimental results provide useful information for preventing and treating allergic diseases.

KEYWORDS

allergic asthma, smog particles, mast cell, MAPK, silica nanoparticles

Introduction

Due to environmental changes, air pollutants, and aeroallergens, the morbidity, and prevalence of allergic respiratory diseases have increased dramatically over the past few decades (1, 2). In addition to lifestyle changes, many epidemiological and experimental studies explicitly highlight the role of air pollution in the development of allergic disease and increase the frequency of emergency department visits and hospitalizations for asthma (3–5). Importantly, pollutants can act as adjuvants to potentiate the development of pollen allergies, and early-life exposure may increase the risk of aeroallergen sensitization (6, 7).

Undoubtedly, air pollution has become a severe threat to global health. According to the World Health Organization (WHO) (https://www.who.int/), ambient air pollution accounts for an estimated 4.2 million deaths per year, and over 90% of people live in places where air quality levels do not reach WHO guideline levels. Air pollution has been of great concern over the last decade in China due to the increasing hazardous dense smog affecting most parts of the country (8). Among the various air pollutants, which are composed of gases (O_3, NO_2, CO, and SO_2) and particulate matter (PM), PM causes the most significant harmful effects during a smog episode (9). Fine particulate matter (PM2.5), one of the main components of smog particles, refers to particulate matter with an aerodynamic diameter ≤ 2.5 μm, which is an extraordinarily complex mixture of diverse chemical, physical and biological components with a wide range of morphological, chemical, physical, and thermodynamic characteristics (10). The composition of smog particles includes not only a large number of biologically active substances, such as pollen, fungal spores, and microorganisms, but also nonbiologically active substances, such as heavy metals, transition metals, organic acids, and polycyclic aromatic hydrocarbons, which are the carriers and catalysts of many pollutants (11, 12). However, which components of smog particles play a significant role in developing allergic diseases have not yet been fully studied.

Mast cells are one of the critical effector cells in allergic diseases and are predominantly localized at sites in the skin, mucous membranes, airways, and intestine where they contact the environment; therefore, mast cells are considered to be the sentinel cells for environmental insults (13). Mast cells can recognize immunological, inflammatory, and environmental factors by various types of receptors, including high-affinity immunoglobulin E (IgE) receptors (FcεRI), G protein-coupled receptors, or ion channels, and release bioactive mediators through IgE pathways or non-IgE pathway activation (14). Previous studies on the effects of smog particles on allergic diseases have primarily focused on complex mixtures. For example, Piao et al. reported that PM2.5 exposure could exacerbate oxidative stress and enhance PM2.5 phagocytosis by activating the NF-κB signaling pathway in an ovalbumin (OVA)-induced allergic rhinitis mouse model (15). Another study found that environmentally relevant metal and transition metal ions, such as Al^{3+}, Cd^{2+}, Sr^{2+}, and Ni^{2+}, could increase the level of allergen-mediated mast cell activation, which indicated that nonbiologically active substances in smog particles also played an essential role in allergic diseases (12).

However, studies on the effects of inorganic components and particulate matter with different particle sizes in smog particles on allergic diseases are limited, and the possible molecular mechanism of inducing allergies is not completely clear. In our previous study, we chose nine typical water-soluble inorganic salts and three water-soluble organic acids

in PM2.5 from Beijing to investigate the cytotoxicity and activation effect on mast cells. The results showed that only malonic acid had a very slight activation effect on mast cells *via* the IgE pathway (16). The source and composition of smog particles are very complex. Elemental analysis shows that mineral elements and metal elements, such as Na, Fe, Al, Si, Ti, K, Mg, Ca, and Mn, are the main constituent elements (17, 18). In the present study, limited by the source of the material, we only selected four common mineral elements with different particle sizes in smog particles, including aluminum oxide (Al_2O_3, 20 nm and 26.93 μm), titanium oxide (TiO_2, 20 nm and 1 μm), iron oxide (Fe_2O_3, 50 nm and 1 μm) and silicon dioxide (SiO_2, 20 nm and 2.34 μm). We studied the relationship and molecular mechanism of smog particle composition, particle size, and allergic effect using mast cells, IgE-mediated passive cutaneous anaphylaxis (PCA) model, and an OVA-induced asthmatic mouse model *in vitro* and *in vivo*. Finally, we found that nano-SiO_2 particles stimulation might synergistically activate IgE-sensitized mast cells by enhancing the mitogen-activated protein kinase (MAPK) signaling pathway and that nano-SiO_2 particles exposure could exacerbate allergic inflammation.

Materials and methods

Reagents and antibodies

Aluminum oxide (Al_2O_3, 20 nm and 26.93 μm), titanium oxide (TiO_2, 20 nm and 1 μm), iron oxide (Fe_2O_3, 50 nm and 1 μm) and silicon dioxide (SiO_2, 20 nm and 2.34 μm) were purchased from Shanghai YunFu Nanotechnology Co., Ltd. (Shanghai, China), Fuchen Chemical Reagent Co., Ltd. (Tianjin, China), and Aladdin (Shanghai, China). Monoclonal anti-dinitrophenol (DNP)-IgE antibody, DNP-human serum albumin (HSA), and 4-nitrophenyl N-acetyl-β-D-glucosaminide were obtained from Sigma–Aldrich (St. Louis, USA). Antibodies as against phosphor-JNK, JNK, phosphor-LYN, LYN, phosphor-Plcγ1, Plcγ1, phosphor-P38, P38, phosphor-ERK1/2, ERK1/2, NF-κB, and β-actin were obtained from Cell Signaling Technology Inc. (Danvers, MA). ERK inhibitor U0126-EtOH and p38 inhibitor SB203580 were purchased from MedChem Express (Monmouth Junction, NJ, USA), PE-anti-mouse CD117 (c-kit), APC-anti-mouse FcεRIα, and FITC-anti-mouse IgE antibodies were purchased from Biolegend (San Diego, CA, USA). Recombinant interleukin (IL)-3 and stem cell factor (SCF) were purchased from PeproTech (Cranbury, NJ, USA). Evans blue and formamide were obtained from Dalian Meilun Biotechnology Co. Ltd. (Dalian, China). The ovalbumin (OVA; grade V) was purchased from Sigma Company (St. Louis, USA), and aluminum hydroxide was purchased from Thermo Fisher Scientific (Massachusetts, USA).

BMMC culture

Mouse bone marrow-derived mast cells (BMMCs) were isolated from BALB/c mouse femurs and cultured in complete RPMI-1640 with 100 U/mL penicillin, 100 U/mL streptomycin, 2 mM L-glutamine, 0.1 mM nonessential amino acids, 10% foetal bovine serum, 10 ng/mL IL-3, and 10 ng/mL SCF. After 4-6 weeks in culture, mast cell purity was evaluated by flow cytometry detection of cell-surface CD117 and FcεRI expression.

Cell viability assay

The BMMCs were seeded in 96-well plates at a density of 1×10^5 cells/well and then were subsequently treated with Al_2O_3 (20 nm and 26.93 μm), TiO_2 (20 nm and 1 μm), Fe_2O_3 (50 nm and 1 μm), and SiO_2 (20 nm and 2.34 μm) at concentrations of 0, 50, 100, and 200 μg/mL for 1 hour. Cell viability was measured with the Cell Counting Kit 8 (CCK8) (Dojindo Laboratories, Tokyo, Japan) according to the manufacturer's protocol.

Measurement of mast cell degranulation in the IgE and non-IgE Pathways

For the IgE pathway, the BMMCs were sensitized with 500 ng/mL mouse anti-DNP IgE for 12 hours and then washed with Tyrode's buffer before being dispensed into 96-well plates. For treated samples, the particles were applied for 1 hour. The molecule inhibitors (ERK inhibitor U0126-EtOH 5 μM/L, and p38 inhibitor SB203580 10 μM/L), were also applied for 1 hour. Subsequently, after stimulation with 100 ng/mL DNP-HSA for 30 min, the supernatant and cell lysate were reacted for 1.5 hours with 1 mM 4-nitrophenyl-N-acetyl-β-D-glucosaminide at 37 °C. The reaction was stopped with 0.2 M glycine solution. The optical density (OD) at 405 nm was measured with Multiskan GO (Thermo Fisher Scientific, Massachusetts, USA). For the non-IgE pathway, the BMMCs were not sensitized with mouse anti-DNP IgE and directly treated with the particles for 1 hour after seeding in 96-well plates. Compound 48/80 (Sigma–Aldrich, St. Louis, USA) served as the positive control. The β-hexosaminidase (β-hex) release was evaluated using the following formula: β-hex release (%) = absorbance of supernatant/(absorbance of supernatant + absorbance of cell lysates) × 100%.

Experimental procedure for animal experiments

Female BALB/c mice, 6-8 weeks old, were purchased from Charles River Laboratories (Beijing, China) and used after 1 week of

quarantine and acclimatization. All mice were maintained at conventional animal facilities under standard conditions. All animal use procedures were conducted in accordance with the National Institutes of Health and approved by Nanjing Medical University's Institutional Animal Care and Use Committee (IACUC-2007037).

For the IgE-mediated PCA model, 20 female BALB/c mice were randomly divided into four groups: blank group, SiO_2 group, DNP-HSA group, and DNP-HSA+SiO_2 group. Briefly, BALB/c mice were injected intradermally with 500 ng of anti-DNP IgE into the left ear. After a 24-hour infiltration period, 200 μl of 5 mg/ml Evan's blue solution containing 100 μg DNP-HSA and/or 10 mg/kg nano-SiO_2 particles (about 200 μg/per mouse) was administered into the tail vein. One hour after the challenge, skin areas were photographed, and the thickness of the ears was measured with a dial thickness gauge after which the mice were euthanized. The dye was extracted from dissected ears in 700 μl of formamide for 12 hours at 62°C and quantitated by a spectrophotometer at 620 nm.

For the allergic asthma mouse model, 24 female BALB/c mice were randomly divided into four groups: blank group, OVA group, SiO_2 group, and OVA+SiO_2 group. The mice were sensitized on Days 0, 7, and 14 by an intraperitoneal injection of 50 μg of OVA (Sigma–Aldrich, Grade V) emulsified with 4 mg of aluminum hydroxide (Thermo Scientific) in 200 μL of phosphate-buffered saline (PBS). On Days 15 to 21, mice in the SiO_2 and OVA+SiO_2 groups were exposed to SiO_2 solution (500 μg/mL, 50 μl per mouse) *via* intranasal instillation. On Days 19-21, mice in the OVA and OVA+SiO_2 groups were challenged with a 1% (W/V) OVA solution *via* intranasal instillation.

Measurement of airway hyperresponsiveness

Twenty-four hours after the last intranasal OVA challenge, airway hyperresponsiveness (AHR) in response to inhaled aerosolized methacholine was measured using the FlexiVent system (SCIREQ, Montreal, Canada) following the manufacturer's protocol. The mice were subjected to tracheostomy and endotracheal intubation after anaesthetization with 50 mg/kg pentobarbital sodium (Sigma–Aldrich, St. Louis, USA) by intraperitoneal injection, and then the mice were connected to a ventilator. Aerosolized normal saline (0.9% NaCl) or a dose of methacholine (Sigma–Aldrich, St. Louis, USA) (6.25, 12.5, 25, and 50 mg/mL) was administered to the mice *via* a nebulizer. AHR was assessed by measuring the changes in lung resistance.

Measurements of IgE, cytokines, histamine, and tryptase in BALF and serum

After measurement of AHR, bronchoalveolar lavage fluid (BALF) was collected by instilling and retrieving 0.5 mL of cold PBS into the lung tissues three times. Then, BALF was centrifuged at 1500 rpm for 10 min at 4°C, and supernatants were stored at −80°C until further use. The cell pellets were resuspended in 50 μL of sterile PBS to calculate the total cell counts using the TC20^{TM} Automated Cell Counter (Bio–Rad Laboratories, Inc.). The levels of IL-4 and IL-6 in BALF supernatant were detected using a commercial ELISA kit (Multisciences (Lianke) Biotech Co., Ltd, Hangzhou, China) according to the manufacturers' instructions. Blood was collected at the end of the experiment, and serum was acquired after allowing the blood to stand at room temperature for at least 2 hours. The levels of OVA-specific IgE (Cusabio Technology LLC, Wuhan, China), histamine (Elabscience Biotechnology Co., Ltd., Wuhan, China), and tryptase (Cusabio Technology LLC, Wuhan, China) in BALF and serum were measured using a commercial ELISA kit according to the manufacturers' instructions.

Lung histology and immunohistochemistry

For histological analysis, the left lung tissues were fixed in 10% neutral-buffered formalin (Biomics Biotech, Nantong, China). Paraffin-embedded lung tissues (5 mm thick) were subjected to hematoxylin and eosin (H&E) and periodic acid-Schiff (PAS) staining to evaluate tissue inflammation and goblet cell metaplasia. Histological scores were determined by randomly selecting 6-8 different fields under a microscope and evaluated by a pathologist. The numbers of peribronchial and perivascular infiltrating inflammatory cells were scored as follows: 0, no cells; 1, a few cells; 2, a ring of inflammatory cells, one cell layer of peribronchial cells; 3, a ring of inflammatory cells, two to four cell layers of peribronchial cells; and 4, a ring of inflammatory cells, more than four cell layers of peribronchial cells. The mucus hypersecretion score by PAS staining was determined as follows: the percentage of the mucus-positive area of the whole bronchus was 0, ≤5%; 1, 5%-25%; 2, 25%-50%; 3, 50%-75%; and 4, >75%.

Immunohistochemistry of mast cell tryptase in lung tissue was performed using an anti-mast cell tryptase antibody (Affinity Biosciences, cat.DF6758). Heat-mediated antigen retrieval was performed after deparaffinization. The tissue sections were blocked with goat serum. Then, the tissue sections were incubated with 1 μg/mL rabbit anti-mast cell tryptase antibody overnight at 4°C. The sections were incubated with horseradish peroxidase (HRP)-conjugated secondary antibody at 37°C for 40 min. The tissue sections were developed using Streptavidin-Biotin-Complex (SABC) with diaminobenzidine (DAB) as the chromogen.

Transmission electron microscopic analysis

For TEM analysis, mast cells were fixed with a fixative solution containing 2% paraformaldehyde and 2%

glutaraldehyde in 0.1 M phosphate buffer (pH 7.4). Cells were then postfixed in 1% OsO4 at 4°C for 2 hours. After rinsing the fixative solution from the cells, the samples were dehydrated with a graded series of ethanol and embedded in epoxy resin. Thin sections were cut with a diamond knife and mounted on copper grids. The grids were stained for 30 min each in Reynolds's lead citrate and aqueous uranyl acetate. Ultrathin sections (thickness 70 nm) were observed under an electron microscope (HT7700, HITACHI, Japan) at 80 kV.

Scanning transmission X-ray microscopy, STXM

The mast cells were detached from the culture medium and washed with phosphate-buffered saline (PBS) three times. Then, they were fixed with 10% neutral formalin for 10 min and dehydrated by a graded dehydration series of ethanol solution, including 70% (40 min), 80% (15 min), 90% (10 min), and 100% (10 min) ethanol solutions, at room temperature (19). Finally, the cell suspension was dropped onto a special microporous gold mesh (UltrAuFoil, Ted Pella Inc.). The mesh size was 2 μm, and the thickness of the gold mesh was only 50 nm, so soft X-rays could still be effectively transmitted. The key question of the possible intake of silicon dioxide nanoparticles by mast cells was studied by scanning transmission microscopy (STXM) at beamline station BL08U1a at Shanghai Synchrotron Radiation Facility (SSRF) (20). The microscope used a soft X-ray in the energy ranging from150-2000 eV to image a sample. The dual-energy imaging method was used in the experiment (21), whereby the value of dual-energy was set as 1840 eV for pre-edge and 1848 eV for on-the-edge. The energy value was calibrated against the reference spectrum recorded from a standard sample (nano-SiO_2).

Flow cytometry detection

Mature BMMCs were collected in 6-well plates. Nano-SiO_2 was incubated with non-IgE-sensitized BMMCs for 12 hours and then added APC anti-mouse FcεRIα antibody (Biolegend, CA, USA) to detect the effect of nano-SiO_2 exposure on the expression of FcεRI in unsensitized mast cells. Similarly, BMMCs were first incubated with anti-DNP IgE to sensitize, washed to remove unbound anti-DNP IgE, then treated with nano-SiO_2 and anti-DNP IgE, and finally added APC anti-mouse FcεRIα antibody (Biolegend, CA, USA) and FITC anti-mouse IgE antibody (Biolegend, CA, USA) to detect the effect of nano-SiO_2 exposure on FcεRI expression and IgE binding in IgE-sensitized mast cells.

Transcriptome sequencing

Mature BMMCs were collected after treatment with nano-SiO_2 particles for transcriptome sequencing analysis. The experiment was divided into four groups: blank control, DNP-HSA, SiO_2, and DNP-HSA+SiO_2. We performed 2×150 bp paired-end sequencing (PE150) on an Illumina Novaseq™ 6000 (LC-BioTechnology CO., Ltd., Hangzhou, China) following the vendor's recommended protocol. Bioinformatics analysis was performed using the OmicStudio tools at https://www.omicstudio.cn/tool.

Western blotting

Western blotting was used to investigate the effects of nano-SiO_2 particles on the activation of the FcεRI signaling regulatory proteins LYN and Plcγ1 and the MAPK signaling proteins P38, JNK, ERK1/2, and NF-κB. BMMCs were sensitized with 500 ng/mL DNP-IgE overnight, washed twice with Tyrode's buffer, and placed in Tyrode's buffer. After incubating with or without nano-SiO_2 particlesat 37°C for 1 hour, BMMCs were stimulated with 100 ng/mL DNP-HSA for 5 to 30 min. Cells were lysed in RIPA buffer (Beyotime, Beijing, China) with protease inhibitor cocktail (Med Chem Express, Monmouth Junction, NJ) and phosphatase inhibitor cocktail (Beyotime, Beijing, China). Cell lysates were centrifuged at 12,000 rpm for 15 min. Supernatants were mixed with a loading sample buffer (Thermo Fisher Scientific) and denatured by heating for 10 min at 100°C. Proteins were separated by sodium dodecyl sulfate-polyacrylamide gel electrophoresis and transferred to polyvinylidene difluoride membranes (Merck Millipore, Billerica MA). After incubation with a primary antibody in Tris-buffered saline with 0.1% Tween 20 buffer that containing 5% bovine serum albumin, the membranes were incubated with horseradish peroxidase-conjugated secondary antibodies for 1 hour at room temperature with shaking. Chemiluminescence reagents (Biosharp, Hefei, China) were applied according to the manufacturer's protocol. Western blot images were captured using a Tanon 5200 Multi chemiluminescent imaging system (Tanon Science & Technology Co., Ltd, Shanghai, China).

Statistical analysis

Descriptive parameters, such as the means and standard deviations (SD) and the frequencies and percentages for

categorical data, were calculated. For normally distributed data, the independent Student's t test or one-way analysis of variance (ANOVA) was used to compare different groups. $P<0.05$ was considered statistically significant. Analyses were performed using GraphPad Prism version 8.0 software (GraphPad Software, Inc., San Diego, CA, USA).

Results

Cytotoxicity of particle exposure on mast cells

First, we determined whether the different-sized particles posed toxic effects on mast cells. BMMCs were incubated with different doses of particles of different sizes (0 to 200 μg/mL). As shown in **Figure 1A**, the results suggested that exposure to high doses (200 μg/mL) of the particles could induce pronounced toxicity to mast cells. In contrast, some particles at low doses (50 and 100 μg/mL) showed minimal toxic effects on BMMCs. Among the particles, both 50 nm and 1 μm Fe_2O_3 showed strong cytotoxicity with increasing concentration.

Particle exposure to non-IgE- and IgE-mediated mast cell degranulation

Mast cell degranulation was assayed by measuring the release of β-hexosaminidase by mast cells into the culture supernatants. For non-IgE pathway-mediated mast cell activation, compared with the blank control, SiO_2 (20 nm and 2.34 μm), Al_2O_3 (26.93 μm), and Fe_2O_3 (50 nm and 1 μm) showed stimulatory effects on mast cell activation with statistical significance at 100 μg/mL. However, the activation effects were very slight to a certain degree, while Fe_2O_3 probably had a cytotoxic effect on mast cells (**Figure 1B**). The activation effects were even milder at low concentrations (25 and 50 μg/mL). Conversely, for IgE-mediated mast cell degranulation, the BMMCs were sensitized with anti-DNP IgE before the addition of the particles at different doses. Compared with the blank control, only the 20 nm SiO_2 particles at 100 μg/mL

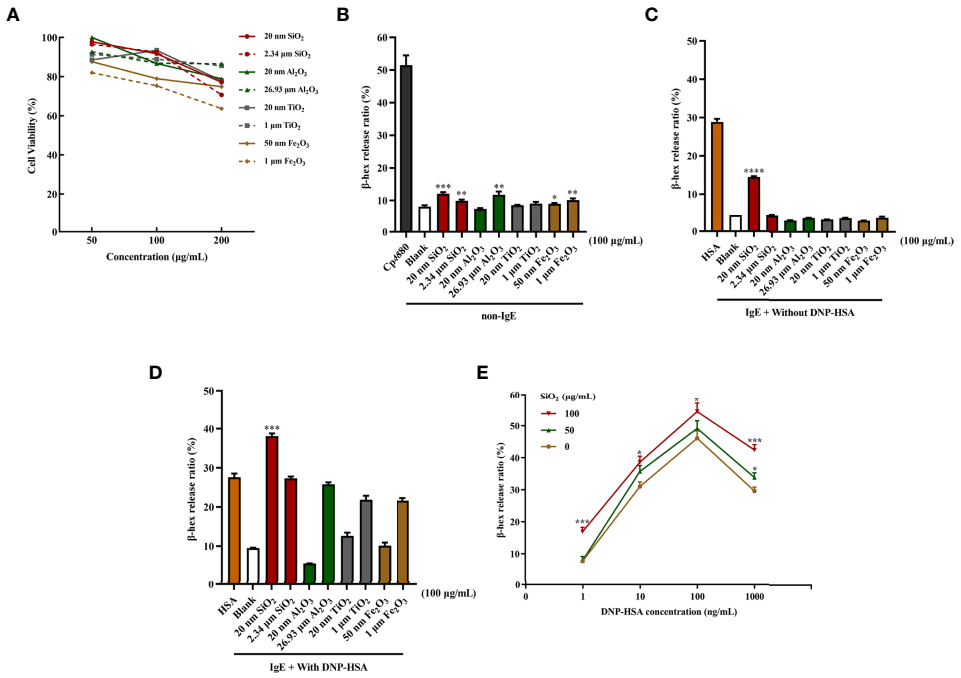

FIGURE 1
Particle exposure induced cytotoxicity and degranulation of mast cells. **(A)** Cytotoxicity of particle exposure on mast cells. **(B)** Non-IgE pathway-mediated mast cell activation. BMMCs were not sensitized with anti-DNP IgE and directly treated with particles of different sizes. Compound 48/80 was used as the positive control. The comparator was the blank control. **(C)** BMMCs were sensitized with anti-DNP IgE before treatment with different particle sizes but without DNP-HSA stimulation. DNP-HSA stimulation was used as the positive control. The comparator was the blank control. **(D)** IgE-mediated mast cell degranulation. BMMCs were sensitized with anti-DNP IgE before treatment with particles of different sizes and stimulated with DNP-HSA. The comparator was the DNP-HSA stimulation group. **(E)** Effects of different doses of 20 nm SiO_2 exposure on FcεRI-mediated mast cell degranulation. All data are presented as the mean ± SD. The unpaired t test or ordinary one-way ANOVA was used to compare different groups. *$P < 0.05$, **$P < 0.01$, ***$P < 0.001$, ****$P < 0.0001$.

significantly activated mast cells after IgE sensitization, improving the activation rate by approximately 10%, while other particles stimulation alone did not (**Figure 1C**). Interestingly, when IgE-sensitized mast cells were first incubated with the particles and then activated by the addition of DNP-HSA, compared with the DNP-HSA stimulation positive control, only the 20 nm SiO_2 particles at 100 μg/mL significantly increased the release of β-hexosaminidase, improving the activation rate by over 10%, while other particles' stimulation alone did not (**Figure 1D**). However, at low concentrations (25 and 50 μg/mL), none of the particles with or without DNP-HSA stimulation significantly activated mast cells. In addition, a dose-response relationship was observed for 20 nm SiO_2 particles exposure with increasing DNP-HSA stimulating concentrations. Mast cells showed the most significant activation effect at a 20 nm SiO_2 particles concentration of 100 μg/mL and DNP-HSA concentration of 100 ng/mL (**Figure 1E**).

Nano-SiO_2 particles Promote IgE-mediated PCA mouse model

We used an IgE-mediated PCA model to examine the effects of nano-SiO_2 particles on IgE-mediated allergic reactions *in vivo*, which was quantified by the amount of Evan's blue dye in the IgE-sensitized mouse area. As shown in **Figure 2**, compared with the blank group, Evan's blue extravasation (**Figures 2A, B**) and ear thickness (**Figure 2C**) in mice were significantly increased after treatment with nano-SiO_2 particles and DNP-HSA, demonstrating vascular hyperpermeability. Compared with the DNP-HSA group, the nano-SiO_2 particles treatment significantly enhanced Evan's blue extravasation.

Nano-SiO_2 particles exposure exacerbates OVA-induced allergic asthma

We used an OVA-induced allergic asthma mouse model to further verify whether nano-SiO_2 particles could activate mast cells *in vivo* and the effects of nano-SiO_2 particles on the development of OVA-induced allergic asthma airway inflammation in mice. Several parameters related to airway inflammation and bronchial hyperresponsiveness were determined to evaluate the impact of nano-SiO_2 particles exposure on the morphological abnormality and dysfunction of the airway.

Airway hyperresponsiveness (AHR) was measured after the last intranasal OVA challenge. Compared with the PBS-treated blank group, airway resistance (Rrs) values were significantly elevated to various degrees in the SiO_2 exposure, OVA, and OVA+SiO_2 groups (**Figure 3B**). In particular, the Rrs values were significantly increased in the OVA+SiO_2 compared with the OVA group ($P<0.01$). These data suggested that exposure to nano-SiO_2 particles could affect airway function and increase airway resistance.

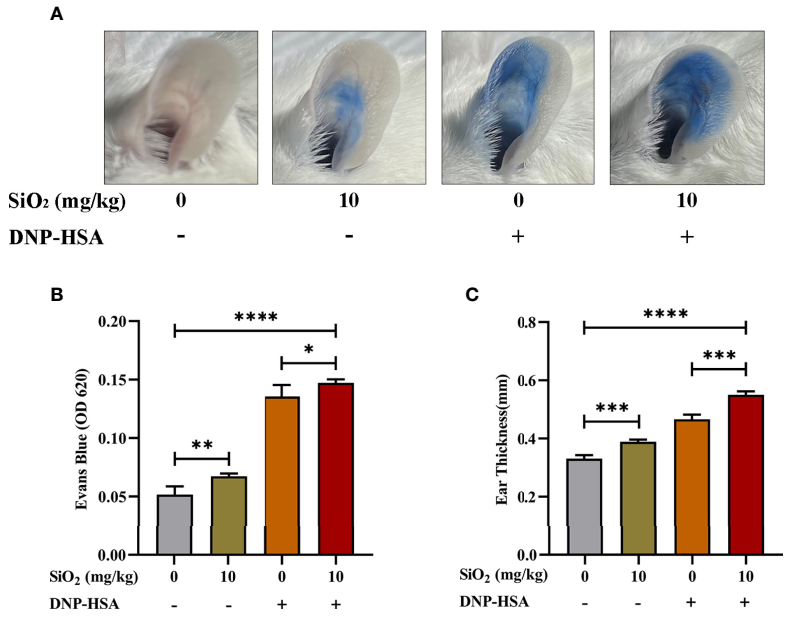

FIGURE 2
Nano-SiO_2 particles promote IgE-mediated PCA in mice. **(A)** Representative images of PCA mouse ears. **(B)** Nano-SiO_2 particles increase PCA-induced Evan's blue extravasation (OD620nm) and **(C)** promote PCA-induced ear thickening. The data are presented as the mean ± SD. The unpaired t test or ordinary one-way ANOVA was used to compare different groups. *$P < 0.05$, **$P < 0.01$, ***$P < 0.001$, ****$P < 0.0001$.

IgE, cytokines, and histamine are important inflammatory transmitters and activators in allergic respiratory diseases. The levels of OVA-specific IgE (sIgE), histamine, and tryptase in BALF and serum were measured. As shown in **Figure 3**, compared with the OVA alone group, the levels of OVA-sIgE in serum were significantly increased when exposed to OVA +SiO_2, although a similar trend was not observed in BALF (**Figures 3C, D**). Moreover, the total BALF inflammatory cells in allergic asthma mice exposed to nano-SiO_2 particles were significantly higher than those in the blank and OVA groups (**Figure 3E**). The levels of IL-4 and IL-6 in the BALF supernatant were detected. Nano-SiO_2 particles exposure significantly increased IL-4 and IL-6 in BALF between the OVA group and OVA+SiO_2 group (**Figures 3F, G**). In addition, compared with that in the blank control group, IL-4 secretion, but not IL-6 secretion, was elevated in the SiO_2 exposure group. Histamine levels in both serum and BALF were increased to varying degrees after exposure to nano-SiO_2 particles compared with the blank control. Moreover, histamine was also significantly higher in the OVA+SiO_2 group than in the OVA alone group (**Figures 4A, B**). However, exposure to nano-SiO_2 particles did not significantly increase the level of tryptase secretion, nor did it show a difference between the OVA alone group and the OVA+SiO_2 group (**Figures 4C, D**).

Representative images of lung histology and immunohistochemistry are shown in **Figure 5**. The blank control group exhibited a normal lung tissue structure and clear pulmonary alveoli. The SiO_2 exposure group showed slight congestion of the alveolar walls, slight thickening of the bronchiolar walls, and a small amount of inflammatory cell infiltration around the bronchioles. Histological analysis showed peribronchial and perivascular inflammation in all OVA-treated groups. OVA+SiO_2 exposure induced more serious alveoli and bronchial injuries than OVA exposure alone. The inflammatory injury was characterized by hemorrhage, edema, a thickened alveolar wall, and pronounced inflammatory infiltrates within the interstitial and alveolar spaces. The alveolar cavity and bronchioles were structurally collapsed, and epithelial

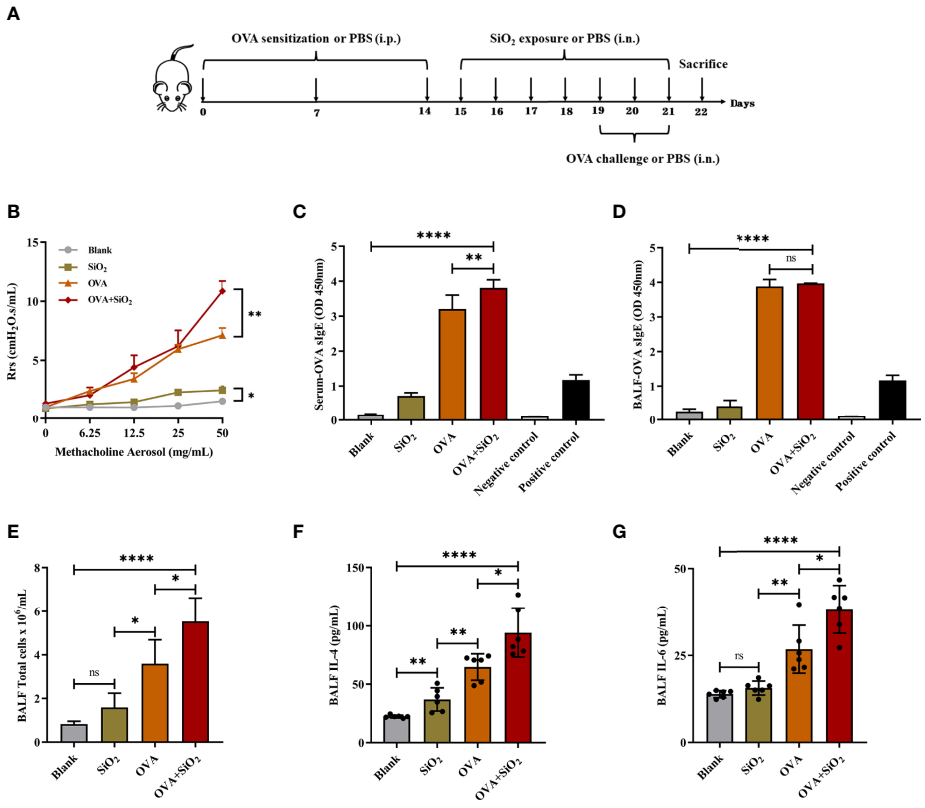

FIGURE 3
Effect of 20 nm SiO_2 exposure on the allergic asthma mouse model. **(A)** The schedule for the OVA-induced asthma model and the procedure of intranasal instillation of 20 nm SiO_2 or PBS in the OVA-induced asthma model. **(B)** Measurement of airway hyperresponsiveness in the OVA-induced asthma model. The values of respiratory system resistance (Rrs) were measured 24 h after the last OVA challenge by exposure to increasing doses of methacholine. Data are presented as the mean ± SEM. **(C, D)** Levels of OVA-specific IgE in BALF and serum. **(E)** Total cell counts in BALF of the OVA-induced asthma model. Data are presented as the mean ± SD. **(F, G)** Levels of IL-4 and IL-6 in BALF supernatant of the OVA-induced asthma model. Data are presented as the mean ± SD. The unpaired t test or ordinary one-way ANOVA was used to compare different groups. *$P < 0.05$, **$P < 0.01$, ****$P < 0.0001$. ns, no significance.

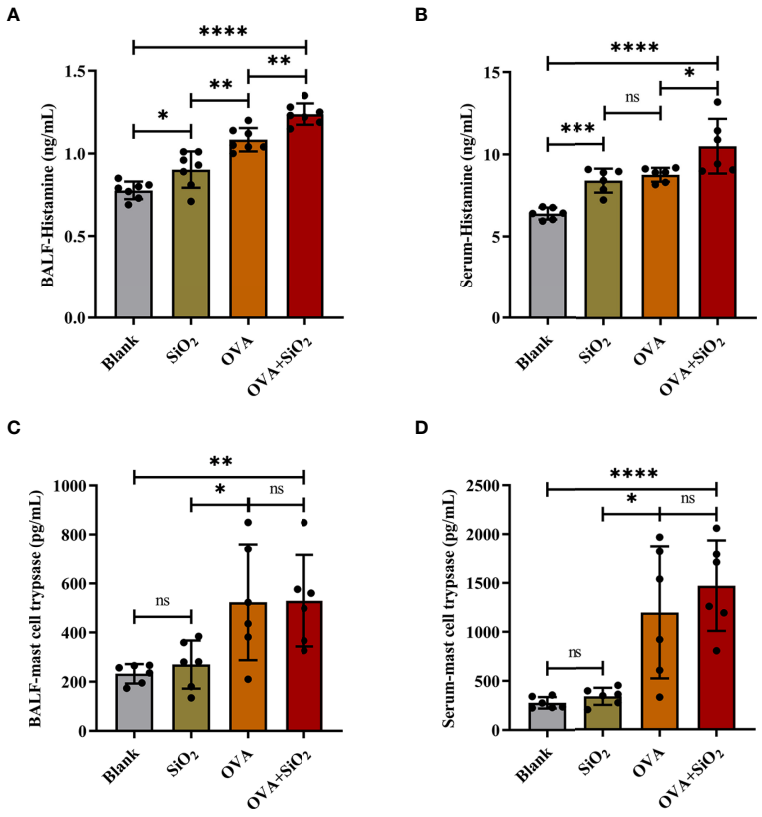

FIGURE 4
The levels of histamine and mast cell tryptase in BALF and serum of the OVA-induced asthma model. Data are presented as the mean ± SD. The unpaired t test or ordinary one-way ANOVA was used to compare different groups. *$P < 0.05$, **$P < 0.01$, ***$P < 0.001$, ****$P < 0.0001$. ns, no significance.

cells were destroyed, with more goblet cell hyperplasia. After exposure to nano-SiO_2, airway inflammation and mucus hypersecretion scores were significantly elevated in the OVA+SiO_2 group (**Figures 5A, B**). Moreover, the immunohistochemistry analysis of mast cell tryptase in lung tissue showed that the anti-mast cell tryptase antibody-positive cells had more aggregation in the OVA+SiO_2 group than in the OVA alone group (**Figure 5C**). Taken together, our data indicated that nano-SiO_2 particles exposure exacerbated allergic airway inflammation, triggered goblet cell proliferation, recruited mast cells, increased histamine secretion, and enhanced airway responsiveness.

STXM and TEM analyses show that nano-SiO_2 can enter the mast cells

The results of dual-energy imaging of the two samples are shown in **Figure 6A**. Sample 16 was a dehydrated cell with silica particles (**Figure 6Aa, b, c**), and sample 27 was an empty cell for comparison (**Figure 6Ad, e, f**). Fig. (c) and (f) show the derived results of dual-energy imaging with diffuse distributions of yellow dots. Because the energy of the silicon K-edge was close to the upper limit of the energy range of the beamline, the light flux dropped to a low level. The counting rate of the signals was low, which led to a poor signal-to-noise ratio in the processed images, so it was impossible to obtain a clear and distinguishable element distribution map. Nevertheless, a statistical analysis of the frequency of occurrence of likelihood (FOL), "yellow dots" in the dual-energy map, could provide helpful hints as to whether SiO_2 particles were included in the sample. A statistical box with a size of 1 μm × 1 μm, shown as white-dashed boxes in the figure, was used in the analysis. They were chosen to be positioned over mesh holes where X-rays have better penetration and therefore more effective signals for silicon content. From the direct-scanned images of Figure (d) and (e), it could be seen that there was no cell coverage on the golden mesh in the Y1 and Y2 areas, so the FOL should be mainly from the background noise. The gold mesh in area J1 was covered with cells, but its FOL was the same as that for the bare area within the error bar of the statistical range (**Table 1**). This result suggested that sample 27 was an empty cell. The same method was used to analyze sample 16 (Figure c). The direct-scanned images are in **Figure 6Aa, b**) revealed no obvious cell sample

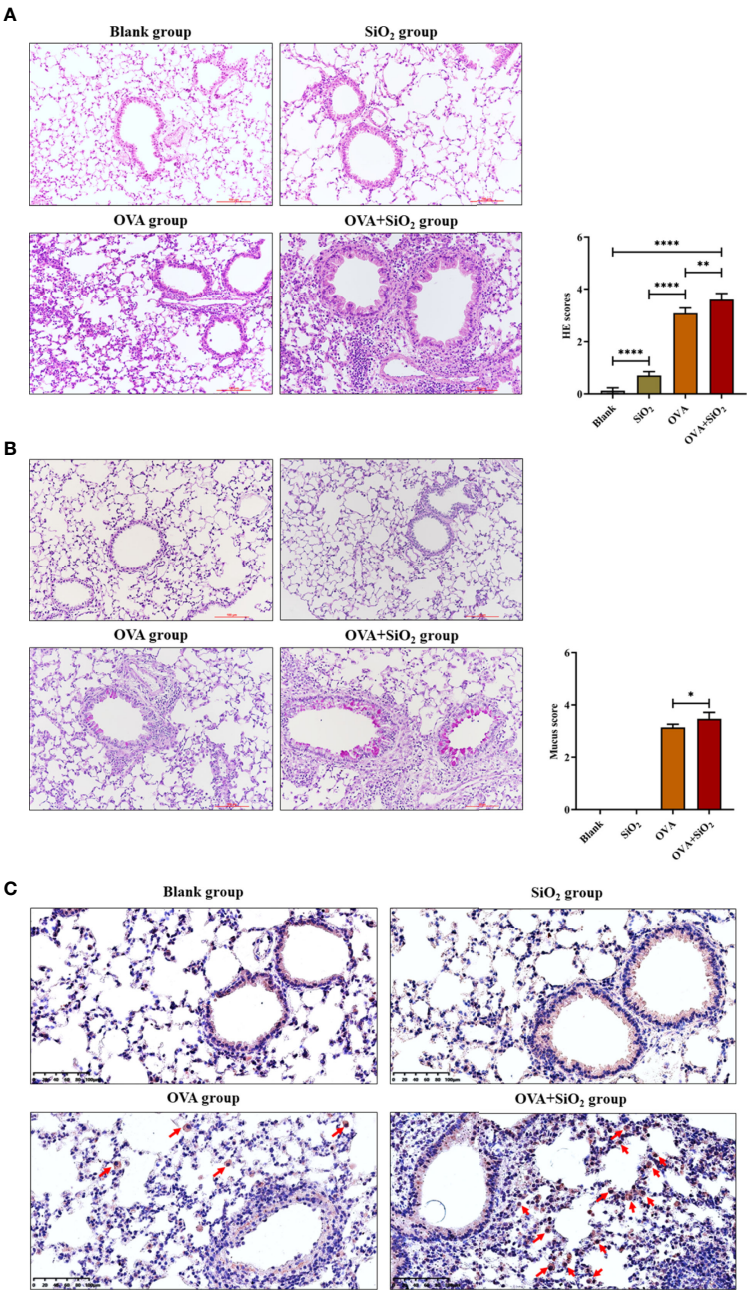

FIGURE 5
Representative images of lung histology and immunohistochemistry. **(A)** Lung tissue stained with hematoxylin and eosin (H&E) (× 200). **(B)** Lung tissue stained with periodic acid-Schiff stain (PAS) (× 200). **(C)** Immunohistochemistry analysis of mast cell tryptase in lung tissue. The arrow indicates anti-mast cell tryptase antibody-positive cells. Data are represented as the means ± SD. The unpaired t test was used to compare different groups. *$P < 0.05$, **$P < 0.01$, ****$P < 0.0001$.

coverage on the golden mesh in areas X1 and X2, and the FOLs for both were relatively close (Table 1), which could be considered background noise. The gold mesh of the I1 region was covered with cells, and a high FOL was recorded, which was almost doubled, strongly suggesting that the cells were loaded with SiO_2 particles. Furthermore, we noted that the background noise for sample16 was greater than that for sample 27, which was related to the instrument and did not necessitate cross-checking. To summarize the dual-energy imaging results, clear elemental distribution mapping was not possible due to the low signal-to-noise ratio. Nevertheless, a statistical analysis of loaded cell samples demonstrated a high FOL number in the area

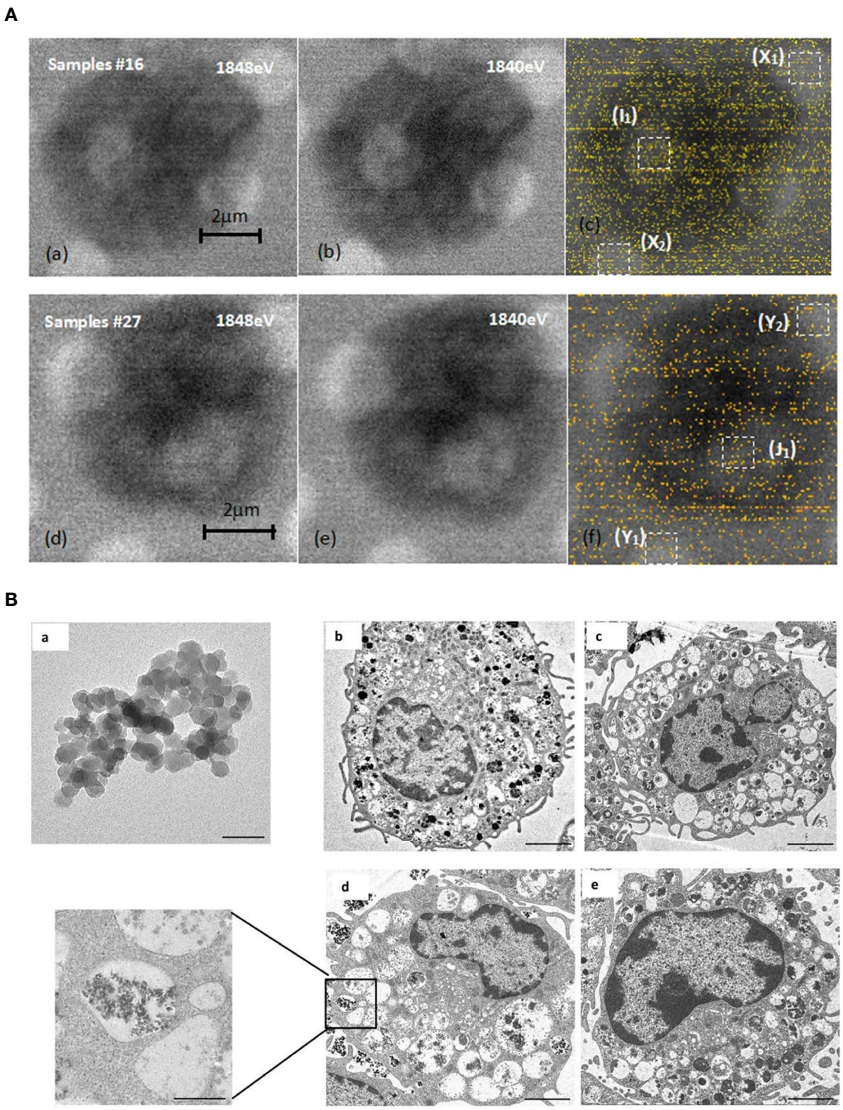

FIGURE 6
STXM and TEM analysis. **(A)** Comparison of dual-energy imaging between cells (samples #16) loaded with SiO_2 nanoparticles, images shown in **(a)**, **(b)**, **(c)**, and empty cells (sample #27), with the images shown in **(d, e, f)**. **(B)** SiO_2 promoted mast cell degranulation. **(a)**. Transmission electron microscope image of 20 nm SiO_2 (×1000 k, bar=50 nm). **(b–e)**. Representative transmission electron microscope images of mast cells. b: Blank group (×2.5 k, bar=2 μm); c: DNP-HSA group (×2.0 k, bar=2 μm); d: DNP-HSA+SiO_2 group (×2.5 k, bar=2 μm; ×10 k, bar=500 nm); e: SiO_2 group (×3.0 k, bar=2 μm).

covered by cells, suggesting the presence of silicon nanoparticles in the cells.

We further investigated whether nano-SiO_2 particles could enter mast cells and promote degranulation. The morphology of mast cells and SiO_2 was investigated by transmission electron microscopy (TEM). Compared with the control group, the cells treated with DNP-HSA or DNP-HSA+SiO_2 exhibited obvious morphological changes, such as deformation, shrinkage, secretory granule release, sparse intracellular particles, and vacuolated cytoplasm, altogether indicating the occurrence of degranulation (**Figure 6B**) (22). However, there was no clear morphological change in mast cells in the SiO_2 group, which seemed to indicate that treatment with SiO_2 alone was insufficient to cause obvious degranulation. Compared with the DNP-HSA group, an increased degree of intracellular vacuoles was observed in DNP-HSA+SiO_2. Moreover, we found nano-SiO_2 particles inside the mast cells. These results showed that nano-SiO_2 particles could enter the mast cells and exert a synergistic sensitization effect through the IgE pathway.

TABLE 1 Statistical analysis of FOL on samples at various areas marked by white-dashed boxes.

Sample	27 (empty cell)			16 (cell with silica particles)		
Area	Y1	Y2	J1	X1	X2	I1
FOL	13 ± 2	13 ± 2	17 ± 2	30 ± 2	36 ± 2	71 ± 2

FOL, frequency of occurrence of likelihood.

Effects of nano-SiO_2 exposure on the gene expression profile in mast cells

To deeply investigate the details of the nano-SiO_2 particles effects, we examined the gene expression profile alterations after nano-SiO_2 particles treatment in BMMCs. The difference analysis between the groups showed that 285 genes were significantly expressed after treatment with nano-SiO_2 particles. The differentially expressed genes were further searched and analyzed in the GeneCards database, and 135 differentially expressed genes were found to be related to oxidative stress, suggesting that the exposure of nano-SiO2 particles may cause oxidative stress in mast cells.

Gene Ontology (GO) and Kyoto Encyclopedia of Genes and Genomes (KEGG) pathway enrichment analyses were used to analyze these differentially expressed genes. As shown in Figure 7A, in terms of biological process, differentially expressed genes were mainly enriched in transcriptional regulation, signal transduction, apoptosis process, inflammatory response, cell proliferation, phosphorylation, and positive regulation of ERK1/2 cascade, etc. In terms of cellular component, the cellular structural positions where differentially expressed genes perform their functions were mainly located in the nucleus, cytoplasm, and cell membrane. In terms of molecular function, the activities of gene products at the molecular level mainly involved protein binding, metal ion binding, DNA and nucleic acid binding, and hydrolase activity. Further, taking the Top 20 terms with the smallest *p*-value for GO enrichment scatterplot display, GO enrichment analysis showed that the genes were enriched in MAP kinase tyrosine/serine/threonine phosphatase activity, protein tyrosine/threonine phosphatase activity, and regulation of the ERK1 and ERK2 cascades (Figure 7B). As shown in Figure 7C, the KEGG enrichment bar plot showed that the differentially expressed genes covered the KEGG Main Class, involving several secondary classifications such as cell growth and death,

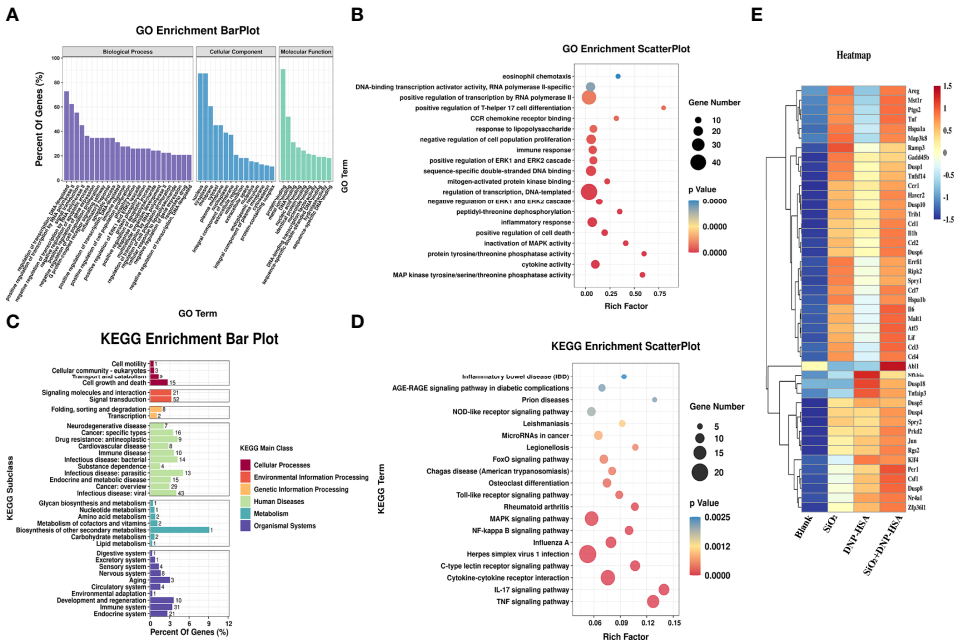

FIGURE 7
Nano-SiO_2 exposure affects the gene expression profile. **(A)** Gene Ontology (GO) enrichment barplot analysis. **(B)** GO enrichment scatterplot analysis. **(C)** Kyoto Encyclopaedia of Genes and Genomes (KEGG) pathway enrichment barplot analysis. **(D)** KEGG pathway enrichment scatterplot analysis. **(E)** Heatmap of clustering analysis for differentially expressed genes related to signaling pathway.

signal transduction, environmental adaptation, metabolism, and immune system, etc. The KEGG pathway enrichment analysis demonstrated that the differentially expressed genes were primarily involved in cytokine-cytokine receptor interactions, the NF-κB signaling pathway, and the MAPK signaling pathway (**Figure 7D**). We further screened differentially expressed genes related to the MAPK signaling pathway, NF-κB signaling pathway, and ERK1/2 cascade positive and negative regulation for cluster analysis. A total of 45 differentially expressed genes were screened (**Figure 7E**). Compared with the blank group, both nano-SiO_2 exposure and DNP-HSA stimulation increased the expression of genes related to the MAPK signaling pathway in mast cells to varying degrees. Exposure to nano-SiO_2 significantly up-regulated the expression of genes such as *Areg*, *Ptgs2*, *Tnf*, *Hspa1a*, *Map3k8*, *Malt1*, *Ccl3*, *Ccl4*, and *Il6*.

Nano-SiO_2 exposure enhances the MAPK signaling pathway

First, we investigated whether nano-SiO_2 particles affected the expression of high-affinity IgE receptors (FcεRI) in mast cells and the ability to bind IgE. BMMCs showed no significant difference in FcεRI expression after incubation with SiO_2 particles compared to the blank control (**Figure 8A**). Then, BMMCs were sensitized by incubation with anti-DNP-IgE, washed to remove unbound IgE, and treated with SiO_2 particles. Flow cytometry detection revealed no significant differences in FcεRI expression or IgE binding capacity compared to the blank control (**Figures 8B, C**). Overall, the above data confirmed that nano-SiO_2 particles exposure did not affect the expression of FcεRI or the ability of mast cells to bind IgE.

Given the transcriptome sequencing analysis results, we further investigated the signaling pathways involved in mast cell activation. BMMCs were sensitized with anti-DNP-IgE, treated with nano-SiO_2 particles, and stimulated with DNP-HSA. Cell lysates were analyzed by Western blotting with different antibodies. As shown in **Figures 8D–G**, the results indicated that nano-SiO_2 particles treatment upregulated p-ERK1/2 expression based on DNP-HSA stimulation. Nano-SiO_2 particles treatment increased p-p38 expression compared with the blank control, while this trend was not observed after DNP-HSA stimulation. The expression of NF-κB, p-Plcγ1 and p-JNK was upregulated after mast cell activation, but no significant differences were observed between the DNP-HSA stimulation group and the DNP-HSA+SiO_2 group. Taken together, nano-SiO_2 particles stimulation may synergistically activate mast cells by enhancing the MAPK signaling pathway, especially the phosphorylation levels of ERK1/2.

Next, we validated using the MAPK signaling inhibitors (ERK inhibitor U0126-EtOH and p38 inhibitor SB203580). As shown in **Figure 8H**), when the BMMCs were pretreated with signaling molecule inhibitors, the β-hex release ratio of the SiO_2 group, the DNP-HSA group, and the DNP-HSA+SiO_2 group all decreased to varying degrees, and the differences were statistically significant ($P<0.0001$). Compared with the 10 μM/L p38 inhibitor, the inhibitory effects of the 5 μM/L ERK inhibitor were more obvious, and the β-hex release ratio was reduced by about 10%-25%.

Discussion

An increasing number of observational studies have demonstrated that air pollution has an adverse impact on allergic respiratory disease. Air pollution exposure is associated with increased asthma and allergy morbidity and is a suspected strong risk factor for the increasing prevalence of allergic conditions (23–25). However, how the different components or PM with different particle sizes in air pollution affect the allergic response is unclear. In the present study, we explored the effects of four common mineral elements with different particle sizes in smog particles on mast cell activation. The results showed that nano-SiO_2 particles stimulation might synergistically activate IgE-sensitized mast cells by enhancing the MAPK signaling pathway, and nano-SiO_2 particles exposure could exacerbate allergic inflammation in an OVA-induced asthmatic mouse model.

Mast cells play an essential role in various allergic disorders, acting as the first line of defense in response to external environmental stimuli (13). Activated mast cells release various mediators, including histamine and inflammatory cytokines in response to various stimuli (26). Numerous studies have confirmed that PM2.5 can promote mast cell degranulation, increase the release of inflammatory cytokines, and aggravate allergic diseases (27–29). However, only a few studies have examined the effects of pollutant components on allergic diseases because pollutants derive from different sources and vary in composition and toxicity (30). In our previous study, nine typical water-soluble inorganic salts (ammonium nitrate, ammonium sulfate, ammonium chloride, sodium nitrate, anhydrous sodium sulfate, potassium nitrate, potassium sulfate, calcium nitrate, and calcium sulfate) and three water-soluble organic acids (malonic acid, succinic acid, oxalic acid) were selected in PM2.5 to investigate the cytotoxicity and activation effect on mast cells. These results indicated that nine typical water-soluble inorganic salts could not induce the release of β-hex on BMMCs through either the IgE pathway or the non-IgE pathway (16). In water-soluble organic acids, only malonic acid was observed to have a very weak activation effect on BMMCs. In the present study, we found that different particle sizes of Al_2O_3, Fe_2O_3, and SiO_2 showed a slight activation effect on mast cell β-hex release in the non-IgE pathway. We also found that SiO_2 at 20 nm was able to increase β-hex release from IgE-sensitized mast cells, while Al_2O_3, TiO_2, Fe_2O_3, and SiO_2

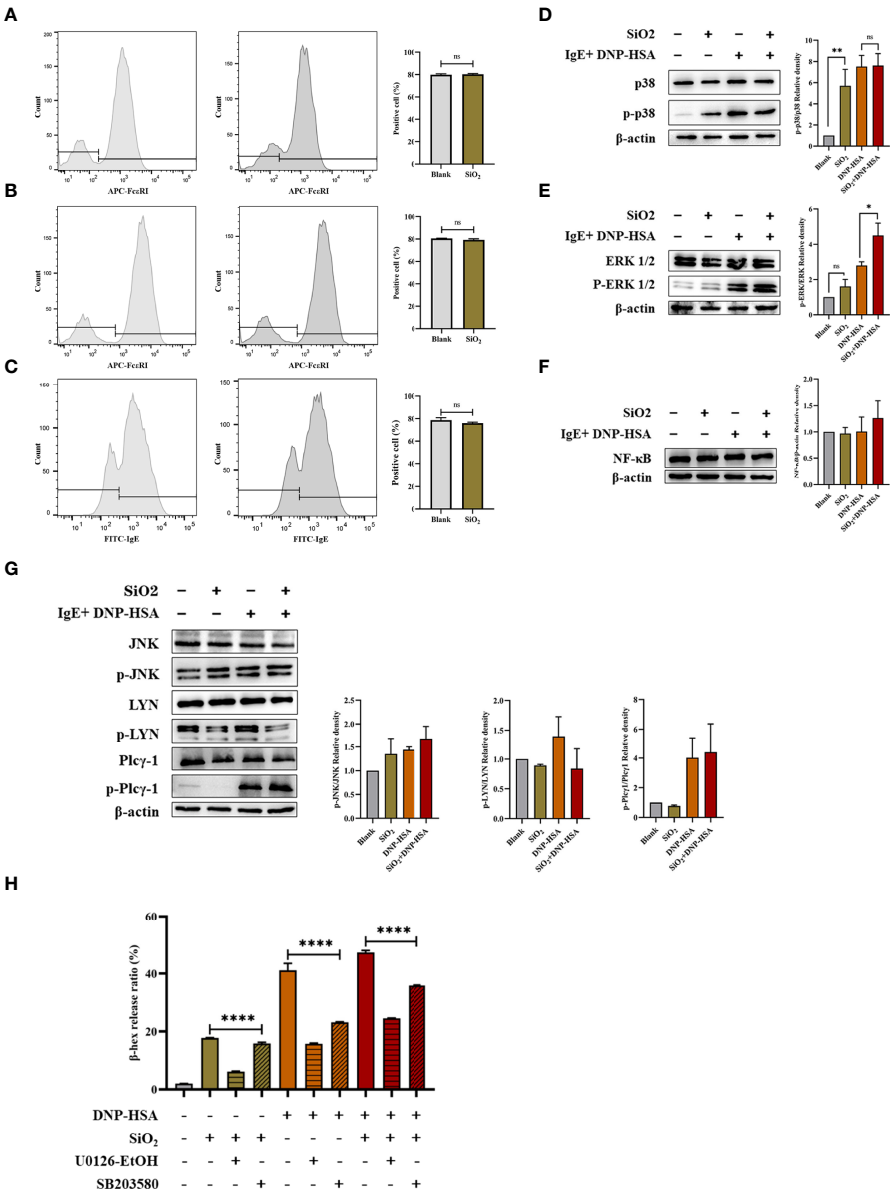

FIGURE 8
FcεRI-mediated signaling in mast cells. **(A)** BMMCs were not sensitized with anti-DNP IgE and treated with nano-SiO_2. The results showed no significant difference in FcεRI expression compared to the blank control. **(B, C)** BMMCs were sensitized with anti-DNP IgE and washed to remove unbound anti-DNP IgE before treatment with nano-SiO_2. There were no significant differences in FcεRI expression **(B)** or IgE binding capacity **(C)** compared to the blank control. **(D–G)** BMMCs were sensitized with anti-DNP-IgE, treated with nano-SiO_2, and stimulated with DNP-HSA. The cell lysates were analyzed by Western blotting with different antibodies against the NF-κB proteins and the phosphorylated and nonphosphorylated forms of the p38, ERK1/2, JNK, LYN, and Plcγ1 proteins. Relative density bars represent the means ± SD. **(H)** β-hexosaminidase release ratio from activated BMMCs pretreated with signaling inhibitors (ERK inhibitor U0126-EtOH 5 μM/L and p38 inhibitor SB203580 10 μM/L). The unpaired t test or ordinary one-way ANOVA was used to compare different groups. *$P < 0.05$, **$P < 0.01$, ****$P < 0.0001$. ns, no significance.

(2.34 μm) did not. Depending on their size and mass, particles can reach different sites within the respiratory tract. For example, PM10 can enter the upper airways, while finer particles, such as PM2.5 and PM0.1, can enter the terminal bronchioles and alveoli. If the particles are small enough, they can enter the blood, which in turn can affect other organ systems (31, 32). In our experiments, due to the different masses of particulate matter, its sedimentation speed in the medium was different, resulting in a difference in the time of sufficient contact with mast cells. In addition, there may also be differences in the

uptake capacity of mast cells to different particle sizes. However, the TEM and STXM results showed that 20 nm SiO_2 particles could enter the mast cells and exert a sensitizing effect. Importantly, we cannot ignore the effect of the protein composition of the cell culture medium on particulate matter. Particles may be bound or coated by bioactive proteins in the medium, which not only impacts the behavior of nanoparticles but also affects the bound proteins. Therefore, in our experiments, only nano-SiO_2 particles was observed to promote the activation of IgE-sensitized mast cells, but this did not exclude those other particles that would not affect mast cells. In fact, several studies have investigated the effects of the chemical composition and redox activity of particles on exacerbating allergic airway sensitization and the type of immune response (33–36). Although our study attempted to investigate the effects on mast cells from single particles of different sizes, further research is needed to understand the immune-modulatory effects of different particles in pollutants and the impact of particle material, other sizes, and surface coating.

Given the results of the *in vitro* cellular experiments, we further verified the effect of nano-SiO_2 particles on allergic diseases *in vivo*. The PCA ear model is a typical acute allergic animal model wherein allergic reactions are induced by antigen stimulation of mast cells in ear skin, which is widely used in the screening of anti-allergic drugs and drug safety assessment (37, 38). In our PCA mouse model, Evan's blue extravasation in mice was significantly increased after treatment with nano-SiO_2 particles, which indicated that the nano-SiO_2 particles exposure might promote the local IgE-sensitized mast cell activation and allergic mediators' secretion, thereby increasing the permeability of local blood vessels and aggravating allergic reactions. Coexposure to nano-SiO_2 particles plus OVA sensitization caused an enhancement of allergic airway inflammation compared with OVA alone. This adjuvant-like effect was manifested by significantly greater OVA-specific serum IgE, airway hyperresponsiveness, lung inflammation injury, mucous cell metaplasia, and cytokine expression compared with mice sensitized to OVA without nano-SiO_2. Our findings were consistent with those of other studies. Han et al. reported that silica nanoparticles with OVA induced more significant inflammatory cell infiltration in BALF, extensive pathological changes, and higher cytokine levels than silica nanoparticles alone or saline/OVA. In particular, mesoporous-type silica nanoparticles showed the most severe airway inflammation in both direct toxicity and adjuvant effect assays (39). Brandenberger et al. suggested that engineered silica nanoparticles promoted the immunologic response towards the allergen and thereby potentiated the adverse allergic responses in the pulmonary airways, and the adjuvant effects of silica nanoparticles were Th2/Th17 related (40). One murine model experiment showed that SiO_2 induced epithelial cells to express IL-33, which in turn activated innate lymphoid cells to produce IL-5 and/or IL-13, contributing to the exacerbation of OVA-induced airway inflammation (41). Another study indicated that silica nanoparticles aggravate airway inflammation and asthma development by increasing the protein expression levels of thioredoxin-interacting protein (TXNIP) and the NOD-like receptor pyrin domain-containing 3 (NLRP3) inflammasome (42). However, Shin JH et al. conducted a subacute inhalation toxicity study of synthetic amorphous silica nanoparticles at low, middle, and high concentrations in rats using a nose-only inhalation system. They did not observe any toxic effects on the lungs of rats at any concentration (43). In Horie M's study, SiO_2 nanoparticles did not affect OVA-specific IgE and IgG1 levels and did not show the potential to aggravate allergic reactions (36).

Obviously, the effect of SiO_2 particles exposure on the body is a very complex process, and the airway epithelial cells and alveolar macrophages are undoubtedly the most concerned. Studies have pointed out that occupational mineral dusts and air pollutant particles can induce airway wall remodeling (44, 45). Using the human airway epithelial cells 16HBE or primary cultured mouse tracheobronchial epithelial cells, researchers found that SiO_2 nanoparticles could inhibit the responses to ATP and inhibit cation channel transient receptor potential vanilloid 4 (TRPV4) in airway epithelial cells, and result in epithelial barrier dysfunction (46, 47). *In vitro* and *in vivo* experiments demonstrated that SiO_2 particles exposure not only caused rapid NLRP3-dependent mitochondrial depolarization and DNA damage in airway epithelial cells but also led to ultrastructural defects in airway cilia and mucus hypersecretion (48, 49). Besides, one review concluded that SiO_2 particles might bind to the scavenger receptor of alveolar macrophages, followed by particle endocytosis with a respiratory burst to generate reactive oxygen species and reactive nitrogen species, which in turn activation of the protein kinase C mediated MAPK signaling cascades resulting in cytokine release (50). In our experiments, we attempted to evaluate the effect of nano-SiO_2 on allergic asthma from the perspective of mast cells *in vivo* based on *in vitro* cell experiments that confirmed the activation of nano-SiO_2 on mast cells. High inhalation doses of silica result in pulmonary fibrosis and silicosis, and silica exposure can activate various immune cells and cause a proinflammatory response (51, 52). We selected a relatively low-concentration nano-SiO_2 exposure *in vivo* to avoid masking its synergistic sensitizing effect due to the apparent toxic reaction. Compared with the blank control group, the nano-SiO_2 exposure alone group exhibited relatively mild pathological changes in the lung tissue, yet some changes persisted in lung function, histamine, and inflammatory factors. Compared with the OVA group, the results showed that nano-SiO_2 exposure resulted in the accumulation of tryptase-positive cells in the airways and increased BALF histamine levels, which is associated with immediate allergic symptoms. These results suggested that airway exposure to nano-SiO_2 could exacerbate

allergic airway inflammation, trigger mast cells, increase histamine secretion, enhance airway responsiveness, and foster more serious manifestations of allergic airway disease.

Finally, we studied the effect of nano-SiO_2 exposure on FcεRI-mediated signaling. *In vitro*, we found that nano-SiO_2 had a very slight activation effect on mast cells without IgE sensitization. However, when IgE-sensitized mast cells were first incubated with nano-SiO_2 and then excited by the addition of DNP-HSA, the nano-SiO_2 showed a synergistic effect, significantly increasing the release of β-hexosaminidase. Therefore, we first investigated whether nano-SiO_2 affected the expression of FcεRI in mast cells and the ability to bind IgE. The experimental results showed that nano-SiO_2 exposure did not affect the expression of FcεRI or the ability of mast cells to bind IgE but synergistically activated mast cells by enhancing the MAPK signaling pathway, especially the phosphorylation levels of ERK1/2, which was consistent with the results of transcriptome sequencing. The gene expression profile in mast cells showed the genes related to the MAPK signaling pathway in mast cells had significant changes, such as the *Gadd45b* and *Nr4a1*. The orphan nuclear receptor *Nr4a1* promoted FcεRI-stimulated mast cell activation and anaphylaxis by counteracting the inhibitory LKB1/AMPK axis (53). *Gadd45b* belongs to the Gadd45 (growth arrest and DNA damage-inducible 45) family of proteins and is involved in environmental stress. It was reported that PM2.5 can promote IgE-mediated mast cell activation through ROS/Gadd45b/JNK axis (54).

Of note, the mechanism underlying the impact of pollutants on diseases is extremely complex. Cao et al. found that PM2.5 could increase the viability of human airway smooth muscle cells, accompanied by increased airway hyperresponsiveness through the kallikrein-bradykinin pathway (29). In addition, Liu et al. confirmed that PM2.5 triggered airway inflammation and bronchial hyperresponsiveness in mice by significantly downregulating the expression and activity of SIRT2, accelerating p65 phosphorylation and acetylation, and activating the NF-κB signaling pathway (55). Specific to mast cells, our results were consistent with Jin's study, which showed that PM2.5 exposure enhanced FcεRI-mediated signaling and mast cell function due to increased phosphorylation of Syk, LAT, SLP-76, PLC-γ1, Akt, ERK1/2 or p38 and activated the PI3K and MAPK pathways (56). However, Wang et al. pointed out that PM2.5 treatment activated MEKK4 and JNK1/2 but not ERK1/2 and p38, facilitating IgE-mediated mast cell activation (54). Moreover, another study on silicosis found that silica can direct mast cell activation, resulting in inflammatory mediators, and enhance IgE-mediated cytokine, chemokine, and protease production. However, these effects were thought to occur in part through mast cell scavenger receptors instead of the alteration of FcεRI-mediated signaling events (57). The cellular mechanisms regulating hyperallergic responses caused by pollutants have not been entirely elucidated. The role of biologically and nonbiologically active components in pollutants, in addition to PM2.5 and nano-SiO_2, in allergic diseases and the underlying molecular mechanisms, still merit attention and further research.

Silica is the most common component found naturally in the Earth's crust and is an important component of respirable particulate matter in urban areas (58). Due to their specific physicochemical properties, silica nanoparticles are widely used in many engineering and medical fields, including fabrication, drug delivery systems, cosmetics, and food packing (59). These factors undoubtedly increase the risk of SiO_2 exposure. The high incidence of allergic diseases and the increasing exposure factors similar to nano-SiO_2 have brought new challenges to preventing and treating allergic diseases. Moreover, our results provide useful information for explaining the acute exacerbation of symptoms and the increase in medical treatment in patients with allergic diseases in smoggy weather. The synergistic effects of nano-SiO_2 exposure promoting mast cell activation in smoggy weather, even in thunderstorms may be one of the reasons for the aggravation of symptoms in allergic patients. Our results also suggest the need to avoid nano-SiO_2 exposure in daily life, especially in individuals with allergic respiratory diseases.

Although *in vitro* and *in vivo* experiments are important for understanding the potential toxicology and immune response to air pollution, our experiments still have some limitations. First, pollutant exposure dosing shows significant effects, but whether these effects represent the density of particles deposited in the airway is questionable, as also observed in similar studies (60). The effects of exposure dose, effective concentration, sedimentation rate, and diffusion rate of particles on cell experiments need to be further evaluated. Second, exposure to particulate matter may involve numerous immune cells such as epithelial cells, macrophages, dendritic cells, and lymphocytes, despite the mast cells localized in the skin, mucous membranes, and airways that are in contact with the environment. The effects of SiO_2 on the immune system and allergic diseases may be far more complex than we have observed. Therefore, there is a need to further study the effects of nano-SiO_2 on immune cells and the impact of nano-SiO_2 on airborne allergens.

In conclusion, our results indicated that nano-SiO_2 stimulation might synergistically activate IgE-sensitized mast cells by enhancing the MAPK signaling pathway and that nano-SiO_2 exposure could exacerbate allergic inflammation. Our experimental results provide useful information for preventing and treating allergic diseases.

Data availability statement

The datasets presented in this study can be found in online repositories. The names of the repository/repositories and

accession number(s) can be found below: GEO under accession number GSE206630.

Ethics statement

The animal study was reviewed and approved by Nanjing Medical University's Institutional Animal Care and Use Committee.

Author contributions

Y-SY: Investigation, Formal analysis, Data Curation, Writing - Original Draft; M-DC: Methodology, Investigation, Validation, Data Curation; AW: Resources, Investigation, Data Curation; Q-ML: Resources, Investigation; D-XZ: Resources, Investigation; YZ: Resources, Investigation; L-LM: Resources, Investigation; ML: Resources, Investigation; YS: Resources, Investigation; D-DX: Conceptualization, Supervision, Writing - Review & Editing; J-FW: Conceptualization, Supervision, Writing - Review & Editing; J-LS: Conceptualization, Supervision, Writing - Review & Editing. All authors contributed to the article and approved the submitted version.

Funding

This work was supported by the National Natural Science Foundation of China (U1832212), Beijing Municipal Natural Science Foundation (7191008) and National Natural Science Foundation of China (12105313).

Conflict of interest

The authors declare that the research was conducted in the absence of any commercial or financial relationships that could be construed as a potential conflict of interest.

Publisher's note

References

1. Cecchi L, D'Amato G, Annesi-Maesano I. Climate change and outdoor aeroallergens related to allergy and asthma: Taking the exposome into account. *Allergy* (2020) 75(9):2361–3. doi: 10.1111/all.14286

2. Gilles S, Akdis C, Lauener R, Schmid-Grendelmeier P, Bieber T, Schäppi G, et al. The role of environmental factors in allergy: A critical reappraisal. *Exp Dermatol* (2018) 27(11):1193–200. doi: 10.1111/exd.13769

3. Pacheco SE, Guidos-Fogelbach G, Annesi-Maesano I, Pawankar R, D' Amato G, Latour-Staffeld P, et al. Climate change and global issues in allergy and immunology. *J Allergy Clin Immunol* (2021) 148(6):1366–77. doi: 10.1016/j.jaci.2021.10.011

4. Poole JA, Barnes CS, Demain JG, Bernstein JA, Padukudru MA, Sheehan WJ, et al. Impact of weather and climate change with indoor and outdoor air quality in asthma: A work group report of the AAAAI environmental exposure and respiratory health committee. *J Allergy Clin Immunol* (2019) 143(5):1702–10. doi: 10.1016/j.jaci.2019.02.018

5. Cecchi L, D'Amato G, Annesi-Maesano I. External exposome and allergic respiratory and skin diseases. *J Allergy Clin Immunol* (2018) 141(3):846–57. doi: 10.1016/j.jaci.2018.01.016

6. Bowatte G, Lodge C, Lowe AJ, Erbas B, Perret J, Abramson MJ, et al. The influence of childhood traffic-related air pollution exposure on asthma, allergy and sensitization: a systematic review and a meta-analysis of birth cohort studies. *Allergy* (2015) 70(3):245–56. doi: 10.1111/all.12561

7. Codispoti CD, LeMasters GK, Levin L, Reponen T, Ryan PH, Biagini Myers JM, et al. Traffic pollution is associated with early childhood aeroallergen sensitization. *Ann Allergy Asthma Immunol* (2015) 114(2):126–33. doi: 10.1016/j.anai.2014.10.020

8. Xu P, Chen Y, Ye X. Haze, air pollution, and health in China. *Lancet* (2013) 382(9910):2067. doi: 10.1016/S0140-6736(13)62693-8

9. Arias-Pérez RD, Taborda NA, Gómez DM, Narvaez JF, Porras J, Hernandez JC. Inflammatory effects of particulate matter air pollution. *Environ Sci pollut Res Int* (2020) 27(34):42390–404. doi: 10.1007/s11356-020-10574-w

10. Committee WGAbtGR. *WHO global air quality guidelines: Particulate matter (PM(2.5) and PM(10)), ozone, nitrogen dioxide, sulfur dioxide and carbon monoxide*. Geneva: World Health Organization 2021 (2021).

11. Chen R, Cheng J, Lv J, Wu L, Wu J. Comparison of chemical compositions in air particulate matter during summer and winter in Beijing, China. *Environ Geochem Health* (2017) 39(4):913–21. doi: 10.1007/s10653-016-9862-9

12. Walczak-Drzewiecka A, Wyczólkowska J, Dastych J. Environmentally relevant metal and transition metal ions enhance fc epsilon RI-mediated mast cell activation. *Environ Health Perspect* (2003) 111(5):708–13. doi: 10.1289/ehp.5960

13. Tikoo S, Barki N, Jain R, Zulkhernain NS, Buhner S, Schemann M, et al. Imaging of mast cells. *Immunol Rev* (2018) 282(1):58–72. doi: 10.1111/imr.12631

14. Plum T, Wang X, Rettel M, Krijgsveld J, Feyerabend TB, Rodewald H-R. Human mast cell proteome reveals unique lineage, putative functions, and structural basis for cell ablation. *Immunity* (2020) 52(2):404–16.e5. doi: 10.1016/j.immuni.2020.01.012

15. Piao CH, Fan Y, Nguyen TV, Shin HS, Kim HT, Song CH, et al. PM Exacerbates oxidative stress and inflammatory response through the Nrf2/NF-κB signaling pathway in OVA-induced allergic rhinitis mouse model. *Int J Mol Sci* (2021) 22(15):8173. doi: 10.3390/ijms22158173

16. An W, Yaping M, Mengda C, Yang S, Lingling M, Jifu W. Distribution characteristics and allergic effect of typical water soluble ions in PM2.5 in shijingshan district of Beijing. *Acta Scientiae Circumstantiae* (2022) 42(3):334–41. doi: 10.13671/j.hjkxxb.2021.0267

17. Zhi M, Zhang X, Zhang K, Ussher SJ, Lv W, Li J, et al. The characteristics of atmospheric particles and metal elements during winter in Beijing: Size distribution, source analysis, and environmental risk assessment. *Ecotoxicol Environ Saf* (2021) 211:111937. doi: 10.1016/j.ecoenv.2021.111937

18. Akram W, Madhuku M, Ahmad I, Xiaolin L, Zhang G, Yan L. Morphology, microstructure and chemical composition of single inhalable particles in shanghai, China. *Environ Monit Assess* (2014) 186(12):8587–98. doi: 10.1007/s10661-014-4026-9

19. Xiu J, Liu Y, Wang B, Xue Y, Chen M, Ji T, et al. Quantitative toxicological study of dose-dependent arsenic-induced cells *via* synchrotron-based STXM and FTIR measurement. *Analyst* (2020) 145(13):4560–8. doi: 10.1039/d0an00346h

20. Zhang L, Xu Z, Zhang X, Yu H, Zou Y, Guo Z, et al. Latest advances in soft X-ray spectromicroscopy at SSRF Nuclear Sci Techniq. (2015) 26(4):040101. doi: 10.13538/j.1001-8042/nst.26.040101

21. Zhang XZ, Xu ZJ, Tai RZ, Zhen XJ, Wang Y, Guo Z, et al. Ratio-contrast imaging of dual-energy absorption for element mapping with a scanning

transmission X-ray microscope. *J Synchrotron Radiat* (2010) 17(6):804–9. doi: 10.1107/S0909049510031250

22. Jiang D, Feng D, Jiang H, Yuan L, Yongqi Y, Xu X, et al. Preliminary study on an innovative, simple mast cell-based electrochemical method for detecting foodborne pathogenic bacterial quorum signaling molecules (N-acyl-homoserine-lactones). *Biosens Bioelectron* (2017) 90:436–42. doi: 10.1016/j.bios.2016.09.096

23. Fan J, Li S, Fan C, Bai Z, Yang K. The impact of PM2.5 on asthma emergency department visits: a systematic review and meta-analysis. *Environ Sci pollut Res Int* (2016) 23(1):843–50. doi: 10.1007/s11356-015-5321-x

24. Amato M D, Cecchi L, Annesi-Maesano I, D Amato G. News on climate change, air pollution, and allergic triggers of asthma. *J Investig Allergol Clin Immunol* (2018) 28(2):91–7. doi: 10.18176/jiaci.0228

25. Riedl MA. The effect of air pollution on asthma and allergy. *Curr Allergy Asthma Rep* (2008) 8(2):139–46. doi: 10.1007/s11882-008-0024-8

26. Wernersson S, Pejler G. Mast cell secretory granules: armed for battle. *Nat Rev Immunol* (2014) 14(7):478–94. doi: 10.1038/nri3690

27. Diaz-Sanchez D, Penichet-Garcia M, Saxon A. Diesel exhaust particles directly induce activated mast cells to degranulate and increase histamine levels and symptom severity. *J Allergy Clin Immunol* (2000) 106(6):1140–6. doi: 10.1067/mai.2000.111144

28. Li Y, Zhou J, Rui X, Zhou L, Mo X. PM2.5 exposure exacerbates allergic rhinitis in mice by increasing DNA methylation in the IFN-γ gene promoter in CD4+T cells *via* the ERK-DNMT pathway. *Toxicol Lett* (2019) 301:98-107. doi: 10.1016/j.toxlet.2018.11.012

29. Cao X, Wang M, Li J, Luo Y, Li R, Yan X, et al. Fine particulate matter increases airway hyperresponsiveness through kallikrein-bradykinin pathway. *Ecotoxicol Environ Saf* (2020) 195:110491. doi: 10.1016/j.ecoenv.2020.110491

30. Ichinose T, Yoshida S, Sadakane K, Takano H, Yanagisawa R, Inoue K, et al. Effects of asian sand dust, Arizona sand dust, amorphous silica and aluminum oxide on allergic inflammation in the murine lung. *Inhal Toxicol* (2008) 20(7):685–94. doi: 10.1080/08958370801935133

31. Yang L, Li C, Tang X. The impact of PM on the host defense of respiratory system. *Front Cell Dev Biol* (2020) 8:91. doi: 10.3389/fcell.2020.00091

32. Xing Y-F, Xu Y-H, Shi M-H, Lian Y-X. The impact of PM2.5 on the human respiratory system. *J Thorac Dis* (2016) 8(1):E69–74. doi: 10.3978/j.issn.2072-1439.2016.01.19

33. Dekkers S, Wagner JG, Vandebriel RJ, Eldridge EA, Tang SVY, Miller MR, et al. Role of chemical composition and redox modification of poorly soluble nanomaterials on their ability to enhance allergic airway sensitisation in mice. *Part Fibre Toxicol* (2019) 16(1):39. doi: 10.1186/s12989-019-0320-6

34. Ban M, Langonné I, Huguet N, Guichard Y, Goutet M. Iron oxide particles modulate the ovalbumin-induced Th2 immune response in mice. *Toxicol Lett* (2013) 216(1):31–9. doi: 10.1016/j.toxlet.2012.11.003

35. Vandebriel RJ, Vermeulen JP, van Engelen LB, de Jong B, Verhagen LM, de la Fonteyne-Blankestijn LJ, et al. The crystal structure of titanium dioxide nanoparticles influences immune activity *in vitro* and *in vivo*. *Part Fibre Toxicol* (2018) 15(1):9. doi: 10.1186/s12989-018-0245-5

36. Horie M, Stowe M, Tabei M, Kuroda E. Pharyngeal aspiration of metal oxide nanoparticles showed potential of allergy aggravation effect to inhaled ovalbumin. *Inhal Toxicol* (2015) 27(3):181–90. doi: 10.3109/08958378.2015.1026618

37. Hou Y-B, Ji K, Sun Y-T, Zhang L-N, Chen J-J. CDK4/6 inhibitor palbociclib suppresses IgE-mediated mast cell activation. *J Transl Med* (2019) 17(1):276. doi: 10.1186/s12967-019-2026-9

38. Hiemori-Kondo M, Morikawa E, Fujikura M, Nagayasu A, Maekawa Y. Inhibitory effects of cyanidin-3-O-glucoside in black soybean hull extract on RBL-2H3 cells degranulation and passive cutaneous anaphylaxis reaction in mice. *Int Immunopharmacol* (2021) 94:107394. doi: 10.1016/j.intimp.2021.107394

39. Han H, Park YH, Park HJ, Lee K, Um K, Park J-W, et al. Toxic and adjuvant effects of silica nanoparticles on ovalbumin-induced allergic airway inflammation in mice. *Respir Res* (2016) 17(1):60. doi: 10.1186/s12931-016-0376-x

40. Brandenberger C, Rowley NL, Jackson-Humbles DN, Zhang Q, Bramble LA, Lewandowski RP, et al. Engineered silica nanoparticles act as adjuvants to enhance allergic airway disease in mice. *Part Fibre Toxicol* (2013) 10:26. doi: 10.1186/1743-8977-10-26

41. Unno H, Arae K, Matsuda A, Ikutani M, Tamari M, Motomura K, et al. Critical role of IL-33, but not IL-25 or TSLP, in silica crystal-mediated exacerbation of allergic airway eosinophilia. *Biochem Biophys Res Commun* (2020) 533(3):493–500. doi: 10.1016/j.bbrc.2020.09.046

42. Ko J-W, Shin N-R, Je-Oh L, Jung T-Y, Moon C, Kim T-W, et al. Silica dioxide nanoparticles aggravate airway inflammation in an asthmatic mouse model *via* NLRP3 inflammasome activation. *Regul Toxicol Pharmacol* (2020) 112:104618. doi: 10.1016/j.yrtph.2020.104618

43. Shin JH, Jeon K, Kim JK, Kim Y, Jo MS, Lee JS, et al. Subacute inhalation toxicity study of synthetic amorphous silica nanoparticles in sprague-dawley rats. *Inhal Toxicol* (2017) 29(12-14):567–76. doi: 10.1080/08958378.2018.1426661

44. Churg A, Wright JL. Airway wall remodeling induced by occupational mineral dusts and air pollutant particles. *Chest* (2002) 122(6 Suppl):306S–9S. doi: 10.1378/chest.122.6_suppl.306s

45. Perkins TN, Peeters PM, Albrecht C, Schins RPF, Dentener MA, Mossman BT, et al. Crystalline silica alters sulfatase-1 expression in rat lungs which influences hyper-proliferative and fibrogenic effects in human lung epithelial cells. *Toxicol Appl Pharmacol* (2018) 348:43–53. doi: 10.1016/j.taap.2018.04.011

46. Sanchez A, Alvarez JL, Demydenko K, Jung C, Alpizar YA, Alvarez-Collazo J, et al. Silica nanoparticles inhibit the cation channel TRPV4 in airway epithelial cells. *Part Fibre Toxicol* (2017) 14(1):43. doi: 10.1186/s12989-017-0224-2

47. Milici A, Sanchez A, Talavera K. Silica nanoparticles inhibit responses to ATP in human airway epithelial 16HBE cells. *Int J Mol Sci* (2021) 22(18):10173. doi: 10.3390/ijms221810173

48. Wu R, Högberg J, Adner M, Ramos-Ramírez P, Stenius U, Zheng H. Crystalline silica particles cause rapid NLRP3-dependent mitochondrial depolarization and DNA damage in airway epithelial cells. *Part Fibre Toxicol* (2020) 17(1):39. doi: 10.1186/s12989-020-00370-2

49. Yu Q, Fu G, Lin H, Zhao Q, Liu Y, Zhou Y, et al. Influence of silica particles on mucociliary structure and MUC5B expression in airways of C57BL/6 mice. *Exp Lung Res* (2020) 46(7):217–25. doi: 10.1080/01902148.2020.1762804

50. Hamilton RF, Thakur SA, Holian A. Silica binding and toxicity in alveolar macrophages. *Free Radic Biol Med* (2008) 44(7):1246–58. doi: 10.1016/j.freeradbiomed.2007.12.027

51. Lee S, Hayashi H, Mastuzaki H, Kumagai-Takei N, Otsuki T. Silicosis and autoimmunity. *Curr Opin Allergy Clin Immunol* (2017) 17(2):78–84. doi: 10.1097/ACI.0000000000000350

52. Hoy RF, Chambers DC. Silica-related diseases in the modern world. *Allergy* (2020) 75(11):2805–17. doi: 10.1111/all.14202

53. Jin F, Li X, Deng Y, Timilshina M, Huang B, Kim D-Y, et al. The orphan nuclear receptor NR4A1 promotes FcεRI-stimulated mast cell activation and anaphylaxis by counteracting the inhibitory LKB1/AMPK axis. *Allergy* (2019) 74 (6):1145–56. doi: 10.1111/all.13702

54. Wang Y, Tang N, Mao M, Zhou Y, Wu Y, Li J, et al. Fine particulate matter (PM2.5) promotes IgE-mediated mast cell activation through ROS/Gadd45b/JNK axis. *J Dermatol Sci* (2021) 102(1):47–57. doi: 10.1016/j.jdermsci.2021.02.004

55. Liu M, Shi Z, Yin Y, Wang Y, Mu N, Li C, et al. Particulate matter 2.5 triggers airway inflammation and bronchial hyperresponsiveness in mice by activating the SIRT2-p65 pathway. *Front Med* (2021) 15(5):750–66. doi: 10.1007/s11684-021-0839-4

56. Jin Y, Zhu M, Guo Y, Foreman D, Feng F, Duan G, et al. Fine particulate matter (PM) enhances FcεRI-mediated signaling and mast cell function. *Cell Signal* (2019) 57:102–9. doi: 10.1016/j.cellsig.2019.01.010

57. Brown JM, Swindle EJ, Kushnir-Sukhov NM, Holian A, Metcalfe DD. Silica-directed mast cell activation is enhanced by scavenger receptors. *Am J Respir Cell Mol Biol* (2007) 36(1):43–52. doi: 10.1165/rcmb.2006-0197OC

58. Liu H, Wang X, Talifu D, Ding X, Abulizi A, Tursun Y, et al. Distribution and sources of PM-bound free silica in the atmosphere of hyper-arid regions in hotan, north-West China. *Sci Total Environ* (2022) 810:152368. doi: 10.1016/j.scitotenv.2021.152368

59. Napierska D, Thomassen LCJ, Lison D, Martens JA, Hoet PH. The nanosilica hazard: another variable entity. *Part Fibre Toxicol* (2010) 7(1):39. doi: 10.1186/1743-8977-7-39

60. Glencross DA, Ho T-R, Camiña N, Hawrylowicz CM, Pfeffer PE. Air pollution and its effects on the immune system. *Free Radic Biol Med* (2020) 151:56–68. doi: 10.1016/j.freeradbiomed.2020.01.179

frontiers | Frontiers in Immunology

TYPE Original Research
PUBLISHED 26 July 2022
DOI 10.3389/fimmu.2022.953714

OPEN ACCESS

EDITED BY
Bao-Hui Cheng,
Institute of ENT and Shenzhen Key Laboratory of ENT, China

REVIEWED BY
Arifumi Iwata,
Chiba University, Japan
Thomas Trian,
Universitéde Bordeaux, France

*CORRESPONDENCE
Dan Xu
dan.xu@xjtu.edu.cn
Ying Chang
changyingcn@hotmail.com

SPECIALTY SECTION
This article was submitted to Immunological Tolerance and Regulation, a section of the journal Frontiers in Immunology

RECEIVED 26 May 2022
ACCEPTED 30 June 2022
PUBLISHED 26 July 2022

CITATION
Wang W, Li Y, Fan J, Qu X, Shang D, Qin Q, Xu T, Hamid Q, Dang X, Chang Y and Xu D (2022) MiR-365-3p is a negative regulator in IL-17-mediated asthmatic inflammation. *Front. Immunol.* 13:953714. doi: 10.3389/fimmu.2022.953714

MiR-365-3p is a negative regulator in IL-17-mediated asthmatic inflammation

Weijia Wang[1], Ying Li[1], Jiaqi Fan[1], Xiaoyan Qu[1], Dong Shang[2], Qiaohong Qin[3], Tun Xu[4], Qutayba Hamid[5,6], Xiaomin Dang[2], Ying Chang[1]* and Dan Xu[1]*

[1]The Key Laboratory of Biomedical Information Engineering of Ministry of Education, School of Life Science and Technology, Xi'an Jiaotong University, Xi'an, China, [2]Department of Respiration, The First Affiliated Hospital, Xi'an Jiaotong University, Xi'an, China, [3]Institute of Basic and Translational Medicine, Xi'an Medical University, Xi'an, China, [4]School of Automation Science and Engineering, Faculty of Electronic and Information Engineering, Xi'an Jiaotong University, Xi'an, China, [5]Meakins-Christie Laboratories and Respiratory Division, The Research Institute of the McGill University Health Centre and Department of Medicine, McGill University, Montreal, QC, Canada, [6]College of Medicine, University of Sharjah, Sharjah, United Arab Emirates

Background: Interleukin-17, the major proinflammatory cytokine secreted by Th17 cells, makes essential contribution to pathogenesis of severe asthma, while the detailed mechanisms, especially the involvement of microRNAs which are also important participants in asthma progression, remains largely unclear.

Methods: In this study, we established a house dust mite (HDM) extract-induced murine asthmatic models and the miRNA expression in the lung tissues of mice were profiled by miRNA microarray assay. The effect of miR-365-3p on IL-17-mediated inflammation was examined by qRT-PCR and immunoblotting analysis. The involvement of ARRB2 as target gene of miR-365-3p was verified by overexpression or RNA interference.

Results: HDM extract-induced asthmatic inflammation was proved to be IL17-mediated and miR-365-3p was screened out to be the only miRNA exclusively responsive to IL-17. miR-365-3p, whose expression was significantly downregulated upon IL-17 stimulation, was demonstrated to exert remarkable anti-inflammatory effect to decrease IL-17-provoked inflammatory cytokines (KC/IL-8 and IL-6) in both airway epithelial cells and macrophages of murine and human origins, verifying its universal antagonizing activity against IL-17-initiated inflammation across the two species. ARRB2 was characterized as the key target of miR-365-3p to negate IL-17-induced inflammatory cytokines.

10.3389/fimmu.2022.953714

Conclusion: Taken together, our data supported the notion that miR-365-3p, which was diminished by IL-17 in murine and human asthmatic pathogenesis, functioned as an essential negative mediator in IL-17-stimuated inflammatory response by targeting ARRB2, which would shed new light to the understanding and therapeutics thereof of asthmatic inflammation.

KEYWORDS

asthma, IL-17KO, miR-365-3p, ARRB2, IL-8

Background

Asthma is a chronic inflammatory airway disease characterized by reversible airflow limitation with complicated pathogenesis involving variety of inflammatory cells and cytokines (1), of which Th17 cells, the crucial mediators between innate immunity and adaptive immunity, are shown to play essential roles in the inflammatory response in asthma (2). Our previous studies found that cytokines secreted by Th17 cells can induce the chemotaxis, proliferation and inflammatory responses of airway smooth muscle cells (ASMCs), revealing the unneglectable participation of Th17 cytokines in the remodeling of airway (3–5). IL-17 (also called IL-17A), the main contributor of the pro-inflammatory activity of Th17 cells (2, 6) has been demonstrated to be positively correlated with severity and steroid insensitivity of asthma (7, 8), whereas the detailed mechanisms remain to be explored.

MicroRNAs, the prominent regulators of gene expression by targeting mRNAs for degradation or translational suppression (9), also actively participate in the airway inflammatory response, as exampled by miR-21 that was identified as an essential regulator in Th1/Th2 imbalance and subsequent AHR, mucus formation and eosinophil infiltration in mice airway inflammation (10), miR34/449 that was suppressed by IL-13 to promote bronchial epithelial cells differentiation and proliferation (11), and miR-19a and miR-221 that played an essential role in proliferation of epithelial cells and airway smooth muscle cells in severe asthmatic patients (12, 13). Although the role of miRNA has been well recognized in asthma, its involvement in IL17-mediated asthmatic inflammation has not been fully understood (9, 14, 15). Nonetheless, a recent study revealed that miRNA was indispensable for IL-17 to induce secretion of inflammatory factors and chemokines by astrocytes in experimental autoimmune encephalomyelitis (16), implying the possibility that miRNA also participates in IL-17 -mediated asthmatic pathogenesis.

To investigate the role of miRNA in IL-17-dependent asthmatic inflammatory response, a chronic asthmatic animal model was established in wild type and IL-17- deficient mice. miRNA profiling assays and analysis revealed that miR-365-3p was significantly downregulated by IL-17. The further mechanistic study demonstrated that miR-365-3p was a negative regulator in IL17-mediated inflammation in both murine and human airway cells *via* miR-365-3p/ARRB2/cytokines axis, which may provide experimental evidence for the potential therapeutic targets of asthma.

Abbreviations: IL, interleukin; HDM, house dust mite; KO knock out; BALF bronchoalveolar lavage fluid; qRT-PCR quantitative reverse transcriptase polymerase chain reaction; WT wild type; AHR airway hyper responsiveness; KC keratinocyte chemoattractant; ARRB2 beta arrestin 2; EAE experimental autoimmune encephalitis; RA rheumatoid arthritis; CXCL C-X-C Motif Chemokine Ligand; ASMC airway smooth muscle cells; PBS phosphate-buffered saline; TNF-α tumor necrosis factor-α; IFN-γ interferon-γ; α-SMA α-smooth muscle actin; FASL Fas-ligand; TRAF3 TNF Receptor Associated Factor 3; Sgk1 Serum/Glucocorticoid Regulated Kinase 1; PIK3R3 phosphoinositide-3-kinase regulatory subunit 3; ADAM10 ADAM metallopeptidase domain 10; ADM Adrenomedullin; DMEM Dulbecco's modified Eagle's medium; HEPES N-2-hydroxyethylpiperazine-N_-2-ethanesulfonic acid; HITES hydrocortisone, insulin, transferrin, estrogen, and selenium; UTR untranslated region; MLE-12 Murine Lung Epithelial-12; NC negative control; SDS sodium dodecyl sulfate; PAGE polyacrylamide gel electrophoresis; PVDF polyvinylidene difluoride; BSA bovine serum albumin; TBS Tris-buffered saline; HRP horseradish peroxidase; ECL enhanced chemiluminescence; ELISA enzyme-linked immunosorbent assay; OVA ovalbumin.

Methods and materials

Animals and establishment of murine asthmatic models

C57BL/6 female mice (6-8 wk) were purchased from Charles River (Montreal, Canada). IL-17KO (IL-17A deficient) mice were prepared as previously described (17). All animals were treated and maintained under a protocol approved by the Animal Care Committee of McGill University, following guidelines set by the Canadian Council on Animal Use and Care. To establish asthmatic model, wild type and IL-17KO mice were exposed to purified home dust mite (HDM) extract (Greer Laboratories, Lenoir, NC)

intranasally (25 μg of protein in 10 μl of saline) for 5 days/week for five consecutive weeks. The equivalent volume of saline was used as the control. Each group contained 10 mice. The mice were sacrificed 24 h after the last exposure.

Preparation of bronchoalveolar lavage fluid

The lungs were lavaged using a cannula inserted in the trachea and the lungs were instilled with 0.5 ml PBS. Cytospins were prepared at a density of 0.5×10^6 cells/ml. Differential cell counts were performed using standard morphological criteria on Hema-Gurr-stained cytospins (500 cells/sample) (Merck, Darmstadt, Germany).

Bronchoalveolar lavage cytokine analysis

Aliquots of cell-free bronchoalveolar lavage fluid (BALF) were frozen in liquid N_2 and stored at -80°C. The levels of IL-17, IL-4, IL-5, IL-13 and KC in BALF were analyzed by the Bio-plex system (Bio-Rad, Mississauga, Ontario, Canada) performed in the Goodman Cancer Centre Transgenic Core Facility, McGill University, Canada.

Immunohistochemistry staining

The immunohistochemistry staining for IL-17A (Santa Cruz Biotechnology, Santa Cruz, CA, USA) and α-SMA (Santa Cruz Biotechnology) was performed on paraffin-embedded mouse lung tissue sections as previously described (18).

miRNA expression array

Equal amount of RNA sample from each mouse of different groups was pooled individually for miRNA profiling assay using μParaflo®Microfluidic Biochip miRNA microarray (LC Sciences, Houston, USA).

Real-time quantitative RT-PCR

Three independent assays were performed using quantitative reverse transcription PCR (qRT-PCR) on all mouse samples for each individual miRNA (miR-207, miR-5112, miR-2861, miR-340-5p, miR-6238, miR-181c-5p, miR-6239, miR-365-3p and miR-133b-3p) (Qiagen, Hilden, Germany) and predicted target genes (FASL, TRAF3, ARRB2, Sgk1, PIK3R3, ADAM10 and ADM) (Bio-rad, Foster City, USA). The inflammatory cytokines expression in MLE-12, J774a.1, A549 and U937 cells were analyzed by qRT-PCR as well. Data were presented relative to U6 for miRNA and β-actin for target genes based on calculations of $2^{(-\sigma Ct)}$. The primer sequences for target genes were listed in Table 1. Statistical significance was defined as $p < 0.05$ as measured by the t-test using GraphPad Prism 5 software (GraphPad, San Diego, USA).

Cell culture

MLE-12, 293T, J774a.1, U937 and A549 cell lines were purchased from ATCC (Manassas, VA). MLE-12 were cultured in HITES medium (50:50, DMEM-Ham's F-12) supplemented with 2% FBS, 1:100 insulin/transferrin/selenium supplement. 293T and J774a.1 was maintained with high glycose DMEM with 10% FBS, while U937 and A549 were maintained in 1640 medium with 10% FBS. All the cells culture medium was supplemented with penicillin (100 U/ml) and streptomycin (100 μg/ml). Before the transfection, U937 was differentiated into macrophage-like cells by 72h stimulation with 200nM PMA (phorbol 12-myristate 13-acetate). HITES medium were purchased from Hyclone (Logan, UT, USA), while DMEM and 1640 medium were provided by Gibco (Grand Island, NY, USA). ITS supplement 100X, penicillin/streptomycin 100X and PMA were supplied by Sigma (St. Louis, MO, USA).

MiR-365-3p transfection

After 24 h of starvation with HITES medium containing 0.1% FBS, MLE-12 cells were cultured with different concentrations (0, 1, 10 and 100ng/ml) of mouse recombinant murine IL-17A (R&D Systems, Minneapolis, USA) for 24h, and the expression of miR-365-3p was examined by qRT-PCR. Alternatively, the mimic (100nM) of miR-365-3p was transfected into the MLE-12 cells using X-tremeGENE siRNA Transfection Regent (Roche, Penzberg, Upper Bavaria, Germany) in Opti-MEM (Gibco) for 24h. Expression of ARRB2 was examined by qRT-PCR and Western blot.

We cultured 4 kinds of cells for MiR-365-3p transfection, including MLE-12, J774a.1, U937 and A549. the cells were transfected with the mimic (100nM) of miR-365-3p for 6h, and 24h later, the transfected cells were incubated with 10ng/ml murine IL-17A or 100 ng/ml human IL-17A (R&D Systems). RNA samples were collected 3h after the IL-17A stimulation. qRT-PCR were performed to evaluate the level of cytokines in IL-17A treated cells.

Luciferase reporter assay

Sense and antisense sequences corresponding to a 406-bp fragment from the 3'UTR of ARRB2 with the predicted binding and mutated sites (position 236–243) were amplified from cDNAs of mouse lung tissue by using primers containing the *SacI* restriction site in the sense oligo and *XbaI* restriction site in the

TABLE 1 The sequence of primers for real-time PCR.

Gene	Sequence (5'-3')	Direction
FASL	GAACTCCGTGAGCCAACCC	Forward
	CCAGAGATCAGAGCGGTTCC	Reverse
TRAF3	GCGTGCCAAGAAAGCATCAT	Forward
	CCTCTGCCTTCATTCCGACA	Reverse
ARRB2	ACACGCCACTTCCTCATGTC	Forward
	TCTTCTTGACGGTCTTGGCA	Reverse
Sgk1	ATCCTGACCAAGCCGGACC	Forward
	AAAATCGTTCAGGCCCATCCTT	Reverse
PIK3R3	AAGATGCAGAGTGGTACTGGG	Forward
	CCTGCATTTTCGTTGAGGCA	Reverse
ADAM10	ACACCAAAAACACCAGCGTG	Forward
	GGAAGTGTCCCTCTTCATTCGT	Reverse
ADM	ATTGGGTTCACTCGCTTTCCT	Forward
	GCTGGATGCTTGTAGTTCCCT	Reverse
KC	GCTTGAAGGTGTTGCCCTCAG	Forward
	AAGCCTCGCGACCATTCTTG	Reverse
Mouse IL-6	ACAAAGCCAGAGTCCTTCAGAG	Forward
	AGGAGAGCATTGGAAATTGGGG	Reverse
Mouse β-actin	GATGCCCTGAGGCTCTTTTCC	Forward
	TCTTTACGGATGTCAACGTCACAC	Reverse
IL-8	GATGCCAGTGAAACTTCAAGC	Forward
	ATTGCATCTGGCAACCCTAC	Reverse
Human IL-6	CCAGAGCTGTGCAGATGAGT	Forward
	ATTTGTGGTTGGGTCAGGGG	Reverse
Human ARRB2	TGTGTCTGGGGTGGGGATAC	Forward
	AGCCGCACAGAGTTCCTTTT	Reverse
Human β-actin	TGGCACCCAGCACAATGAA	Forward
	CTAAGTCATAGTCCGCCTAGAAGCA	Reverse

antisense oligo (Sense: 5'-ATCGAGCTCCTGTCCACCC GAGATACAC-3'; Antisense: 5'-AGCTCTAGAGGTACCCT GCAGATGTAGAA-3'; GenePharma, Shanghai, China). To construct luciferase reporter plasmids for ARRB2, the annealed synthetic oligos were cloned downstream to the firefly luciferase into *SacI-XbaI* double digested pmirGLO Dual-Luciferase miRNA target expression vector (Promega, WI, USA).

For the luciferase reporter assay, 293T cells were co-transfected with 250 ng of luciferase reporter plasmid harboring the wild type/mutant binding sites of ARRB2 respectively along with 25nM mimic control/miR-365-3p mimic using X-tremeGENE siRNA Transfection Regent (Roche) in Opti-MEM (Gibco). After 48h of transfection, cells were washed in PBS and lysed in Reporter lysis buffer (Promega), and luciferase activity was measured in a FlexStation 3 microplate reader (Molecular Devices, Sunnyvale, CA, USA) using the Dual-Luciferase reporter assay kit (Promega) according to the manufacturer's instructions. Firefly luciferase activity was normalized to Renilla luciferase activity, and relative luciferase activity was calculated taking firefly luciferase activity of empty pmirGLO transfected cells as 100 percent.

ARRB2 overexpression and knockdown assay

Mouse *ARRB2* mRNA was cloned from cDNA of mouse lung tissue by PCR, the primers containing *NheI* restriction site in the sense oligo and *HindIII* restriction site in the antisense oligo (Sense: 5'- CTAGCTAGCATGGGAGAAAAACCCGGGAC -3'; Antisense: 5'- CAGAAGCTTCTAGCAAAACTGGTCATCACA GTC-3'; TsingKe, Beijing, China). To construct ARRB2-overexpression vector, the gene were cloned into the multiple cloning site of *NheI- HindIII* double digested pcDNA3.1 plasmid (Invitrogen, CA, USA). To knock down the expression of ARRB2, the siRNA was purchased from TsingKe (Sense: 5'- GGACCAGGG UCUUCAAGAATT -3'; Antisense: 5'- UUCUUGAAGACCC UGGUCCTT-3'). For the ARRB2 overexpression or knockdown assay, the pcDNA3.1-ARRB2 plasmid (1μg) and ARRB2-siRNA (130ng) were transfected into MLE-12 cells by X-tremeGENE siRNA Transfection Regent (Roche) in Opti-MEM (Gibco). After 24h transfection, the transfected cells were treated with IL-17 (10ng/ml) for 3 hours and examined by qRT-PCR and Western blot.

Western blot

The protein samples of mouse lung tissue or MLE-12 cells were loaded (5 μg) on a 10% acrylamide SDS-PAGE gel (Bio-Rad, Hercules, USA) for protein separation, followed by transfer to PVDF membranes (Bio-Rad). The blots were then blocked with 1% BSA in 0.1% Tween 20/TBS for 1 h at room temperature and then incubated overnight at 4°C with antibodies specific for ARRB2 (Novus Biologicals, Centennial, CO, USA). After washing with 0.1% Tween 20 in TBS, the membranes were incubated with a 1: 3000 dilution of goat anti-rabbit IgG HRP (EMD Millipore Corp, Burlington, Massachusetts, USA) in 1% solution of powdered milk in TBS/0.1% Tween 20. The membranes were exposed to ECL solution (Bio-Rad) and imaged by chemiluminescence (Clinx Science Instrument, Shanghai, China).

Statistical analysis

Results are expressed as means ± SE. Statistical analysis for expression of IL-17A in mouse lung tissue (Figure 1A) was performed by Mann-Whitney test. The differences between the four groups of mice (Figures 1, 2, 3B, 6B and Supplementary Figures 1, 2) were evaluated by Kruskal-Wallis test. The results of cell culture experiments (Figures 3C, 4, 5, 6C–H) were assessed by t-test. Probability values of $P < 0.05$ were considered significant. Data analysis was performed by using the GraphPad Prism 5 software (GraphPad, San Diego, CA, USA).

Results

IL-17 is indispensable for asthmatic phenotype in HDM-induced murine model

To examine the alteration of IL-17 in asthmatic pathogenesis, a murine model was generated by repeated intranasal challenge with house dust mite extract (HDM) 5 times a week for 5 weeks. The level of IL-17 in bronchoalveolar lavage fluid (BALF) in the asthmatic group were 4-fold higher than control group ($P<0.01$, Figure 1A), which was further confirmed by the elevated proportion of IL-17-positive areas in the lung tissue of asthmatic animals as shown by immunohistochemical analysis (Figures 1B and 1C). According to their morphology, most of the IL-17 expressing cells were categorized as macrophages (19) and lymphocytes. The indispensability of IL-17 to maintain asthmatic phenotype was then verified in IL-17KO mice, which developed significantly less pronounced symptoms upon induction of HDM extract as evidenced by thinner airway wall and reduced inflammatory cell infiltration compared with wild-type asthmatic mice (Supplementary Figure 1). As a typical asthmatic histopathological feature, the thickened layer of smooth muscle was much more prominent in wild-type asthmatic model than IL-17KO asthmatic model, as shown in immunohistochemical staining (Figures 1D, E), which coincided with the distinguishable collagen deposition between the lung tissues of wildtype and IL-17KO asthmatic model (Figures 1F, G).

IL-17 is pivotal for the inflammatory response in murine asthmatic model

To further elucidate the role of IL-17 in the inflammatory response in the murine asthmatic model, inflammatory cells of different types in BALF were firstly numerated, which showed that wildtype asthmatic mice had significantly higher number of inflammatory cells including macrophages, neutrophils and lymphocytes in their BALF than mock treatment (Figure 2A and Supplementary Figure 2). In stark contrast, inflammatory cells in the BALF of mice with IL-17 deficiency were significantly less than wildtype counterparts upon HDM stimulation (Figure 2A), indicating the IL-17 was the main contributor to increase inflammatory cells in BALF during asthmatic pathogenesis.

Moreover, the Th2 cytokines in BALF of HDM-stimulated wild-type mice increased by 6.6-fold for IL-4, 3.4-fold for IL-5 and 4.8-fold for IL-13, respectively, along with 10.6-fold elevation of pro-inflammatory cytokine KC (human IL-8 homologue), which was believed to be the main effector cytokine to recruit neutrophils in asthma. Nevertheless, inflammatory response represented by these cytokines was largely abolished in IL-17KO asthmatic model animals (Figure 2B). The level of IFN-gamma did not show obvious alterations upon HDM treatment in both wildtype and IL-17KO mice, indicating that IFN-gamma did not play a significant role in this asthmatic model (Supplementary Figure 3). Collectively, our data implied that IL-17 was pivotal for the inflammatory response in HDM-induced murine asthma model.

miR-365-3p is downregulated in wildtype asthmatic mice but not in IL-17 KO asthmatic mice

To investigate the miRNAs involved in IL-17-dominated asthmatic pathogenesis, the miRNA expression in the lung tissues of mice were profiled by miRNA microarray assay. The results showed that the expression of 31 miRNAs in WT model mice changed by more than 1.5 times compared with WT control group (Figure 3A), of which 9 were selected for the further analysis due to their exclusive responsiveness to IL-17 since they were not altered between IL-17KO model and IL-17KO control mice. We further verified the expressions of the 9 miRNAs in mouse lung tissue by qRT-PCR (Supplementary Figure 4), which confirmed that only miR-340-5p and miR-365-3p were significantly different between wildtype control and

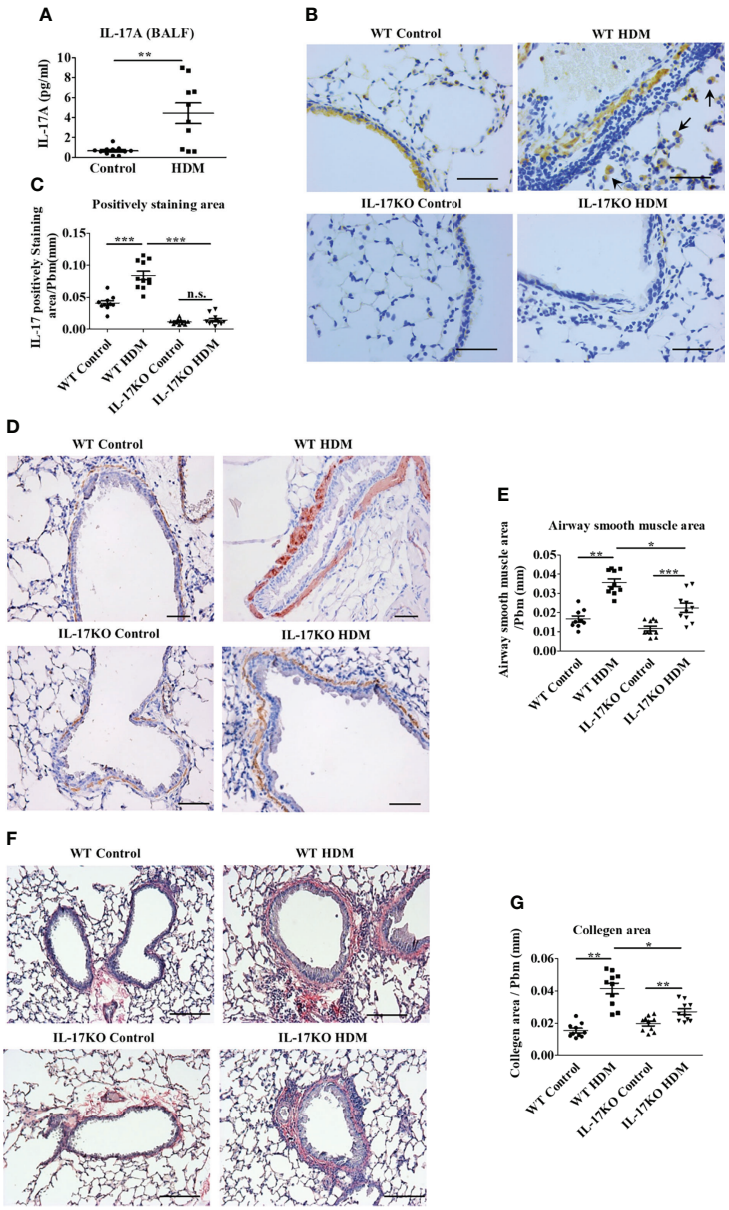

FIGURE 1
IL-17 is necessary to maintain asthmatic phenotype in HDM-induced murine model. **(A)** The level of IL-17A in mouse Bronchoalveolar lavage fluid (BALF) detected by Bio-Plex. N=10. **(B, C)** IHC staining **(B)** and quantitative analysis **(C)** of IL-17 positive cells in mouse lung tissue section. The brown area represents IL-17 positive. Black arrows indicate stained macrophage. Scale bar =50μm. N=10. **(D, E)** IHC staining **(D)** and quantitative analysis **(E)** of airway smooth muscle mass (indicated by Alpha-Smooth Muscle Actin) in mouse lung tissue section. The brown areas represent the airway smooth muscle cells. Scale bars= 100μm. N=10. **(F, G)** collagen deposition analysis in mouse lung tissue. Collagen was stained by Picro Sirius red, the color red indicates the positive staining. Scale bars=100μm. N=10. *, P<0.05, **, P<0.01, ***, P<0.001. n.s., not statistically significant.

wildtype asthmatic group, whereas miR-365-3p is the only one that was exclusively responsive to IL-17 (Figure 3B). The negative regulatory effect of IL-17 on miR-365-3p was further confirmed by a ~90% reduction of expression level upon treatment with 10 ng/mL IL-17 in mouse alveolar epithelial cells (MLE-12) (Figure 3C).

IL-17 induces inflammatory response through downregulating miR-365-3p

Since miR-365-3p was the only miRNA selected to be responsive to IL-17, we next, logically, investigated the mechanisms how miR-365-3p participated in IL-17-mediated inflammatory response in asthma.

10.3389/fimmu.2022.953714

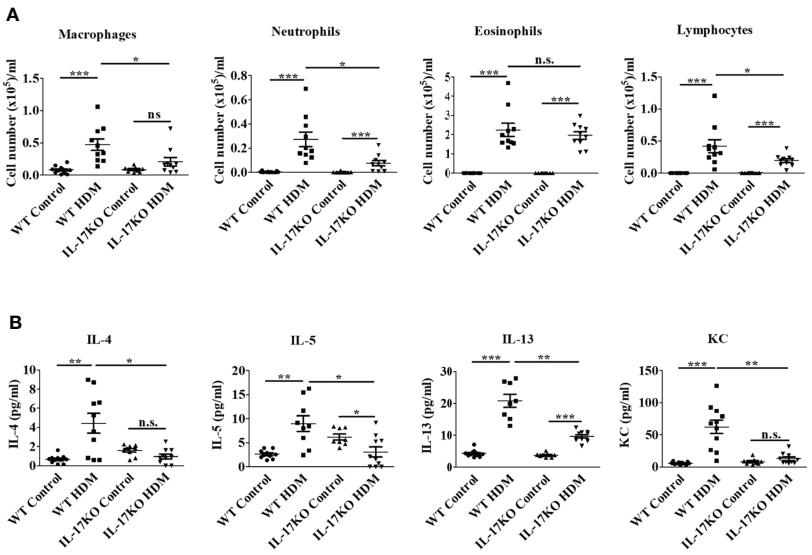

FIGURE 2
Indispensable role of IL-17 in the inflammatory response of HDM-induced asthma in murine model. **(A)** Counts of inflammatory cells in BALF. N=10. **(B)** The level of inflammatory cytokines in BALF. The inflammatory cytokines in BALF were detected by Bio-Plex. N=10. *, P<0.05, **, P<0.01, ***, P<0.001. n.s., not statistically significant.

Both mouse alveolar epithelial cells (MLE-12) and macrophages (J774a.1) were used to examine the role of miR-365-3p in IL-17-mediated inflammation. We then examined the influence of miR-365-3p on the pro-inflammatory activity of IL-17 by transfecting cells with miR-365-3p mimic which effectively rescued the endogenous level of the microRNA (Supplementary Figure 5). While IL-17 stimulated dramatic increase of two representative pro-inflammatory cytokines, IL-6 and KC (official symbol Cxcl1) as shown in qRT-PCR analysis (Figure 4A), rescue of miR-365-3p level could significantly reduce the expression of these two cytokines upon IL-17 treatment, suggesting that miR-365-3p exerted negative regulatory activity on the pro-inflammatory effects of IL-17 in MLE12 cells. Additionally, the negating role of miR-365-3p was also found in mouse monocyte macrophage J774a.1 as well. Increased IL-6 expression of IL-17-stimulated J774a.1 cells was tuned down to the baseline upon addition of miR-365-3p mimic (Figure 4B).

miR-365-3p also serves as negative regulator in IL-17 induced inflammatory response in human airway epithelial cells and macrophages

We then wondered whether miR-365-3p is also negative regulator of IL-17 in human airway cells. By comparing human and murine microRNA sequences using the miRBase database, miR-365-3p was found to be conservatively expressed in both human and mouse, sharing identical sequence (Figure 5A). has-miR-365a-3p, the human homologue of murine miR-365-3p, has been reported to be downregulated in severe asthmatic patients (20, 21), necessitating further examination of its role in IL-17 dominated human asthmatic inflammation response. As expected, human IL-17 (hIL-17) was effective to promote expression of IL-8 (official symbol CXCL8) and IL-6 in human lung epithelial A549 cells by ~2 folds (P<0.01) and ~1.5 folds (P<0.05), respectively, while rescue of endogenous of miR-365-3p almost abolished the IL-17-elevated IL-8 and IL-6 expression (Figure 5B). The negative regulatory effect of miR-365-3p on pro-inflammatory effects of human IL-17 was also verified in human macrophages. Human monocyte U937 was differentiated into macrophages with 200 ng/ml PMA for three days, followed by treatment with hIL-17, which in turn stimulated expression of IL-6. As expected, the supplementation of miR-365-3p mimic negated the increase of IL-6 induced by IL-17 treatment (Figure 5C). Taken together, the data obtained on human cells indicated that miR-365-3p also served as a negative regulator in IL17-mediated inflammation in human airway cells.

ARRB2 is the key mediator of miR-365-3p negated proinflammatory effect of IL-17

To further illustrate the mechanisms how miR-365-3p downregulated IL-17-mediated inflammatory response, we firstly examined the activation of NF-kB pathway, the major signaling pathway of IL-17 and found that phosphorylation level of p65, the key player of Nf-κB pathway did not change in miR-365-3p-

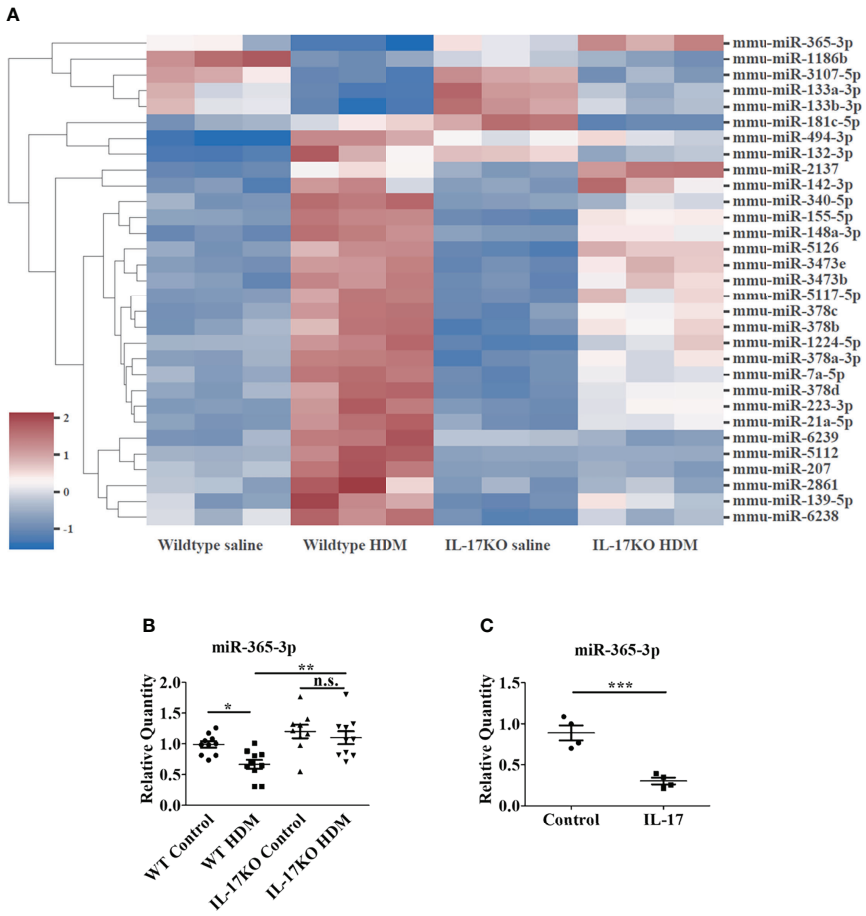

FIGURE 3
miR-365-3p is downregulated in wildtype HDM-induced mice but not in IL-17 KO HDM-induced mice. **(A)** Microarray of dysregulated miRNA in wildtype saline and HDM-induced mice, N=3. **(B)** The level of miR-365-3p examined by qRT-PCR in wild-type and IL-17KO mice. N=10. **(C)** The effect of IL-17 in miR-365-3p expression in MLE-12 cells. The MLE-12 cells were treated by IL-17, and the miR-365-3p expression was tested by qRT-PCR N=4. *, P<0.05, **, P<0.01, ***, P<0.001. n.s., not statistically significant.

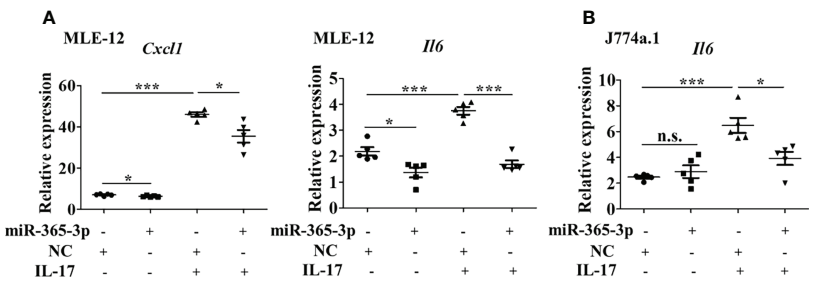

FIGURE 4
miR-365-3p negates IL-17-induced inflammatory cytokines expression in murine epithelial cells and macrophages. **(A)** Effect of miR-365-3p mimic on mRNA expression of KC and IL-6 in MLE-12 cells upon IL-17 treatment. N=5. **(B)** Effect of miR-365-3p mimic on mRNA expression of IL-6 in J774a.1 cells upon IL-17 treatment. N=3. *, P<0.05, ***, P<0.001. n.s., not statistically significant.

10.3389/fimmu.2022.953714

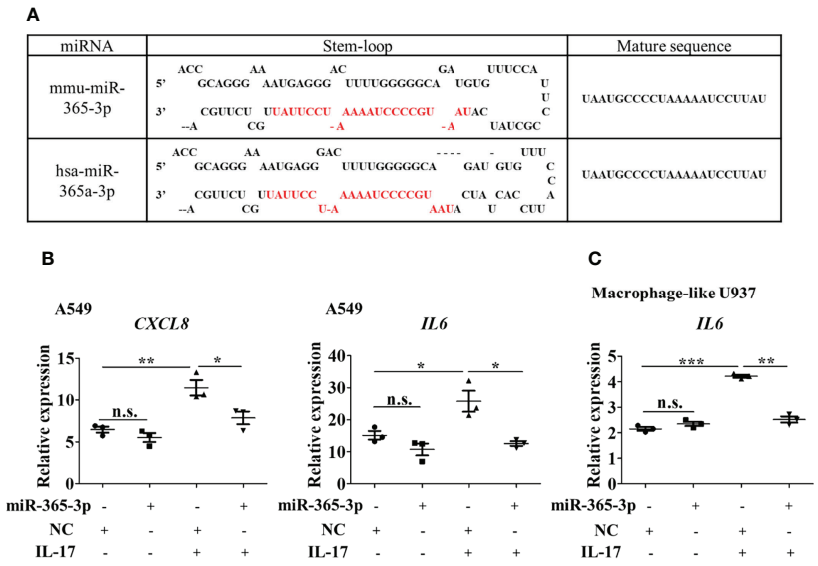

FIGURE 5
miR-365-3p also serves as a negative regulator in hIL-17 induced inflammatory response in human airway epithelial cells and macrophages. **(A)** Sequence comparison of mmu-miR-365-3p and has-miR-365a-3p. **(B)** Effect of miR-365-3p mimic on mRNA expression of IL-8 and IL-6 in human A549 cells upon hIL-17 treatment. N=3. **(C)** Effect of miR-365-3p mimic on mRNA expression of IL-6 in PMA-differentiated U937 cells upon hIL-17 treatment. N=3. *, P<0.05, **,P<0.01, ***, P<0.001. n.s., not statistically significant.

transfected cells in comparison with mock-treated control cells (Supplementary Figure 6), indicating that NF-κB signaling pathway was not involved in the negative regulatory function of miR-365-3p on IL-17 signaling. We then used Targetscan database to predict the potential target genes of miR-365-3p. Among these predicted target genes, critical transcription factors such as Rel, Ets1, Bcl11b, Prdm1, Maf, and Ikzf4, and asthma-related molecules including TRAF3, ARRB2, Sgk1, PIK3R3, ADAM10, ADM Pten and Nr3c1 are the ones that have been reported in PubMed to be involved in pulmonary inflammation response of asthma (Figure 6A), whose expression were subsequently examined in mouse lung tissue (Supplementary Figure 7). The qRT-PCR results showed that the expression of ARRB2, the essential regulator of GPCR signaling pathway, was significantly higher in wildtype asthmatic group than control group, while IL-17 deficiency diminished its responsiveness to HDM stimulation (Figures 6B and Supplementary Figure 7), indicating its involvement of IL-17-mediated pathogenesis.

To validate whether ARRB2 was directly targeted by miR-365-3p, luciferase reporter assay constructed with ARRB2 3'UTR was performed. As shown in Figure 6C, the addition of miR-365-3p mimic reduced the luciferase activity to ~50% of the original level, suggesting mRNA of ARRB2 gene was directed targeted by miR-365-3p, in consistence with the following qRT-PCR and immunoblotting analysis that showed miR-365-3p mimic reduced the expression of ARRB2 in MLE-12 cells at both mRNA and protein level (Figures 6D, E). The regulatory effect of miR-365-3p on ARRB2 expression was further examined in murine lung tissue (Supplementary Figure 8) and human airway cells. As shown in Figure 6F, while hIL-17 elevated the expression of ARRB2, miR-365-3p supplementation significantly decreased the expression of ARRB2, validating the existence of regulatory relationship between miR-365-3p and ARRB2 in human airway cells. These data, convincingly, demonstrated that ARRB2 was one of direct targets of miR-365-3p in both murine and human asthmatic pathogenesis.

We then, logically, investigated whether ARRB2 was the effector of miR-365-3p to negate IL-17-provoked inflammation. To validate the mediator role of ARRB2, its expression level was manipulated by RNA interfering (RNAi) or overexpressing plasmid in MLE-12 cells. Cytokines production from MLE-12 cells transfected with either ARRB2-siRNA or ARRB2-expressing pcDNA3.1 plasmid was quantified by qRT-PCR. As the result shown in **Figures 6G–J**, the expression of KC was significantly reduced in ARRB2-knockdown cells and elevated in ARRB2-overexpression cells.

Collectively, our data supported the notion that miR-365-3p, which was diminished by IL-17 in murine and human asthmatic pathogenesis, functioned as an essential negative mediator in IL-17-stimuated inflammatory response by targeting ARRB2 (Figure 7).

Discussion

Previous studies have unraveled the role of IL-17 in provoking the release of pro-inflammatory cytokines and chemokines such as IL-6, TNF-α, IL-1β, CXCL1, IL-8 and MCP-1 (22) in various inflammatory diseases, of which asthma was highlighted since IL-

10.3389/fimmu.2022.953714

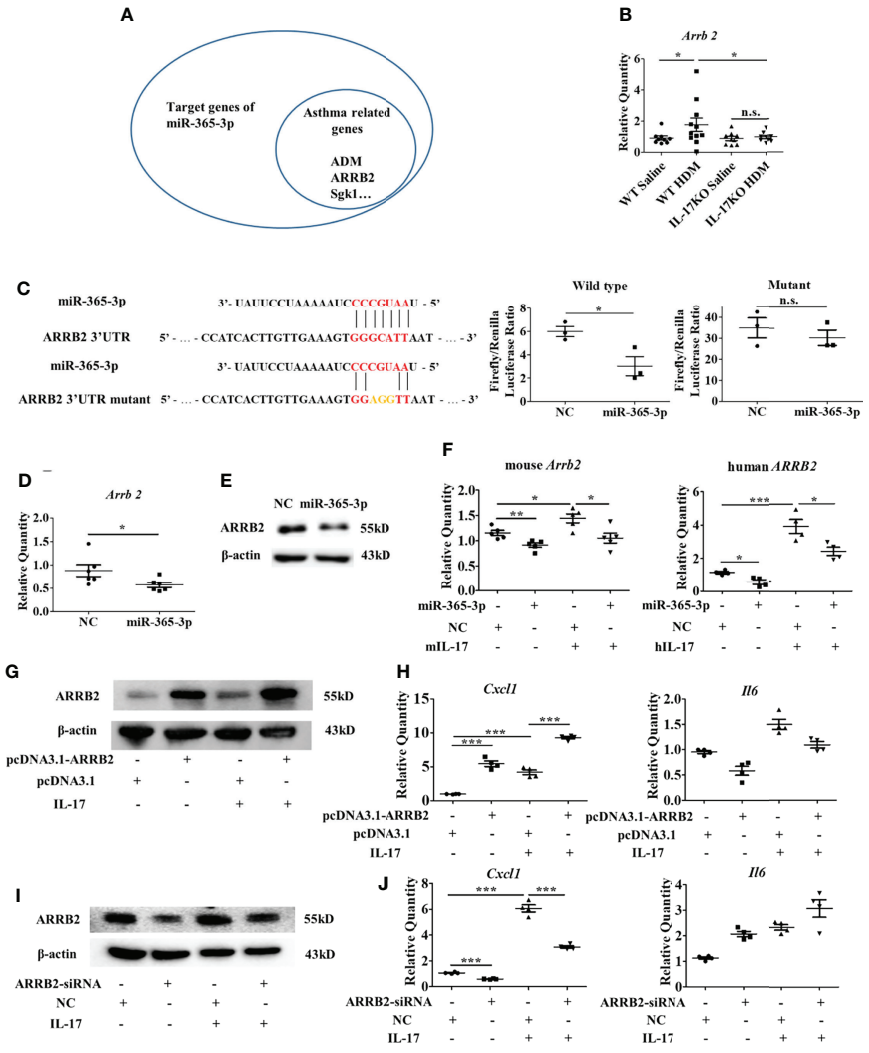

FIGURE 6
ARRB2 is the target gene of miR-365-3p to negate proinflammatory effect of IL-17. **(A)** target genes of miR-365-3p that are related with asthma. **(B)** mRNA expression of *ARRB2* detected by qRT-PCR. N=5. **(C)** The targeting role of miR-365-3p on *ARRB2* examined by reporter fluorescence assays, N=3. **(D)** Effect of miR-365-3p rescue on mRNA level of *ARRB2*. N=6. **(E)** Effect of miR-365-3p rescue on protein level of ARRB2. **(F)** regulatory effect of miR-365-3p on ARRB2 expression in both mouse MLE-12 (left) and human A549 (right) epithelial cells. **(G)** immunoblotting analysis of ARRB2 overexpression from pcDNA3.1 vector in MLE-12 cells. **(H)** expression of KC and IL-6 in ARRB2-overexpression MLE-12 cells upon IL-17 treatment. N=4. **(I)** immunoblotting analysis of ARRB2 knockdown by siRNA in MLE-12 cells. **(J)** expression of KC and IL-6 in ARRB2-knockdown MLE-12 cells upon IL-17 treatment. N=4. *, P<0.05, **, P<0.01, ***, P<0.001. n.s., not statistically significant.

17-orchestrated IL-8 synthesis is crucial to promote neutrophil recruitment and disrupt neutrophil homeostasis in severe and fatal asthma (23). Consistent with previous animal model studies, the asthmatic animal model established in our study using HDM extract induction verified the pivotal role of IL-17 to o maintain the inflammatory phenotype of asthma (24, 25). Nonetheless, due to the different types of allergen and mice used in our asthmatic model, the results obtained in this study slightly differed from the previous murine models. As shown in our results, IL-17 deficiency prohibited neutrophil infiltration rather than eosinophil infiltration in lung tissue and reduces level of KC in BALF, supporting the dominant role of IL-17 in recruiting neutrophils. Furthermore, in our models, IL-17 deficiency did not diminish HDM-induced airway hyper-responsiveness (AHR) (data not shown), which is different from the promoting role of IL-17 in asthmatic airway hyper-responsiveness in previous reports (26).

Although deficiency of Th2 cytokines is believed to promote IL-17 expression in human and IL-17 mediated inflammation in mice (27, 28), severe asthmatic patients frequently display mixed patterns of inflammation including Th2-induced eosinophils and Th17-induced neutrophils (29). Our results, nonetheless, revealed that IL-17 deficiency was also effective to reduce the production of Th-2

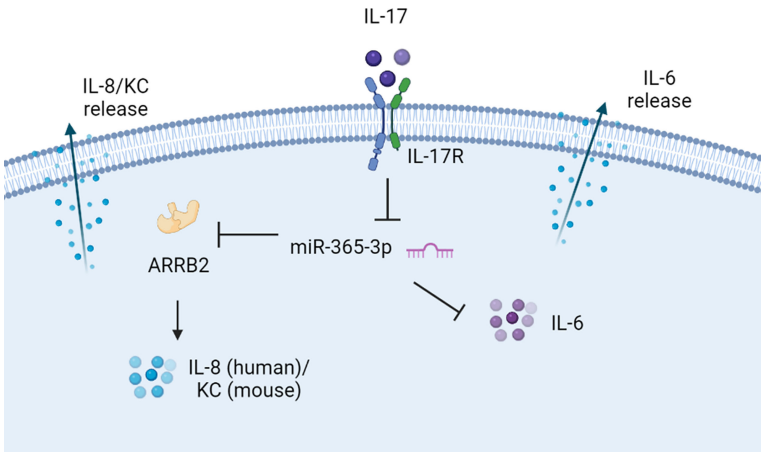

FIGURE 7
The proposed scheme of negative regulating role of miR-365-3p in IL-17 induced KC and IL-6 production. miR-365-3p, which was diminished by IL-17 in murine and human asthmatic pathogenesis, functioned as an essential negative mediator to suppress IL8 (KC for mouse) and IL-6 upon IL-17 stimulation by targeting ARRB2.

cytokines such as IL-4, IL-5, and IL-13, implying a synergistic interaction between Th2 and Th17 responses. However, IL-17 deficiency did not reduce the eosinophil recruitment in the asthmatic mouse model. Given that anti-IL5 therapy had limited impact on eosinophil recruitment and asthma exacerbations (30, 31), there might be a potential alternative mechanism of eosinophil infiltration.

To our knowledge, this is the first report describing a link between miR-365-3p and IL-17 in asthma. A total of 31 miRNAs were dysregulated in WT HDM mice compared with WT control group. Among these altered miRNAs, miR-155-5p (32), miR-148a-3p (14), miR-494-3p (33), miR-142-3p (34), miR-378d (35), miR-181c-5p (36), miR-21a-5p (37), miR-3107-5p (38) and miR-133a-3p (39) have been reported to be involved in asthma, but none of them were associated with IL-17 activity in our analysis. Nevertheless, we found miR-365-3p is negatively regulated by IL-17 in HDM-induced asthma mice, which coincided with the observations in human asthma patients demonstrating that human homologue of murine miR-365-3p, hsa-miR-365a-3p, was negatively correlated with severity of asthma and serum IL-17 level (20, 21). And reasonably, miR-365-3p has the potential to be a biomarker for the IL17-dominated asthmatic inflammation.

Whether the downregulated miR-365-3p was active participator or just bystander in IL-17-mediated inflammation was examined by manipulating its level through introducing exogeneous miR-365-3p mimics. Our results confirmed that miR-365-3p actively antagonized IL-17-mediated inflammatory cytokine elevation from airway epithelial cells and macrophages, not only in murine cells but also in human cells, revealing the universal negating effect of miR-365-3p against IL-17 across the two species. Although various pathways including p38, Erk, NF-κB and PI3K/Akt-dependent pathways have been reported to be involved in the pro-inflammatory activity of IL-17 in previous studies (40, 41), the participation and possible role of microRNA in IL-17-initiated asthmatic inflammation has been barely referred. Our current finding, for the first time, established the correlation between IL-17 and miRNA in asthmatic pathogenesis. Nonetheless, since role of miRNAs has been well recognized in asthma, our current finding added a new expected piece to the puzzle, reinforcing a recent study that miRNA was indispensable for IL-17 to induce secretion of inflammatory factors and chemokines by astrocytes in experimental autoimmune encephalomyelitis (16).

To further illustrate the downstream targets of miR-365-3p to negate IL-17-mediated asthmatic inflammation, ARRB2 (beta-arrestin-2), an essential regulator of G protein-coupled receptor signaling, was selected out in the lung tissue of diseased animals. ARRB2, well known to regulate G protein-coupled receptor function and receptor internalization (42), has been also recognized as an important pro-inflammatory mediator by promoting $CD4^+$ T cells migration, Th2 cell chemotaxis, and inflammatory cytokine production in asthma (43, 44). Increased ARRB2 expression in OVA (ovalbumin)-challenged mice and diminished inflammatory responses in ARRB2 deficiency mice (45) implied the key role of ARRB2 in the pathogenesis of asthma. Consistently, our study reinforced the essential regulatory role of ARRB2, as the target of miR-365-3p, in the inflammatory response in IL-17-dependent asthma pathogenesis.

Although both miR-365-3p and ARRB2 have been reported to exert the regulatory roles in cytokine production individually (46, 47), this study provided the first clue to connect these two regulators together in IL-17-mediated asthmatic airway inflammation and proposed the possible IL-7/miR-365-3p/ARRB2/KC(IL-8) axis in asthmatic inflammation (Figure 7). It

was also noted that alteration of ARRB2 expression did not influence IL-6 synthesis upon IL-17 stimulation. Given the previous study indicating that miR-365-3p could directly target IL-6 mRNA for degradation (48), ARRB2 may not participate in the regulation of IL-6.

In summary, through miRNAs expression profiling in wildtype and IL-17KO chronic asthmatic mouse models, we established the first connection between miR-365-3p and IL-17 in asthmatic pathogenesis and elucidated the possible mechanisms thereof, whereas more details remain to be further explored. This current study provides a new perspective to understand the pathological role of miRNA in IL-17-mediated asthmatic inflammation and may inspire new therapeutic strategies to alleviate neutrophilic airway inflammation in asthmatic pathogenesis.

Conclusions

Taken together, these findings suggest that IL-17 plays an important role in the inflammatory response and airway remodeling, and miR-365-3p may be a key miRNA involved in this regulation.

Data availability statement

The data that support the findings of this study are available from the corresponding authors upon request. The miRNA microarray data presented in the study are deposited in the GEO repository, accession number GSE207659. Website Address: https://www.ncbi.nlm.nih.gov/geo/query/acc.cgi?acc=GSE207659.

Ethics statement

The animal study was reviewed and approved by Animal Care Committee of McGill University.

Author contributions

WW and JF performed qRT-PCR, western blotting and analyzed the results. YL coordinated the animal experiments. XQ cultured the cells, DS coordinated the histochemistry staining. QQ coordinated the animal experiments. TX did the data analysis. QH revised the manuscript. XD performed ELISA. DX and YC designed the study, performed the animal experiments, and drafted the manuscript. All authors contributed to the article and approved the submitted version.

Funding

This study was supported by the National Natural Science Foundation of China (32070134 to DX and 31501044 to YC), Natural Science Basic Research Plan in Shaanxi Province of China (2020JM-002), International Cooperation, Exchange Program of Science and Technology of Shaanxi Province (2020KW-046), and The Science and Technology Innovation Base-Open and Sharing Platform of Science and Technology Resource Project of Shaanxi Province (2019PT-26).

Acknowledgments

We thank H. Li from School of Life Science and Technology, Xi'an Jiaotong University and Instrument Analysis Center of Xi'an Jiaotong University for their (Z. Ren and Y. Chen) technical assistance.

Conflict of interest

The authors declare that the research was conducted in the absence of any commercial or financial relationships that could be construed as a potential conflict of interest.

Publisher's note

Supplementary material

The Supplementary Material for this article can be found online at: https://www.frontiersin.org/articles/10.3389/fimmu.2022.953714/full#supplementary-material

References

1. Girodet PO, Ozier A, Bara I, Tunon de Lara JM, Marthan R, Berger P. Airway remodeling in asthma: new mechanisms and potential for pharmacological intervention. *Pharmacol Ther* (2011) 130:325–37. doi: 10.1016/j.pharmthera.2011.02.001

2. Gurczynski SJ, Moore BB. IL-17 in the lung: the good, the bad, and the ugly. *Am J Physiol Lung Cell Mol Physiol 314* (2018) 314(1):L6–L16. doi: 10.1152/ajplung.00344.2017

3. Chang Y, Al-Alwan L, Risse PA, Roussel L, Rousseau S, Halayko AJ, et al. TH17 cytokines induce human airway smooth muscle cell migration. *J Allergy Clin Immunol* (2011) 127:1046–53 e1-2. doi: 10.1016/j.jaci.2010.12.1117

4. Chang Y, Al-Alwan L, Risse PA, Halayko AJ, Martin JG, Baglole CJ, et al. Th17-associated cytokines promote human airway smooth muscle cell proliferation. *FASEB J* (2012) 26:5152–60. doi: 10.1096/fj.12-208033

5. Al-Alwan LA, Chang Y, Baglole CJ, Risse PA, Halayko AJ, Martin JG, et al. Autocrine-regulated airway smooth muscle cell migration is dependent on IL-17-induced growth-related oncogenes. *J Allergy Clin Immunol* (2012) 130:977–85 e6. doi: 10.1016/j.jaci.2012.04.042

6. Chesne J, Braza F, Mahay G, Brouard S, Aronica M, Magnan A. IL-17 in severe asthma. where do we stand? *Am J Respir Crit Care Med* (2014) 190:1094–101. doi: 10.1164/rccm.201405-0859PP

7. Al-Ramli W, Prefontaine D, Chouiali F, Martin JG, Olivenstein R, Lemiere C, et al. T(H)17-associated cytokines (IL-17A and IL-17F) in severe asthma. *J Allergy Clin Immunol* (2009) 123:1185–7. doi: 10.1016/j.jaci.2009.02.024

8. Bullens DM, Truyen E, Coteur L, Dilissen E, Hellings PW, Dupont LJ, et al. IL-17 mRNA in sputum of asthmatic patients: linking T cell driven inflammation and granulocytic influx? *Respir Res* (2006) 7:135. doi: 10.1186/1465-9921-7-135

9. Oglesby IK, McElvaney NG, Greene CM. MicroRNAs in inflammatory lung disease–master regulators or target practice? *Respir Res* (2010) 11:148. doi: 10.1186/1465-9921-11-148

10. Lu TX, Munitz A, Rothenberg ME. MicroRNA-21 is up-regulated in allergic airway inflammation and regulates IL-12p35 expression. *J Immunol* (2009) 182:4994–5002. doi: 10.4049/jimmunol.0803560

11. Solberg OD, Ostrin EJ, Love MI, Peng JC, Bhakta NR, Hou L, et al. Airway epithelial miRNA expression is altered in asthma. *Am J Respir Crit Care Med* (2012) 186:965–74. doi: 10.1164/rccm.201201-0027OC

12. Haj-Salem I, Fakhfakh R, Berube JC, Jacques E, Plante S, Simard MJ, et al. MicroRNA-19a enhances proliferation of bronchial epithelial cells by targeting TGFbetaR2 gene in severe asthma. *Allergy* (2015) 70:212–9. doi: 10.1111/all.12551

13. Perry MM, Baker JE, Gibeon DS, Adcock IM, Chung KF. Airway smooth muscle hyperproliferation is regulated by microRNA-221 in severe asthma. *Am J Respir Cell Mol Biol* (2014) 50:7–17. doi: 10.1165/rcmb.2013-0067OC

14. Specjalski K, Jassem E. MicroRNAs: Potential biomarkers and targets of therapy in allergic diseases? *Arch Immunol Ther Exp (Warsz)* (2019) 67:213–23. doi: 10.1007/s00005-019-00547-4

15. Maneechotesuwan K. Role of microRNA in severe asthma. *Respir Investig* (2019) 57:9–19. doi: 10.1016/j.resinv.2018.10.005

16. Liu X, He F, Pang R, Zhao D, Qiu W, Shan K, et al. Interleukin-17 (IL-17)-induced microRNA 873 (miR-873) contributes to the pathogenesis of experimental autoimmune encephalomyelitis by targeting A20 ubiquitin-editing enzyme. *J Biol Chem* (2014) 289:28971–86. doi: 10.1074/jbc.M114.577429

17. Nakae S, Komiyama Y, Nambu A, Sudo K, Iwase M, Homma I, et al. Antigen-specific T cell sensitization is impaired in IL-17-deficient mice, causing suppression of allergic cellular and humoral responses. *Immunity* (2002) 17:375–87. doi: 10.1016/S1074-7613(02)00391-6

18. Chang Y, Nadigel J, Boulais N, Bourbeau J, Maltais F, Eidelman DH, et al. CD8 positive T cells express IL-17 in patients with chronic obstructive pulmonary disease. *Respir Res* (2011) 12:43. doi: 10.1186/1465-9921-12-43

19. Song C, Luo L, Lei Z, Li B, Liang Z, Liu G, et al. IL-17-producing alveolar macrophages mediate allergic lung inflammation related to asthma. *J Immunol* (2008) 181:6117–24. doi: 10.4049/jimmunol.181.9.6117

20. Woeller CF, Thatcher TH, Van Twisk D, Pollock SJ, Croasdell A, Kim N, et al. Detection of serum microRNAs from department of defense serum repository: Correlation with cotinine, cytokine, and polycyclic aromatic hydrocarbon levels. *J Occup Environ Med* (2016) 58:S62–71. doi: 10.1097/JOM.0000000000000742

21. Zhang S, Laryea Z, Panganiban R, Lambert K, Hsu D, Ishmael FT. Plasma microRNA profiles identify distinct clinical phenotypes in human asthmatics. *J Trans Genet Genomics* (2018) 72(12)1962–1971. doi: 10.20517/jtgg.2018.22

22. Bettelli E, Korn T, Oukka M, Kuchroo VK. Induction and effector functions of T(H)17 cells. *Nature* (2008) 453:1051–7. doi: 10.1038/nature07036

23. Pelletier M, Maggi L, Micheletti A, Lazzeri E, Tamassia N, Costantini C, et al. Evidence for a cross-talk between human neutrophils and Th17 cells. *Blood* (2010) 115:335–43. doi: 10.1182/blood-2009-04-216085

24. Chenuet P, Fauconnier L, Madouri F, Marchiol T, Rouxel N, Ledru A, et al. Neutralization of either IL-17A or IL-17F is sufficient to inhibit house dust mite induced allergic asthma in mice. *Clin Sci (Lond)* (2017) 131:2533–48. doi: 10.1042/CS20171034

25. Chesne J, Braza F, Chadeuf G, Mahay G, Cheminant MA, Loy J, et al. Prime role of IL-17A in neutrophilia and airway smooth muscle contraction in a house dust mite-induced allergic asthma model. *J Allergy Clin Immunol* (2015) 135:1643–1643 e3. doi: 10.1016/j.jaci.2014.12.1872

26. Kudo M, Melton AC, Chen C, Engler MB, Huang KE, Ren X, et al. IL-17A produced by alphabeta T cells drives airway hyper-responsiveness in mice and enhances mouse and human airway smooth muscle contraction. *Nat Med* (2012) 18:547–54. doi: 10.1038/nm.2684

27. Newcomb DC, Boswell MG, Zhou W, Huckabee MM, Goleniewska K, Sevin CM, et al. Human TH17 cells express a functional IL-13 receptor and IL-13 attenuates IL-17A production. *J Allergy Clin Immunol* (2011) 127:1006–13 e1-4. doi: 10.1016/j.jaci.2010.11.043

28. Newcomb DC, Boswell MG, Huckabee MM, Goleniewska K, Dulek DE, Reiss S, et al. IL-13 regulates Th17 secretion of IL-17A in an IL-10-dependent manner. *J Immunol* (2012) 188:1027–35. doi: 10.4049/jimmunol.1102216

29. Pelaia G, Vatrella A, Busceti MT, Gallelli L, Calabrese C, Terracciano R, et al. Cellular mechanisms underlying eosinophilic and neutrophilic airway inflammation in asthma. *Mediators Inflammation* (2015) 2015:879783. doi: 10.1155/2015/879783

30. Farne HA, Wilson A, Powell C, Bax L, Milan SJ. Anti-IL5 therapies for asthma. *Cochrane Database Syst Rev 9* (2017) 9(9):CD010834. doi: 10.1002/14651858.CD010834.pub3

31. Flood-Page PT, Menzies-Gow AN, Kay AB, Robinson DS. Eosinophil's role remains uncertain as anti-interleukin-5 only partially depletes numbers in asthmatic airway. *Am J Respir Crit Care Med* (2003) 167:199–204. doi: 10.1164/rccm.200208-789OC

32. Zhou H, Li J, Gao P, Wang Q, Zhang J. miR-155: A novel target in allergic asthma. *Int J Mol Sci 17* (2016) 17(10):1773. doi: 10.3390/ijms17101773

33. Wang Y, Yang L, Li P, Huang H, Liu T, He H, et al. Circulating microRNA signatures associated with childhood asthma. *Clin Lab* (2015) 61:467–74. doi: 10.7754/Clin.Lab.2014.141020

34. Munitz A, Karo-Atar D, Foster PS. Asthma diagnosis: MicroRNAs to the rescue. *J Allergy Clin Immunol* (2016) 137:1447–8. doi: 10.1016/j.jaci.2016.02.013

35. Li P, Lang X, Xia S. Elevated expression of microRNA-378 in children with asthma aggravates airway remodeling by promoting the proliferation and apoptosis resistance of airway smooth muscle cells. *Exp Ther Med* (2019) 17:1529–36. doi: 10.3892/etm.2018.7141

36. Taka S, Tzani-Tzanopoulou P, Wanstall H, Papadopoulos NG. MicroRNAs in asthma and respiratory infections: Identifying common pathways. *Allergy Asthma Immunol Res* (2020) 12:4–23. doi: 10.4168/aair.2020.12.1.4

37. Plank MW, Maltby S, Tay HL, Stewart J, Eyers F, Hansbro PM, et al. MicroRNA expression is altered in an ovalbumin-induced asthma model and targeting miR-155 with antagomirs reveals cellular specificity. *PloS One* (2015) 10: e0144810. doi: 10.1371/journal.pone.0144810

38. Tang GN, Li CL, Yao Y, Xu ZB, Deng MX, Wang SY, et al. MicroRNAs involved in asthma after mesenchymal stem cells treatment. *Stem Cells Dev* (2016) 25:883–96. doi: 10.1089/scd.2015.0339

39. Chen Y, Mao ZD, Shi YJ, Qian Y, Liu ZG, Yin XW, et al. Comprehensive analysis of miRNA-mRNA-lncRNA networks in severe asthma. *Epigenomics* (2019) 11:115–31. doi: 10.2217/epi-2018-0132

40. Hwang SY, Kim JY, Kim KW, Park MK, Moon Y, Kim WU, et al. IL-17 induces production of IL-6 and IL-8 in rheumatoid arthritis synovial fibroblasts *via* NF-kappaB- and PI3-kinase/Akt-dependent pathways. *Arthritis Res Ther* (2004) 6: R120–8. doi: 10.1186/ar1038

41. Laan M, Lotvall J, Chung KF, Linden A. IL-17-induced cytokine release in human bronchial epithelial cells *in vitro*: role of mitogen-activated protein (MAP) kinases. *Br J Pharmacol* (2001) 133:200–6. doi: 10.1038/sj.bjp.0704063

42. Ha H, Debnath B, Neamati N. Role of the CXCL8-CXCR1/2 axis in cancer and inflammatory diseases. *Theranostics* (2017) 7:1543–88. doi: 10.7150/thno.15625

43. Wang G, Liu Y, Yang M, Liu S, Ma L, Gong S. Effect of β-arrestin 2 on cytokine production of CD4+ T lymphocytes of mice with allergic asthma. *Indian J Exp Biol* (2011) 49pp:585–93.

44. Nichols HL, Saffeddine M, Theriot BS, Hegde A, Polley D, El-Mays T, et al. β-Arrestin-2 mediates the proinflammatory effects of proteinase-activated receptor-2 in the airway. *Proc Natl Acad Sci* (2012) 109:16660–5. doi: 10.1073/pnas.1208881109

45. Walker JK, Fong AM, Lawson BL, Savov JD, Patel DD, Schwartz DA, et al. Beta-arrestin-2 regulates the development of allergic asthma. *J Clin Invest* (2003) 112:566–74. doi: 10.1172/JCI200317265

46. Xu Z, Xiao SB, Xu P, Xie Q, Cao L, Wang D, et al. miR-365, a novel negative regulator of interleukin-6 gene expression, is cooperatively regulated by Sp1 and NF-kappaB. *J Biol Chem* (2011) 286:21401–12. doi: 10.1074/jbc.M110.198630

47. Gaffal E, Jakobs M, Glodde N, Schroder R, Kostenis E, Tuting T. Beta-arrestin 2 inhibits proinflammatory chemokine production and attenuates contact allergic inflammation in the skin. *J Invest Dermatol* (2014) 134:2131–7. doi: 10.1038/jid.2014.117

48. Lin B, Feng DG, Wang F, Wang JX, Xu CG, Zhao H, et al. MiR-365 participates in coronary atherosclerosis through regulating IL-6. *Eur Rev Med Pharmacol Sci* (2016) 20:5186–92.

frontiers | Frontiers in Immunology

TYPE Original Research
PUBLISHED 28 July 2022
DOI 10.3389/fimmu.2022.937832

OPEN ACCESS

EDITED BY
Bao-Hui Cheng,
Institute of ENT and Shenzhen Key Laboratory of ENT, China

REVIEWED BY
Zhe Xing,
Zhengzhou University, China
Tao Han,
Northern Theater General Hospital, China

*CORRESPONDENCE
Ji Wang
doctorwang2009@126.com
Xiaoshan Zhao
zhaoxs0609@163.com

†These authors have contributed equally to this work

SPECIALTY SECTION
This article was submitted to Immunological Tolerance and Regulation, a section of the journal Frontiers in Immunology

RECEIVED 06 May 2022
ACCEPTED 04 July 2022
PUBLISHED 28 July 2022

CITATION
Yang F, Wang T, Yan P, Li W, Kong J, Zong Y, Chao X, Li W, Zhao X and Wang J (2022) Identification of pyroptosis-related subtypes and establishment of prognostic model and immune characteristics in asthma. *Front. Immunol.* 13:937832. doi: 10.3389/fimmu.2022.937832

Identification of pyroptosis-related subtypes and establishment of prognostic model and immune characteristics in asthma

Fan Yang[1,2], Tieshan Wang[3], Peizheng Yan[4], Wanyang Li[5], Jingwei Kong[1,2], Yuhan Zong[1,2], Xiang Chao[1], Weijie Li[6], Xiaoshan Zhao[7*†] and Ji Wang[2*†]

[1]College of Traditional Chinese Medicine, Beijing University of Chinese Medicine, Beijing, China, [2]National Institute of Traditional Chinese Medicine (TCM) Constitution and Preventive Medicine, Beijing University of Chinese Medicine, Beijing, China, [3]Beijing Research Institute of Chinese Medicine, Beijing University of Chinese Medicine, Beijing, China, [4]College of Pharmacy, Shandong University of Traditional Chinese Medicine, Jinan, China, [5]Department of Clinical Nutrition, Chinese Academy of Medical Sciences - Peking Union Medical College, Peking Union Medical College Hospital, Beijing, China, [6]College of Traditional Chinese Medicine, Shandong University of Chinese Medicine, Jinan, China, [7]School of Chinese Medicine, Southern Medical University, Guangzhou, China

Background: Although studies have shown that cell pyroptosis is involved in the progression of asthma, a systematic analysis of the clinical significance of pyroptosis-related genes (PRGs) cooperating with immune cells in asthma patients is still lacking.

Methods: Transcriptome sequencing datasets from patients with different disease courses were used to screen pyroptosis-related differentially expressed genes and perform biological function analysis. Clustering based on K-means unsupervised clustering method is performed to identify pyroptosis-related subtypes in asthma and explore biological functional characteristics of poorly controlled subtypes. Diagnostic markers between subtypes were screened and validated using an asthma mouse model. The infiltration of immune cells in airway epithelium was evaluated based on CIBERSORT, and the correlation between diagnostic markers and immune cells was analyzed. Finally, a risk prediction model was established and experimentally verified using differentially expressed genes between pyroptosis subtypes in combination with asthma control. The cMAP database and molecular docking were utilized to predict potential therapeutic drugs.

Results: Nineteen differentially expressed PRGs and two subtypes were identified between patients with mild-to-moderate and severe asthma conditions. Significant differences were observed in asthma control and FEV1 reversibility between the two subtypes. Poor control subtypes were closely related to glucocorticoid resistance and airway remodeling. BNIP3 was identified as a diagnostic marker and associated with immune cell infiltration

such as, M2 macrophages. The risk prediction model containing four genes has accurate classification efficiency and prediction value. Small molecules obtained from the cMAP database that may have therapeutic effects on asthma are mainly DPP4 inhibitors.

Conclusion: Pyroptosis and its mediated immune phenotype are crucial in the occurrence, development, and prognosis of asthma. The predictive models and drugs developed on the basis of PRGs may provide new solutions for the management of asthma.

KEYWORDS

pyroptosis-related genes, asthma, prognostic model, immune cell, DPP4

Introduction

Asthma is a respiratory disease characterized by chronic inflammation of airways. Its prominent features include airway hyperresponsiveness and recurrent attacks. Although asthma has been extensively investigated, pathogenesis requires further investigation and existing studies mainly focus on the airway inflammatory mechanism, immune regulation mechanism, neuromodulatory mechanism, and genetic and environmental factors (1). Severe asthma refers to the type that requires step 4 or 5 treatment, as recommended by Global Initiative for Asthma (GINA). This kind of asthma is more difficult to control than its mild-to-moderate counterpart (2), thereby reducing the quality of life and increasing the mortality of patients in this group. A variety of immune cells are involved throughout the course of asthma. The GINA guidelines indicated that monoclonal antibody-based immunotherapy is recommended for patients with severe asthma (3). Although severe asthma is mostly characterized by type-I immunity, drugs typically used are generally under target type-I immunity and sometimes unavailable (4). Therefore, cutting off the progression of mild-to-moderate to severe asthma cases is still the key to asthma management given the disease characteristics and health economic expenditure because sensitive assessment tools are required in identifying early mild-to-moderate asthma patients and the development of drugs to treat asthma from other pathophysiological perspectives and help patients achieve clinical control (5).

Cell pyroptosis has gradually become an important research direction in the exploration of asthma pathogenesis. Pyroptosis is a new mode of programmed cell death that has been confirmed in recent years. Pyroptosis is characterized by the change of osmotic pressure inside and outside the cell due to the perforation of activated gasdermin D (GSDMD) in the cell membrane and flow of extracellular material into the cell that result in its final rupture and release of massive proinflammatory factors (6). Gasdermin B (GSDMB) intervenes in various physiological and pathological processes, such as inflammation, coagulation, and cell differentiation, by regulating cell pyroptosis. Moreover, gene polymorphism of GSDMB is highly correlated with the pathogenesis of asthma (7). The expression of GSDMB in airway epithelial cells of patients with asthma is upregulated. Cell pyroptosis induced by the GSDMB protein can be eliminated when deleting the entire exon 6 from the splicing variant rs11078928 of the GSDMB gene to reduce the risk of asthma (8). Additionally, immune cells mediate the progression of asthma through cell pyroptosis. Activated caspase-11 induces pyroptosis, alveolar macrophages from patients with asthma exhibit increased expression of caspase-4 (human homologue of caspase-11), and prostaglandin E2 can exert protective effects against allergic airway inflammation by inhibiting caspase-11-/caspase-4-dependent pyroptosis in mouse and human macrophages (9). Although existing studies have initially reported the role of pyroptosis and pyroptosis-related genes (PRGs) in the development and progression of asthma, research on expression differences of PRGs between mild-to-moderate and severe asthma cases is still lacking and the role of cell pyroptosis in immune responses in airway epithelial tissues remains unclear. Moreover, studies that combine the situation of asthma control and immune imbalance as well as comprehensively analyze the role of PRGs in asthma are limited.

We excluded key PRGs related to the progression and control of asthma using machine learning method, compared the differences of immune cell infiltration under different PRG expression patterns, and established the relationship between key PRGs and immune cells in this study. A pyroptosis-related prognostic model was constructed to predict the control of asthmatic patients, and animal experiments were performed to verify the effectiveness of the model and screen potential therapeutic agents for high-risk patients.

Materials and methods

Data source

The microarray datasets GSE89809 and GSE104468 are downloaded from the GEO database (https://www.ncbi.nlm.nih.gov/geo/) (10, 11). The "*limma*" package was used to screen differentially expressed genes (DEGs) (12), and $P < 0.05$ and $|\log2\ FC| > 0.585$ were considered statistically significant. The 227 pyroptosis-related genes are from the Genecards (https://www.genecards.org/) website. The site uses GeneCards Inferred Functionality Scores (GIFtS) to annotate each relevant gene and generate a correlation score. In this study, pyroptosis was used as the keyword to search related genes, and 227genes with GIFtS > 30 were included for follow-up study.

Classification and functional enrichment analysis of PRG-related subtypes in asthma

Unsupervised cluster analysis was carried out according to the difference of PRG expression between mild-to-moderate and severe asthma cases to identify various subtypes of asthma (13, 14). A consensus clustering algorithm was used to evaluate the cluster numbers and robustness. The R package "*ConsensuClusterPlus*" was applied to implement these steps for 1000 iterations to guarantee the robustness of classification (15). Weighted gene coexpression network analysis for specific subtypes was performed with the R package "*WGCNA*." (16, 17) We first determined the appropriate soft threshold power to achieve a scale-free topology. Hierarchical clustering was then performed to identify modules, and a phylogenetic cluster map was constructed to divide similar gene expression levels into different modules. The correlation between the phenotype composed of various clinical information and each module was evaluated using Pearson correlation analysis. The module with the maximum correlation with the trait was selected for subsequent analysis. The ChEA3 database (https://maayanlab.cloud/chea3/) includes a large number of independently published ChIP-seq data and integrates transcription factor coexpression data on the basis of RNA-seq data (18). The transcriptional regulatory network of key modules is predicted from this database. Gene set enrichment analysis (GSEA) was performed on the gene expression matrix through the "*clusterProfiler*" package, and "*c2.cp.kegg.v7.0.symbols.gmt*" was selected as the reference gene set. We used the "*clusterProfiler*" and "*ggplot2*" packages to perform Gene Ontology (GO) and Kyoto Encyclopedia of Genes and Genomes (KEGG) enrichment analyses on DEGs, respectively (19, 20).

Screening, expression regulation, and immune cell infiltration analyses of diagnostic markers associated with pyroptosis subtypes

We used least absolute shrinkage and selection operator (LASSO) logistic regression to perform feature selection of screening diagnostic markers for asthma (21). LASSO is a popular algorithm, which was extensively utilized in medical studies (22–26). The LASSO algorithm was applied with the "*glmnet*" package (27). The regulatory prediction of noncoding RNAs for diagnostic markers was first analyzed using databases, including RNA22, miRDB, and RNAInter, to select miRNAs with intersections (28). The literature was then reviewed to select miRNAs with biological roles in asthma for further analysis. miRNet 2.0 database (www.mirnet.ca/miRNet/home.xhtml) and starBase (http://starbase.sysu.edu.cn/)) are utilized to predict the target lncRNA of miRNA and finally establish the ceRNA network (29, 30). The degree of immune cell infiltration in the airway epithelium was assessed using the CIBERSORT algorithm to determine the abundance of 22 immune cell subsets, and differences in immune cell infiltration between groups were visualized through the "*ggplot2*" package (31, 32). Finally, Spearman correlation analysis was performed on all immune cells and diagnostic markers, and the positive or negative correlation between them was determined with the "*ggstatsplot*" package.

Construction of a risk signature associated with asthma control

The univariate Cox regression model was utilized to select genes related to the control of patients with asthma. $P < 0.05$ was considered statistically significant. The optimal genome for constructing risk characteristics was screened using LASSO regression to establish the risk score as follows: Risk score = $(expr_{gene1} \times Coef_{gene1}) + (expr_{gene2} \times Coef_{gene2}) + \ldots + (expr_{genen} \times Coef_{genen})$ (33). Patients with asthma were divided into low- and high-risk groups according to the median risk score. Principal component analysis (PCA) and t-distributed stochastic neighbor embedding (t-SNE) were used to evaluate the classification accuracy of risk scores. In addition, a Cox proportional hazards regression model was applied to identify the risk score as an independent predictor, and Kruskal test was selected to compare infiltrating immune cell abundance scores in two different risk patterns.

Identification of small-molecule therapeutic drugs that block the progression of asthma

The Broad Institute Connectivity Map (cMAP) database (https://portals.broadinstitute.org/cmap) was used to identify small-molecule drugs associated with asthma progression. Gene sets with log2FC > 0.585 were entered into the cMAP database for enrichment analysis to identify drug candidates (34). The PubChem database (https://pubchem.ncbi.nml.gov) was utilized to extract details of small molecules and obtain their

3D structures. Molecular docking was then carried out, and the predicted crystal structure information of the target protein (human source) was searched in the PDB (https://www.rcsb.org/) database. The receptor protein was pretreated with dehydration and hydrogenation using AutoDockTool software, and the molecular docking between the target protein and small molecular drugs was carried out Vina software to predict the binding ability of the two proteins. A negative binding energy value and an absolute value greater than 5 kcal/mol demonstrate significant binding possibilities.

Animal experiment

BALB/c mice (female, 17–20 g, 6–8 weeks old) were obtained from Beijing Vital River Laboratory Animal Technology Co., Ltd. in China. The mice were kept under specific pathogen-free conditions in Beijing University of Chinese Medicine. All mice were kept in a controlled room (25°C ± 1°C, 45%–60% humidity). All animal studies were conducted in accordance with the institutional animal care regulations of Beijing University of Chinese Medicine and AAALAC and IACUC guidelines. The allergic asthma model of mice was established through OVA sensitization and atomization inhalation stimulation. Briefly, mice were intraperitoneally injected with 2 mg of OVA (Sigma–Aldrich, Cat#A5503) mixed with 2 mg of Imject™ Alum Adjuvant (Invitrogen, Cat#77161) and PBS on days 0 and 14. The challenge phase was from the 21st day to the 25th day after injection, and the mice were atomized with 1% OVA for 30 minutes. The animals were then sacrificed, and lung tissues were snap-frozen in liquid nitrogen and stored in a freezer at −80°C for further analysis.

Western blot

Rabbit anti-BNIP3 antibody (bs-4239R) was purchased from Biosynthesis Biotechnology Inc. (Beijing, China). Horseradish peroxidase-labeled goat antirabbit IgG antibodies (GB23303) was obtained from Wuhan Service Bio Technology Co., Ltd. We extracted the protein from lung tissues according to the manufacturer's instructions after obtaining the total protein from lung tissues using radio immune precipitation assay (RIPA) lysis buffer containing 0.1% phenyl methyl sulfonyl fluoride (PMSF). We used the BCA protein detection kit to measure the protein concentration. Equal amounts of protein samples were separated with sodium dodecyl sulfate–polyacrylamide gel electrophoresis (SDS-PAGE) and transferred to polyvinylidene fluoride (PVDF) membranes. Nonfat milk (5%) in TBST was incubated overnight with primary antibodies against BNIP3 (diluted 1:1,000) at 4°C after blocking. We incubated the sample using goat antirabbit secondary antibody for 1.5 h at room temperature and then washed it four times with TBST to form protein bands on the membrane with an enhanced chemiluminescence reagent. AlphaEase FC software was applied to detect the gray value of protein bands.

Quantitative real-time polymerase chain reaction

mRNA was extracted from lung tissues using a universal RT-PCR kit (Solarbio Science & Technology Co., Ltd., Shanghai, China) following the manufacturer's instructions. Samples were treated with DNase and then purified using an RNeasy kit (Qiagen, Hilden, Germany). Glyceraldehyde-3-phosphate dehydrogenase (GAPDH) was utilized as the internal reference. PCR primer sequences include the following: SLC4A1: forward primer: 5'-CTTCTTCTCGTTCTGTGAAAGCAAT-3', reverse primer: 5'-CATAAGTCTGTTGTAGTGGGTAGTCC-3', SERPINB2: forward primer: 5'-AGGTGAAATCCCAAACCTGCTAC-3', reverse primer: 5'-CACGGAAAGGATAAAGCCCAT-3', BNIP3: forward primer: 5'-TTCCAGCCTCCGTCTCTATTTA-3', reverse primer: 5'-AATCTTCCTCAGACAGAGTGCTG-3', TAAR9: forward primer: 5'-TTACACGGGAGCCAATGAGG-3', reverse primer: 5'-TGGCTGTACCCTCTATCTTCCTA-3', GAPDH: forward primer: 5'-CCTCGTCCCGTAGACAAAATG-3', and reverse primer: 5'-TGAGGTCAATGAAGGGGTCGT-3'.

Statistical analysis

Data were shown as mean ± standard deviation (SD). The differences between the two groups were evaluated by independent sample t-test and nonparametric test. A $P < 0.05$ was considered statistically significant. Statistical analyses and figures were obtained using IBM SPSS Statistics 23.0 (IBM SPSS Software, NY, USA) and GraphPad Prism Version 8.0 (GraphPad Software, San Diego, CA, USA).

Results

Landscape of PRGs between mild-to-moderate and severe asthma samples

This study involved 227 PRGs. Nineteen differentially expressed PRGs were included in the mild-to-moderate and severe asthma samples, among which CAPN1, NLRP1, TRIM31, NOS2, and CDC37 showed the highest difference ($P<0.01$, Figure 1A). The analysis of the coexpression relationship of 19 PRGs demonstrated that a close correlation exists between gene

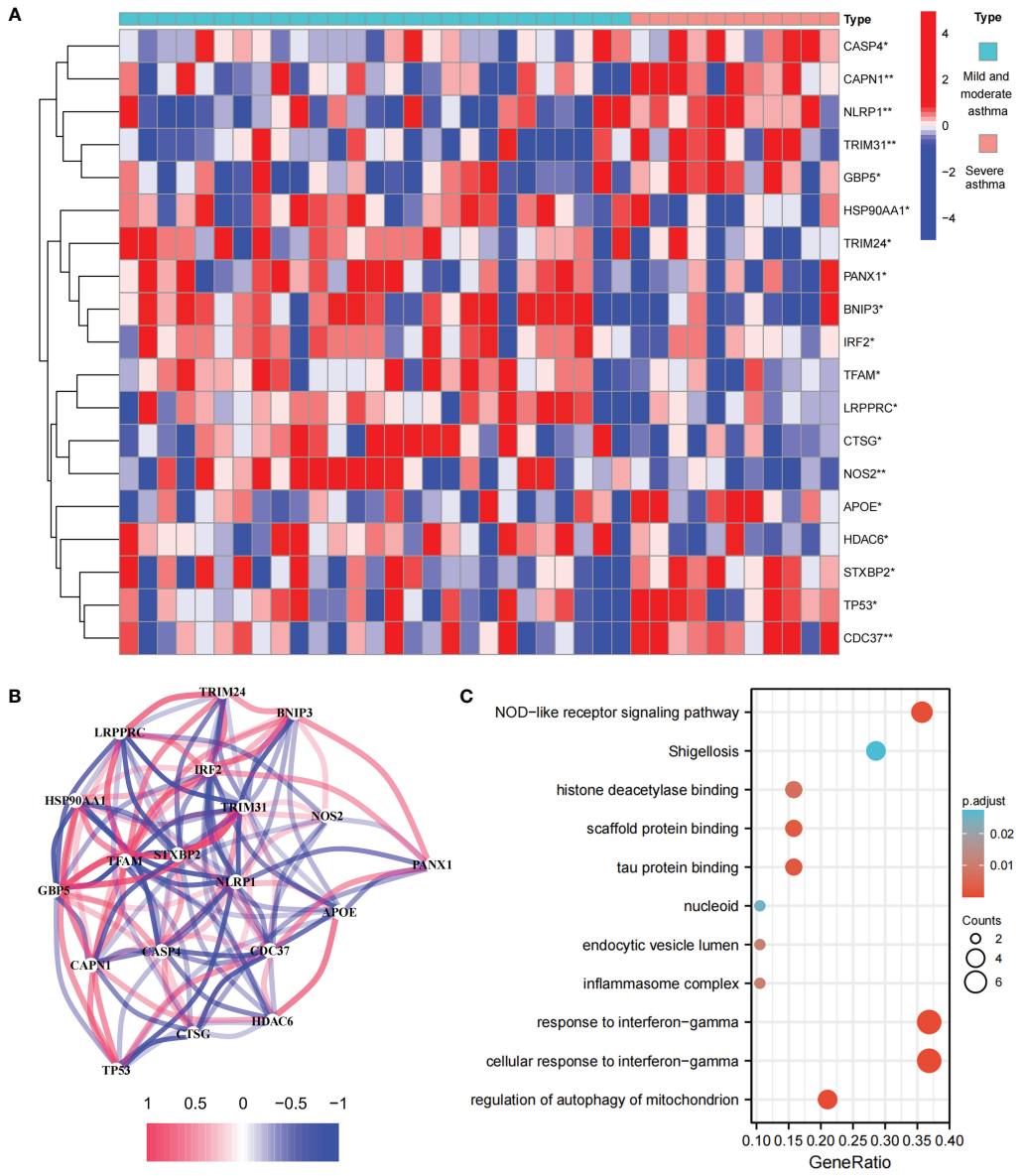

FIGURE 1
Expression and biological function of PRG in mild to moderate asthma and severe asthma. **(A)** 19 differentially expressed PRGs between mild to moderate and severe asthma. **(B)** Co-expression network of 19 PRGs. **(C)** GO and KEGG enrichment analysis of differentially expressed PRG. *P < 0.05 , **P < 0.01.

expression levels (Figure 1B). GO and KEGG analyses demonstrated that differentially expressed PRGs are mainly involved in biological processes and signaling pathways, such as cellular response to interferon-gamma and NOD-like receptor signaling pathway (Figure 1C). These findings suggested that differences likely exist in the cell pyroptosis level in the airway epithelium of mild-to-moderate and severe asthma patients and PRGs may be involved in the evolution of clinical symptoms or disease course of patients through mediated inflammatory processes.

Differentially expressed PRGs between mild-to-moderate and severe asthma cases are divided into two subtypes

We performed an unsupervised consensus cluster analysis of asthma samples on the basis of the expression of 19 PRGs to investigate the role of PRGs in asthma. According to the cumulative distribution function curve, k=2 is selected as the best number of clusters (Figure 2A). This finding indicated that two pyroptosis-related molecular subtypes (C1 and C2) are

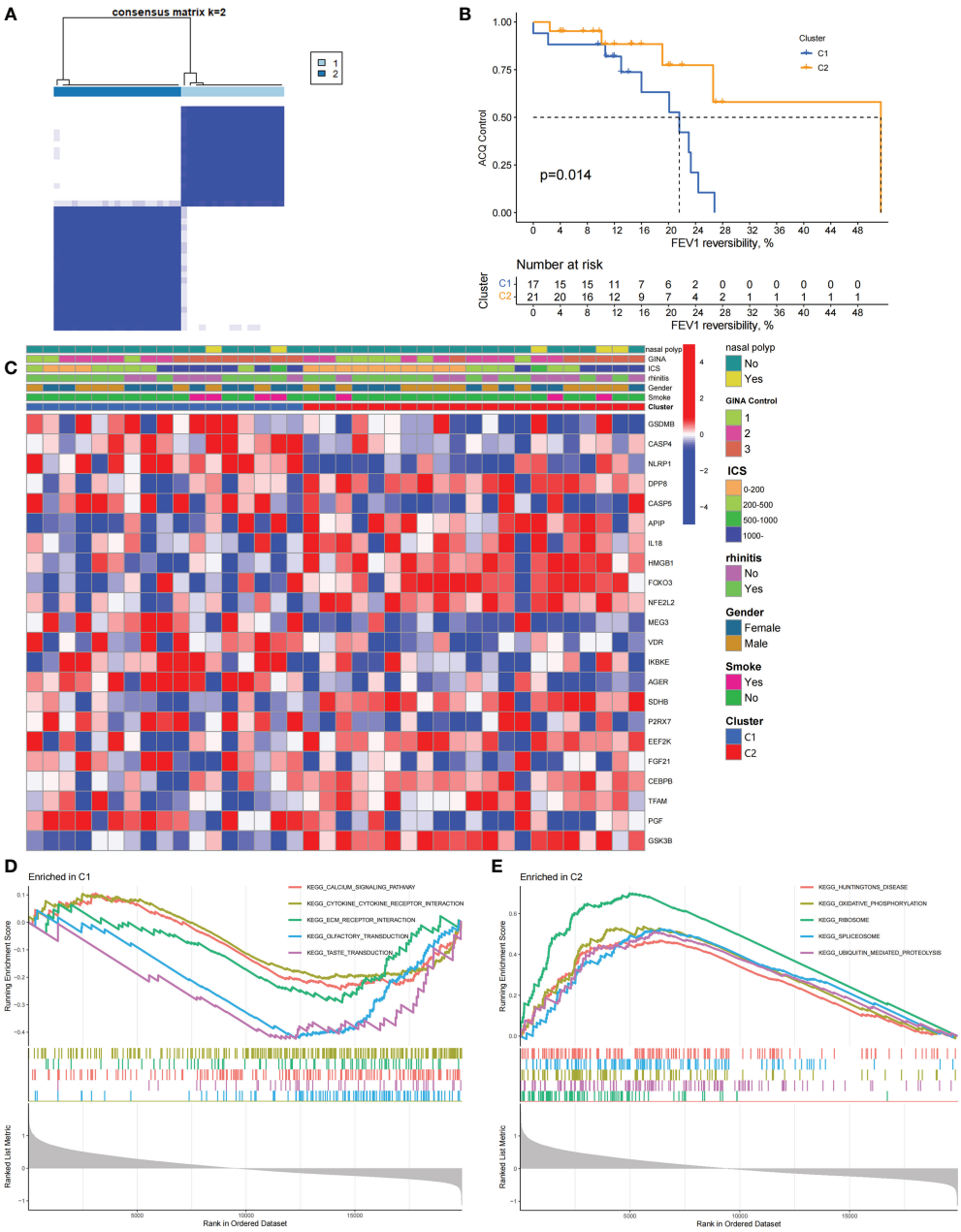

FIGURE 2
Two different pyroptosis-related subtypes identified in asthma by unsupervised clustering of 19 PRGs. **(A)** Heatmap of the matrix of co-occurrence proportions for asthma samples. **(B)** Kaplan–Meier curves of different gene subtypes ACQ Control and FEV1 reversibility. **(C)** Composite heatmap showing the relationship between the expression levels of 22 PRGs and clinical features. **(D, E)** GSEA analysis of C1 and C2 subtypes.

observed in asthma. FEV1 reversibility, a marker of airway hyperresponsiveness (AHR), is positively correlated with the severity of asthma (35, 36). The asthma control questionnaire (ACQ) is a widely used standardized questionnaire of asthma control that can stably and effectively evaluate the degree of control in patients (37–39). Joint analysis of the two major key clinical features of ACQ control and FEV1 reversibility revealed that patients with the C1 subtype present severely poor asthma control (P = 0.014, Figure 2B). Twenty-two differentially expressed PRGs were observed between C1 and C2 subtypes. The analysis of relevant clinical characteristics showed that the C1 subtype (0–200 μg: three cases, 1000 μg or more: seven cases) is higher than the C2 subtype (0–200 μg: 10 cases, 1000 μg or more: five cases) when ICS is used. This finding suggested that

poor asthma control in patients with the C1 subtype may be due to a certain degree of glucocorticoid resistance (Figure 2C). GO and KEGG enrichment analyses of DEGs among subtypes were performed, and biological processes, such as ribosomal translation and threonine-type endopeptidase activity, were significantly enriched (Figure S1). GSEA enrichment analysis showed that the difference of main signal pathways between C1 and C2 subtypes (Figures 2D, E) is that the C1 subtype is mainly enriched in the calcium signaling pathway, cytokine–cytokine receptor interaction, and other pathways closely related to allergy and asthma. These results suggested that PRGs involved in the exacerbation of asthma present a satisfactory classification function that can be used can be used in clinical practice for the detection and intervention of PRGs.

Biological characteristics of the C1 subtype

We constructed scale-free networks and determined optimal soft thresholds on the basis of clinical features to explore related genes that affect asthma control in C1 subtype patients (Figures 3A, B). The TOM matrix was utilized to detect the gene module and analyze the correlation with clinical characteristics. The results showed that the MEpink4 module presents the maximum correlation with asthma control (cor = −0.72, $P = 0.006$). Hence, this module was selected for subsequent analysis (Figure 3C). Genes within the same cluster often share common transcription factors. We predicted and analyzed the transcription factors of genes in the MEpink4 module and visualized the mutual regulatory relationship between the top 10 transcription factors in the mean rank (Figure S2). The association of these transcription factors with asthma was partially demonstrated. For example, SNPs of ZBTB10 affect the asthma risk through the cis-regulation of its genes (40). Functional enrichment analysis of genes in the MEpink4 module showed their primary involvement in biological processes and cellular components related to allergic reactions and airway remodeling, such as motile cilium assembly, regulation of muscle cell apoptotic process, and calcium channel complex, which are closely related to glucocorticoid resistance and poor control of the C1 subtype (Figure 3D).

Determination of pyroptosis-related diagnostic markers among subtypes and their correlation with immune cells

We applied the LASSO logistic regression algorithm on the basis of DEGs and differentially expressed PRGs between C1 and C2 subtypes (Figure 4A) to identify the BNIP3 gene as a pyroptosis-related diagnostic marker for asthma (Figure 4B). Expression levels of BNIP3 in C1 and C2 subtypes were significantly different ($P<0.01$), and expression levels of the C1 subtype were lower than those of the C2 subtype (Figure 4C). This finding suggested that the low expression of BNIP3 may lead to poor asthma control. Animal experiments confirmed that the content of BNIP3 protein in the lung tissue of the asthma mouse model is significantly downregulated (Figures 4D, E) and the BNIP3 mRNA shows the same trend ($P<0.01$, Figure 4F) compared with those of normal mice. Meanwhile, the ROC curve showed the satisfactory classification performance of BNIP3 for C1 and C2 subtypes (AUC: 0.947, Figure 4G). Samples were divided into two groups with high- and low-BNIP3 expression levels for single-gene GSEA analysis to explore the role of BNIP3 in asthma. The results showed that a significant difference exists in the enrichment degree of cell differentiation of Th1 and Th2 in the key pathway of asthma between the two groups ($P = 0.0017$, Figure 4H) biological processes, such as metabolism of xenobiotics by cytochrome P450 and glutathione metabolism, are primarily involved (Figure 4I). Notably, the low expression of BNIP3 was highly correlated with the T cell receptor signaling pathway, cell differentiation of Th1 and Th2, Th17 cell differentiation, and other immune processes (Figsures 4J, K). We quantified the level of immune cell infiltration with the composition of 22 immune cells in all samples between the two subtypes shown in histograms to assess the immune landscape of C1 and C2 subtypes (Figure 5A). Statistical differences in immune cell infiltration between the two subtypes showed that infiltration of M2 macrophages is less in the C1 subtype compared with that in the C2 subtype ($P=0.01$, Figure S3). The relationship between immune cells is illustrated in the thermogram in Figure 5B. Several immune cells closely related to asthma showed a strong correlation. M2 macrophages were positively correlated with activated mast cells and eosinophils, and plasma cells were negatively correlated with activated mast cells and eosinophils. Spearman correlation analysis tested the correlation between BNIP3 and immune cells (Figure 5C) and revealed that it was significantly positively correlated with M2 macrophages ($R=0.53$, $P=0.00069$) and significantly negatively correlated with regulatory T cells ($R=-0.41$, $P=0.011$, Figure 6A). The noncoding RNA regulatory mechanism of BNIP3 was subsequently explored, and 64 miRNAs were predicted from three databases (Figure 6B), of which four miRNAs presented functions in asthma. Finally, a ceRNA network, including 14 LncRNAs and four miRNAs, was constructed (Figure 6C). However, their regulatory relationship and biological significance in asthma still need further investigation.

Establishment of a prognostic model, immunological characteristics, and drug prediction based on asthma control

Combined with clinical data, we identified 12 PRGs that can predict asthma control (Figure 7A). LASSO Cox regression analysis

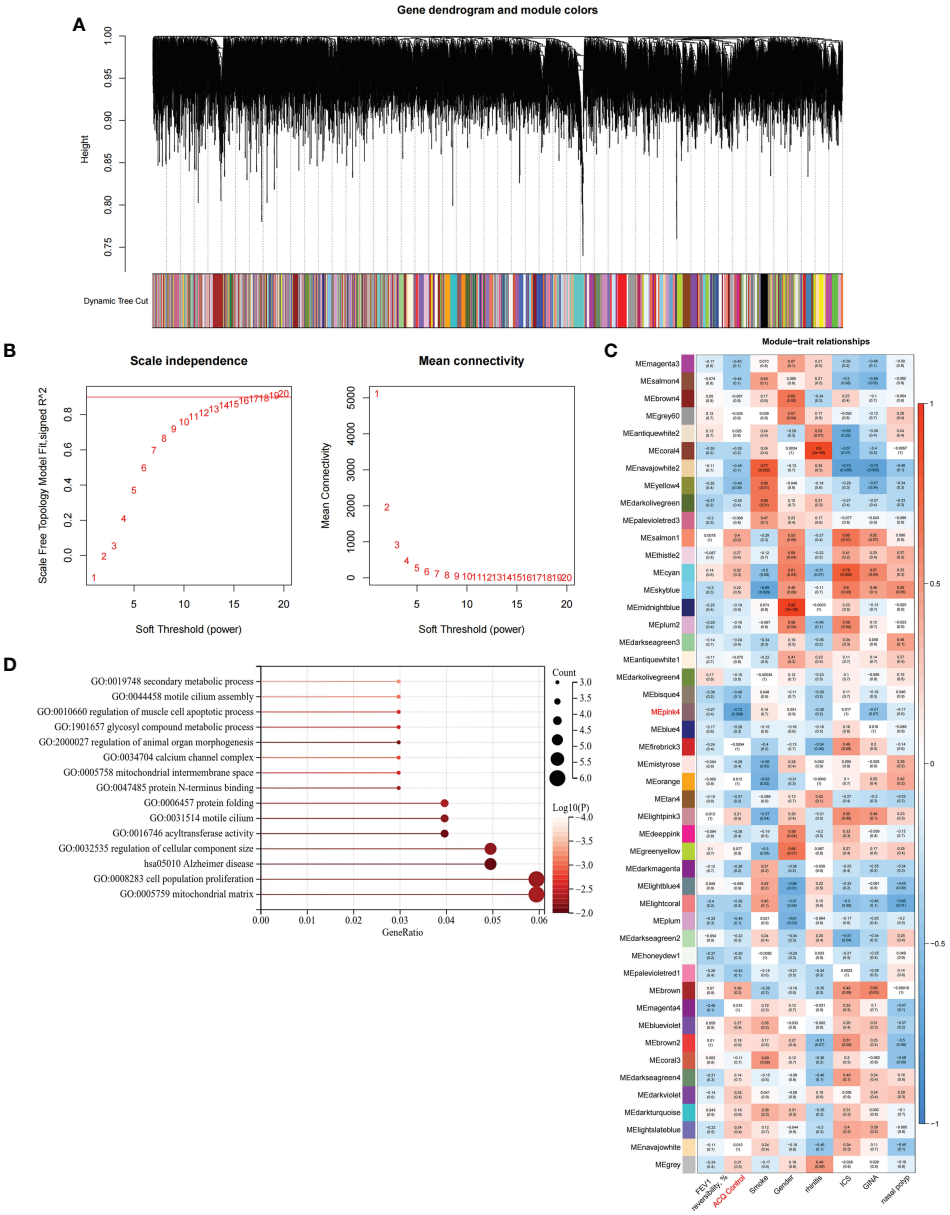

FIGURE 3
Identification and functional enrichment analysis of asthma control related genes in C1 subtype. **(A)** WGCNA of the C1 subtype to obtain a cluster dendrogram of coexpressed genes. **(B)** Analysis of the scale free ft index and analysis of the mean connectivity for various soft −thersholding powers. **(C)** Module − trait relationships for C1 subtypes. Each module contains the corresponding correlation and *P*-value. **(D)** GO and KEGG functional enrichment analysis of genes in MEpink4 module.

was performed on DEGs between subtypes of different cell pyroptosis levels to obtain a prediction model consisting of four genes (Figures 7B, C). The composition of the model is as follows: risk score = (−0.131 × C12orf75 expression level) + (−0.138 × SERPINB2 expression level) + (0.434 × SLC4A1 expression level) + (0.029 × TAAR9 expression levels). This model named P-score can be used to divide patients into high- and low-risk groups on the basis of the median cut-point value of the score. The results showed that the rate of asthma control level in the high-risk group declines faster than that in the low-risk group with the increase of FEV1 reversibility ($P < 0.001$, Figure 7D). Joint analysis of the patients' p-score, FEV1 reversibility, and asthma control revealed that patients with poor control demonstrate high p-score and FEV1 reversibility (Figures 7E, F). PCA and t-SNE analyses were performed on gene expression data to test the classification ability of the P-score. The results showed a clear distribution difference between the two

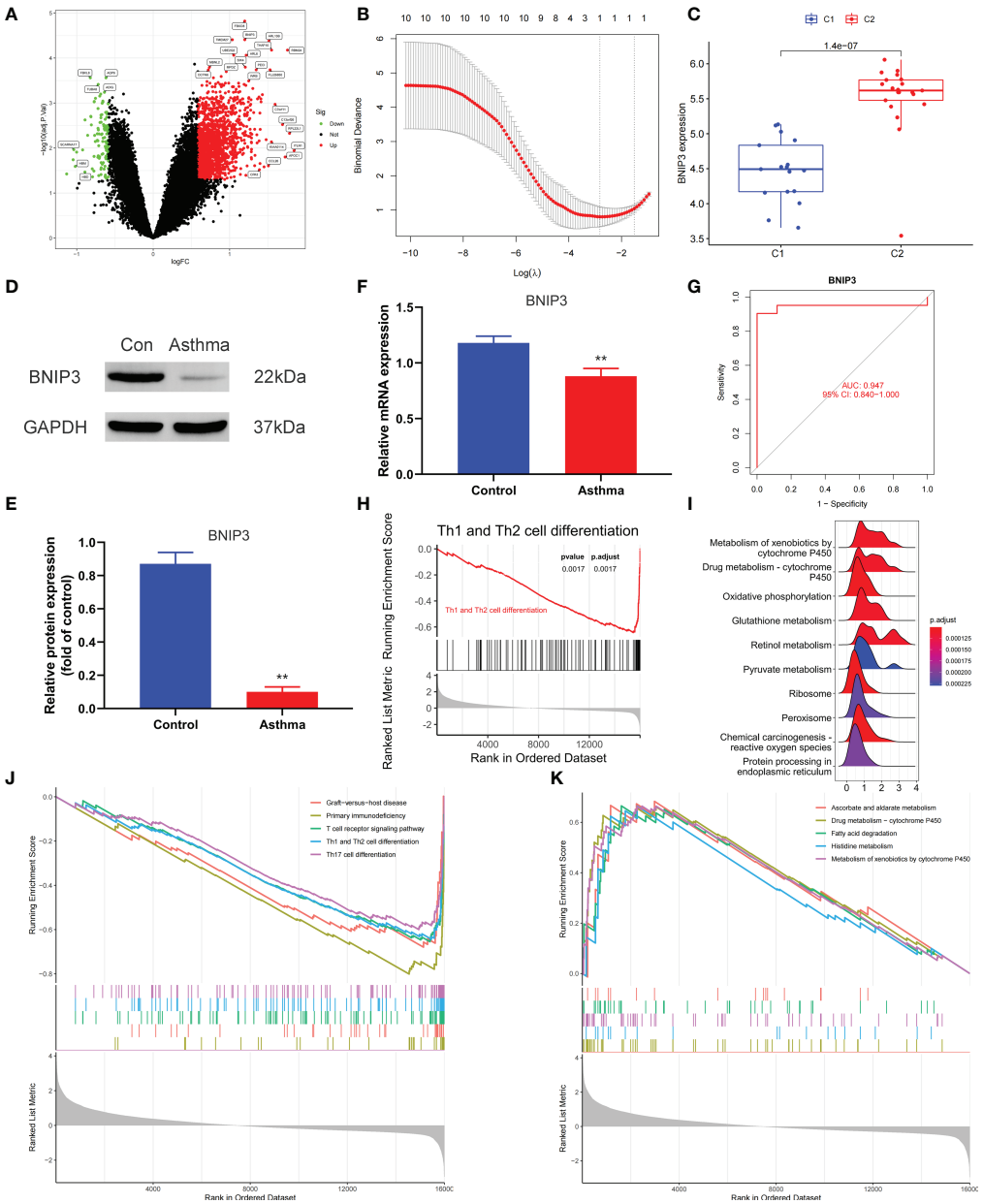

FIGURE 4
Screening of pyroptosis-related diagnostic markers. **(A)** Volcano map of DEGs. red represents up-regulated differential genes, black represents no significant difference genes, and green represents down-regulated differential genes. **(B)** LASSO logistic regression algorithm to screen diagnostic markers. **(C)** Difference of BNIP3 gene expression between C1 and C2 subtypes. **(D, E)** Differential expression of BNIP3 between normal and asthmatic mice. **(F)** Differential expression of BNIP3 mRNA between normal and asthmatic mice. **(G)** ROC curve for verifying the efficacy of BNIP3 gene diagnosis. **(H)** Enrichment difference of Th1 and Th2 cell differentiation pathway between BNIP3 high expression group and low expression group. **(I)** Functional enrichment analysis of DEGs between BNIP3 high expression group and low expression group. **(J, K)** GSEA enrichment analysis of DEGs between BNIP3 high expression group and low expression group. **P < 0.01.

groups (Figures 7G, H). Furthermore, the multivariate regression analysis indicated that the P-score is an independent risk factor for asthma control (HR = 39.845, $P < 0.001$) (Figure 7I). We then explored the expression levels of four genes in the P-score of high- and low-risk groups and demonstrated that C12orf75 and SERPINB2 are downregulated while SLC4A1 and TAAR9 are upregulated in the high-risk group (Figure 8A). PCR analysis of SERPINB2, SLC4A1, and TAAR9 genes, which also exist in the mouse model of asthma, was conducted to verify the accuracy of the results. The findings showed that the level of SERPINB2 mRNA in

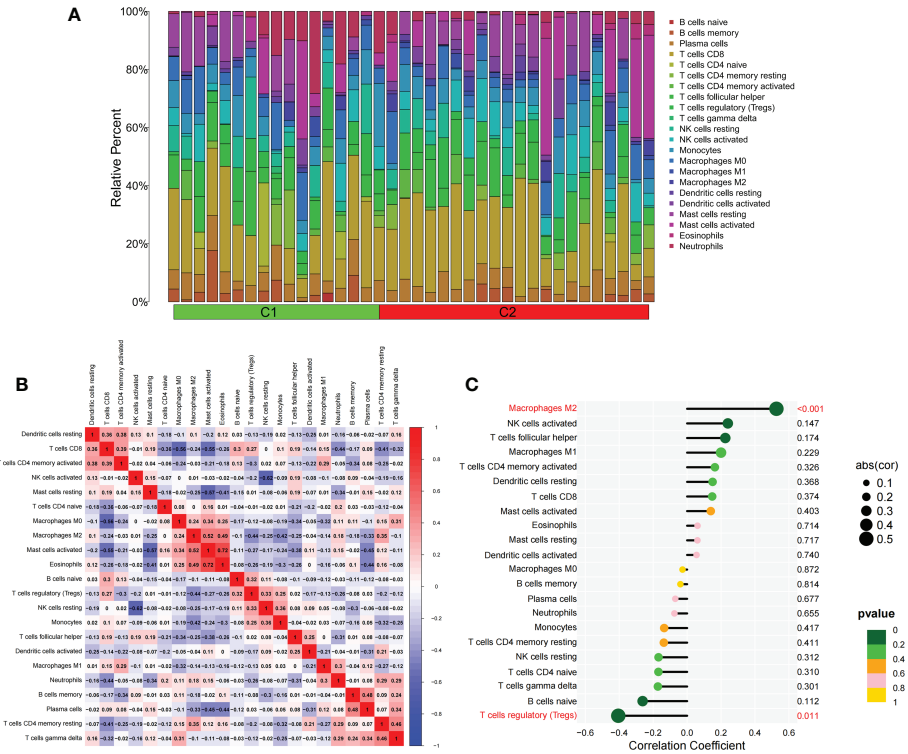

FIGURE 5
The difference of immune cell infiltration among subtypes. **(A)** The histogram of the infiltration ratio of 22 kinds of immune cells in C1 group and C2 subtype samples. **(B)** The correlation among 22 kinds of immune cells. **(C)** The lollipop diagram shows the correlation between BNIP3 gene and 22 kinds of immune cells, and red marks indicate $P < 0.05$.

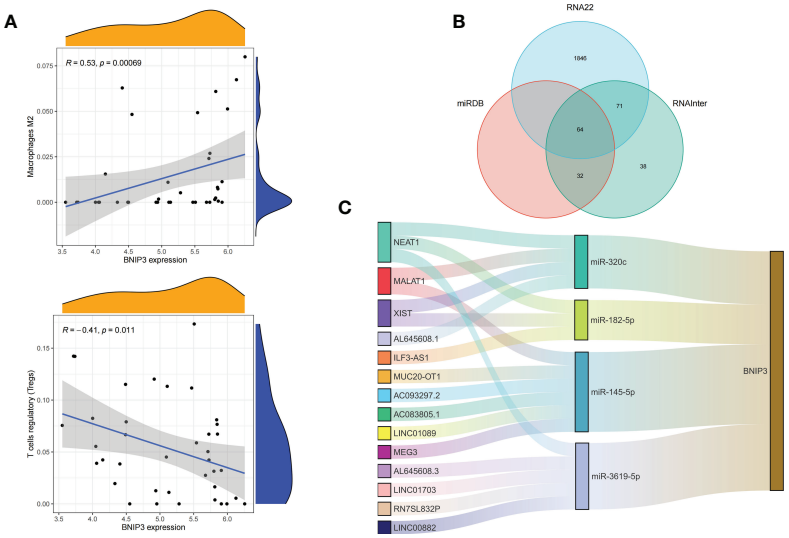

FIGURE 6
Correlation of BNIP3 with immune cell infiltration and its gene expression regulatory network. **(A)** Mountain diagram showing the correlation between the BNIP3 gene and immune cells. **(B)** The intersection of the prediction results of the three databases. **(C)** CeRNA networks involved in the regulation of BNIP3 gene expression.

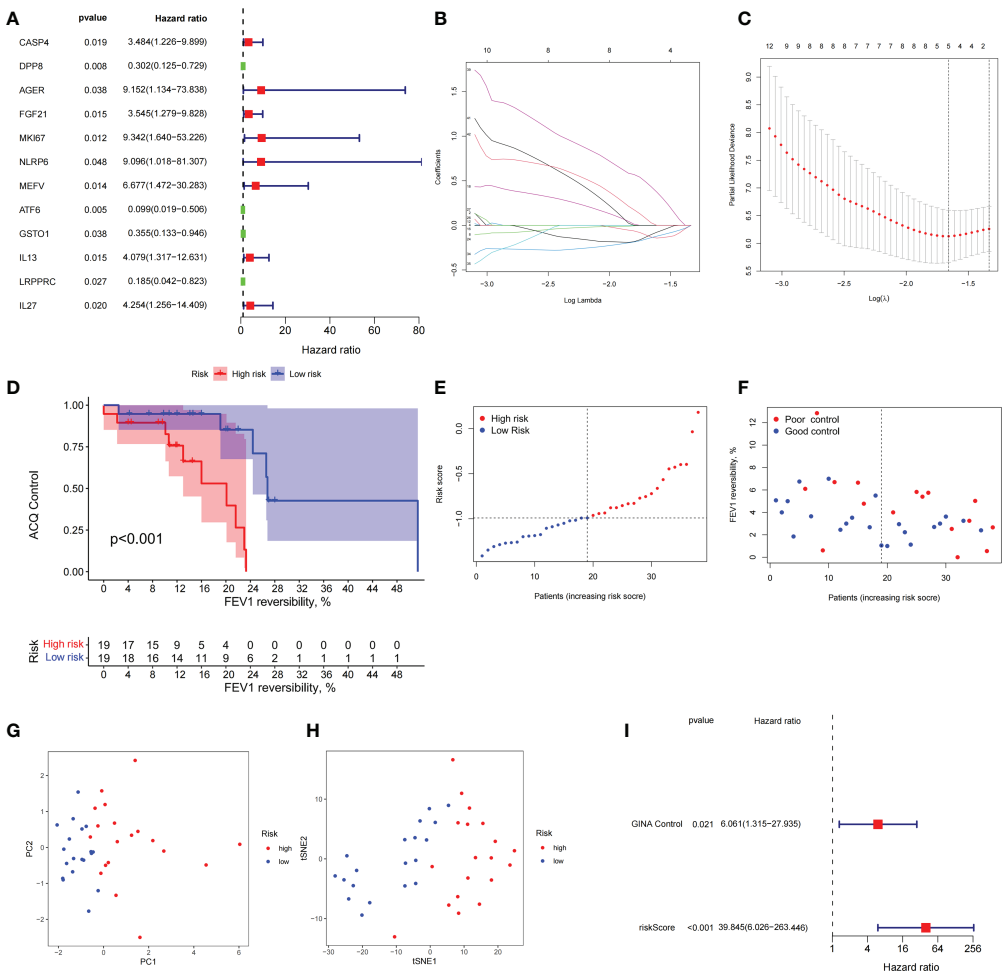

FIGURE 7
The prognostic model constructed by differentially expressed genes from different pyroptosis patterns can distinguish between high- and low-risk patients with asthma. **(A)** DEGs associated with asthma control status. Red and green colors represent high- and low-risk genes, respectively. **(B, C)** Distribution of LASSO coefficients for DEGs. Tenfold cross-validation for tuning parameter selection in the LASSO regression. Dotted vertical lines are drawn at the optimal values by minimum criteria and 1 – SE criteria. **(D)** Kaplan–Meier curves of ACQ control and FEV1 reversibility in patients with different risk groups. **(E)** P-score distribution of patients with different risks. **(F)** The distribution of FEV1 reversibility and asthma control among different risk samples. **(G, H)** PCA and t-SNE was used to determine whether the samples could be grouped correctly based on the P-score. **(I)** Multivariate Cox regression analysis of P-score was shown by forest plot.

the model of asthma is downregulated while that of SLC4A1 mRNA and TAAR9mRNA is upregulated compared with those of normal mice (Figure 8B). In order to verify the value of P-score, we used GSE104468 as the verification set to test the diagnostic efficacy of the three core genes. It is found that the AUC values of SERPINB2, SLC4A1, TAAR9 in patients with asthma and normal people are 0.854, 0.819 and 0.688, respectively (Figure S4). These conclusions suggested that the P-score can effectively predict the control status of asthma patients. We explored its immune cell abundance and biological processes using ssGSEA and GO analyses to understand the differences in immune microenvironment and biological functional characteristics among different degrees of risk groups mediated by cell pyroptosis. Relative to those in the low-risk group, the degree of B and Th1 cell infiltration was higher, and the degree of NK cell infiltration was lower in the high-risk group ($P<0.05$, Figure S5). Notably, DEGs between high- and low-risk groups were mainly concentrated in extracellular vesicle-related biological processes. This finding suggested that cell pyroptosis in asthma may be closely related to the occurrence of extracellular vesicles and intercellular communication (Figure S6). Finally, 10 small-molecule drugs targeting high-risk asthma were screened using the cMAP database, and their correlation with DPP4 targets was significant (Figure 8C). Sitagliptin and diprotin-A were selected for molecular docking with DPP4 to confirm the binding ability between the drug and the target. The results showed that affinities between them are all less than −5 kcal/mol. The molecular docking patterns of the two

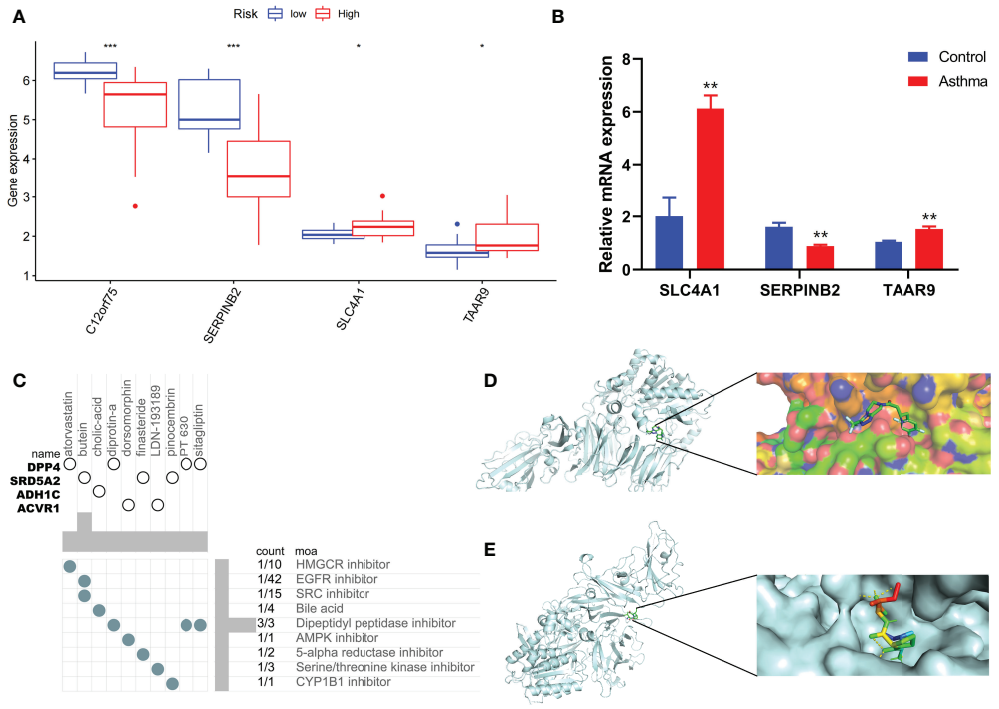

FIGURE 8
Immune status of patients at different risks and prediction of potential therapeutic drugs. **(A)** The expression differences of P-score constituent genes among different risk groups. **(B)** The difference of expression of P-score constituent genes between normal mice and asthmatic mice. **(C)** Correlation between potential therapeutic drugs and corresponding targets. **(D)** Binding conformation of DPP4 and diprotin-A (binding energy = −6.4 kcal/mol). **(E)** Binding conformation of DPP4 and sitagliptin (binding energy = −7.8 kcal/mol). *$P < 0.05$, **$P < 0.01$, ***$P < 0.001$.

molecules are shown in Figures 8D, E confirmed that the drug and the target show significant binding ability, which may play a potential therapeutic role in asthma.

Discussion

Asthma is a common chronic disease. Existing treatment goals for asthma are mainly to prevent exacerbations and reduce the risk of further exacerbations. However, its heterogeneity increases the difficulty in achieving these goals. Th2-driven asthma is a common clinical manifestation typically characterized by elevated levels of type-2 inflammatory factors, serum IgE, and blood eosinophils. However, these indicators are ineffective diagnostic markers for differentiating asthma control (41). By contrast, the relatively rare Th1-driven and severe asthma cases caused by various factors are usually poorly controlled, with limited choice of drugs and lacking predictive tools. Moreover, early identification of Th1-driven and severe asthma in patients at risk of poor control is challenging due to the unclear pathogenesis of asthma (42). Therefore, conducting an in-depth discussion on the basis of clinical and transcriptome characteristics of patients with different disease courses demonstrates high clinical and practical significance.

Although the pathogenesis and immune characteristics of asthma based on cell pyroptosis have been investigated, the role of pyroptosis in asthma remains unclear. Recent reports have shown that NLRP3-related inflammatory response is a key driver of asthma pathogenesis and the allergen Der f1 induces bronchial asthma by mediating caspase-1-dependent pyroptosis through the NLRP3 pathway (43, 44). Furthermore, the expression of canonical PRGs, such as GSDMB, caspase-4, and NLRP1, was upregulated in the poorly controlled asthma subtype. Therefore, the inhibition of pyroptosis in bronchial epithelial cells can reduce the inflammatory response of asthma. GSDMB can be cleaved into several short fragments when coexpressed with caspase-1, of which the N fragment (GSDMB-N) can induce significant cell pyroptosis (8). This phenomenon may explain why different GSDMB genotypes are associated with various phenotypes of adult asthma (45). Chromosome 17q12-q21 is the most replicated genetic locus in childhood asthma. The main mechanism is to regulate its SNPs to affect the abundance of GSDMB transcripts in airway epithelial cells and the functional properties of GSDMB proteins (46). The machine learning results of our study showed that BNIP3 is a diagnostic marker of different pyroptosis subtypes that affects the cell pyroptosis of

cardiomyocytes and coronary artery endothelial cells by mediating caspase-3/GSDME and oxidative stress (47, 48). Note that the expression of BNIP3 was upregulated in properly controlled asthma subtypes but positively correlated with typical type-2 inflammatory cells, such as M2 macrophages, in subsequent immune infiltration analyses. This finding indicated that the asthma phenotype of poorly controlled groups may be different from type-2 inflammation in pyroptosis-based asthma typing. Moreover, among the various phenotypes of asthma, the expression of NLRP3, caspase-1, caspase-4, and other PRGs in neutrophil asthma significantly increases and NLRP3 inflammatory bodies can drive animal asthma models to produce glucocorticoid resistance (49, 50). Furthermore, asthma subtypes with upregulated NLRPs and caspase-1 exhibit high glucocorticoid use and poor asthma control. The consistency in these conclusions indicated that PRG-based typing methods show high potential in identifying immunophenotypes of patients with asthma and can be used to guide the use of glucocorticoid.

Although severe asthma will likely demonstrate poor control compared with mild-to-moderate asthma, poor control caused by gene expression differences, environmental stimulation, medication habits, infections, and other factors can occur in both mild-to-moderate and severe asthma cases (51). Therefore, we constructed the P-score model to predict the control profile of asthma by combining the differential expression levels of PRGs with clinical features. The role of the four genes that make up the P-score in asthma is also partially supported by previous studies. For example, meta-analysis based on the results of sputum transcriptome sequencing of asthmatic patients identified SERPINB2 as a potential signature gene associated with asthma pathogenesis and miR-34b as a key miRNA that regulates the SERPINB2 gene expression (52). Environmental pollutants, such as diesel engine exhaust particles, can promote the expression of the SERPINB2 gene in bronchial epithelial cells while inducing an asthma attack, and its expression level is significantly correlated with the severity of asthma (53, 54). Moreover, glucocorticoid treatment response is a crucial control for asthma accompanied by changes in the expression level of SERPINB2 (55). Although the P-score presents satisfactory risk prediction and discriminating ability, the association of the three other genes with asthma, except for SERPINB2, remains unverified. Hence, the mechanism of the P-score-predicting asthma control requires further experimentation. On the basis of DEGs of high-risk patients, the cMAP database identified targets and drugs with potential therapeutic value for asthma, among which DPP4 demonstrated the highest enrichment score as a drug action target. The level of DPP4 increases in airway epithelial cells of asthmatic patients, and its ability to promote airway smooth muscle cell proliferation *in vitro* implied that DPP4 is likely associated with airway remodeling in asthma (56). Interleukin 13 (IL-13) secreted by Th2 cells is associated with airway inflammation in asthma, and data based on transcriptome sequencing of asthmatic patients confirmed that a positive correlation exists between the DPP4 gene and IL-13 mRNA levels. This finding indicated that a DPP4 can play a potentially important role in asthma (57). Notably, the resulting DPP4 inhibitor sitagliptin predicted in this study can ameliorate airway inflammation in murine asthma models by downregulating inflammatory factors, such as IL-13. Therefore, these drugs may exert important effects on the treatment and control of asthmatic patients although they still need further investigations.

Asthma was successfully classified on the basis of the differential expression of PRGs between mild-to-moderate and severe asthma cases, and the significance of pyroptosis-mediated immunophenotype in the occurrence, development, and prognosis of asthma was systematically revealed in this study. The prognostic model can be used as a powerful tool in predicting asthma control. However, this study presents the following limitations. Existing asthma transcriptome sequencing datasets generally lack corresponding clinical data; hence, the number of patients that can be included in the study is small and the validation set is lacking. Moreover, further experiments are needed to provide new insights into the biological functions of other PRGs in asthma.

Conclusions

We obtained pyroptosis-related genes associated with the progression of asthma in this study. We differentiated two pyroptosis-related subtypes and explored the relationship between key diagnostic markers and immune cells by assessing the expression levels of these genes. We also constructed a pyroptosis-related risk score model with acceptable predictive value and predicted the potential therapeutic drugs using this model. Our findings initially revealed the role of pyroptosis in asthma and promoted the improvement of treatment strategies.

Data availability statement

The datasets presented in this study can be found in online repositories. The names of the repository/repositories and accession number(s) can be found in the article/supplementary material.

Ethics statement

The animal study was reviewed and approved by experimental animal ethics subcommittee of Academic Committee of Beijing University of Traditional Chinese Medicine.

Author contributions

FY designed and conducted the whole research. TW, PY, and WYL carried out animal experiments and molecular biological analysis. JK and YZ applied for the GEO dataset analysis of asthma. FY, XC, and WJL completed the data analysis and drafted the manuscript. XZ and JW revised and finalized the manuscript. All authors contributed to the article and approved the submitted version.

Funding

This work was supported by the National Key R&D Program of China (2020YFC2003100, 2020YFC2003101), National Natural Science Foundation of China (No. 82174243, No. 81973715, No. 82004233), General project of Beijing Natural Science Foundation (No. 7202110), Innovation Team and Talents Cultivation Program of National Administration of Traditional Chinese Medicine (No. ZYYCXTD-C-202001).

Conflict of interest

The authors declare that the research was conducted in the absence of any commercial or financial relationships that could be construed as a potential conflict of interest.

Publisher's note

Supplementary material

The Supplementary Material for this article can be found online at: https://www.frontiersin.org/articles/10.3389/fimmu.2022.937832/full#supplementary-material.

References

1. Thakore P, Earley S. STIM1 is the key that unlocks airway smooth muscle remodeling and hyperresponsiveness during asthma. *Cell Calcium* (2022) 104:102589. doi: 10.1016/j.ceca.2022.102589

2. Wu S, Li S, Zhang P, Fang N, Qiu C. Recent advances in bronchial thermoplasty for severe asthma: a narrative review. *Ann Transl Med* (2022) 10 (6):370. doi: 10.21037/atm-22-580

3. Chan R, Stewart K, Misirovs R, Lipworth BJ. Targeting downstream type 2 cytokines or upstream epithelial alarmins for severe asthma. *J Allergy Clin Immunol Pract* (2022) 10(6):1497–505. doi: 10.1016/j.jaip.2022.01.040

4. Namakanova OA, Gorshkova EA, Zvartsev RV, Nedospasov SA, Drutskaya MS, Gubernatorova EO. Therapeutic potential of combining IL-6 and TNF blockade in a mouse model of allergic asthma. *Int J Mol Sci* (2022) 23(7):3521. doi: 10.3390/ijms23073521

5. Pelaia C, Pelaia G, Crimi C, Maglio A, Gallelli L, Terracciano R, et al. Tezepelumab: A potential new biological therapy for severe refractory asthma. *Int J Mol Sci* (2021) 22(9):4369. doi: 10.3390/ijms22094369

6. Ruan J, Wang S, Wang J. Mechanism and regulation of pyroptosis-mediated in cancer cell death. *Chem Biol Interact* (2020) 323:109052. doi: 10.1016/j.cbi.2020.109052

7. Feng S, Fox D, Man SM. Mechanisms of gasdermin family members in inflammasome signaling and cell death. *J Mol Biol* (2018) 430(18 Pt B):3068–80. doi: 10.1016/j.jmb.2018.07.002

8. Panganiban RA, Sun M, Dahlin A, Park HR, Kan M, Himes BE, et al. A functional splice variant associated with decreased asthma risk abolishes the ability of gasdermin b to induce epithelial cell pyroptosis. *J Allergy Clin Immunol* (2018) 142(5):1469–78.e2. doi: 10.1016/j.jaci.2017.11.040

9. Zasłona Z, Flis E, Wilk MM, Carroll RG, Palsson-McDermott EM, Hughes MM, et al. Caspase-11 promotes allergic airway inflammation. *Nat Commun* (2020) 11(1):1055. doi: 10.1038/s41467-020-14945-2

10. Singhania A, Wallington JC, Smith CG, Horowitz D, Staples KJ, Howarth PH, et al. Multitissue transcriptomics delineates the diversity of airway T cell functions in asthma. *Am J Respir Cell Mol Biol* (2018) 58(2):261–70. doi: 10.1165/rcmb.2017-0162OC

11. Yang IV, Richards A, Davidson EJ, Stevens AD, Kolakowski CA, Martin RJ, et al. The nasal methylome: A key to understanding allergic asthma. *Am J Respir Crit Care Med* (2017) 195(6):829–31. doi: 10.1164/rccm.201608-1558LE

12. Ritchie ME, Phipson B, Wu D, Hu Y, Law CW, Shi W, et al. Limma powers differential expression analyses for RNA-sequencing and microarray studies. *Nucleic Acids Res* (2015) 43(7):e47. doi: 10.1093/nar/gkv007

13. Zhang B, Wu Q, Li B, Wang D, Wang L, Zhou YL. m(6)A regulator-mediated methylation modification patterns and tumor microenvironment infiltration characterization in gastric cancer. *Mol Cancer* (2020) 19(1):53. doi: 10.1186/s12943-020-01170-0

14. Zhang X, Zhang S, Yan X, Shan Y, Liu L, Zhou J, et al. m6A regulator-mediated RNA methylation modification patterns are involved in immune microenvironment regulation of periodontitis. *J Cell Mol Med* (2021) 25 (7):3634–45. doi: 10.1111/jcmm.16469

15. Wilkerson MD, Hayes DN. ConsensusClusterPlus: a class discovery tool with confidence assessments and item tracking. *Bioinformatics* (2010) 26 (12):1572–3. doi: 10.1093/bioinformatics/btq170

16. Langfelder P, Horvath S. WGCNA: an r package for weighted correlation network analysis. *BMC Bioinf* (2008) 9:559. doi: 10.1186/1471-2105-9-559

17. Langfelder P, Horvath S. Fast r functions for robust correlations and hierarchical clustering. *J Stat Software* (2012) 46(11):i11. doi: 10.18637/jss.v046.i11

18. Fu Z, Xu Y, Chen Y, Lv H, Chen G, Chen Y. Construction of miRNA-mRNA-TF regulatory network for diagnosis of gastric cancer. *BioMed Res Int* (2021) 2021:9121478. doi: 10.1155/2021/9121478

19. Ginestet C. ggplot2: Elegant graphics for data analysis. *J R Stat Soc: Ser A (Statistics Society)* (2011) 174(1):245–56. doi: 10.1111/j.1467-985X.2010.00676_9.x

20. Yu G, Wang LG, Han Y, He QY. clusterProfiler: an r package for comparing biological themes among gene clusters. *Omics* (2012) 16(5):284–7. doi: 10.1089/omi.2011.0118

21. Robert T. Regression shrinkage and selection via the lasso. *J R Stat Soc Ser B (Methodol)* (1996) 58(1):267-88. doi: 10.1111/j.2517-6161.1996.tb02080.x

22. Liu Z, Liu L, Weng S, Guo C, Dang Q, Xu H, et al. Machine learning-based integration develops an immune-derived lncRNA signature for improving outcomes in colorectal cancer. *Nat Commun* (2022) 13(1):816. doi: 10.1038/s41467-022-28421-6

23. Liu Z, Xu H, Weng S, Ren Y, Han X. Stemness refines the classification of colorectal cancer with stratified prognosis, multi-omics landscape, potential mechanisms, and treatment options. *Front Immunol* (2022) 13:828330. doi: 10.3389/fimmu.2022.828330

24. Liu Z, Lu T, Li J, Wang L, Xu K, Dang Q, et al. Development and clinical validation of a novel six-gene signature for accurately predicting the recurrence risk of patients with stage II/III colorectal cancer. *Cancer Cell Int* (2021) 21(1):359. doi: 10.1186/s12935-021-02070-z

25. Liu Z, Guo C, Dang Q, Wang L, Liu L, Weng S, et al. Integrative analysis from multi-center studies identities a consensus machine learning-derived lncRNA signature for stage II/III colorectal cancer. *EBioMedicine* (2022) 75:103750. doi: 10.1016/j.ebiom.2021.103750

26. Xing Z, Liu Z, Fu X, Zhou S, Liu L, Dang Q, et al. Clinical significance and immune landscape of a pyroptosis-derived LncRNA signature for glioblastoma. *Front Cell Dev Biol* (2022) 10:805291. doi: 10.3389/fcell.2022.805291

27. Friedman J, Hastie T, Tibshirani R. Regularization paths for generalized linear models *via* coordinate descent. *J Stat Software* (2010) 33(1):1–22. doi: 10.18637/jss.v033.i01

28. Li JH, Liu S, Zhou H, Qu LH, Yang JH. starBase v2.0: decoding miRNA-ceRNA, miRNA-ncRNA and protein-RNA interaction networks from large-scale CLIP-seq data. *Nucleic Acids Res* (2014) 42(Database issue):D92–7. doi: 10.1093/nar/gkt1248

29. Chang L, Zhou G, Soufan O, Xia J. miRNet 2.0: network-based visual analytics for miRNA functional analysis and systems biology. *Nucleic Acids Res* (2020) 48(W1):W244–w51. doi: 10.1093/nar/gkaa467

30. Liu XS, Gao Y, Wu LB, Wan HB, Yan P, Jin Y, et al. Comprehensive analysis of GLUT1 immune infiltrates and ceRNA network in human esophageal carcinoma. *Front Oncol* (2021) 11:665388. doi: 10.3389/fonc.2021.665388

31. Newman AM, Liu CL, Green MR, Gentles AJ, Feng W, Xu Y, et al. Robust enumeration of cell subsets from tissue expression profiles. *Nat Methods* (2015) 12 (5):453–7. doi: 10.1038/nmeth.3337

32. Deng YJ, Ren EH, Yuan WH, Zhang GZ, Wu ZL, Xie QQ. GRB10 and E2F3 as diagnostic markers of osteoarthritis and their correlation with immune infiltration. *Diagn (Basel)* (2020) 10(3):171. doi: 10.3390/diagnostics10030171

33. Wang Y, Liu X, Guan G, Zhao W, Zhuang M. A risk classification system with five-gene for survival prediction of glioblastoma patients. *Front Neurol* (2019) 10:745. doi: 10.3389/fneur.2019.00745

34. Lamb J, Crawford ED, Peck D, Modell JW, Blat IC, Wrobel MJ, et al. The connectivity map: using gene-expression signatures to connect small molecules, genes, and disease. *Science* (2006) 313(5795):1929–35. doi: 10.1126/science.1132939

35. Thayyezhuth D, Venkataram R, Bhat VS, Aroor R. A study of spirometric parameters in non asthmatic allergic rhinitis. *Heliyon* (2021) 7(11):e08270. doi: 10.1016/j.heliyon.2021.e08270

36. Ye Q, Liao A, D'Urzo A. FEV(1) reversibility for asthma diagnosis: a critical evaluation. *Expert Rev Respir Med* (2018) 12(4):265–67. doi: 10.1080/17476348.2018.1439741

37. Rhee H, Love T, Mammen J. Comparing asthma control questionnaire (ACQ) and national asthma education and prevention program (NAEPP) asthma control criteria. *Ann Allergy Asthma Immunol* (2019) 122(1):58–64. doi: 10.1016/j.anai.2018.09.448

38. Schuler M, Faller H, Wittmann M, Schultz K. Asthma control test and asthma control questionnaire: factorial validity, reliability and correspondence in assessing status and change in asthma control. *J Asthma* (2016) 53(4):438–45. doi: 10.3109/02770903.2015.1101134

39. Nguyen JM, Holbrook JT, Wei CY, Gerald LB, Teague WG, Wise RA. Validation and psychometric properties of the asthma control questionnaire among children. *J Allergy Clin Immunol* (2014) 133(1):91–7.e1-6. doi: 10.1016/j.jaci.2013.06.029

40. Li X, Hastie AT, Hawkins GA, Moore WC, Ampleford EJ, Milosevic J, et al. eQTL of bronchial epithelial cells and bronchial alveolar lavage deciphers GWAS-identified asthma genes. *Allergy* (2015) 70(10):1309–18. doi: 10.1111/all.12683

41. Liu L, Gao Y, Si Y, Liu B, Liu X, Li G, et al. MALT1 in asthma children: A potential biomarker for monitoring exacerbation risk and Th1/Th2 imbalance-mediated inflammation. *J Clin Lab Anal* (2022) 36(5):e24379. doi: 10.1002/jcla.24379

42. Hinks TSC, Levine SJ, Brusselle GG. Treatment options in type-2 low asthma. *Eur Respir J* (2021) 57(1):2000528. doi: 10.1183/13993003.00528-2020

43. Theofani E, Semitekolou M, Samitas K, Mais A, Galani IE, Triantafyllia V, et al. TFEB signaling attenuates NLRP3-driven inflammatory responses in severe asthma. *Allergy* (2022) 77(7):2131–46. doi: 10.1111/all.15221

44. Tsai YM, Chiang KH, Hung JY, Chang WA, Lin HP, Shieh JM, et al. Der f1 induces pyroptosis in human bronchial epithelia *via* the NLRP3 inflammasome. *Int J Mol Med* (2018) 41(2):757–64. doi: 10.3892/ijmm.2017.3310

45. Kitazawa H, Masuko H, Kanazawa J, Shigemasa R, Hyodo K, Yamada H, et al. ORMDL3/GSDMB genotype is associated with distinct phenotypes of adult asthma. *Allergol Int* (2021) 70(4):495–97. doi: 10.1016/j.alit.2021.04.004

46. Schoettler N, Dissanayake E, Craven MW, Yee JS, Eliason J, Schauberger EM, et al. Children's Respiratory and Environmental Workgroup. New insights relating gasdermin b to the onset of childhood asthma. *Am J Respir Cell Mol Biol* (2022). doi: 10.1165/rcmb.2022-0043PS

47. Zheng X, Zhong T, Ma Y, Wan X, Qin A, Yao B, et al. Bnip3 mediates doxorubicin-induced cardiomyocyte pyroptosis *via* caspase-3/GSDME. *Life Sci* (2020) 242:117186. doi: 10.1016/j.lfs.2019.117186

48. Wang Y, Song X, Li Z, Liu N, Yan Y, Li T, et al. MicroRNA-103 protects coronary artery endothelial cells against H(2)O(2)-induced oxidative stress *via* BNIP3-mediated end-stage autophagy and antipyroptosis pathways. *Oxid Med Cell Longev* (2020) 2020:8351342. doi: 10.1155/2020/8351342

49. Simpson JL, Phipps S, Baines KJ, Oreo KM, Gunawardhana L, Gibson PG. Elevated expression of the NLRP3 inflammasome in neutrophilic asthma. *Eur Respir J* (2014) 43(4):1067–76. doi: 10.1183/09031936.00105013

50. Kim RY, Pinkerton JW, Essilfie AT, Robertson AAB, Baines KJ, Brown AC, et al. Role for NLRP3 inflammasome-mediated, IL-1β-Dependent responses in severe, steroid-resistant asthma. *Am J Respir Crit Care Med* (2017) 196(3):283–97. doi: 10.1164/rccm.201609-1830OC

51. Mulugeta T, Ayele T, Zeleke G, Tesfay G. Asthma control and its predictors in Ethiopia: Systematic review and meta-analysis. *PloS One* (2022) 17(1):e0262566. doi: 10.1371/journal.pone.0262566

52. Singh P, Sharma A, Jha R, Arora S, Ahmad R, Rahmani AH, et al. Transcriptomic analysis delineates potential signature genes and miRNAs associated with the pathogenesis of asthma. *Sci Rep* (2020) 10(1):13354. doi: 10.1038/s41598-020-70368-5

53. Meldrum K, Gant TW, Leonard MO. Diesel exhaust particulate associated chemicals attenuate expression of CXCL10 in human primary bronchial epithelial cells. *Toxicol In Vitro* (2017) 45(Pt 3):409–16. doi: 10.1016/j.tiv.2017.06.023

54. El-Badawy NE, Abdel-Latif RS, El-Hady HA. Association between SERPINB2 gene expression by real time PCR in respiratory epithelial cells and atopic bronchial asthma severity. *Egypt J Immunol* (2017) 24(1):165–81.

55. Woodruff PG, Boushey HA, Dolganov GM, Barker CS, Yang YH, Donnelly S, et al. Genome-wide profiling identifies epithelial cell genes associated with asthma and with treatment response to corticosteroids. *Proc Natl Acad Sci U.S.A.* (2007) 104(40):15858–63. doi: 10.1073/pnas.0707413104

56. Shiobara T, Chibana K, Watanabe T, Arai R, Horigane Y, Nakamura Y, et al. Dipeptidyl peptidase-4 is highly expressed in bronchial epithelial cells of untreated asthma and it increases cell proliferation along with fibronectin production in airway constitutive cells. *Respir Res* (2016) 17:28. doi: 10.1186/s12931-016-0342-7

57. Poole A, Urbanek C, Eng C, Schageman J, Jacobson S, O'Connor BP, et al. Dissecting childhood asthma with nasal transcriptomics distinguishes subphenotypes of disease. *J Allergy Clin Immunol* (2014) 133(3):670–8.e12. doi: 10.1016/j.jaci.2013.11.025

frontiers | Frontiers in Immunology

TYPE Original Research
PUBLISHED 02 August 2022
DOI 10.3389/fimmu.2022.939127

OPEN ACCESS

EDITED BY
Bao-Hui Cheng,
Institute of ENT and Shenzhen Key Laboratory of ENT, China

REVIEWED BY
Jin-Lyu Sun,
Peking Union Medical College Hospital, China
(Dylan) Xi Wang,
Dartmouth College, United States

*CORRESPONDENCE
Rongfei Zhu
zrf13092@163.com
Lin Yang
yanglin_tjmu@sina.com

†These authors have contributed equally to this work and share first authorship

SPECIALTY SECTION
This article was submitted to Immunological Tolerance and Regulation, a section of the journal Frontiers in Immunology

RECEIVED 08 May 2022
ACCEPTED 21 June 2022
PUBLISHED 02 August 2022

CITATION
Chen H, Zhang X, Zhu L, An N, Jiang Q, Yang Y, Ma D, Yang L and Zhu R (2022) Clinical and immunological characteristics of *Aspergillus fumigatus*-sensitized asthma and allergic bronchopulmonary aspergillosis. *Front. Immunol.* 13:939127. doi: 10.3389/fimmu.2022.939127

Clinical and immunological characteristics of *Aspergillus fumigatus*-sensitized asthma and allergic bronchopulmonary aspergillosis

Hao Chen[1†], Xinyu Zhang[2†], Li Zhu[3†], Nairui An[2], Qing Jiang[1], Yaqi Yang[1], Dongxia Ma[1], Lin Yang[1*] and Rongfei Zhu[1*]

[1]Department of Allergy, Tongji Hospital, Tongji Medical College, Huazhong University of Science and Technology, Wuhan, China, [2]Department of Allergy and Clinical Immunology, Guangzhou Institute of Respiratory Health, State Key Laboratory of Respiratory Disease, National Clinical Research Center of Respiratory Disease, First Affiliated Hospital of Guangzhou Medical University, Guangzhou, China, [3]Department of Hematology, Tongji Hospital, Tongji Medical College, Huazhong University of Science and Technology, Wuhan, China

Background: *Aspergillus fumigatus* (*A.f*) is a common airborne allergen that contributes to allergic asthma. In some patients, *A.f* can colonize in the airway and lead to allergic bronchopulmonary aspergillosis (ABPA). However, our understanding of the pathogenesis of *A.f*-sensitized asthma and ABPA remains inadequate.

Objective: We aimed to investigate the clinical and immunological characteristics of *A.f*-sensitized asthma and ABPA.

Methods: A total of 64 ABPA and 57 A.*f*-sensitized asthma patients were enrolled in the study, and 33 non-*A.f*-sensitized asthma patients served as the control group. The clinical and immunological parameters included lung function, fractional exhaled nitric oxide (FeNO), induced sputum and blood cell analysis, specific IgE/IgG/IgA of A.f and its components, cytokines (IL-33, IL-25, and TSLP) and $CD4^+$T cell subsets.

Results: The eosinophils in blood, induced sputum, and FeNO were significantly higher in ABPA patients compared to that in *A.f*-sensitized patients. The combination of FeNO and eosinophils (EO) parameters presented good diagnostic efficiency in differentiating *A.f* (+) asthma from ABPA, with a sensitivity of 80% and a specificity of 100%. Specific IgE, IgG, and IgA against *A.f* also increased in ABPA patients. However, serum IL-25, IL-33, and TSLP showed no significant differences between the two groups. Cell analysis showed an increase in IFN-γ^+Th1 cells in the ABPA patients. FlowSOM analysis further confirmed that the frequency of $CD3^+CD4^+PD\text{-}1^+CD127^+$IFN-$\gamma^+$T cells was higher in ABPA patients.

10.3389/fimmu.2022.939127

Conclusion: Our findings suggest the distinct humoral and cell immunological responses in *A.f*-sensitized asthma and ABPA patients. ABPA patients have more severe eosinophilic inflammation and enhanced Th1 responses compared with *A.f*-sensitized asthma patients.

KEYWORDS

***Aspergillus fumigatus*, asthma, allergic bronchopulmonary aspergillosis, CD4$^+$T cell, IgE**

Introduction

Asthma is a heterogeneous disease characterized by chronic airway inflammation and airway hyperresponsiveness. The main clinical manifestations are recurrent wheezing, shortness of breath, chest tightness, or cough (1). According to recent epidemiological surveys in China (2), more than 45 million adults over the age of 20 suffered from asthma, and the majority of them suffered from allergic asthma. Fungi, especially *Aspergillus fumigatus* (*A.f*), are common airborne allergens that cause allergic asthma (3). The colonies of *A.f* are fluffy or flocculated and can grow rapidly. With thermophilic feature, *A.f* can colonize in the airway and cause invasive infection; its sensitization is also a risk factor for severe asthma (4).

Allergic bronchopulmonary aspergillosis (ABPA) is a chronic inflammation triggered by repeated exposure to *A.f*, which has colonized for a long time in the airway (5). The clinical manifestations include chronic asthma or bronchiectasis and recurrent wandering pulmonary shadows or mucus blockage in lung images (6). While ABPA was mostly found in patients with bronchial asthma or cystic fibrosis in Western countries, it was more common in patients with asthma and bronchiectasis in China (7). A study revealed that the estimated prevalence of ABPA in adults with asthma was at 2.5% (8) and could rise up to 45% in patients with *A.f*-sensitized asthma (9). As the symptoms were extremely similar to those of asthma and other airway diseases, ABPA was always misdiagnosed in clinical practice. A study in China revealed that nearly 70% of the ABPA patients in the country had been misdiagnosed. Among them, 21% were misdiagnosed as tuberculosis and received anti-tuberculosis therapy for at least 1 year. Some patients would receive high-dosage inhalant or systemic steroids and antibiotics but were always resistant to the treatments (10). Thus, it is of great significance to distinguish ABPA from asthma, especially *A.f*-sensitized asthma.

Currently, the diagnosis for ABPA mainly relies on total IgE (tIgE), specific IgE (sIgE) against *A.f*, pulmonary imaging, and blood eosinophil count. However, most of these indicators are non-specific and not very sensitive. A detailed mechanism and surrogate indicators of ABPA and *A.f*-sensitized asthma still need further investigation. In this study, we investigated clinical and immunological characteristics of ABPA and *A.f*-sensitized asthma with a view of elucidating the underlying mechanism and exploring potential biomarkers to discriminate ABPA from *A.f*-sensitized asthma.

Materials and methods

Patients

This study was conducted from September 2018 to June 2021 in the Department of Respiratory Medicine at the First Affiliated Hospital of Guangzhou Medical University and the Department of Allergy, Tongji Hospital, Tongji Medical College. The inclusion criteria for patients enrolled in our study were those who were diagnosed with asthma or ABPA, based on Global Initiative for Asthma (GINA) guidelines (http://ginasthma.org/) and ABPA criteria (11). The exclusion criteria were (1) patients with chronic diseases such as tuberculosis, chronic obstructive pulmonary disease, coronary heart disease, hypertension, diabetes, and tumor and (2) patients who received systemic glucocorticoids or monoclonal antibodies within 1 month that might affect the levels of eosinophil or tIgE before enrollment. The study was approved by the Independent Ethical Committee of First Affiliated Hospital of Guangzhou Medical University (No. GYFYY-2016-73) and Tongji Hospital (No. TJ-IRB20210761). Each participant or their guardian provided a written informed consent.

Based on clinical data, sIgE against *A.f*, chest computerized tomography (CT) reports, and peripheral blood eosinophil counts, the enrolled patients were divided into three groups: non-*A.f*-sensitized asthma [*A.f* (−) asthma], *A.f*-sensitized asthma [*A.f* (+) asthma], and ABPA. The demographic data included gender, age, height, weight, and other basic information of the patients. The count and percentage of peripheral blood cells including white blood cell (WBC), neutrophils (NEUT), lymphocytes (LY), and eosinophils (EO)

and infection-related indicators such as erythrocyte sedimentation rate (ESR) and procalcitonin (PCT) were also collected in the first detection after hospitalization. According to the GINA guideline, asthma control test (ACT) was used for each patient in the enrollment stage to evaluate the control level of these three groups. The total score of ACT was 25, in which ≥20 was defined as controlled and <20 was uncontrolled.

Clinic and immunological parameters

Lung function and fractional exhaled nitric oxide

Lung function was measured by spirometry on a MasterScreen Pneumo (Jaeger, Wurzburg, Germany) spirometer. The parameters for such measurement included forced vital capacity (FVC), forced expiratory volume in 1 s (FEV1), FEV1/FVC, peak expiratory flow (PEF), maximum mid-expiratory flow (MMEF), maximal expiratory flow 50 (MEF50), and maximal expiratory flow 25 (MEF25). Fractional exhaled nitric oxide (FeNO) level was measured with a portable electrochemical device (NIOX MINO; Aerocrine AB, Stockholm, Sweden), and the upper normal limit was 25 ppb.

Induced sputum cytology classification

After gargling with water, the subjects underwent sputum induction by inhaling 3% sodium chloride solution with ultrasonic atomization for 15 min and coughed up the sputum to the Petri dish. Sputum of 3–5 ml was weighed and added into 0.1% dithionitol solution with four times volume. After 1 min of vortex shock, the sputum was incubated in a 37°C water bath for 10 min until the specimen was liquefied. The samples were filtered by a 300-mesh nylon filter, and the filtrate was centrifuged at 3,000 rpm for 10 min. The cell precipitate was prepared into cell smears, which were dried in a 55°C oven. The cell smears were fixed with 10% formaldehyde and stained with Raysgiemsa for 15–20 min. Sputum cells including eosinophils (SEO), neutrophils (SNEUT), macrophages (SMø), and lymphocytes (SLY) were classified and counted under a microscope.

IgE, IgG, and IgA detection

The serum sample was collected to analyze tIgE and *A.f*-sIgE using ImmunoCAP 1000 provided by Thermo Fisher Scientific Inc. Positive sIgE was categorized into six classes: class 1 (≥0.35–<0.70 KU/L), class 2 (≥0.70–<3.50 KU/L), class 3 (≥3.50–<17.50 KU/L), class 4 (≥17.50–<50 KU/L), class 5 (≥50–<100 KU/L), and class 6 (≥100 KU/L).

Specific IgA, IgG4, and IgE against *A.f* and its components (Asp f1, Asp f3, and Asp f9) were measured by *A.f* components test kit (Hangzhou Zheda Dixun Biological Gene Engineering Co, Ltd, Hangzhou, China). The recombinant *A.f* and its components (Asp f1, Asp f3, and Asp f9) were precoated on the chip. After serum was incubated on the chip for 1 h, anti-human IgE/IgA/IgG4 antibodies (conjugated by biotin) and alkaline phosphatase–streptavidin were added consecutively. The concentrations of IgE/IgA/IgG4 against *A.f* were calculated by a series of protein standardization. The positive cutoff value of sIgG4 was set by 95% percentile of upper limit of 210 healthy non-allergic donors; sIgG4 above 156 U_A/ml, sIgA above 10 U/ml, and sIgE above 0.35 IU/ml were defined as positive.

Interleukin-33, IL-25, thymic stromal lymphopoietin assay

Concentrations of interleukin (IL)-33 (EHC151, Neobioscience, China), IL-25 (EHC180, Neobioscience, China), and TSLP (EK0958, BOSTER, China) in serum were determined using their specific enzyme-linked immunosorbent assay (ELISA) kits according to the manufacturer's instructions.

Cell staining and flow cytometric analysis

Peripheral blood mononuclear cells (PBMCs) of patients were isolated and stored in liquid nitrogen. Thawed PBMCs of ABPA patients and *A.f* (+) asthma patients were incubated with 25 μg/ml *A.f* allergen extracts and 100 ng/ml PMA (phorbol-12-myristate 13-acetate, MCE, China) for 6 h. PBMCs of house dust mite (HDM)-positive group were incubated with 25 μg/ml HDM and 100 ng/ml PMA also for 6 h as control, and then, the harvested cells were prepared at a concentration of 1×10^6 in 100 μl flow cytometry (FACS) staining buffer and were stained with Live/Dead Fixable Read cell stain kit (Invitrogen, USA), anti-human CD3, CD4, CD183 (CXCR3), CD294 (CRTH2), CD25, CD127, IL-4, IL-13, and IFN-γ antibodies (Biolegend, USA), and CD279 (PD-1), IL-10, and CD185 (CXCR5) (BD Biosciences, USA). T subsets were gated by Th1 ($CD3^+CD4^+CXCR3^+$), Th2 ($CD3^+CD4^+CRTH2^+$), Tfh ($CD3^+CD4^+CXCR5^+PD\text{-}1^+$), and Treg ($CD3^+CD4^+CD25^+CD127^{low/-}$) (12, 13). Stained cells were acquired with FACS Caliber (BD, Biosciences, Milpitas, CA, USA), and the data were analyzed with FlowJo software.

FlowSOM algorithm

The FlowSOM algorithm helps to obtain an overview of all markers and expression on all cells to identify novel subsets. Viable cells were downsampled to 1,000 cells per triplicate and donor using the Downsample version 3.3 plugin for FlowJo and were concatenated to one sample per group. FlowSOM was performed for each study group separately. Flow cytometry standard (FCS) files were manually pregated as $CD3^+CD4^+$ Live/Dead and were sorted into 15 metaclusters, which provided sufficient metaclusters to capture the expected number of unique cell types while potentially uncovering other

biologically interesting populations. For the second study group, we chose the option "apply on map" of the first analyzed study group. Heat maps were generated for both study groups including all parameters. The resulting metaclusters were manually inspected for the expression of marker using the heat map.

Statistical analysis

Continuous variables with normal distribution were represented as mean ± standard deviation (SD), while non-normal distribution was represented by median and range interquartile. Quantitative data among multiple groups was analyzed by ANOVA and Kruskal–Wallis tests. Categorical variables in terms of frequency and percentage were expressed and were compared using the χ^2 or Fisher's exact tests as appropriate. Spearman rank test was used for correlation evaluation. Multivariate logistic regression models were constructed, and least absolute shrinkage and selection operator (LASSO) regression method was used for feature selection, and the area under receiver operating characteristic (ROC) curve (AUC) was used to verify the sensitivity and specificity of models. Statistical analyses were performed using SPSS version 20.0 (IBM, Chicago, IL) and R package version 3.5.1. $p<0.05$ was considered as statistically significant.

Results

Patient characteristics

A total of 154 patients were recruited and divided into three groups, including 33 patients with *A.f* (−) asthma, 57 patients with *A.f* (+) asthma, and 64 ABPA patients. There was a significant difference in age between ABPA and *A.f* (+) asthma ($p<0.05$). The parameters of lung function showed that FVC (%), FEV1 (%), FEV1/FVC (%), PEF (%), MEF75/25 (%), MEF50 (%), and MEF25 (%) in the ABPA group and the *A.f* (+) asthma group were lower than those in the *A.f* (−) asthma group (both $p<0.05$), but these parameters showed no statistical significance between the ABPA and *A.f* (+) asthma groups. FeNO in the ABPA group was higher than that in the *A.f* (+) asthma and the *A.f* (−) asthma group (both $p<0.01$). In venous blood cell analysis, both EO and EO% in ABPA group were higher than those in *A.f* (+) asthma and *A.f* (−) asthma group ($p<0.001$). In the induced sputum cytology classification, the SEO% of the ABPA group was higher than that of *A.f* (+) asthma and *A.f* (−) asthma groups ($p<0.05$), and SNEUY% and SMø% in the ABPA group presented significant difference compared with *A.f* (−) asthma group (both $p<0.05$) (Table 1).

There was no difference in tIgE, but significant difference in *A.f*-sIgE among the three groups, in which the ABPA group had significantly higher sIgE level than the other two groups (10.24 *vs.* 1.15 *vs.* 0.07, $p<0.05$). ACT scores were statistically different (15 *vs.* 18 *vs.* 21, $p<0.01$) among the three groups, and the lowest was found in the ABPA group (Figure 1).

It should be noted that 95.20% of ABPA patients did not reach the control level; the percentage was 74.30% in *A.f* (+)-asthma patients and only 27.30% in *A.f* (−)-asthma patients (Figure 2A). The level of *A.f*-sIgE in 76.2% of the ABPA patients was classified as high concentration (classes 3–6), while only 25.7% of the *A.f* (+) asthma patients had sIgE level equal or above class 3 (Figure 2B).

Correlation of clinical and immunological parameters in different groups

There were positive correlations between ACT score and all lung function parameters ($p<0.01$) and negative correlations between ACT and *A.f*-sIgE, FeNO, SEO%, EO%, and EO ($p<0.01$). *A.f*-sIgE was positively correlated with FeNO value, SEO%, EO%, and EO ($p<0.01$) and negatively correlated with ACT score and all lung function parameters ($p<0.01$). All lung function parameters except MEF50 (%) were negatively correlated with FeNO and SEO% ($p<0.05$). FeNO value was positively correlated with SEO%, EO%, and EO ($p<0.01$) (Figure 3).

For the ABPA group, ACT was positively correlated with all lung function parameters ($p<0.05$), *A.f*-sIgE value was positively correlated with tIgE ($p<0.05$), and tIgE value was negatively correlated with EO ($p<0.05$). For the *A.f* (+)-asthma group, ACT score was positively correlated with all lung function parameters ($p<0.01$); all the lung function parameters except FEV1 (%) were negatively correlated with SEO% ($p<0.05$). FeNO was positively correlated with SEO% ($p<0.01$). For the *A.f* (−)-asthma group, ACT value was positively correlated with FEV1 (%), FEV1/FVC (%), MEF75/25(%), MEF50 (%), and MEF25 (%) ($p<0.05$); A.f-sIgE was negatively correlated with MEF50 (%) ($p<0.05$); FeNO was positively correlated with SEO% and EO ($p<0.05$); and FVC (%) and MEF50 (%) were positively correlated with EO% ($p<0.05$) (Figure 4).

Predictive value of clinical parameters in *A.f* (+) asthma and ABPA

ROC curve was used to analyze the predictive value of clinical parameters for *A.f* (+) asthma and ABPA. We found that *A.f*-sIgE, FeNO, SEO%, EO%, and EO had a higher predictive value (cutoff, 4.108; AUC=0.749; CI, 0.629–0.869; cutoff, 55.5; AUC=0.811; CI, 0.707–0.916; cutoff, 6.625; AUC=0.738; CI, 0.619–0.857; cutoff, 8.7; AUC=0.738; CI, 0.619–0.857; cutoff, 0.815; AUC=0.922; CI, 0.856–0.988) than other parameters (Figures 5A–D). In differentiating *A.f* (+) asthma from ABPA, the combination of FeNO and EO

TABLE 1 The comparison of clinical parameters in the three groups.

	[a]ABPA (n=64)	[b]*A.f* (+) Asthma (n=57)	[c]*A.f* (–) Asthma (n=33)	Comparison (p-value)		
				a vs. b	*a vs. c*	*b vs. c*
Age (years)	45.0 (33.5–52.8)	33.0 (14.5–52.0)	38.0 (9.0–61.5)	**0.026**	0.161	0.703
Male/Female	40/24	34/23	20/13	0.926	0.924	0.772
BMI (kg/m^2)	20.73 (18.64–24.29)	21.64 (18.36–24.80)	20.98 (16.78–25.50)	0.830	0.827	0.976
Lung function						
FVC (%)	79.87 ± 16.97	83.19 ± 19.07	94.73 ± 15.98	0.649	**0.000**	**0.007**
FEV1 (%)	64.35 (46.25–84.32)	60.20 (41.00–90.50)	88.90 (76.65–102.20)	0.919	**0.000**	**0.001**
FEV1/FVC (%)	78.34 ± 20.76	75.46 ± 18.70	90.39 ± 11.17	0.638	**0.005**	**0.001**
PEF (%)	64.28 ± 25.39	62.65 ± 26.25	85.80 ± 19.55	0.656	**0.000**	**0.000**
MMEF75/25 (%)	33.08 (12.80–57.83)	22.00 (14.50–60.60)	55.10 (41.36–76.15)	0.379	**0.006**	**0.001**
MEF50 (%)	37.05 (15.40–63.25)	22.30 (15.00–68.20)	54.41 (44.05–75.05)	0.258	**0.009**	**0.000**
MEF25 (%)	29.45 (13.67–54.80)	24.60 (10.20–53.42)	48.50 (32.25–69.23)	0.425	**0.021**	**0.003**
FeNO	76.00 (52.00–89.50)	40.00 (32.00–52.00)	44.00 (23.50–69.00)	**0.000**	**0.001**	0.782
Venous blood cell analysis						
WBC (10^9/L)	8.00 (6.74–9.86)	8.52 (6.93–9.90)	8.50 (6.20–10.02)	0.882	0.979	0.745
NEUT%	58.61 ± 13.30	59.40 ± 15.35	58.16 ± 14.79	0.581	0.856	0.659
LY%	22.90 (18.03–35.00)	28.40 (18.40–34.00)	27.10 (20.40–41.40)	0.709	0.134	0.401
EO%	10.60 (7.20–12.55)	4.10 (1.20–7.30)	4.30 (1.20–7.15)	**0.000**	**0.000**	0.917
NEUT (10^9/L)	4.25 (3.35–6.28)	4.50 (3.30–6.40)	4.40 (3.60–6.25)	0.716	0.898	0.859
LY (10^9/L)	1.80 (1.48–2.53)	2.40 (1.50–2.60)	2.10 (1.55–3.05)	0.528	0.293	0.735
EO (10^9/L)	1.65 (1.09–2.26)	0.33 (0.10–0.54)	0.27 (0.09–0.65)	**0.000**	**0.000**	0.606
Induced sputum cytology classification						
SNEUT%	71.95 ± 20.41	60.39 ± 24.92	54.24 ± 25.66	0.067	**0.003**	0.261
SMø%	5.00 (0.50–20.30)	9.50 (1.00–25.00)	16.00 (4.63–44.59)	0.367	**0.024**	0.135
SEO%	21.15 (7.60–35.75)	5.55 (2.50–14.50)	5.85 (2.75–9.50)	**0.000**	**0.000**	0.681
SLY%	1.02 (0.50–2.00)	1.05 (0.50–1.50)	1.25 (1.00–2.50)	0.844	0.146	0.116
Infection index						
ESR (mm/h)	18.00 (8.50–26.25)	12.00 (7.00–20.00)	12.00 (10.00–21.50)	0.320	0.473	0.623
PCT (positive rate)	80.95%	77.14%	75.76%	0.682	0.586	0.893

ABPA, allergic bronchopulmonary aspergillosis; A.f (+) asthma, Aspergillus fumigatus-sensitized asthma; A.f (–) asthma, non-Aspergillus fumigatus-sensitized asthma; BMI, body mass index; FVC, forced vital capacity; FEV1, forced expiratory volume in 1 s; PEF, peak expiratory flow; MMEF, maximum mid-expiratory flow; MEF50, maximal expiratory flow 50; MEF25, maximal expiratory flow 25; FeNO, fractional exhaled nitric oxide; SNEUT, sputum neutrophils; SMø, sputum macrophages; SEO, sputum eosinophils; SLY, sputum lymphocytes; WBC, white blood cell; NEUT, neutrophils; LY, lymphocytes; EO, eosinophils; ESR, erythrocyte sedimentation rate; PCT, procalcitonin. Bold font indicates statistical significance (p<0.05).

parameters can optimize the diagnostic efficiency, and the sensitivity and specificity were 80% and 100%, respectively (AUC=0.948; CI, 0.897–0.999) (Figure 5E).

As for the immunological parameters, no significant difference was found with IL-33, IL-17E, and TSLP among these groups (p>0.05) (Figure 6).

Compared with specific antibodies and their components between ABPA and *A.f* (+) asthma, the levels of *A.f*-sIgG4, *A.f*-sIgA, and *A.f*-sIgE in ABPA were significantly higher than those in the *A.f* (+) asthma group (105.3 *vs.* 15.6, p=0.023; 0.15 *vs.* 0.03, p=0.014; 8.4 *vs.* 1.44, p=0.002, respectively). sIgA and sIgE components also presented significant differences in IgA of Asp f9 (0.46 *vs.* 0.05, p=0.003) and IgE of Asp f3 (2.43 *vs.* 0.06, p=0.007) and Asp f9 (19.24 *vs.* 0.06, p=0.001) between ABPA and *A.f* (+) asthma (Figure 7).

The PBMCs from seven ABPA patients, six *A.f* (+)-asthma patients, and seven HDM-sensitized asthma [HDM (+)-asthma] patients were collected and exposed to 25 μg/ml *A.f* or HDM extracts, respectively, for 6 h. The percentages of Th1 ($CD3^+CD4^+CXCR3^+$), Th2 ($CD3^+CD4^+CRTH2^+$), Tfh ($CD3^+CD4^+CXCR5^+PD\text{-}1^+$), and Treg ($CD3^+CD4^+CD25^+CD127^{low/-}$) had no significant differences among the three groups. After exposure to allergen, only the Th2 in the HDM group increased significantly (all p<0.05). The signature cytokine-secreting T-cell subsets including Th1 (IFN-γ), Th2 (IL-4 and IL-13), Tfh (IL-13), and Treg (IL-10) were also detected; the percentage of IFN-γ-positive Th1 in the ABPA group was 69.62% ± 13.52%, which was higher than that in the HDM group (34.23% ± 9.95%) (p<0.05). After allergen exposure, the IFN-γ-positive Th1 cells of both ABPA and *A.f* (+)-asthma patients decreased; however, there

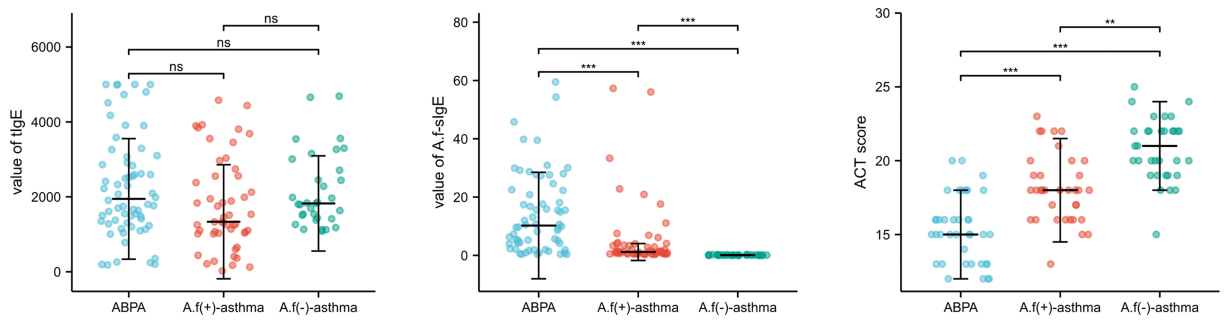

FIGURE 1
The comparison of tIgE, *A.f*-sIgE, and ACT score in three groups. ABPA, allergic bronchopulmonary aspergillosis; *A.f* (+) asthma, *Aspergillus fumigatus*-sensitized asthma; *A.f* (–) asthma, non-*Aspergillus fumigatus* sensitized asthma. ns, no significance; **p<0.01; ***p<0.001.

was no statistical change in the HDM group after HDM exposure (Figure 8).

The FlowSOM algorithm was further used to cluster, visualize, and compare the differences of $CD3^+CD4^+$T cells among the ABPA, *A.f* (+)-asthma patients, and HDM (+)-asthma patients before and after exposure. The result identified that the frequency of metaclusters of pop 10 ($CD3^+CD4^+PD\text{-}1^+CD127^+IFN\text{-}\gamma^+$), pop 13 ($CD3^+CD4^+PD\text{-}1^+IFN\text{-}\gamma^+$) and pop 6 ($CD3^+CD4^+CD127^+CXCR5^+$) were higher in the ABPA group compared with that in the *A.f* (+)-asthma group; meanwhile, pop 13 ($CD3^+CD4^+$ $PD\text{-}1^+IFN\text{-}\gamma^+$) increased and pop 11 ($CD3^+CD4^+CD25^+CD127^+PD\text{-}1^+$) decreased after exposure to allergen in the ABPA patients. The metaclusters of pop 13 also increased in the *A.f* (+)-asthma group after exposure; however, pop 11 was slightly changed by stimulation. For the HDM-allergic patients, the frequencies of pop 3, pop 4, pop 10, pop 11, pop 12, and pop 13 were all lower compared to ABPA group patients (Figure 9).

We further defined the metacluster of $CD3^+CD4^+$ $CD25^+CD127^+$ cells as the activated Tregs and compared these metacluster cells with Treg ($CD3^+CD4^+$ $CD125^+CD127^{low/-}$). The metaclusters of the three groups all increased after stimulation [from 2.85% ± 1.62% to 3.49% ± 1.89% in the ABPA group; from 2.95% ± 2.58% to 3.97% ± 1.63% in the *A.f* (+)-asthma group; from 3.20% ± 0.85% to 4.0% ± 1.73% in the HDM (+)-asthma group]. For the ABPA group, the IL-4, IL-13 and IFN-γ^+ expression on the metacluster all decreased after allergen exposure; however, the expression of these cytokines barely changed in the metacluster of *A.f* (+) asthma, Treg of ABPA, and *A.f* (+) asthma. These cytokines even increased in the metacluster of the HDM (+)-asthma group. The IL-4 expression statistically upregulated in the metacluster in the HDM group after allergen exposure (Figure 10). The metacluster of $CD3^+CD4^+PD\text{-}1^+$ also increased in all groups after stimulation; however, only the $CD3^+CD4^+PD\text{-}1^+IFN\text{-}\gamma^+$ of ABPA decreased (Supplementary Figure).

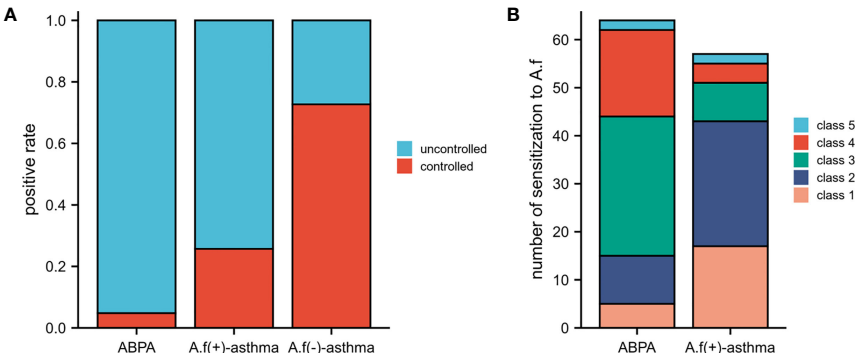

FIGURE 2
Control situation and class of *A.f*-sIgE in different groups. **(A)** Control situation among ABPA, *A.f* (+) asthma, and *A.f* (–) asthma. **(B)** Class of *A.f*-sIgE between ABPA and *A.f* (+) asthma. ABPA, allergic bronchopulmonary aspergillosis; *A.f* (+) asthma, *Aspergillus fumigatus*-sensitized asthma; *A.f* (–) asthma, non-*Aspergillus fumigatus*-sensitized asthma.

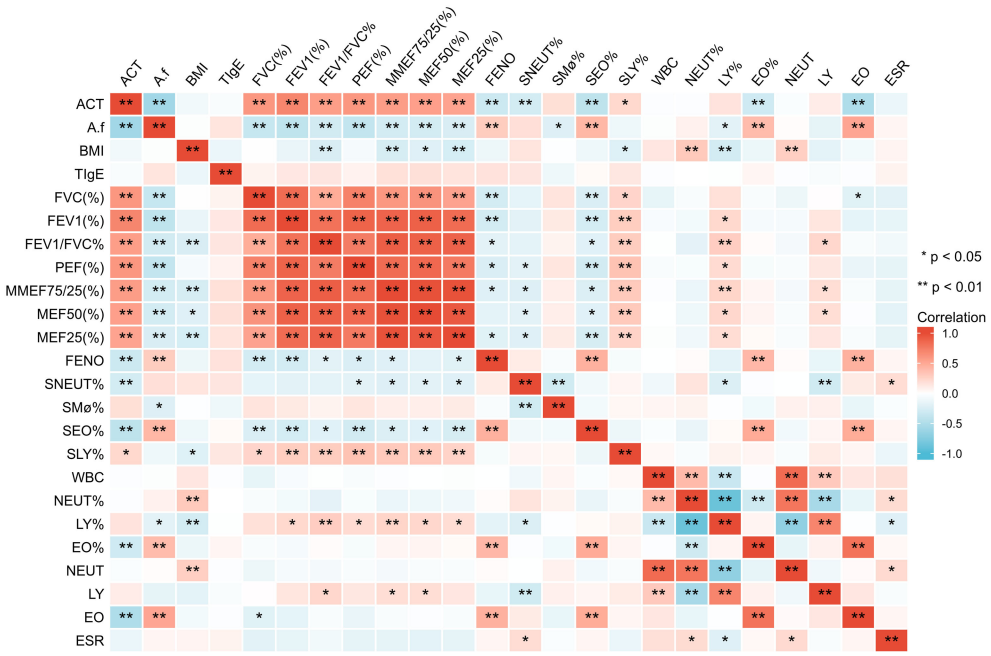

FIGURE 3
Correlation of clinical parameters in all the patients. ACT, asthma control test; *A.f*, *Aspergillus fumigatus*; BMI, body mass index; tIgE, total IgE; FVC, forced vital capacity; FEV1, forced expiratory volume in 1 s; PEF, peak expiratory flow; MMEF, maximum mid-expiratory flow; MEF50, maximal expiratory flow 50; MEF25, maximal expiratory flow 25; FeNO, fractional exhaled nitric oxide; SNEUT, sputum neutrophils; SMø, sputum macrophages; SEO, sputum eosinophils; SLY, sputum lymphocytes; WBC, white blood cell; NEUT, neutrophils; LY, lymphocytes; EO, eosinophils; ESR, erythrocyte sedimentation rate; PCT, procalcitonin. *p<0.05; **p<0.01.

Discussion

In this study, we compared the clinical and immunological characteristics in ABPA and *A.f*-sensitized asthma patients. We found that the eosinophils in blood and induced sputum and FeNO were significantly higher in ABPA patients compared to *A.f*-sensitized patients. Immunological analysis showed that *A.f*-specific IgE, IgG, IgA, and IFN-γ+Th1 cells also increased in

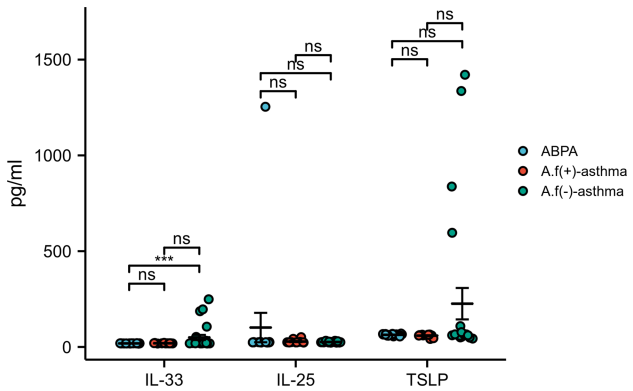

FIGURE 4
Correlation of clinical parameters in the three groups. ACT, asthma control test; *A.f*, *Aspergillus fumigatus*; BMI, body mass index; tIgE, total IgE; FVC, forced vital capacity; FEV1, forced expiratory volume in 1 s; PEF, peak expiratory flow; MMEF, maximum mid-expiratory flow; MEF50: maximal expiratory flow 50; MEF25, maximal expiratory flow 25; FeNO, fractional exhaled nitric oxide; SNEUT, sputum neutrophils; SMø, sputum macrophages; SEO, sputum eosinophils; SLY, sputum lymphocytes; WBC, white blood cell; NEUT, neutrophils; LY, lymphocytes; EO, eosinophils; ESR, erythrocyte sedimentation rate; PCT, procalcitonin. ***p < 0.001; ns indicates no statistical significance.

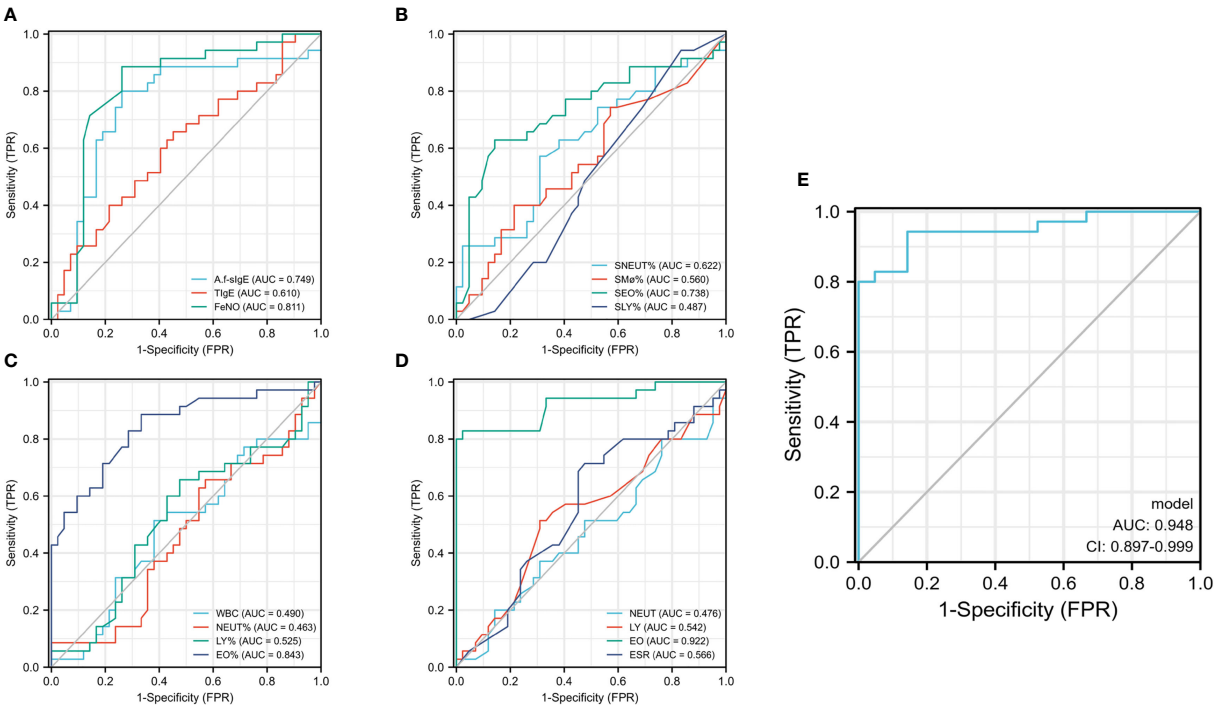

FIGURE 5
Predictive value of clinical parameters in *A.f* (+) asthma and ABPA. *A.f* (+) asthma, *Aspergillus fumigatus*-sensitized asthma; ABPA, allergic bronchopulmonary aspergillosis. **(A–D)** ROC curve analyzed the predictive value of clinical parameters for *A.f* (+) asthma and ABPA; **(E)** ROC curve analyzed the predictive value of combination of FeNO and EO parameters.

ABPA patients. These findings suggested ABPA patients had more severe eosinophilic inflammation and enhanced Th1 responses compared with *A.f*-sensitized asthma patients. In addition, we first showed that the combination of FeNO and eosinophils parameters had good diagnostic efficiency in differentiating *A.f* (+) asthma from ABPA and thus provided an easy tool other than sIgE and tIgE tests in clinical practice.

The first important thing about this tool is that our study highlighted the importance of eosinophils in the diagnosis of ABPA. Like fungus-sensitized asthma—a type-2 (T2) inflammation caused by eosinophilia (14), ABPA is also a chronic lung inflammation with eosinophilia (14). In fact, eosinophilia has been considered as an important indicator for the diagnosis of ABPA (15). Just as fungal sensitization, whose

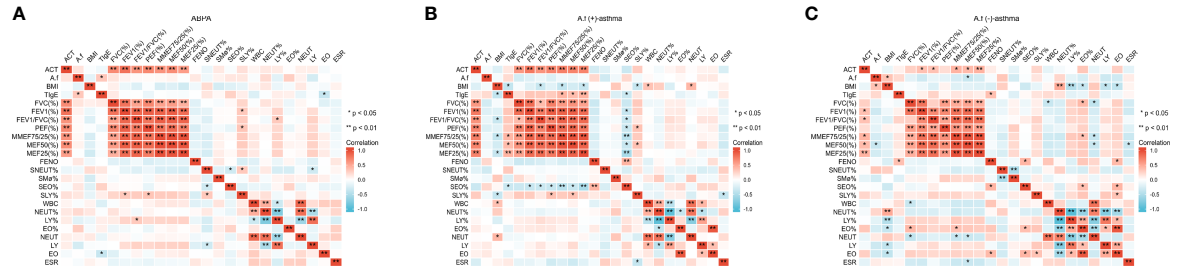

FIGURE 6
IL-33, IL-25, and TSLP levels in different groups. **(A)** IL-33, IL-25, and TSLP levels in ABPA group; **(B)** IL-33, IL-25, and TSLP levels in *A.f* (+) asthma group; **(C)** IL-33, IL-25, and TSLP levels in *A.f* (–) asthma group. IL-33, interleukin 33; IL-25, interleukin 25; IL-17E, interleukin 17E (can be as IL-25); TSLP, thymic stromal lymphopoietin; ABPA, allergic bronchopulmonary aspergillosis; *A.f* (+) asthma, *Aspergillus fumigatus*-sensitized asthma; *A.f* (–) asthma, non-*Aspergillus fumigatus*-sensitized asthma. *p<0.05 and **p<0.01.

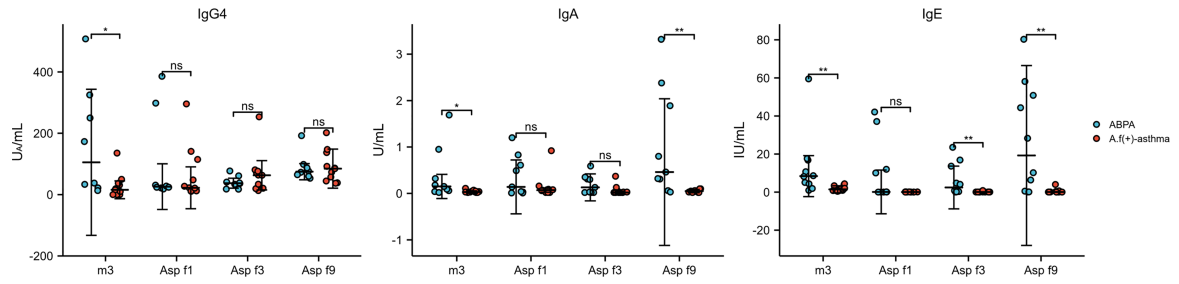

FIGURE 7
The level of IgG4, IgA, and IgE against *A.f* in different groups. ABPA, allergic bronchopulmonary aspergillosis; *A.f* (+) asthma, *Aspergillus fumigatus*-sensitized asthma; m3, crude extract of A.f; Asp f1, Asp f3, and Asp f9, components of *A.f*; ns, no significance; *p<0.05; **p<0.01.

incidence in patients ranges from 35% to 75% (16), tends to make asthma more severe (17), in our study, we observed that the SEO%, EO, and EO% in induced sputum and peripheral blood of ABPA patients were significantly higher than in *A.f*- and HDM-sensitized asthma patients, which further proved the importance of eosinophils in the diagnosis of ABPA. In addition, we found that in the ABPA group, FeNO levels, which had been regarded as an indicator of eosinophil inflammation in the airway, were significantly higher than those in the other two groups. Our study suggested that ABPA had more severe eosinophilic airway inflammation than *A.f*-sensitized asthma, and FeNO could be considered as a surrogate indicator in the diagnosis of ABPA.

Apart from an emphasis on eosinophilia, we also want to underscore that the measurement of lung function played an important role in the management of asthma and ABPA (18). In the early stage of ABPA, there might be no shadow on lung imaging, but peripheral bronchi and small airway had been involved (19); therefore, it was necessary to assess airway injury with a lung function test. The lung function of ABPA patients was mainly characterized by reversible obstructive ventilatory dysfunction in acute phase, and it was mixed ventilatory dysfunction with reduced diffusion function in chronic phase (20). We found that the lung function parameters decreased in all the three groups, with those in *A.f* (+)-asthma and ABPA groups decreasing more obviously, suggesting that *A.f* might be one of the main reasons leading to accelerated deterioration of lung function. However, there was no statistical difference between the ABPA and the *A.f* (+)-asthma group, which was similar to previous studies (21, 22). Some studies found that bronchiectasis and more severe airflow obstruction were associated with *A.f* sensitization.

Another specific indicator of ABPA was also reviewed in our study. *A.f*-sIgE was considered to be the most sensitive of all laboratory indicators in ABPA diagnosis (21, 22). We analyzed the sensitization of *A.f* in ABPA and *A.f* (+)-asthma groups and found that the level of *A.f*-sIgE in the ABPA group was higher than that in the *A.f* (+)-asthma group. Many studies had shown that the IgE titer of recombinant *A.f* in ABPA patients was higher than that in non-ABPA asthma, which indicated that ABPA patients had a stronger T2 immune response to *A.f* and produce a high level of sIgE and tIgE (23, 24). Thus, the level of *A.f*-sIgE could be used to distinguish ABPA from *A.f*-sensitized asthma; moreover, the cutoff value of *A.f*-sIgE as a diagnostic indicator for ABPA should be elevated at a higher level and investigated in large population rather than the *A.f*-sIgE test result just being positive (above 0.35 KU/L).

Our understanding of ABPA and asthma, despite their similarities in symptoms and treatments, was enhanced not only by our study of the indicators but also by the correlations between these indicators. We used ACT to assess control of *A.f* (+) asthma, *A.f* (−) asthma and ABPA and found that ABPA had the lowest ACT score among the three groups. In the correlation analysis, we also found that ACT was positively correlated with all lung function parameters and negatively correlated with *A.f*-sIgE, FeNO, SEO%, EO%, and EO. Studies had shown that the acute phase of ABPA was associated with a reversible decline in lung function (25), and eosinophils were the primary mediators of inflammatory activity in ABPA (26), which was consistent with our findings that ABPA had the worst control level, which may be accounted for by the decreased lung function and eosinophilia. In addition, we found a negative correlation between lung function parameters and SEO% in the three groups; however, no correlation between peripheral blood eosinophils and lung function parameters was observed in the ABPA group, which suggested that sputum eosinophils were more sensitive in reflecting exacerbation of lung function in ABPA than blood eosinophils.

Nitric oxide (NO) mediated a variety of physiological reactions at low level, while a high level of NO was involved in the occurrence of innate immunity and chronic inflammatory diseases (27). In our study, there was a significant negative correlation between ACT score and FeNO in the three groups, which indicated that patients with higher FeNO tend to suffer

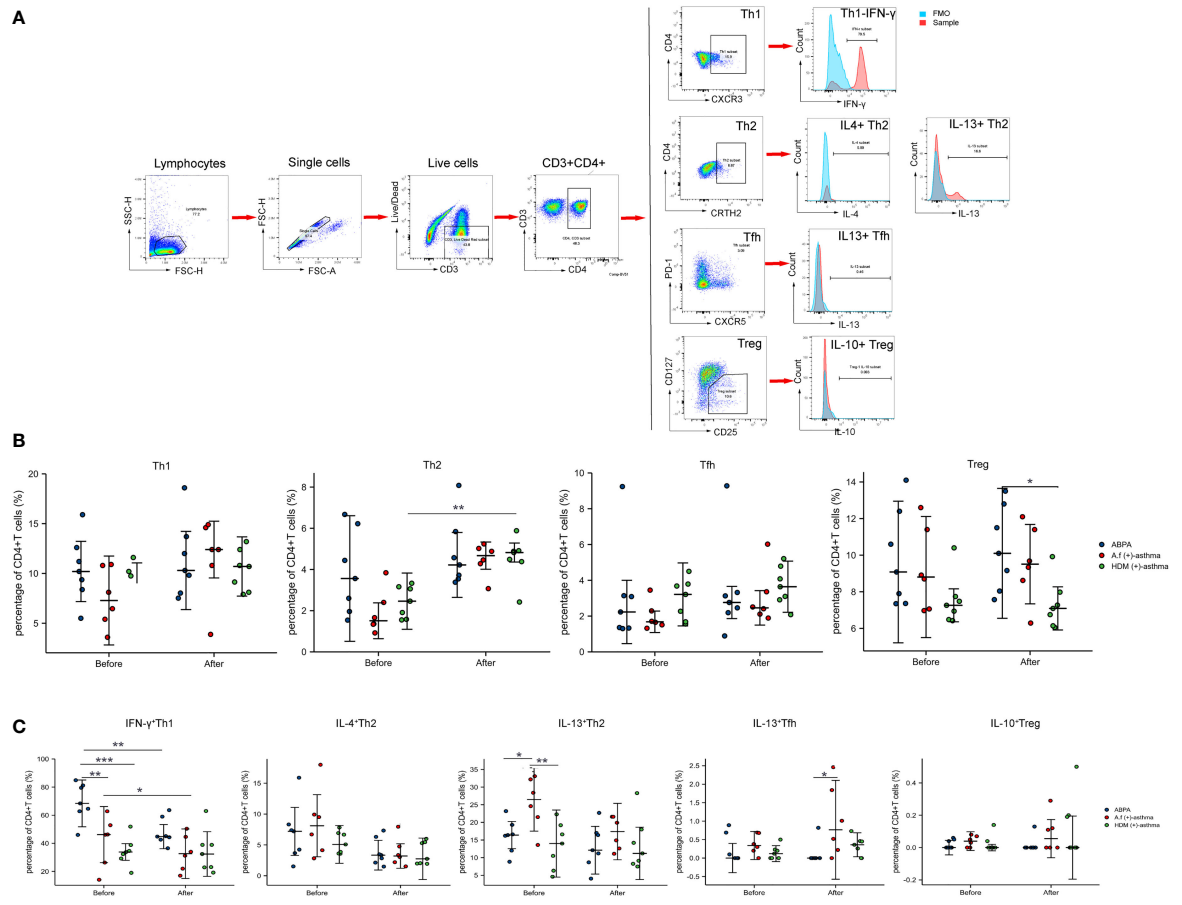

FIGURE 8
$CD4^+$ T-cell subsets and cytokines expression. **(A)** Manual gating strategy for $CD4^+$ T-cell subsets and representative plots for Th1 ($CD3^+CD4^+CXCR3^+$), Th2 ($CD3^+CD4^+CRTH2^+$), Tfh ($CD3^+CD4^+CXCR5^+PD\text{-}1^+$), and Treg ($CD3^+CD4^+CD25^+CD127^{low/-}$). IFN-$\gamma^+$Th1, IL-$4^+$ Th2, IL-13^+ Th2, IL-13^+ Tfh, and IL-10^+ Treg were representatively exhibited and compared with FMO control. **(B)** The dot plot figures showed $CD4^+$ T-cell subsets; **(C)** the cytokines of the Th1 (IFN-γ), Th2 (IL-4 and IL-13), Tfh (IL-13), and Treg (IL-10). ABPA, allergic bronchopulmonary aspergillosis; *A.f* (+) asthma, *Aspergillus fumigatus*-sensitized asthma; HDM (+) asthma, house dust mite-sensitized asthma; Th1, T helper cells 1; Th2, T helper cells 2; Tfh, follicular helper T cells; Treg, regulatory T cells; IFN-γ, interferon γ; IL-4, interleukin 4; IL-13, interleukin 13; IL-10, interleukin 10. *p<0.05, **p<0.01; ***p<0.001.

from uncontrolled asthma or ABPA. It is suggested that FeNO could be a biomarker that integrates both airway inflammation and lung function changes (28), which was consistent with our findings that a negative correlation existed between FeNO and lung function parameters. We also found that *A.f*-sIgE was positively correlated with FeNO, SEO%, EO%, and EO and negatively correlated with ACT and all lung function parameters, which re-confirmed the relationship of sensitization of *A.f* and poor control of asthma and ABPA.

To distinguish *A.f* (+)-asthma patients from ABPA accurately, we further compared the ROC curves of the potential clinical indicators. Our study suggested that some parameters such as *A.f*-sIgE, FeNO, SEO%, EO%, and EO had good diagnostic efficiency. However, the cutoff values of these indicators were different from the current criteria. For example, the current criteria proposed that *A.f*-sIgE is >0.35 KAU/L and EO >0.5×10^9/L for the diagnosis of ABPA (11), while we found that the best diagnostic efficiency could be achieved when the cutoff value of *A.f*-sIgE was 4.108 KU/L and EO was 0.815×10^9/L. We strongly suggest that the optimal cutoff values of these indicators should be investigated and validated in a large population. We also tried to incorporate the indicators into the ROC analysis. Just as we expected, a sensitivity of 80% and a specificity of 100% were obtained in the combined FeNO and EO diagnostic model, which implied that for *A.f*(+)-asthma and ABPA with high-level tIgE, the combination of FeNO and EO for differential diagnosis was reliable and had the advantages of convenience and low cost.

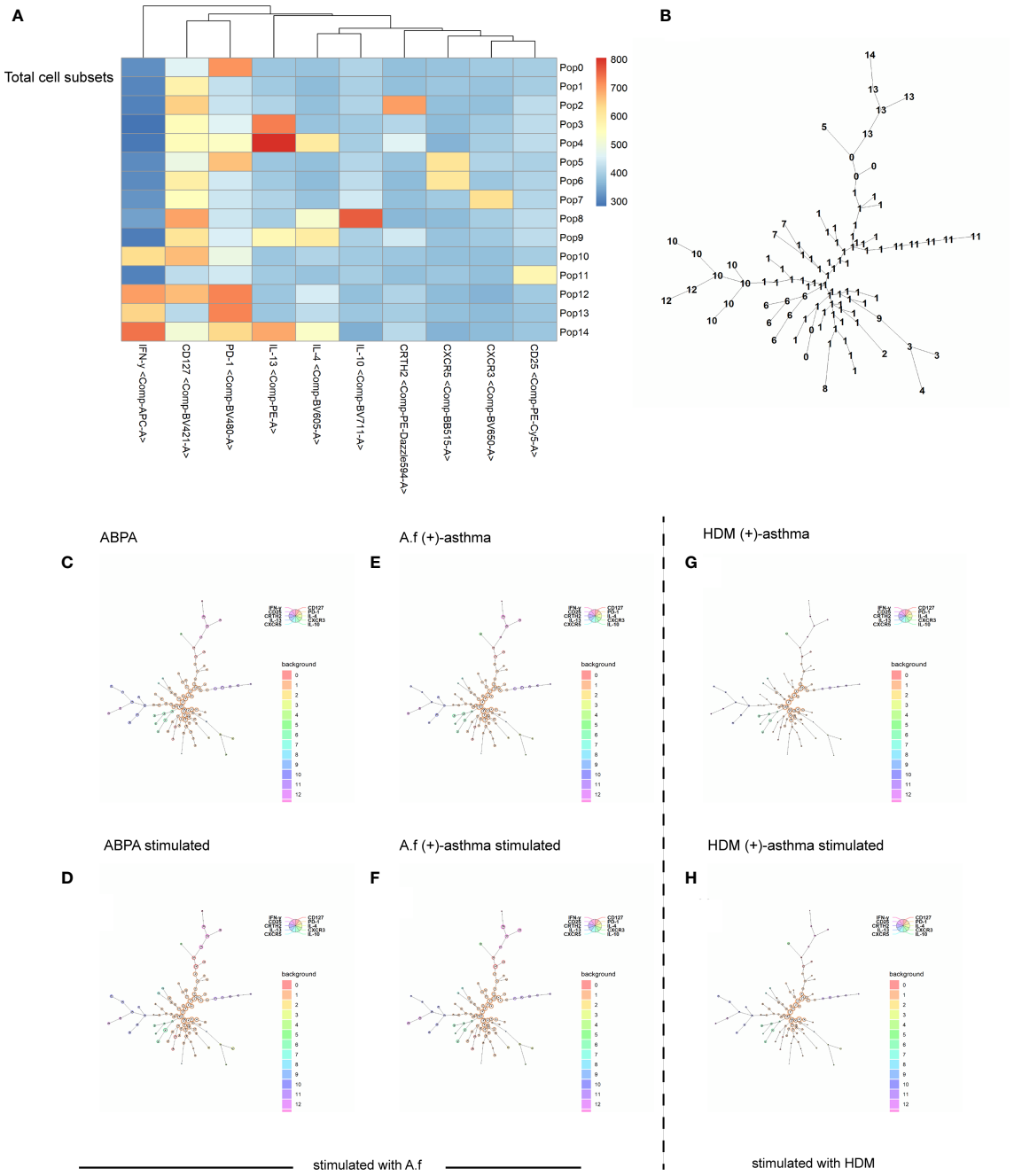

FIGURE 9
FlowSOM algorithm. Spanning tree visualization of a self-organizing map using compensated flow cytometric data. Data were taken from the lineage (CD3+, CD4+) gate. **(A)** heatmap of the FlowSOM clustering; **(B)** minimal spanning tree for 15 metaclusters; **(C–H)** FlowSOM nodes represent clusters of cells. Metaclusters of the nodes, determined by the map, are represented by the background color of the nodes. *A.f* (+) asthma, *Aspergillus fumigatus*-sensitized asthma; HDM (+) asthma, house dust mite-sensitized asthma.

We also studied epithelial-cell-derived IL-33, IL-25, and TSLP, which were regarded as alarmins and played pivotal roles in the initiation of allergic inflammation in asthma (29). Their receptors widely expressed in structural cells and innate and adaptive immune cells, contributing to the airway disease by driving inflammatory processes (30). The expression of IL-33, IL-25, and TSLP should be higher in ABPA and asthma theoretically. However, we did not find a significant difference

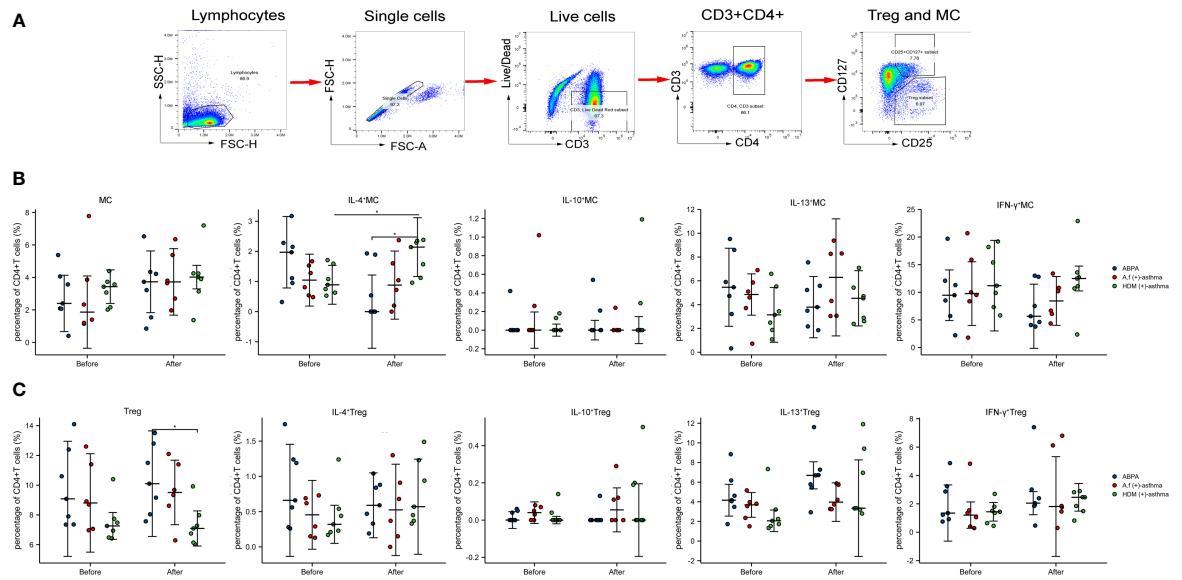

FIGURE 10
Treg ($CD3^+CD4^+CD25^+CD127^{low/-}$), metacluster ($CD3^+CD4^+CD25^+CD127^+$), and their cytokines expression. **(A)** Manual gating strategy for metacluster ($CD3^+CD4^+CD25^+CD127^+$); **(B)** the dot plot figures showed the percentage of Treg and the cytokines of the IL-4, IL-10, IL-13, and IFN-γ; **(C)** the percentage and cytokines (IL-4, IL-10, IL-13, and IFN-γ) of metacluster ($CD3^+CD4^+CD25^+CD127^+$) are shown. MC, metacluster ($CD3^+CD4^+CD25^+CD127^+$); ABPA, allergic bronchopulmonary aspergillosis; *A.f* (+) asthma, *Aspergillus fumigatus*-sensitized asthma; HDM (+) asthma, house dust mite-sensitized asthma; Th1, T helper cells 1; Th2, T helper cells 2; Tfh, follicular helper T cells; Treg, regulatory T cells; IFN-γ, interferon γ; IL-4, interleukin 4; IL-13, interleukin 13; IL-10, interleukin 10. *p<0.05.

in serum IL-33, IL-25, and TSLP among ABPA, *A.f*-sensitized asthma, and non-*A.f*-sensitized asthma, which was consistent with previous studies (26). The explanation for the absence of increased IL-33, IL-25, and TSLP may be that we examined these cytokines in serum samples rather than in bronchial epithelium. It is possible that these cytokines in the sputum will provide more favorable information. However, lack of enough sputum samples did not allow us further pursuit, which was a limitation of our study. Simultaneously measuring the cytokine secretion and mRNA expression of the epithelium cells may provide robust evidence for roles of these cytokines in ABPA and *A.f*-sensitized asthma.

Genetic factors and activation of bronchial epithelial cells in asthma or cystic fibrosis are responsible for $CD4^+$Th2 lymphocyte activation and production of A.f-sIgE, A.f-sIgG and A.f-sIgA (31). ABPA is a disease commonly associated with asthma and cystic fibrosis; theoretically, specific antibodies to *A.f* in ABPA would be higher. In our study, we found that sIgG4, sIgA, and sIgE in ABPA were higher than those in *A.f*-sensitized asthma, which coincided with the previous study (32). Similarly, one study that looked into the total IgG4 level (not *A.f*-IgG4) also found that IgG4 levels in ABPA patients were higher than that in asthma (33). Apart from the *A.f*-specific antibodies analysis, we further investigated the *A.f* component antibodies profiles in the ABPA and *A.f*-sensitized asthma patients. Asp f1 was the major component of *A.f*, and Asp f3 and Asp f9 were components that often caused cross-sensitization. In our study, we that found Asp f9-sIgA and Asp f9-sIgE and Asp f3-sIgE in the ABPA group was significantly higher than those in *A.f*-sensitized asthma, however, specific antibodies (including IgG4, IgE, and IgA) against Asp f1 showed no difference in the two groups. Our study was not consistent with previous studies that suggested that sIgE against Asp f 1, Asp f 2, Asp f 4, and Asp f 6 in ABPA were higher than that in *A.f*-sensitized asthma (34). This discordance may be attributed to small sample sizes in the relevant studies. In addition, the clinical significance of specific antibody levels of Asp f3 and Asp f9 between the two groups remains unclear. Our study provided preliminary information of specific antibodies against Asp f3 and Asp f9 in ABPA and *A.f*-sensitized asthma and the detailed role of these antibodies need to be elucidated in further studies.

ABPA- and *A.f*-sensitized asthmas are regarded as type 2 inflammation, and the activation of Th2 cells play important roles in their pathogenesis. Becker et al. reported that A.f plays a primary role in the induction of a Th2 response in human PBMCs (35). Emerging data have supported that APBA pathophysiology shifted from immune deviation toward favored

Th2 responses (36). However, A.f is an invasive fungus and could also elicit type 1 inflammation by pathogen-associated molecular patterns (PAMPs) in which innate immune cells and antigen presenting cells were involved (37). In our study, we found that the IFN-γ^+Th1 cells especially $CD3^+CD4^+PD\text{-}1^+CD127^+IFN\text{-}\gamma^+T$ cells significantly increased in ABPA patients when compared to A.f-sensitized patients, which suggested that there might be more severe airway epithelial damage in the ABPA patients, driving a shift to Th1 inflammation. However, we did not find the difference in epithelial damage-related cytokines such as IL-25, IL-33, and TSLP in sera of the two groups. As we mentioned above, we think the cytokine analysis that directly targeted epithelial cells will provide more details of mucus barriers dysfunction in ABPA. The FlowSOM algorithm confirmed that the frequency of $CD3^+CD4^+PD\text{-}1^+CD127^+IFN\text{-}\gamma^+T$ cells was higher in ABPA patients. It was reported that PD-1 maintains tolerance and CD127 could be upregulated in activated Treg cells (38, 39). We further gated metacluster ($CD3^+CD4^+$ $CD25^+$ $CD127^+$) and metacluster ($CD3^+CD4^+$ $PD\text{-}1^+$), the two metaclusters increased in all the groups after stimulation. However, cytokines, especially the IFN-γ of the two metaclusters declined only in ABPA, although no statistical significance was found. The decline in the cytokine expression in ABPA patients might impair the tolerance function of the cells and lead to disease progression. However, more samples are needed to confirm our findings.

In conclusion, *A.f* sensitization was an important factor leading to the decline of lung function and the worsening of asthma control in asthma and ABPA patients. ABPA patients showed a higher FeNO level and eosinophils in blood and induced sputum, suggesting a more severe eosinophilic inflammation in ABPA pathogenesis. The combined application of FeNO and EO was reliable and convenient for the differential diagnosis of ABPA and *A.f*-sensitized asthma. These findings help to discriminate ABPA from *A.f*-sensitized patients, and the indicators should be further validated in large population.

Data availability statement

The raw data supporting the conclusions of this article will be made available by the authors, without undue reservation.

Ethics statement

This study was reviewed and approved by Independent Ethical Committee of First Affiliated Hospital of Guangzhou Medical University and Tongji Hospital, Tongji Medical College, Huazhong University of Science and Technology. Written informed consent to participate in this study was provided by the participants' legal guardian/next of kin.

Author contributions

RZ and HC conceived and designed the project. HC was responsible for data analysis and wrote the first draft of the manuscript. RZ revised the raw manuscript. XZ and NA were responsible for patient's enrollment and data analysis. YY and DM collected clinical data. LY and LZ were responsible for allergen components tests and FCM. QJ contributed to IgE test by ImmunoCAP. All authors contributed to the article and approved the submitted version.

Acknowledgments

We express our gratitude to Hangzhou Zheda Dixun Biological Gene Engineering Co, LTD for the kindly providing *A.f* extract and components of sIgE, sIgA, and sIgG4 test kits. We also thank ALK (Horsholm, Denmark) for supplying HDM extract.

Conflict of interest

The authors declare that the research was conducted in the absence of any commercial or financial relationships that could be construed as a potential conflict of interest.

The reviewer PZ declared a shared affiliation with the authors XZ, NA to the handling editor at time of review.

Publisher's note

Supplementary material

The Supplementary Material for this article can be found online at: https://www.frontiersin.org/articles/10.3389/fimmu.2022.939127/full#supplementary-material

SUPPLEMENTARY FIGURE
The percentage and cytokines (IL-13 and IFN-γ) of metacluster ($CD3^+CD4^+PD\text{-}1^+$). MC: metacluster ($CD3^+CD4^+PD\text{-}1^+$); ABPA: allergic bronchopulmonary aspergillosis; A.f (+) asthma: aspergillus fumigatus sensitized asthma; HDM (+) asthma: house dust mite sensitized asthma; IFN-γ: Interferon γ; IL-13: interleukin 13. * was $P<0.05$.

References

1. Bateman ED, Hurd SS, Barnes PJ, Bousquet J, Drazen JM, FitzGerald JM, et al. Global strategy for asthma management and prevention: GINA executive summary. *Eur Respir J* (2008) 31:143–78. doi: 10.1183/09031936.00138707

2. Huang K, Yang T, Xu J, Yang L, Zhao J, Zhang X, et al. Prevalence, risk factors, and management of asthma in China: A national cross-sectional study. *Lancet* (2019) 394:407–18. doi: 10.1016/S0140-6736(19)31147-X

3. Hedayati MT, Pasqualotto AC, Warn PA, Bowyer P, Denning DW. Aspergillus flavus: Human pathogen, allergen and mycotoxin producer. *Microbiol (Reading)* (2007) 153:1677–92. doi: 10.1099/mic.0.2007/007641-0

4. Schwartz HJ, Citron KM, Chester EH, Kaimal J, Barlow PB, Baum GL, et al. A comparison of the prevalence of sensitization to aspergillus antigens among asthmatics in Cleveland and London. *J Allergy Clin Immunol* (1978) 62:9–14. doi: 10.1016/0091-6749(78)90065-9

5. Hogan C, Denning DW. Allergic bronchopulmonary aspergillosis and related allergic syndromes. *Semin Respir Crit Care Med* (2011) 32:682–92. doi: 10.1055/s-0031-1295716

6. Agarwal R, Muthu V, Sehgal IS, Dhooria S, Prasad KT, Aggarwal AN. Allergic bronchopulmonary aspergillosis. *Clin Chest Med* (2022) 43:99–125. doi: 10.1016/j.ccm.2021.12.002

7. Zeng Y, Xue X, Cai H, Zhu G, Zhu M, Wang J, et al. Clinical characteristics and prognosis of allergic bronchopulmonary aspergillosis: A retrospective cohort study. *J Asthma Allergy* (2022) 15:53–62. doi: 10.2147/JAA.S345427

8. Denning DW, Pleuvry A, Cole DC. Global burden of allergic bronchopulmonary aspergillosis with asthma and its complication chronic pulmonary aspergillosis in adults. *Med Mycol* (2013) 51:361–70. doi: 10.3109/13693786.2012.738312

9. Ma Y, Zhang W, Yu B, Chen Y, Mu S, Cui Y. Prevalence of allergic bronchopulmonary aspergillosis in Chinese patients with bronchial asthma. *Zhonghua Jie He He Hu Xi Za Zhi* (2011) 34:909–13. doi: 10.3760/cma.j.issn.1001-0939.2011.12.009

10. Zhang C, Jiang Z, Shao C. Clinical characteristics of allergic bronchopulmonary aspergillosis. *Clin Respir J* (2020) 14:440–6. doi: 10.1111/crj.13147

11. Agarwal R, Maskey D, Aggarwal AN, Saikia B, Garg M, Gupta D, et al. Diagnostic performance of various tests and criteria employed in allergic bronchopulmonary aspergillosis: A latent class analysis. *PLoS One* (2013) 8:e61105. doi: 10.1371/journal.pone.0061105

12. Sharif H, Acharya S, Dhondalay G, Varricchi G, Krasner-Macleod S, Laisuan W, et al. Altered chromatin landscape in circulating T follicular helper and regulatory cells following grass pollen subcutaneous and sublingual immunotherapy. *J Allergy Clin Immunol* (2021) 147:663–76. doi: 10.1016/j.jaci.2020.10.035

13. Varricchi G, Harker J, Borriello F, Marone G, Durham SR, Shamji MH. T Follicular helper (Tfh) cells in normal immune responses and in allergic disorders. *Allergy* (2016) 71:1086–94. doi: 10.1111/all.12878

14. Wardlaw AJ, Rick EM, Pur OL, Scadding A, Gaillard EA, Pashley CH. New perspectives in the diagnosis and management of allergic fungal airway disease. *J Asthma Allergy* (2021) 14:557–73. doi: 10.2147/JAA.S251709

15. Agarwal R, Chakrabarti A. Allergic bronchopulmonary aspergillosis in asthma: Epidemiological, clinical and therapeutic issues. *Future Microbiol* (2013) 8:1463–74. doi: 10.2217/fmb.13.116

16. Del GS, Bakirtas A, Bel E, Custovic A, Diamant Z, Hamelmann E, et al. Allergy in severe asthma. *Allergy* (2017) 72:207–20. doi: 10.1111/all.13072

17. Goh KJ, Yii A, Lapperre TS, Chan AK, Chew FT, Chotirmall SH, et al. Sensitization to aspergillus species is associated with frequent exacerbations in severe asthma. *J Asthma Allergy* (2017) 10:131–40. doi: 10.2147/JAA.S130459

18. Shah A, Panjabi C. Allergic bronchopulmonary aspergillosis: A perplexing clinical entity. *Allergy Asthma Immunol Res* (2016) 8:282–97. doi: 10.4168/aair.2016.8.4.282

19. Neyaz Z, Hashim Z, Kumar S, Nath A, Khan A, Mohindro N. Correlation of asthma severity, IgE level, and spirometry results with HRCT findings in allergic bronchopulmonary aspergillosis. *Indian J Radiol Imaging* (2020) 30:163–9. doi: 10.4103/ijri.IJRI_443_19

20. Li J, Jing M, Jin J, Dong L, Cai S, Ying S, et alConsensus of experts on diagnosis and treatment of allergic bronchopulmonary aspergillosis. *Nalt Med J China* (2017) 97:2650–6. doi: 10.3760/cma.j.issn.0376-2491.2017.34.003

21. Woolnough KF, Richardson M, Newby C, Craner M, Bourne M, Monteiro W, et al. The relationship between biomarkers of fungal allergy and lung damage in asthma. *Clin Exp Allergy* (2017) 47:48–56. doi: 10.1111/cea.12848

22. Menzies D, Holmes L, McCumesky G, Prys-Picard C, Niven R. Aspergillus sensitization is associated with airflow limitation and bronchiectasis in severe asthma. *Allergy* (2011) 66:679–85. doi: 10.1111/j.1398-9995.2010.02542.x

23. Tanimoto H, Fukutomi Y, Yasueda H, Takeuchi Y, Saito A, Watai K, et al. Molecular-based allergy diagnosis of allergic bronchopulmonary aspergillosis in aspergillus fumigatus-sensitized Japanese patients. *Clin Exp Allergy* (2016) 46:381. doi: 10.1111/cea.12698

24. Muthu V, Sehgal IS, Dhooria S, Aggarwal AN, Agarwal R. Utility of recombinant aspergillus fumigatus antigens in the diagnosis of allergic bronchopulmonary aspergillosis: A systematic review and diagnostic test accuracy meta-analysis. *Clin Exp Allergy* (2018) 48:1107–36. doi: 10.1111/cea.13216

25. Nichols D, Dopico GA, Braun S, Imbeau S, Peters ME, Rankin J. Acute and chronic pulmonary function changes in allergic bronchopulmonary aspergillosis. *Am J Med* (1979) 67:631–7. doi: 10.1016/0002-9343(79)90246-8

26. Kozlova Y, Frolova E, Uchevatkina A, Filippova L, Aak O, Burygina E, et al. Diagnostic markers of allergic bronchopulmonary aspergillosis in patients with severe asthma. *Mycoses* (2020) 63:596–603. doi: 10.1111/myc.13083

27. Ricciardolo FL, Sorbello V, Ciprandi G. A pathophysiological approach for FeNO: A biomarker for asthma. *Allergol Immunopathol (Madr)* (2015) 43:609–16. doi: 10.1016/j.aller.2014.11.004

28. Haccuria A, Michils A, Michiels S, Van Muylem A. Exhaled nitric oxide: A biomarker integrating both lung function and airway inflammation changes. *J Allergy Clin Immunol* (2014) 134:554–9. doi: 10.1016/j.jaci.2013.12.1070

29. Yi L, Cheng D, Zhang K, Huo X, Mo Y, Shi H, et al. Intelectin contributes to allergen-induced IL-25, IL-33, and TSLP expression and type 2 response in asthma and atopic dermatitis. *Mucosal Immunol* (2017) 10:1491–503. doi: 10.1038/mi.2017.10

30. Whetstone CE, Ranjbar M, Omer H, Cusack RP, Gauvreau GM. The role of airway epithelial cell alarmins in asthma. *Cells-Basel* (2022) 11(7):1–26. doi: 10.3390/cells11071105

31. Tillie-Leblond I, Tonnel AB. Allergic bronchopulmonary aspergillosis. *Allergy* (2005) 60:1004–13. doi: 10.1111/j.1398-9995.2005.00887.x

32. Hemmann S, Ismail C, Blaser K, Menz G, Crameri R. Skin-test reactivity and isotype-specific immune responses to recombinant asp f 3, a major allergen of aspergillus fumigatus. *Clin Exp Allergy* (1998) 28:860–7. doi: 10.1046/j.1365-2222.1998.00329.x

33. Flament T, Marchand-Adam S, Gatault P, Dupin C, Diot P, Guilleminault L. What are the characteristics of asthma patients with elevated serum IgG4 levels? *Respir Med* (2016) 112:39–44. doi: 10.1016/j.rmed.2016.01.014

34. Luo W, Hu H, Wu Z, Wei N, Huang H, Zheng P, et al. Molecular allergen sensitization of aspergillus fumigatus between allergic bronchopulmonary aspergillosis and a fumigatus-sensitized asthma in guangzhou, southern China. *J Clin Lab Anal* (2020) 34:e23448. doi: 10.1002/jcla.23448

35. Becker KL, Gresnigt MS, Smeekens SP, Jacobs CW, Magis-Escurra C, Jaeger M, et al. Pattern recognition pathways leading to a Th2 cytokine bias in allergic bronchopulmonary aspergillosis patients. *Clin Exp Allergy* (2015) 45:423–37. doi: 10.1111/cea.12354

36. Tracy MC, Okorie C, Foley EA, Moss RB. Allergic bronchopulmonary aspergillosis. *J Fungi (Basel)* (2016) 2(2):1–18. doi: 10.3390/jof2020017

37. Gresnigt MS, Netea MG, van de Veerdonk FL. Pattern recognition receptors and their role in invasive aspergillosis. *Ann N Y Acad Sci* (2012) 1273:60–7. doi: 10.1111/j.1749-6632.2012.06759.x

38. Pyzik A, Grywalska E, Matyjaszek-Matuszek B, Smolen A, Pyzik D, Rolinski J. Frequencies of PD-1- positive T CD3+CD4+, T CD3+CD8+ and b CD19+ lymphocytes in female patients with graves' disease and healthy controls-preliminary study. *Mol Cell Endocrinol* (2017) 448:28–33. doi: 10.1016/j.mce.2017.03.006

39. Simonetta F, Chiali A, Cordier C, Urrutia A, Girault I, Bloquet S, et al. Increased CD127 expression on activated FOXP3+CD4+ regulatory T cells. *Eur J Immunol* (2010) 40:2528–38. doi: 10.1002/eji.201040531

frontiers | Frontiers in Immunology

TYPE Original Research
PUBLISHED 10 August 2022
DOI 10.3389/fimmu.2022.937577

OPEN ACCESS

EDITED BY
Bao-Hui Cheng,
Longgang ENT Hospital, China

REVIEWED BY
Saskia Braber,
Utrecht University, Netherlands
Mirjam Kool,
Nutricia Research, Netherlands

*CORRESPONDENCE
Inken Schmudde
i.schmudde@uni-luebeck.de

†These authors have contributed equally to this work and share last authorship

SPECIALTY SECTION
This article was submitted to Immunological Tolerance and Regulation, a section of the journal Frontiers in Immunology

RECEIVED 06 May 2022
ACCEPTED 18 July 2022
PUBLISHED 10 August 2022

CITATION
Lingel I, Wilburn AN, Hargis J, McAlees JW, Laumonnier Y, Chougnet CA, Deshmukh H, König P, Lewkowich IP and Schmudde I (2022) Prenatal antibiotics exposure does not influence experimental allergic asthma in mice.
Front. Immunol. 13:937577.
doi: 10.3389/fimmu.2022.937577

Prenatal antibiotics exposure does not influence experimental allergic asthma in mice

Imke Lingel[1,2], Adrienne N. Wilburn[3,4], Julie Hargis[3], Jaclyn W. McAlees[3], Yves Laumonnier[2,5], Claire A. Chougnet[3,6], Hitesh Deshmukh[6,7], Peter König[1,2†], Ian P. Lewkowich[3,6†] and Inken Schmudde[1,2*†]

[1]Institute of Anatomy, University of Lübeck, Lübeck, Germany, [2]Airway Research Center North (ARCN), Member of the German Center for Lung Research (DZL), Lübeck, Germany, [3]Division of Immunobiology, Cincinnati Children's Hospital Medical Center, Cincinnati, OH, United States, [4]Immunology Graduate Program, University of Cincinnati, Cincinnati, OH, United States, [5]Institute for Systemic Inflammation Research, University of Lübeck, Lübeck, Germany, [6]Department of Pediatrics, University of Cincinnati, Cincinnati, OH, United States, [7]Division of Neonatology and Pulmonary Biology, Cincinnati Children's Hospital Medical Center, Cincinnati, OH, United States

Changes in microbiome (dysbiosis) contribute to severity of allergic asthma. Preexisting epidemiological studies in humans correlate perinatal dysbiosis with increased long-term asthma severity. However, these studies cannot discriminate between prenatal and postnatal effects of dysbiosis and suffer from a high variability of dysbiotic causes ranging from antibiotic treatment, delivery by caesarian section to early-life breastfeeding practices. Given that maternal antibiotic exposure in mice increases the risk of newborn bacterial pneumonia in offspring, we hypothesized that prenatal maternal antibiotic-induced dysbiosis induces long-term immunological effects in the offspring that also increase long-term asthma severity. Therefore, dams were exposed to antibiotics (gentamycin, ampicillin, vancomycin) from embryonic day 15 until birth. Six weeks later, asthma was induced in the offspring by repeated applications of house dust mite extract. Airway function, cytokine production, pulmonary cell composition and distribution were assessed. Our study revealed that prenatally induced dysbiosis in mice led to an increase in pulmonary Th17$^+$ non-conventional T cells with limited functional effect on airway resistance, pro-asthmatic Th2/Th17 cytokine production, pulmonary localization and cell-cell contacts. These data indicate that dysbiosis-related immune-modulation with long-term effects on asthma development occurs to a lesser extent prenatally and will allow to focus future studies on more decisive postnatal timeframes.

KEYWORDS

asthma, microbiome, dysbiosis, ILCs, Th17 response, RORγt

Introduction

Several risk factors ranging from genetic predisposition, increasing allergen prevalence, decline in parasite infections and changes in microbial colonization are known to contribute to the increasing asthma prevalence particularly in developed countries. These factors critically drive asthma development or asthma severity at different developmental stages. Although maternal exposures have been implicated in long term development of inflammatory diseases, this might be through altering the trajectory over which microbial colonization in offspring occurs. This trajectory is influenced by the transfer of microbiota that starts *in utero via* pioneer microbiota that settle in the meconium and the fetal gut (1–6). These microbiota resemble either vaginal or oral microbiome suggesting that they cross the placental barrier and subsequently colonize the fetus by translocation from vagina or following oral dissemination (2, 5, 6). During and after birth these pioneer skin and gut microbiota are replenished and displaced by bacteria transmitted during passage through the birth canal and/or breast feeding (7–12). Within the first two years of life the microbiome undergoes further choreographed consolidation driven by environmental factors and nutrition, finally reaching the mature colonization pattern (13–16). Thus, early life exposures during this "neonatal window of opportunity" can change the trajectory through which this mature colonization pattern is established. This results in variable interactions between microbiota and host, and is thought to play a critical role in establishing life-long homeostasis (17, 18). However, whether changes to the maternal microbiome during pregnancy are sufficient to alter asthma risk in offspring *via* gut-lung axis remains unclear.

Analyzing the modulation of asthma risk by changes of the microbiome requires basal understanding of immune cells involved in asthma development. Severe allergic asthma is synergistically driven by maladaptive T helper (Th) 2 and Th17 immune responses against harmless air-born allergens presented by dendritic cells. Together these pathways initiate a mixed eosinophilic/neutrophilic inflammation driven by IL-5 and IL-17, respectively (19). Also airway hyperreactivity (AHR), airway remodeling and mucus production are modulated by combined Th2/Th17 immune responses (20–22). Other cellular components are lymphoid-derived cells like innate lymphoid cells (ILC) and non-conventional T cells, which contribute to immediate inflammatory responses by expression of cytokines and receptors, phagocytosis capacitites and release of toxic granules (23, 24). ILCs originate from a common lymphoid progenitor, express similar cytokines as T cells, but do not express the T cell receptor. They reside in the tissues and contribute to inflammation by cytokine release (25, 26). Among the ILC subpopulations, ILC2 and ILC3 contribute to an allergic asthmatic phenotype by secretion of IL-5/IL-13 and IL-17A, respectively (27–29). Non-conventional T cells comprise γδ T cells, invariant NKT cells and mucosal-associated invariant T cell (30). In contrast to conventional T cells they do not express an αβ T cell receptor and rather contribute to innate immunity, since they lack the ability to induce allergen-specific B cell activation (31). They can rapidly respond to pathogens *via* IL-17A secretion In the context of allergic asthma they have the potential to fuel Th2/Th17 induced asthma responses (32, 33). To date it is not clear whether any of these cells are long-term regulated in allergic asthma by early-life changes in microbiome.

In order to test whether changes to the maternal microbiome during late pregnancy are sufficient to alter asthma risk in offspring by modulating lung immune responses, pregnant mice were given antibiotics (Abx) during late pregnancy, to induce dysbiosis in offspring. Control and dysbiosis-exposed offspring were weaned and subsequently exposed to the allergen house dust mite (HDM) in a well-described mouse model of allergic asthma. Compared to control HDM-exposed animals, dysbiosis-exposed offspring subsequently exposed to HDM displayed an increase in the frequency of pulmonary IL-17A$^+$ non-conventional T cells localized around airways. However, this altered IL-17A$^+$ non-conventional T cell frequency was not associated with any functional effect on airway resistance and pro-asthmatic cytokine production. Establishing a staining protocol for immunohistochemistry (IHC) enabled us further demonstrate that prenatal antibiotic exposure does not alter Th17 cell localization as indicated by RORγt staining – either in the airways or in relation to pulmonary CD11c$^+$ antigen presenting cells. Our study suggests that prenatal maternal Abx treatment has insignificant effects on the asthma phenotype in the offspring, indicating that the postnatal colonization may be more important for the pathogenesis of allergic asthma. Thereby, our study will allow to focus future studies on more decisive postnatal timeframes.

Methods

Mice

C57BL/6 mice (in-house breeding) used for establishing microscopic analyses were maintained in the University of Lübeck specific pathogen-free facility and used at 8-12 weeks of age. Animal care was provided in accordance with German animal protection laws. Studies using these mice were reviewed and approved by the Schleswig-Holstein state authorities (registration number 39(44-5/18)). A/J, A/J RORC-GFP as well as C57BL/6 mice (in-house breeding) used for *in vivo* HDM immunization were maintained in the AAALAC-accredited CCHMC animal facility and used at 6-8 weeks of age. Studies using these mice were reviewed and approved by the CCHMC Institutional Animal Care and Use Committee (registration

number 2013-0180). All mice were kept under specific-pathogen-free conditions and received sterile food and drinking water *ad libitum*.

Animal handling

Experiments including Abx treatment and asthma induction were performed in the CCHMC animal facility. For breeding, one male and 2-3 female C57BL/6 mice were mated overnight, and the following morning the presence of vaginal plugs was assessed. For confirmed pregnant female mice, on embryonic day 15 (E15) drinking water was replaced with water containing 0.5 % sucralose, or 0.5 % sucralose with ampicillin, gentamycin and vancomycin (all from Gold Biotechnology Inc.; all at 1.0 mg/mL) as previously published (34). After birth, Abx treatment was discontinued immediately. Offspring of both biological sexes were weaned at the age of 3-4 weeks. Litter sizes ranged from 3 to 10 pups. At 6-8 weeks, asthma was induced in control and Abx-exposed offspring. Mice were immunized intraperitoneally (i.p.) with 10 µg/100 µL of HDM (Greer Laboratories) on experimental day 0 and 7 dissolved in phosphate-buffered saline (PBS; pH7.4; 685 mM NaCl, 13.5 mM KCl, 50 mM NaH_2PO_4*H_2O, 10 mM Na_2HPO_4*H_2O; all from Carl Roth GmbH). Mice originating from one litter were split into both asthma and control group. After 14 and 21 days, mice were treated with 100 µg/40 µL HDM intratracheally (i.t.). Intratracheal treatments were carried out under general anesthesia with ketamine (provided by the veterinary service of CCHMC; 120 mg/kg bodyweight) and xylazine (provided by the veterinary service of CCHMC; 8 mg/kg bodyweight). Control mice received a comparable treatment using PBS. 72 h after the last treatment, lung function was assessed using the flexiVent system (SciReq) and the asthma phenotype was assessed.

Measurement of allergen-induced AHR

AHR was measured in mice anesthetized with sodium pentobarbital (provided by the veterinary service of CCHMC; 70 mg/kg body weight) and xylazine (10 mg/kg body weight). Briefly, the mouse trachea was exposed by surgical incision of the skin, submaxillary glands and muscles surrounding the trachea. Trachea was cannulated using a 20 G cannula that was inserted and tightened by surgical suture. Mice were mechanically ventilated using a flexiVent System at a positive end-expiratory pressure of 3 cm H_2O with 150 breaths per minute. Complete muscle relaxation was induced by i.p. injection of pancuronium bromide (Sigma-Aldrich Inc.; 1 mg/kg body weight). Aerosolized Acetyl-β-Methyl-Choline (methacholine; Sigma-Aldrich Inc.) was generated by an ultrasonic nebulizer and delivered with increasing doses (0, 12.5, 50, 100 mg/ml) inline through the inhalation port for 10 s. Airway resistance (R_{RS}) was measured 2 minutes later.

Collection of bronchoalveolar lavage (BAL) fluid

After lung function measurement, lungs were lavaged three times with 1 mL ice-cold Hank's Balanced Salt Solution (HBSS; Thermo Fisher Scientific Inc.). To isolate BAL cells, samples were centrifuged (300g, 6 min) and erythrocytes lysed using ACK buffer (Lonza AG). Lysis was stopped by adding ice-cold PBS containing 5 % fetal bovine serum (FBS; Thermo Fisher Scientific) and subsequent centrifugation (300g, 6 min). Total BAL cell counts were determined using a Neubauer chamber. 5-10 x 10^4 cells were transferred to objective slides by cytospin centrifugation (400 rpm, 4 min). Cytospins were stained with DiffQuick stain (RAL Diagnostics) and 500 cells were morphologically differentiated by light microscopy.

Isolation of pulmonary cells and cytokine measurements

The postcaval lobe was removed and snap frozen for mRNA isolation. Other lobes were minced and incubated in 7 mL RPMI 1640 (Gibco Life Technologies Corp.) containing Liberase™ Research Grade (Sigma-Aldrich Inc.; 1.5 mg/mL), DNAse I (Roche AG; 0.5 mg/mL) and Penicillin/Streptomycin/L-Glutamine (Gibco Life Technologies Corp.; 1 % v/v) for 45 min at 37°C. Single cell suspensions were prepared by passing minced lobes through a 70 µm strainer. Lung cells were centrifuged (400g, 8 min) and erythrocytes were lysed by incubation with ACK buffer (3 min). Cell numbers were determined using a Neubauer chamber and adjusted to 4 x 10^6 cells/mL and used for cytokine measurements and flow cytometry.

Cytokine measurement

1 x 10^6 lung cells were restimulated *ex vivo* with 0.03 mg/mL HDM in RPMI 1640 (10 % FBS, 1 % Penicillin/Streptomycin, 0.1 % β-Mercaptoethanol (Thermo Fisher Scientific Corp.)) for 72 h at 37°C. Supernatants were harvested. Production of interleukin (IL)-4, IL-5, IL-13 and IL-17A in culture supernatants was determined using matched antibody pairs from Invitrogen. ELISA plates were coated with 50 µL of diluted antibodies (IL-4: clone 11B11; IL-5: clone TRFK5; IL-13: clone eBio13A; IL-17A: clone eBio17CK15A5) overnight at 4°C. 1:2 Standard dilution series with a minimum concentration of 4.88 pg/mL were prepared using recombinant IL-4, IL-5, IL-

13 and IL-17A (all Invitrogen). Plates were washed and 50 µL of sample were applied overnight at 4°C. Subsequently, plates were washed and biotinylated antibodies (IL-4: clone BVD6-24G2; IL-5: clone TRFK4; IL-13: clone eBio16H; IL-17A: clone eBio17B7) were added for 2 h at RT. Plates were washed and HRP-Avidin (Invitrogen) was added for 30 min at RT. After a final washing step Super AquaBlue Invitrogen™ (Invitrogen Inc.) was added to the wells, and after developing time of 8 - 30 min (until concentration gradient had fully developed) optical density of ELISA plates was determined with a BioTek plate reader (BioTek Instruments Inc.).

Intracellular cytokine measurement by flow cytometry

2.5 x 10^5 lung cells were restimulated *ex vivo* in 250 µL Iscove's modified Dulbeccos's Medium (IMDM; Thermo Fisher Scientific Inc.) with Phorbol 12-myristate 13-acetate (PMA)/ionomycin (all Sigma-Aldrich Inc.; 50 ng/mL and 500 ng/mL) and 1x Brefeldin/Monensin (Sigma-Aldrich Inc.) for 4 h at 37°C. Cells were centrifuged (400g, 3 min) and the pellet was resuspended in PBS/bovine serum albumin (BSA; 0.5 %; Sigma-Aldrich Inc.). Nonspecific antibody binding was blocked using anti-CD16/CD32 Mouse BD Fc-block™ (Becton, Dickinson Inc.) for 15 min at 37°C. Cells were stained with anti-CD90.2-BV605 (clone 53-2.1, BioLegend Inc.), anti-TCRβ-AF700/AF488 (clone H57-597, BioLegend Inc.) and anti-CD3ε-APC-Cy7 (clone eBio500A2, Invitrogen Inc.) for 30 min at 37°C. Cells were washed and BD Horizon Viability Dye V500 (Becton Dickinson Inc.) was added in PBS in darkness for 15 min at RT. Cells were washed and then fixed/permeabilized using Cytofix/Cytoperm™ (Becton Dickinson Inc) in darkness for 60 min at RT. After additional blocking with Fc-Block, intracellular staining with anti-IL-17A-PE (clone eBio17B7; Invitrogen Inc.) for 30 min at 4°C was performed. Flow cytometric measurements were performed using a BD™ LSR II flow cytometer (Becton Dickinson Inc.). IL-17A$^+$ cells were analyzed as depicted in Supplementary Figure 1.

RNA extraction

RNA from the postcaval lobe was isolated using TRIzol™ reagent (Thermo Fisher Scientic Inc.) according to the manufacturer's instructions. Reverse transcription was performed using random primers (Invitrogen Inc.), dNTP mix (Thermo Fisher Scientific Inc.), 1st strand buffer (Thermo Fisher Scientific Inc.), Dithiothreitol (USP grade; Thermo Fisher Inc.), RNase out (New England BioLabs Inc.), Superscript™ II Reverse Transcriptase (Invitrogen Inc.). Quantitative PCR was done using Light Cycler 480® SYBR Green I Master Mix (Roche AG) on a LightCycler® 480 Instrument II (Roche) using the following primers (Bio-Rad Laboratories Inc.): *S14* 5'-GAG GAG TCT GGA GAC GAC GA-3' (sense) and 5'-TGG CAG ACA CCA CCA ACA TT-3' (antisense), *Il17a* 5'-CAG ACT ACC TCA ACC GTT CCA C-3' (sense) and 5'-TCC AGC TTT CCC TCC GCA TTG A-3' (antisense), *Il17f* 5'-TGC CAG GAG GTA GTA TGA AGC TT-3' (sense) and 5'-ATG CAG CCC AAG TTC CTA CAC T-3' (antisense), *Il22* 5'-ACG CAA GCA TTT CTC AGA GA-3' (sense) and 5'-AAC ATG AGT CCA GGG AGA GC-3' (antisense), *Mpo* 5'-TCC CAC TCA GCA AGG TCT T-3' (sense) and 5'-TAA GAG CAG GCA AAT CCA G-3' (antisense), *Muc5b* 5'-TGT ACT GCC CCC AGG ATG GGC-3' (sense) and 5'-AGC TCA GCT CTG CCT GAC CCT-3' (antisense), *Muc5ac* 5'-CCA TGC AGA GTC CTC AGA ACA A-3' (sense) and 5'-TTA CTG GAA AGG CCC AAG CA-3' (antisense), *Gob5* 5'-ACT AAG GTG GCC TAC CTC CAA-3' (sense) and 5'-GGA GGT GAC AGT CAA GGT GAG A-3' (antisense).

Tissue removal and cryosectioning

The small intestines of A/J WT and RORC-GFP mice were removed and 10 cm of intestine were rinsed with PBS. The intestinal lumen was filled with 1 % Paraformaldehyde (PFA; Agar Scientific Ltd.), coiled into a spiral and placed between two sponges in a tissue cassette. Tissue was fixed using Cytofix/Cytoperm™ (Becton Dickinson Inc.) 1:4 diluted with PBS overnight at 4°C. Tissue was washed with PBS for 8 h at 4°C. Embedding was prepared by incubation in 30 % sucrose solution (Carl Roth GmbH) diluted 1:1 with TissueTek® O.C.T Compound™ (Science Services GmbH) overnight at 4°C. Tissue was embedded in TissueTek® O.C.T Compound™ and frozen in liquid nitrogen. 18 µm cryosections were generated and used for IHC staining.

To examine pulmonary histology, lungs were perfused *via* the right ventricle with 3 mL ice cold Ringer solution (ph7.4; 5.6 mM KCl, 136.4 mM NaCl, 1 mM $MgCl_2$*6 H_2O, 2.2 mM $CaCl_2$*2 H_2O; all Carl Roth GmbH; 11 mM Glucose, 10 mM HEPES; both Sigma-Aldrich Inc.) containing 5 % heparin (Braun). 3 % LM agarose (Universal Medical Inc.) in Ringer solution at 37°C was injected into the lungs *via* the trachea. Filled lungs were removed and transferred to ice cold Ringer solution. 300 µm sections were sliced using a vibratome, fixed with 1 % PFA in PBS for 15 min at RT while shaking, washed three times in PBS each for 15 min at RT while shaking, incubated with 20 % sucrose overnight at 4°C and used for IHC staining.

Immunofluorescence staining

Lung or intestinal sections were incubated with IHC blocking buffer (PBS, 0,3 % v/v Triton X-100 (Thermo Fisher Scientific Inc.), 10 % v/v normal mouse serum (Invitrogen Inc.)) for 20 min at RT. Sections were incubated in IHC blocking buffer with purified anti-RORγt (AFKJS-9; Invitrogen Inc.) and where indicated with anti-α-SMA-FITC (1A4; Invitrogen Inc.), anti-TCRβ-AF647/AF488 (H57-597; BioLegend Inc.) or anti-CD11c-AF647 (N418; BioLegend Inc.) diluted in PBS (overnight

(intestinal sections) or 60 h (lung sections), 4°C). After three washing steps, sections were incubated with secondary polyclonal anti-rat IgG-DyLight-549/AF647 (Jackson ImmunoResearch Inc.) in PBS supplemented with 5 % normal mouse serum (Invitrogen Inc.) for 60 min at RT. For double-labeling with CD3, an additional blocking step with 10 % normal rat serum (Linaris Biologische Produkte) was performed for 1h at RT, followed by incubation with anti-CD3-AF647 (17A2; BioLegend Inc.) for 2h, at RT. Slices were rinsed three times and cover slipped with Mowiol mounting medium (12 g Mowiol 4-88 (Sigma-Aldrich), 30 mL A. bidest., 60 mL Tris buffer (0.2 M; Invitrogen Inc.), 30 g Glycerin (pH 8.5; Merck)) with or without 1 µg/mL Hoechst dye (Thermo Fisher Scientific Inc.).

Laser scanning confocal microscopy

Stained slices were evaluated with confocal microscopy. Z-stacks (40 µm with a resolution of 1 µm) were recorded to allow a three-dimensional presentation of lung structures including possible cell interactions. Airway and blood vessels were identified by the use of anti-α-SMA-FITC (1A4; Invitrogen) or using autofluorescence (excitation: 488nm; detection: 490-530 nm). Analysis was performed using a laser scanning confocal microscope Zeiss 710 meta (Carl Zeiss AG).

Statistical analysis

Statistical analysis was performed using the GraphPad Prism version 5 (GraphPad Software Inc.). Outliers were excluded after Grubbs test. Data are represented as mean and standard error of the mean (SEM). Statistical differences for the comparison of multiple independent treatment groups were analyzed for normality using D'Agostino and Pearson omnibus normality Test. Gaussian distributed samples were evaluated by one-way ANOVA followed by Tukey Post Test. Non-Gaussian samples were evaluated by Kruskal-Wallis-Test and Dunns's Post Test. For comparison of multiple dependent measurements two-way ANOVA followed by Bonferroni Post Test was chosen. Statistical difference between two groups was evaluated by Student T Test after passing D'Agostino and Pearson omnibus normality Test or Mann-Whitney-U-Test. p values < 0.05 were considered statistically significant.

Results

Prenatally induced dysbiosis of dams increases recruitment of IL-17A producing cells to the lung in allergen-exposed offspring

To date, human and mouse studies tried to correlate early life dysbiosis with long-term asthma susceptibility and severity. However, it remains unclear when and how dysbiosis most strongly influences asthma outcomes. To determine if prenatal maternal dysbiosis is sufficient to induce changes in allergen-induced cellular recruitment, we treated dams from E15 until birth with a cocktail of three Abx (Ampicillin, Vancomycin and Gentamicin) in sucralose-sweetened drinking water, or sucralose-sweetened drinking water alone (Figure 1A). After birth, mothers were switched to conventional water. This model has been shown to induce profound neonatal dysbiosis and increased susceptibility to neonatal pneumonia (34). At 6-8 weeks of age, animals were exposed to an extract of the aeroallergen HDM. To this end, animals were administered two doses of 100 µg of HDM in saline, or saline alone i.p. one week apart. Starting one week after the final i.p HDM exposure, animals were given two doses of i.t. 100 µg HDM one week apart. 72 hours after the final HDM exposure, recruitment of cytokine-producing cells to the airways was measured. To quantify *in situ* cytokine production in the lung at the time of sacrifice, we tested the capacity of lung cells to accumulate IL-13 and IL-17A in response to PMA/ionomycin in presence of Brefeldin/monensin by flow cytometry. After dead cell exclusion lymphocytes were identified as $CD90.2^+$ cells (Supplementary Figure 1). As expected, the compartment of IL-13- and IL-17A-expressing cells was slightly increased in lung cells purified from HDM immunized lungs. Although the number of IL-13-expressing cells was not further regulated by prenatal antibiotic exposure (Supplementary Figure 2), the frequency and number of IL-17A-expressing lung cells were significantly increased in the HDM-treated offspring of Abx-treated dams (Figure 1B, Supplementary Figure 3A). Further analyses of the $IL\text{-}17A^+$ cell compartment following a gating scheme considering TCRβ and CD3 expression (Supplementary Figure 1) allowed the identification of ILCs ($CD3^-TCR\beta^-$), αβ T cells ($CD3^+TCR\beta^+$) and non-conventional T cells ($CD3^+TCR\beta^-$). $IL\text{-}17A^+$ cells were predominantly (>50 %) αβ T cells (Figure 1C). ILCs and non-conventional T cells accounted each for approximately 20 % of $IL\text{-}17A^+$ lung cells. Prenatal treatment with Abx did not affect the frequency of $IL\text{-}17A^+CD4^+$ T cells, or ILCs following HDM-exposure, whereas the frequency of non-conventional T cells was significantly increased in offspring of HDM-exposed, Abx-treated dams. In terms of absolute cell numbers all three subpopulations were significantly increased due to the increase of total $IL\text{-}17A^+$ cells (Supplementary Figure 3B).

Given the increase in $IL\text{-}17A^+$ cells, the expression of Th17-related cytokines *Il17a*, *I17f* and *Il22* was analyzed in whole lung homogenates (Figure 1D). A trend towards increased gene expression of *Il17a*, *I17f* and *Il22* was observed upon HDM immunization compared to PBS-treated control mice. Further, although prenatal Abx treatment tended to increase the expression of *Il17a* and *Il17f* in asthmatic mice, expression of *IL22* was not regulated by prenatal Abx treatment. Since IL-17 is known to regulate the migration of neutrophils and activate airway mucus production we analyzed the expression of neutrophil-

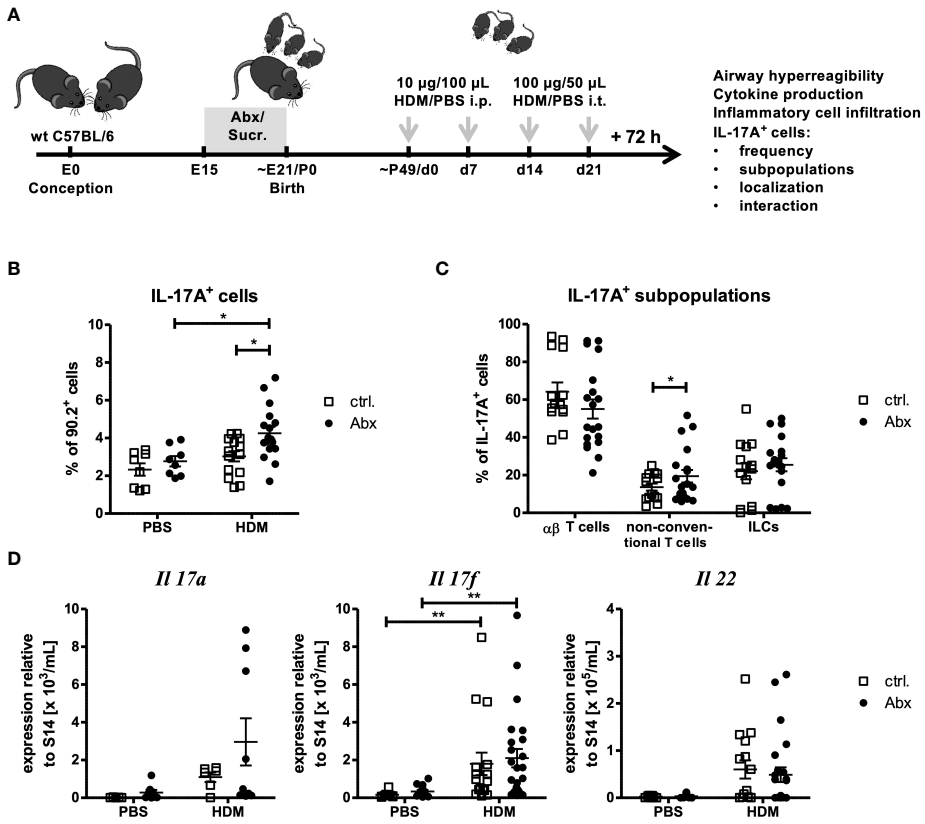

FIGURE 1
Prenatal antibiotic exposure increases the frequency of IL-17A$^+$ pulmonary cells without affecting gene expression. **(A)** C57BL/6 mice were treated with vancomycin, ampicillin and gentamycin (all at 1.0 mg/mL)(Abx) from prenatal day 15 until birth. Mice treated with sucralose served as controls (ctrl.). At 6-8 weeks, offspring C57BL/6 mice were immunized i.p. with 10 µg/100 µL of HDM. Seven days later mice received an additional i.p. injection of HDM. After 14 and 21 days mice were treated with 100 µg/40 µL HDM i.t. Mice treated with PBS served as non-asthmatic controls (B, D). 72 h after the last treatment the asthma phenotype was assessed. **(B)** Single lung cell suspensions were restimulated with PMA (50 ng/mL) and ionomycin (0.5 mg/mL). After intracellular staining of IL-17A, CD90.2$^+$ lymphocytes were analyzed regarding IL-17A production by flow cytometry. **(C)** To further differentiate IL-17A$^+$ populations, CD3 and TCRβ expression was analyzed to identify CD3$^+$TCRβ$^+$ αβ T cells, CD3$^+$TCRβ$^-$ non-conventional T cells and CD3$^-$TCRβ$^-$ ILCs. **(D)** Further, 72 h after the last *in vivo* treatment RNA expression of Th17-related cytokines normalized to the expression of the housekeeping gene S14 by pulmonary cells was assessed. Scatter plot with mean ± SEM; n = 5-25 mice. Each dot represents one mouse. Differences between groups were tested by one-way ANOVA (after passing D'Agostino and Pearson omnibus normality Test) and Tukey Post Test)(B), Student T Test (after passing D'Agostino and Pearson omnibus normality Test) (C) or Kruskal-Wallis-Test and Dunns's Post Test for significance (D); * $p < 0.05$, ** $p < 0.01$.

associated genes (*Mpo*) and mucus-associated genes (*Muc5b*, *Muc5ac* and *Gob5)*. No significant Abx-mediated regulation of these genes was observed in HDM-exposed mice (Supplementary Figures 4A, B). In summary prenatal Abx treatment increased the number of non-conventional T cells capable of producing IL-17A$^+$ cells in the lung, but did not directly induce pulmonary neutrophilia, or augment mucus production.

Prenatally induced maternal dysbiosis does not alter allergen-induced asthma development in offspring

Given observed changes in allergen-induced recruitment of IL-17A$^+$ cells in dysbiosis exposed offspring, and the described role of IL-17A-producing cells in driving the development of asthma, we next examined the impact of prenatally induced dysbiosis on the asthma phenotype. As expected, HDM exposure induced marked changes in airway function in offspring of sucralose-exposed dams (Figure 2A). Offspring of dams treated with prenatal Abx developed comparable airway responses to HDM-treated offspring of control animals. Accordingly, the total number of inflammatory cells present in the BAL fluid (Figure 2B) was comparable in offspring of HDM-treated control dams, and offspring of Abx-treated dams. Similarly, the composition of the inflammatory infiltrate (monocytes, lymphocytes, eosinophils, neutrophils) was not different in HDM-exposed offspring of control dams, or offspring of Abx-exposed dams (Figure 2C). These data are complemented by the observation that HDM sensitization significantly increased the

concentrations of the Th2 cytokines IL-4, -5 and -13 by pulmonary cells restimulated *ex vivo* with HDM independent of prenatal antibiotic exposure (Figure 2D). IL-17A was not measurably induced under any condition (data not shown). Taken together, although HDM immunization induced an asthmatic phenotype in the offspring, maternal dysbiosis did not alter these effects.

Pulmonary cells expressing the IL-17A transcription factor RORγt can be identified *in situ*

Based on the observation of Gray et al. (34) that dysbiosis interrupts migration of ILC3s to the lung by modulating the expression of CCR4, we aimed to investigate *via* IHC whether dysbiosis also influences the localization of IL-17A$^+$ cells *in situ* or affects interactions with other immune cells. Since detection of cytokine signals is difficult by IHC (Brefeldin A-mediated inhibition of secretion is not possible in IHC), the key transcription factor of IL-17A$^+$ cells RORγt was chosen as a marker for IL-17A expression. Using intestinal slides from A/J RORC-GFP reporter mice we tested the RORγt antibody for specificity and applicability in IHC (Supplementary Figure 5). Co-staining with anti-RORγt antibodies and Hoechst stain expectedly revealed a nuclear localization of the anti-RORγt (data not shown). In order to further prove specificity of the anti-RORγt antibody and to test suitability for lung staining, co-expression with CD3 in the lung was analyzed (Figures 3A, C). About 90 % of RORγt$^+$ cells co-expressed the T cell marker CD3. Further, as a proof of concept less than 10 % of RORγt cells expressed the key Th2 transcription factor GATA3 (Figure 3B, D). In summary, staining with anti-RORγt allows identification of RORγt$^+$ cells in the lung *in situ* without substantial overlap with the Th2 cell compartment.

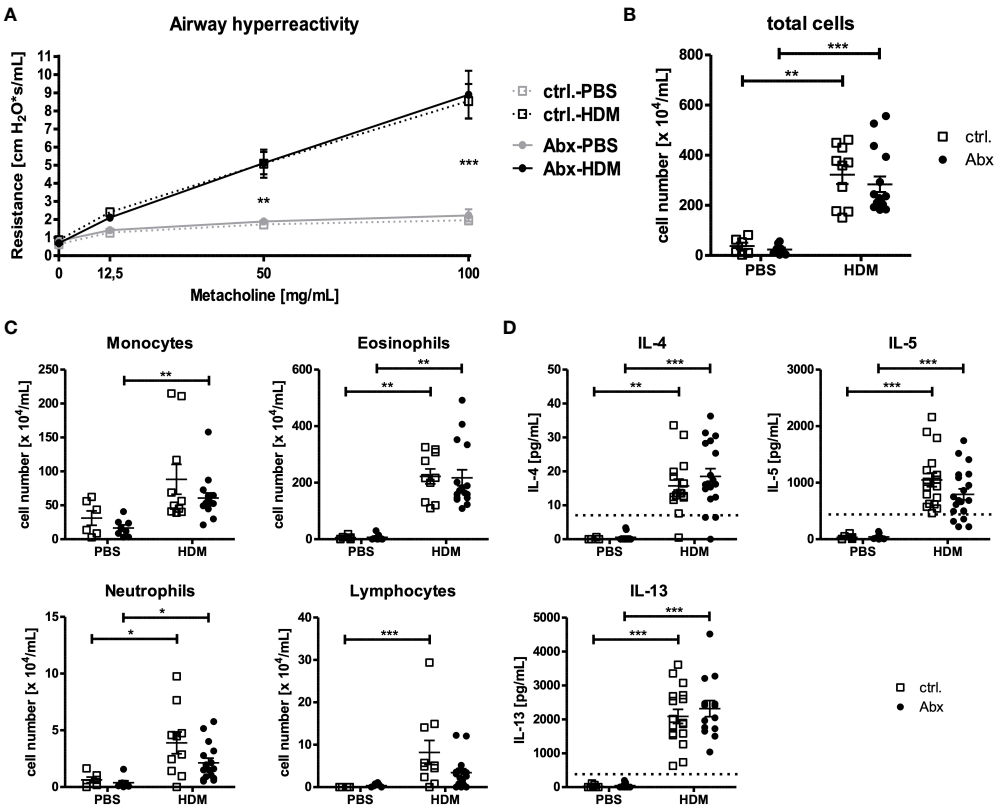

FIGURE 2
Prenatal antibiotic exposure of dams does not influence the asthma phenotype of the offspring. C57BL/6 mice were treated with vancomycin, ampicillin and gentamycin (all at 1.0 mg/mL)(Abx) from prenatal day 15 until birth. Mice treated with sucralose served as controls (ctrl.). At 6-8 weeks, offspring C57BL/6 mice were immunized i.p. with 10 µg/100 µL of HDM. Seven days later mice received an additional i.p. injection of HDM. After 14 and 21 days, mice were treated with 100 µg/40 µL HDM i.t. Mice treated with PBS served as non-asthmatic controls. 72 h after the last treatment AHR in response to i.t. administration of methacholine measured as airway resistance using Flexivent **(A)**, cellular infiltration of the airways **(B, C)** and cytokine production of single lung cell suspensions after 72 h *ex vivo* cell culture **(D)** were assessed. Scatter plot with mean ± SEM, n = 6-18 mice. Each dot represents one mouse. Dotted lines (D) indicate the detection limit. Differences between groups were tested by two-way ANOVA and Bonferroni Post Test (A) or Kruskal-Wallis-Test and Dunns's Post Test (B–D) for significance; * $p < 0.05$, ** $p < 0.01$, *** $p < 0.001$.

Prenatally induced dysbiosis of dams does not influence localization of offspring pulmonary RORγt$^+$ cells

To determine whether prenatal Abx-induced dysbiosis affects later life distribution of pulmonary IL-17A-producing cells, we used the previously established method of α-SMA staining (35) and autofluorescence in combination with the stain of RORγt. This allowed discrimination between large airways, small airways/blood vessels and the pleura/alveolar region as confirmed by TCR-β staining (Supplementary Figure 6). A major proportion (>70 %) of pulmonary RORγt$^+$ cells were localized around larger airways in HDM-exposed animals (Figures 4A, D). In contrast, ~29 % and <1 % were

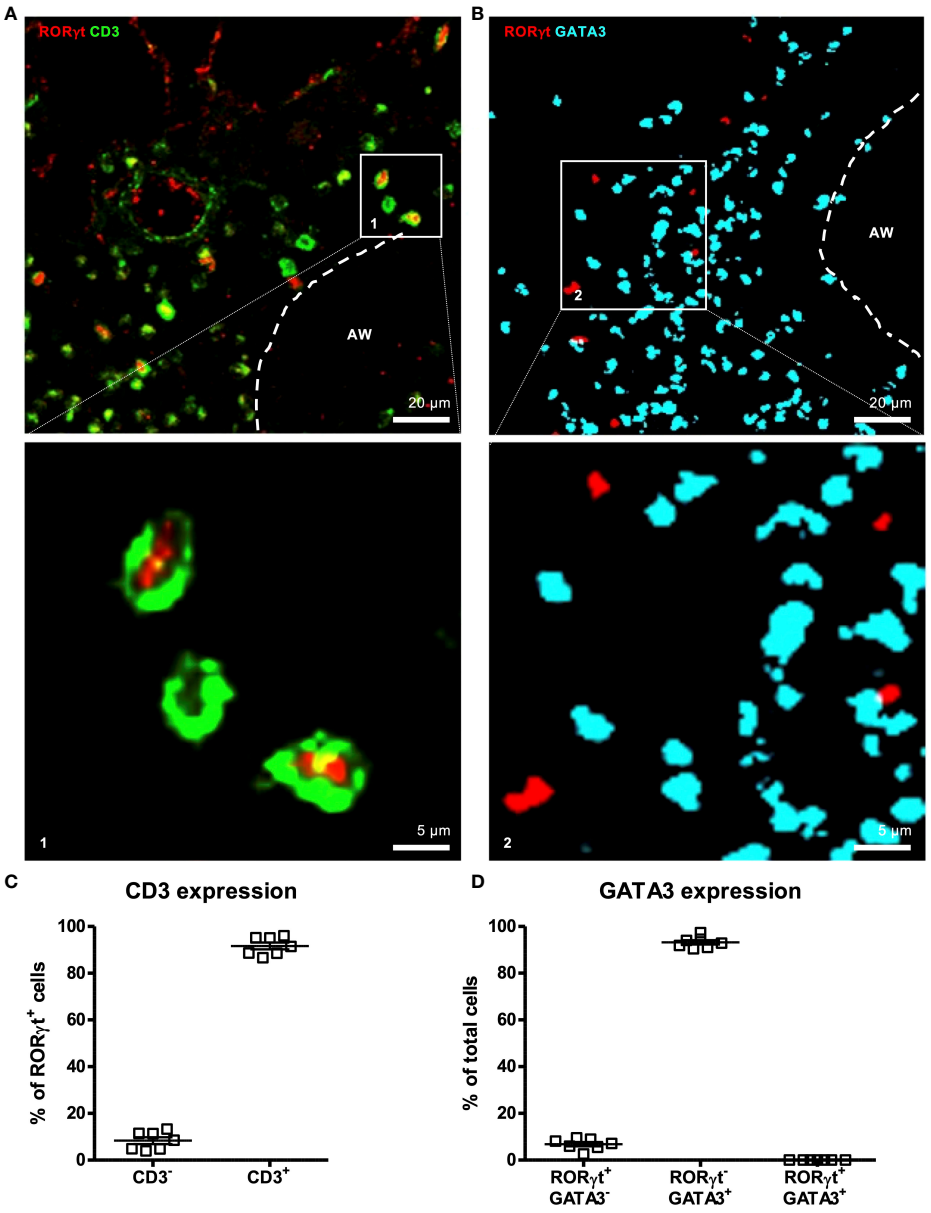

FIGURE 3
RORγt is suitable as a marker for pulmonary IL-17A$^+$ cells *in situ*. At 6-8 weeks C57BL/6 mice were immunized i.p. with 10 µg/100 µL of HDM. Seven days later mice received an additional i.p. injection of HDM. After 14 and 21 days mice were treated with 100 µg/40 µL HDM i.t. 72 h after the last treatment 300 µm lung sections of agarose filled lungs were prepared and stained with anti-RORγt (red) and anti-CD3 (green) **(A)** or anti-RORγt (red) and anti-GATA3 (turquoise) **(B)**. **(C)** RORγt$^+$ cells were analyzed regarding CD3 expression. **(D)** Total cells were analyzed regarding RORγt and GATA3 expression. Stained slices were evaluated with confocal microscopy. Abbreviations: AW, airway. Data are representative of two independent experiments. Scatter plot with mean ± SEM; n = 7 mice. Each dot represents the Z-stack of one mouse.

found around small airways/blood vessels and at the pleura/alveolar region, respectively (Figures 4B–D). Importantly, prenatally induced dysbiosis did not affect the pulmonary distribution of RORγt$^+$ cells after HDM exposure (Figure 4D).

As we observed an increased frequency of IL-17A-producing pulmonary non-conventional T cells *in vivo* in HDM-exposed offspring of Abx-exposed mothers, we next determined whether IL-17A$^+$ non-conventional T cells were increased in specific subregions within the lung. To this end, we combined the methods to determine pulmonary subregions based on autofluorescence (36), with *in situ* IHC staining of CD3 and TCRβ. Using this approach, we were able to discriminate αβ T cells (CD3$^+$TCRβ$^+$) (Figure 5A) and non-conventional T cells (CD3$^+$TCRβ$^-$) (Figure 5B) and ILCs (CD3$^-$TCRβ$^-$) (Figure 5C) expressing RORγt in lung sections and to assign them specifically to pulmonary subregions comprising large airways and small airways/blood vessels. Consistent with our flow based studies, the majority of RORγt$^+$ cells in HDM-exposed animals were αβ T cells (61 %) (Figures 5D, E) whereas non-conventional T cells and ILCs represented only minor RORγt$^+$ cell fractions with a frequency of 31 % and 7 %, respectively. This distribution was not affected by prenatally induced dysbiosis. Further, a similar distribution of RORγt$^+$ cells was seen around larger airways (Figure 5F) as well as smaller airways/blood vessels

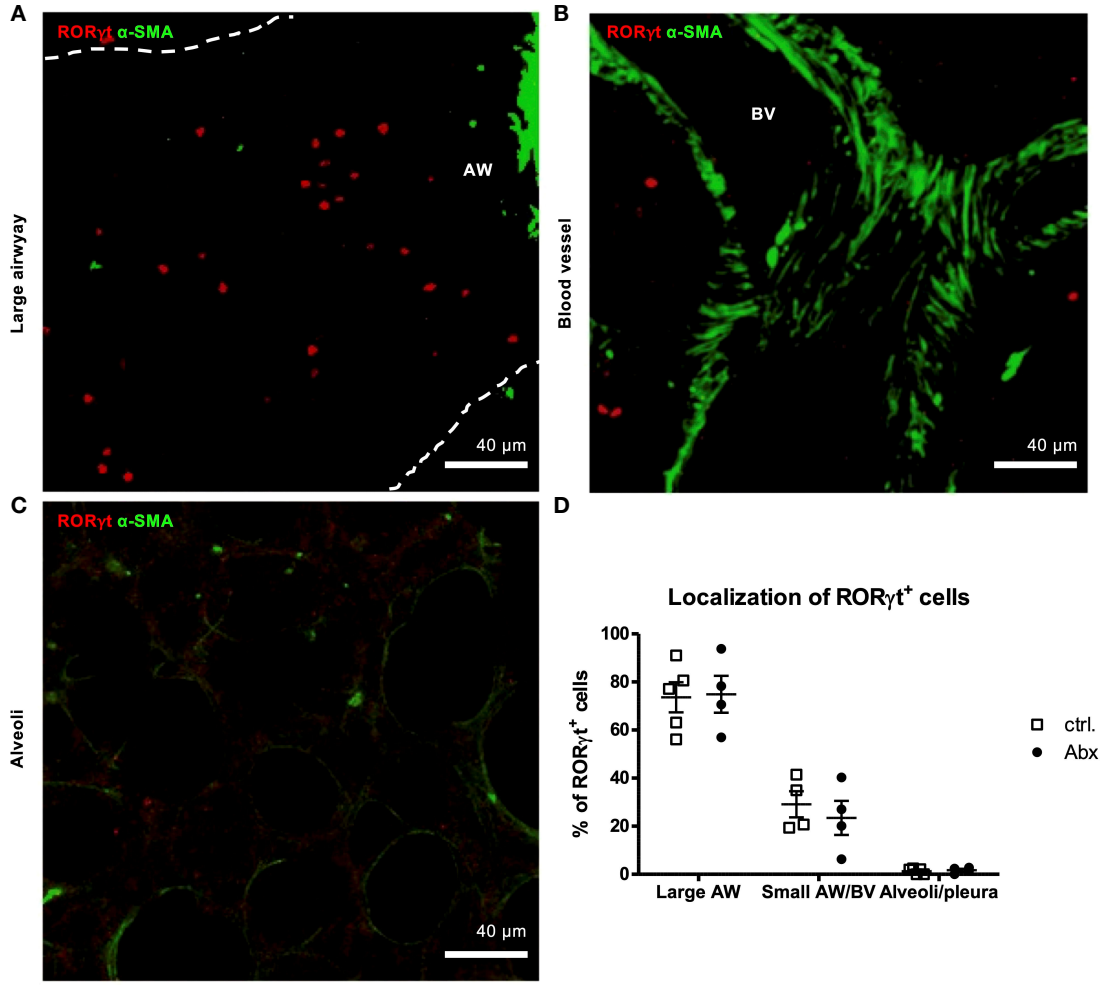

FIGURE 4
Prenatal antibiotic exposure of dams does not influence localization of offspring pulmonary RORγt$^+$ cells *in situ*. C57BL/6 mice were treated with vancomycin, ampicillin and gentamycin (all at 1.0 mg/mL)(Abx) from prenatal day 15 until birth. Mice treated with sucralose served as controls (ctrl.). At 6-8 weeks, offspring C57BL/6 mice were immunized i.p. with 10 µg/100 µL of HDM. Seven days later mice received an additional i.p. injection of HDM. After 14 and 21 days mice were treated with 100 µg/40 µL HDM i.t. 72 h after the last treatment 300 µm lung sections of agarose filled lungs were prepared. **(A, B)** For visualization of airways and blood vessels anti-aSMA (green) was added. **(C)** Alveoli were identified by autofluorescence. **(D)** Stained slices were evaluated with laser scanning confocal microscopy generating Z-Stacks for localization of RORγt$^+$ cells (red). Abbreviations: AW, airway; BV, blood vessel. Data are representative of at least four independent experiments. Scatter plot with mean ± SEM. n = 4-5 mice. Each dot represents the Z-stack of one mouse.

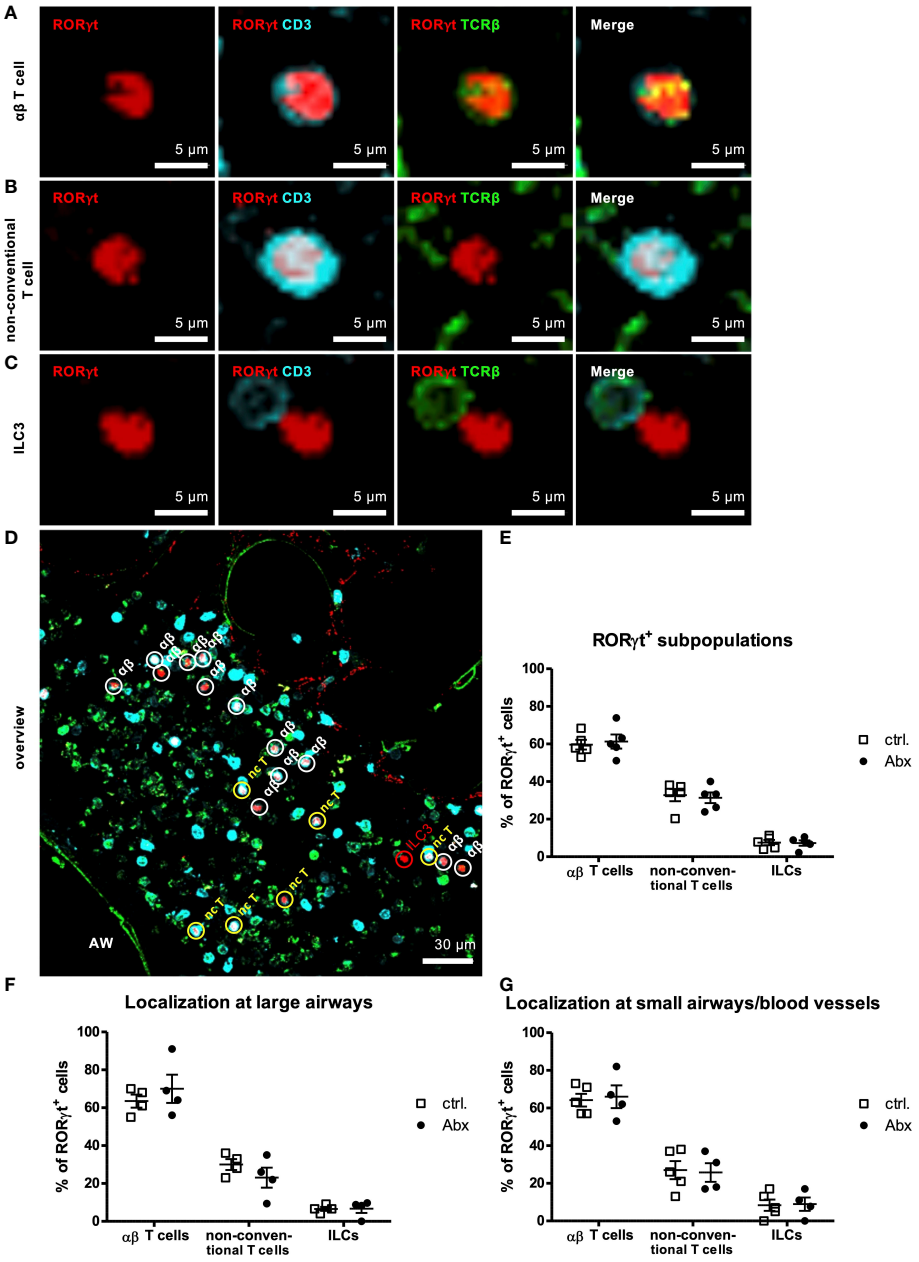

FIGURE 5
Prenatal antibiotic exposure of dams does not influence localization of offspring pulmonary RORγt$^+$ subpopulations *in situ*. C57BL/6 mice were treated with vancomycin, ampicillin and gentamycin (all at 1.0 mg/mL)(Abx) from prenatal day 15 until birth. Mice treated with sucralose served as controls (ctrl.). At 6-8 weeks, offspring C57BL/6 mice were immunized i.p. with 10 µg/100 µL of HDM. Seven days later mice received an additional i.p. injection of HDM. After 14 and 21 days mice were treated with 100 µg/40 µL HDM i.t. 72 h after the last treatment 300 µm lung sections of agarose filled lungs were prepared. Staining with anti-RORγt (red), anti-CD3 (turquoise) and anti-TCRβ (green) allowed discrimination of CD3$^+$TCRβ$^+$ αβ T cells **(A)**, CD3$^+$TCRβ$^-$ non-conventional T cells **(B)** and CD3$^-$TCRβ$^-$ ILC3s **(C)**. Stained slices were evaluated with laser scanning confocal microscopy generating Z-Stacks. **(D)** A representative overview of a large airway is shown. Frequencies of αβ T cells, non-conventional T cells (nc T) and ILC3s among RORγt$^+$ cells were determined in total lungs **(E)** around large **(F)** and small airways/blood vessels **(G)**. Abbreviations: AW, airway. Data are representative of at least four independent experiments. Scatter plot with mean ± SEM. n = 4-5 mice. Each dot represents the Z-stack of one mouse.

(Figure 5G), and prenatal Abx treatment had no impact on the subpopulation assignment. Altogether, these experiments revealed no impact of prenatal Abx treatment on the distribution of subpopulations of pulmonary RORγt$^+$ cells *in situ*.

Prenatally induced dysbiosis of dams does not influence the frequency of contacts between RORγt$^+$ cells and CD11c$^+$ cells

As T cell activation requires prior interaction with proinflammatory dendritic cells (DC), we analyzed the *in situ* interaction between RORγt-expressing cells and CD11c$^+$ DCs as was previously also shown for lung ILC3s (34). 3D-analyses of Z-stacks including analyses of each 1 µm thick slice of the Z-stack revealed that the majority of 71 % of RORγt$^+$ cells were in close contact (<15 nm) with CD11c$^+$ DCs (Figures 6A–C). Perinatal Abx treatment did not affect the frequency of RORγt$^+$ cells interacting with CD11c$^+$ cells (Figure 6C). Collectively these data suggest that while prenatal allergen exposure may influence initial seeding of the lung with non-conventional T cells after HDM exposure, it has little impact on asthma severity later in life. This study thus excludes the prenatal time window as a particularly critical window for maternal antibiotic exposure in mice.

Discussion

Events that occur in fetal and early postnatal life influence the development of tolerance and long lasting risk of inflammatory diseases like asthma (34, 37, 38). However, the relative importance of pre- and postnatal time points critical for

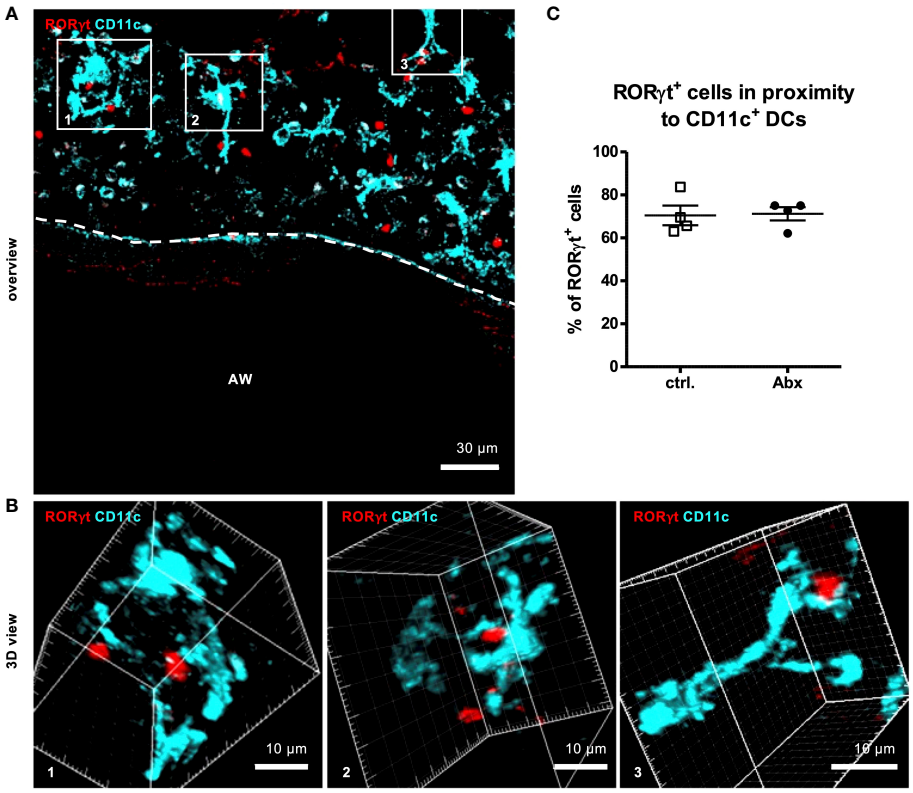

FIGURE 6
Prenatal antibiotic exposure of dams does not influence the frequency of contacts between RORγt$^+$ cells and CD11c$^+$ cells *in situ*. C57BL/6 mice were treated with vancomycin, ampicillin and gentamycin (all at 1.0 mg/mL)(Abx) from prenatal day 15 until birth. Mice treated with sucralose served as controls (ctrl.). At 6-8 weeks, offspring C57BL/6 mice were immunized i.p. with 10 µg/100 µL of HDM. Seven days later mice received an additional i.p. injection of HDM. After 14 and 21 days mice were treated with 100 µg/40 µL HDM i.t. 72 h after the last treatment 300 µm lung sections of agarose filled lungs were prepared. Staining with anti-RORγt (red) and anti-CD11c (turquoise) allowed evaluation of interactions between RORγt$^+$ cells and CD11c$^+$ DCs. Stained slices were evaluated with laser scanning confocal microscopy generating Z-Stacks. **(A)** A representative overview of a large airway is shown. Enlarged 3D views **(B)** of framed areas allowed 3D analysis of contact rates of RORγt$^+$ cells with CD11c$^+$ DCs **(C)**. Abbreviations: AW, airway. Data are representative of at least four independent experiments. Scatter plot with mean ± SEM. n = 4 mice. Each dot represents the Z-stack of one mouse.

development of tolerance remain unclear. Herein, we address whether dysbiosis induced by prenatal Abx-treatment of dams evokes long lasting effects on asthma severity in offspring. Therefore, we exposed dams to a combination of ampicillin, gentamycin and vancomycin, which are commonly used to treat pregnant woman and newborn infants (39). A previous publication using this treatment already described the dysbiosis 4 days after birth by a 10-fold decrease of 16s rDNA copies/mg intestinal content and a change in microbial composition. Strongest effects were seen for Lactobacillales and Enterobacteriales being reduced in numbers upon Abx treatment and Actinomycetales and Bacteroida which were increased in numbers. Dysbiotic colonization showed a trend towards eubiosis already at the end of the window of investigation after 14 days (34). Using an equal treatment approach in the same animal facility, we demonstrate that prenatally induced dysbiosis was associated with increased numbers of non-conventional T cells with a potential for IL-17A-production following allergen sensitization and challenge. Knowing that γδ T cells, that belong together with invariant NKT cells and mucosal-associated invariant T cells to the IL-17A-producing non-conventional T cell compartment, and ILC3s develop between day 10 and 14 of pregnancy, whereas αβ T cells develop only after birth, the increase of non-conventional T cells within the IL-17A$^+$ population appears consistent in a model of prenatally induced dysbiosis (40, 41). However, this modest observed increase in frequency of IL-17A$^+$ non-conventional T cells does not alter asthma severity, as characterized by airway resistance, pro-asthmatic Th2/Th17 cytokine production, pulmonary localization and cell-cell contacts. Thus, our findings indicate that prenatal, maternal dysbiosis-related immune-modulation does not impact overall magnitude of asthma responses. However, given that in our model of experimental allergen-induced asthma, significant airway dysfunction is observed in all allergen-exposed animals (i.e. penetrance of asthma-like disease is 100 %), we cannot fully exclude the possibility that prenatal (maternal) dysbiosis might alter risk of asthma development in a less penetrant model of asthma-like disease.

The newborn lung harbors a Th2-biased immunological environment dominated by Th2 cells, ILC2s, eosinophils and basophils accumulating in the lung in an IL-33-dependent manner (42, 43). After birth, in mice within the first four weeks of life, this balance between Th cells shifts from the Th2 dominant first wave towards a Th1 phenotype and upregulation of regulatory T cells (Treg) (44, 45). In the context of allergic asthma, the Th1 shift appears relevant as asthma is a Th2-driven maladaptive immune response towards harmless aeroallergens. It is posited that intestinal commensals essentially drive the physiological Th2/Th1 conversion of the immune system (44). Thus, changes in the microbiome have the potential to modulate asthma severity by consolidating or alleviating the pro-asthmatic Th2 response or to alter asthma development/risk by altering the development of tolerogenic processes that naturally occur in the lung. Indeed, previous reports have demonstrated that Abx treatment worsens asthma severity in later life (37, 38). Mice treated with Abx peri- and postnatally (start of gestation till the end of the experiment) or solely postnatally (3-6 weeks) developed more severe asthma in OVA- or HDM-induced asthma models (37, 38). This observation correlated with reduced microbial diversity including loss of pro-regulatory organisms. The underlying mechanism relied on reduced Treg numbers in response to reduced *Clostridium* species (38, 45). Surprisingly then, administration of Abx did not affect asthma severity in our model. However, our study profoundly differs from these studies by solely investigating prenatal Abx treatment. Although we include in our considerations that the impact of antibiotic exposures persists into the early postnatal period (as reported previous (34)) when the lung and immune system continue to develop, our study focuses on earlier developmental windows than previous studies. To date, one additional study investigated prenatal Abx administration and the impact on asthma severity. Vancomycin was administered at different doses to dams. This treatment changed the gut microbiome in both mothers and pups and increased later life asthma severity in pups (46). Accordingly, we used vancomycin complemented with gentamycin and ampicillin to induce dysbiosis. Major experimental differences existed in the model allergen used for asthma induction. While Alhasan et al. (46) used ovalbumin without further adjuvant for asthma induction, our study used HDM as an allergen that better relates to human asthma. Comparing cellular influx into the lung, as indicated by BAL cells, HDM induces a much stronger allergic response than the OVA/adjuvant-free model. Likely, the strong asthma induction by HDM overwhelms the regulatory effects of Abx dosage. In combination with the naturally given differences between cohort microbiomes in different animal facilities, this may explain the different experimental outcomes.

Although we found increased numbers of IL-17A$^+$ cells, particularly non-conventional T cells, in HDM-exposed offspring of Abx-treated dams, we were not able to detect any differences in cytokine production - either at baseline or following HDM restimulation - in lung cells isolated from offspring of sucralose or Abx-exposed dams by ELISA. A possible explanation relies on methodological differences. The frequency of IL-17A$^+$ non-conventional T cells was assessed after *ex vivo* PMA/ionomycin stimulation while Th17-associated protein production was assessed after 72 hours of *in vitro* HDM restimulation. In detail, the former method aims at mostly stimulating allergen-specific αβ T cells (31, 32). As we do not actually see changes in the frequency of IL-17A$^+$ conventional CD4$^+$ T cells, this discrepancy may represent a technical limitation of *ex vivo* allergen restimulation as it is unclear to what extent pulmonary non-conventional T cells are activated

by HDM in *ex vivo* cell cultures. In contrast, as flow-based methods for identification of IL-17$^+$ producing cells utilize polyclonal stimulation (PMA/Ionomycin) it is also conceivable that the observed increase in IL-17A-producing non-conventional T cells represents expansion of non-HDM-specific non-conventional T cells that are exclusively captured using polyclonal stimulation techniques.

The mechanisms that might regulate altered non-conventional T cell recruitment to the lungs remain unclear, however, it is to be expected that dysbiosis induces changes in the maternal microbiome. Altered microbes or microbial metabolites might be retained by maternal IgG, and subsequently co-migrate to the uterus. After passage to the fetal intestine, they might lead to altered frequencies of non-conventional T cells. Such transplacental regulation was already demonstrated for ILC3s (47) where bacterial metabolites transferred from mother to offspring were able to regulate expression of antimicrobial peptides and influence microbial colonization in the fetal gut. While much of this work focused on changes in gut of offspring, recruitment of ILC3s to the neonatal lung were shown to be regulated by gut microbes. Further, these ILC3s had major implications for susceptibility to neonatal pneumonia (34). Specifically, CD103$^+$CD11b$^+$ DCs that capture antigen from gut commensal bacteria induced CCR4 expression on gut ILC3s licensing them for migration to the lung as well. This effect was diminished in Abx-treated mice leading to more severe pneumonia (34). Even γδ T cells that are part of the non-conventional T cells subpopulation were already shown to be regulated by antibiotic exposure, albeit the underlying experiment relied on postnatal antibiotic exposure and investigated long lasting effects on psoriasis (48). Altogether, these studies are consistent with our observation that early life shifts in microbiota induced by antibiotic exposure can cause dysregulated accumulation of IL-17 producing cells that may contribute to altered development of inflammatory diseases later in life.

Considering the reported changes in lung homing of ILC3s in response to prenatally induced dysbiosis and our observations that prenatally induced dysbiosis upregulated non-conventional T cells, we aimed at investigating effects on cellular distribution and interaction in the adult lung *in situ* (34, 49). This is of particular interest as T cell activation occurs *via* two pathways. It either involves MHC-mediated antigen-specific contacts with innate immune cells such as DCs accompanied by IL-6 secretion comparable to the pneumonia model and/or antigen-unspecific cell contact-independent cytokine secretion of IL-23 (50–52). Observing cellular contacts *in situ* allows for discrimination between these pathways. To assess cellular distribution we established an IHC staining approach enabling identification of potentially IL-17-producing cells in lung slices using the transcription factor RORγt (53). Staining with GATA3 to exclude Th2 cells as well as Hoechst staining to prove nuclear localization of the transcription factor RORγt validated this staining approach. *In situ* IHC analyses did not reproduce the observed increase of IL-17A$^+$ cells in HDM-exposed offspring of antibiotic treated mothers as observed by FACS. Possibly, PMA/ionomycin stimulation, as used in the FACS approach, serves as a strong stimulant of IL-17A expression that may overcome a more homeostatic RORγt expression probed by IHC. Moreover, Yang et al. suggest that RORα$^+$RORγt$^{-/-}$ cells may have some residual IL-17A-producing capacity (54), suggesting that RORγt-expression may not serve as a perfect surrogate for IL-17A expression. We were unable to examine the distribution of RORα-expressing cells in our models. Nonetheless, we observed localization of RORγt$^+$ cells in HDM-exposed offspring mostly close to large and only to a lower extent around small airways/blood vessels *via* IHC. In general, this localization is in accordance with the described localization of pulmonary immune cell populations (55). Further, it seems plausible that IL-17A$^+$ cells accumulate around larger airways as they contribute to regulation of mucus production which was shown to occur mainly at this localization. Looking at the specific distribution of RORγt subpopulations (αβ T cells, non-conventional T cells and ILCs) within the HDM-exposed lung, revealed that dysbiosis did not affect cellular localization. Since the effects of IL-17A could also depend on activation instead of localization of RORγt$^+$ cells, we determined the contact with CD11c$^+$ DCs. RORγt$^+$ cells were, independent of prior dysbiosis, mostly localized in close proximity with CD11c$^+$ cells. Since activation of RORγt$^+$ cells not only depends on cell-cell contact but also on IL-23 stimulation future studies will have to address this question in the context of prenatally induced dysbiosis.

In summary, our study revealed that solely prenatally induced dysbiosis exerts only minor effects on asthma severity later in life. To date, we cannot estimate whether this is a general observation or whether it rather is related to the individual microbiome of the experimental cohort or translationally the individual asthma patient. Thereby it emphasizes the need of individual considerations (e.g. dietary habit, microbial colonization, medication) in the context of microbiome regulated diseases. Further, it may help to direct future research on dysbiosis and its effects on allergic asthma to the postnatal time window. It also underlines the findings of existing studies that found major contribution of perinatal and postnatal factors such as mode of birth, lactation and postnatal contacts with microbiota in establishing a healthy commensal repertoire and subsequently contributing to appropriate barrier formation and alveolarization in the lung. By showing that prenatally induced dysbiosis affects IL-17$^+$ cells in the offspring, we qualify IL-17-mediated inflammatory processes as the most sensitive and at first regulated processes in response to early dysbiosis.

Data availability statement

The raw data supporting the conclusions of this article will be made available by the authors, without undue reservation.

Ethics statement

The animal study was reviewed and approved by Schleswig-Holstein state authorities and CCHMC Institutional Animal Care and Use Committee.

Author contributions

All authors revised the manuscript. IL performed the majority of the experiment in Cincinnati and Lübeck, and analyzed the data. AW, JH, and JM assisted with experiments in Cincinnati. YL critically discussed the data. CC and HD contributed to study design and data discussion. PK designed the research, supervised and took the responsibility of all experiments performed in Lübeck. IPL designed the research, supervised and took the responsibility of all experiments performed in Cincinnati. IS discussed the data and wrote the manuscript. All authors contributed to the article and approved the submitted version.

Funding

This project was supported by Deutsche Forschungsgemeinschaft Grants IRTG 1911 (project A2 to PK), NHLBI R01 HL122300 (to IPL), and NHLBI R01 HL149366 (to IPL).

Conflict of interest

The authors declare that the research was conducted in the absence of any commercial or financial relationships that could be construed as a potential conflict of interest.

Publisher's note

All claims expressed in this article are solely those of the authors and do not necessarily represent those of their affiliated organizations, or those of the publisher, the editors and the reviewers. Any product that may be evaluated in this article, or claim that may be made by its manufacturer, is not guaranteed or endorsed by the publisher.

Supplementary material

The Supplementary Material for this article can be found online at: https://www.frontiersin.org/articles/10.3389/fimmu.2022.937577/full#supplementary-material

References

1. Jiménez E, Marín ML, Martín R, Odriozola JM, Olivares M, Xaus J. Is meconium from healthy newborns actually sterile? *Res Microbiol* (2008) 159 (3):187–93. doi: 10.1016/j.resmic.2007.12.007

2. Aagaard K, Ma J, Antony KM, Ganu R, Petrosino J, Versalovic J. The placenta harbors a unique microbiome. *Sci Transl Med* (2014) 6(237):237ra65. doi: 10.1126/scitranslmed.3008599

3. Collado MC, Rautava S, Aakko J, Isolauri E, Salminen S. Human gut colonisation may be initiated *in utero* by distinct microbial communities in the placenta and amniotic fluid. *Sci Rep* (2016) 6:23129. doi: 10.1038/srep23129

4. Stout MJ, Conlon B, Landeau M, Lee I, Bower C, Zhao Q. Identification of intracellular bacteria in the basal plate of the human placenta in term and preterm gestations. *Am J Obstet Gynecol* (2013) 208(3):226.e1–7. doi: 10.1016/j.ajog.2013.01.018

5. Han YW, Shen T, Chung P, Buhimschi IA, Buhimschi CS. Uncultivated bacteria as etiologic agents of intra-amniotic inflammation leading to preterm birth. *J Clin Microbiol* (2009) 47(1):38–47. doi: 10.1128/JCM.01206-08

6. Doyle RM, Harris K, Kamiza S, Harjunmaa U, Ashorn U, Nkhoma M. Bacterial communities found in placental tissues are associated with severe chorioamnionitis and adverse birth outcomes. *PloS One* (2017) 12(7):e0180167. doi: 10.1371/journal.pone.0180167

7. Palmer C, Bik EM, DiGiulio DB, Relman DA, Brown PO. Development of the human infant intestinal microbiota. *PloS Biol* (2007) 5(7):e177. doi: 10.1371/journal.pbio.0050177

8. Jost T, Lacroix C, Braegger CP, Rochat F, Chassard C. Vertical mother-neonate transfer of maternal gut bacteria *via* breastfeeding. *Environ Microbiol* (2014) 16(9):2891–904. doi: 10.1111/1462-2920.12238

9. Biasucci G, Rubini M, Riboni S, Morelli L, Bessi E, Retetangos C. Mode of delivery affects the bacterial community in the newborn gut. *Early Hum Dev* (2010) 86 Suppl 1:13–5. doi: 10.1016/j.earlhumdev.2010.01.004

10. Dominguez-Bello MG, Costello EK, Contreras M, Magris M, Hidalgo G, Fierer N. Delivery mode shapes the acquisition and structure of the initial microbiota across multiple body habitats in newborns. *Proc Natl Acad Sci U S A* (2010) 107(26):11971–5. doi: 10.1073/pnas.1002601107

11. Guaraldi F, Salvatori G. Effect of breast and formula feeding on gut microbiota shaping in newborns. *Front Cell Infect Microbiol* (2012) 2:94. doi: 10.3389/fcimb.2012.00094

12. Jost T, Lacroix C, Braegger C, Chassard C. Impact of human milk bacteria and oligosaccharides on neonatal gut microbiota establishment and gut health. *Nutr Rev* (2015) 73(7):426–37. doi: 10.1093/nutrit/nuu016

13. Butel MJ, Waligora-Dupriet AJ, Wydau-Dematteis S. The developing gut microbiota and its consequences for health. *J Dev Orig Health Dis* (2018) 1–8. doi: 10.1017/S2040174418000119

14. Yatsunenko T, Rey FE, Manary MJ, Trehan I, Dominguez-Bello MG, Contreras M. Human gut microbiome viewed across age and geography. *Nat* (2012) 486(7402):222–7. doi: 10.1038/nature11053

15. Mueller S, Saunier K, Hanisch C, Norin E, Alm L, Midtvedt T. Differences in fecal microbiota in different European study populations in relation to age, gender, and country: a cross-sectional study. *Appl Environ Microbiol* (2006) 72(2):1027–33. doi: 10.1128/AEM.72.2.1027-1033.2006

16. Quigley EMM. Leaky gut - concept or clinical entity? *Curr Opin Gastroenterol* (2016) 32(2):74–9. doi: 10.1097/MOG.0000000000000243

17. Renz H, Adkins BD, Bartfeld S, Blumberg RS, Farber DL, Garssen J. The neonatal window of opportunity-early priming for life. *J Allergy Clin Immunol* (2018) 141(4):1212–4. doi: 10.1016/j.jaci.2017.11.019

18. Torow N, Hornef MW. The neonatal window of opportunity: Setting the stage for life-long host-microbial interaction and immune homeostasis. *J Immunol Baltim Md 1950* (2017) 198(2):557–63. doi: 10.4049/jimmunol.1601253

19. Barnes PJ. The cytokine network in asthma and chronic obstructive pulmonary disease. *J Clin Invest* (2008) 118(11):3546–56. doi: 10.1172/JCI36130

20. Lajoie S, Lewkowich IP, Suzuki Y, Clark JR, Sproles AA, Dienger K. Complement-mediated regulation of the IL-17A axis is a central genetic determinant of the severity of experimental allergic asthma. *Nat Immunol* (2010) 11(10):928–35. doi: 10.1038/ni.1926

21. Hall SL, Baker T, Lajoie S, Richgels PK, Yang Y, McAlees JW. IL-17A enhances IL-13 activity by enhancing IL-13-induced signal transducer and activator of transcription 6 activation. *J Allergy Clin Immunol* (2017) 139 (2):462–471.e14. doi: 10.1016/j.jaci.2016.04.037

22. Fujisawa T, Velichko S, Thai P, Hung LY, Huang F, Wu R. Regulation of airway MUC5AC expression by IL-1beta and IL-17A; the NF-kappaB paradigm. *J Immunol Baltim Md 1950* (2009) 183(10):6236–43. doi: 10.4049/jimmunol.0900614

23. Gasteiger G, D'Osualdo A, Schubert DA, Weber A, Bruscia EM, Hartl D. Cellular innate immunity: An old game with new players. *J Innate Immun* (2017) 9 (2):111–25. doi: 10.1159/000453397

24. Takeuchi O, Akira S. Pattern recognition receptors and inflammation. *Cell* (2010) 140(6):805–20. doi: 10.1016/j.cell.2010.01.022

25. Ignacio A, Breda CNS, Camara NOS. Innate lymphoid cells in tissue homeostasis and diseases. *World J Hepatol* (2017) 9(23):979–89. doi: 10.4254/wjh.v9.i23.979

26. Mortha A, Chudnovskiy A, Hashimoto D, Bogunovic M, Spencer SP, Belkaid Y. Microbiota-dependent crosstalk between macrophages and ILC3 promotes intestinal homeostasis. *Sci* (2014) 343(6178):1249288. doi: 10.1126/science.1249288

27. Neill DR, Wong SH, Bellosi A, Flynn RJ, Daly M, Langford TKA. Nuocytes represent a new innate effector leukocyte that mediates type-2 immunity. *Nat* (2010) 464(7293):1367–70. doi: 10.1038/nature08900

28. Yasuda K, Muto T, Kawagoe T, Matsumoto M, Sasaki Y, Matsushita K. Contribution of IL-33-activated type II innate lymphoid cells to pulmonary eosinophilia in intestinal nematode-infected mice. *Proc Natl Acad Sci U S A* (2012) 109(9):3451–6. doi: 10.1073/pnas.1201042109

29. Hoffmann JP, Kolls JK, McCombs JE. Regulation and function of ILC3s in pulmonary infections. *Front Immunol* (2021) 12:672523. doi: 10.3389/fimmu.2021.672523

30. Kaminski H, Couzi L, Eberl M. Unconventional T cells and kidney disease. *Nat Rev Nephrol Dezember* (2021) 17(12):795–813. doi: 10.1038/s41581-021-00466-8

31. Born WK, Huang Y, Reinhardt RL, Huang H, Sun D, O'Brien RL. γδ T cells and b cells. *Adv Immunol* (2017) 134:1–45. doi: 10.1016/bs.ai.2017.01.002

32. Chiba A, Murayama G, Miyake S. Mucosal-associated invariant T cells in autoimmune diseases. *Front Immunol* (2018) 9:1333. doi: 10.3389/fimmu.2018.01333

33. Díaz-Basabe A, Strati F, Facciotti F. License to kill: When iNKT cells are granted the use of lethal cytotoxicity. *Int J Mol Sci* (2020) 21(11):E3909. doi: 10.3390/ijms21113909

34. Gray J, Oehrle K, Worthen G, Alenghat T, Whitsett J, Deshmukh H. Intestinal commensal bacteria mediate lung mucosal immunity and promote resistance of newborn mice to infection. *Sci Transl Med* (2017) 9(376):eaaf9412. doi: 10.1126/scitranslmed.aaf9412

35. Paddenberg R, König P, Faulhammer P, Goldenberg A, Pfeil U, Kummer W. Hypoxic vasoconstriction of partial muscular intra-acinar pulmonary arteries in murine precision cut lung slices. *Respir Res* (2006) 7:93. doi: 10.1186/1465-9921-7-93

36. Hoffmann FM, Berger JL, Lingel I, Laumonnier Y, Lewkowich IP, Schmudde I. Distribution and interaction of murine pulmonary phagocytes in the naive and allergic lung. *Front Immunol* (2018) 9:1046. doi: 10.3389/fimmu.2018.01046

37. Adami AJ, Bracken SJ, Guernsey LA, Rafti E, Maas KR, Graf J. Early-life antibiotics attenuate regulatory T cell generation and increase the severity of murine house dust mite-induced asthma. pediatr res. *September* (2018) 84(3):426–34. doi: 10.1038/s41390-018-0031-y

38. Russell SL, Gold MJ, Hartmann M, Willing BP, Thorson L, Wlodarska M. Early life antibiotic-driven changes in microbiota enhance susceptibility to allergic asthma. *EMBO Rep* (2012) 13(5):440–7. doi: 10.1038/embor.2012.32

39. Tripathi N, Cotten CM, Smith PB. Antibiotic use and misuse in the neonatal intensive care unit. *Clin Perinatol* (2012) 39(1):61–8. doi: 10.1016/j.clp.2011.12.003

40. Ivanov S, Paget C, Trottein F. Role of non-conventional T lymphocytes in respiratory infections: the case of the pneumococcus. *PloS Pathog* (2014) 10(10): e1004300. doi: 10.1371/journal.ppat.1004300

41. Vermijlen D, Prinz I. Ontogeny of innate T lymphocytes - some innate lymphocytes are more innate than others. *Front Immunol* (2014) 5:486. doi: 10.3389/fimmu.2014.00486

42. de Kleer IM, Kool M, de Bruijn MJW, Willart M, van Moorleghem J, Schuijs MJ. Perinatal activation of the interleukin-33 pathway promotes type 2 immunity in the developing lung. *Immun* (2016) 45(6):1285–98. doi: 10.1016/j.immuni.2016.10.031

43. Saluzzo S, Gorki AD, Rana BMJ, Martins R, Scanlon S, Starkl P. First-Breath-Induced type 2 pathways shape the lung immune environment. *Cell Rep* (2017) 18(8):1893–905. doi: 10.1016/j.celrep.2017.01.071

44. Schlosser-Brandenburg J, Ebner F, Klopfleisch R, Kühl AA, Zentek J, Pieper R. Influence of nutrition and maternal bonding on postnatal lung development in the newborn pig. *Front Immunol* (2021) 12:734153. doi: 10.3389/fimmu.2021.734153

45. Atarashi K, Tanoue T, Shima T, Imaoka A, Kuwahara T, Momose Y. Induction of colonic regulatory T cells by indigenous clostridium species. *Sci* (2011) 331(6015):337–41. doi: 10.1126/science.1198469

46. Alhasan MM, Cait AM, Heimesaat MM, Blaut M, Klopfleisch R, Wedel A. Antibiotic use during pregnancy increases offspring asthma severity in a dose-dependent manner. *Allergy* (2020) 75(8):1979–90. doi: 10.1111/all.14234

47. Gomez de Agüero M, Ganal-Vonarburg SC, Fuhrer T, Rupp S, Uchimura Y, Li H. The maternal microbiota drives early postnatal innate immune development. *Sci* (2016) 351(6279):1296–302. doi: 10.1126/science.aad2571

48. Zanvit P, Konkel JE, Jiao X, Kasagi S, Zhang D, Wu R. Antibiotics in neonatal life increase murine susceptibility to experimental psoriasis. *Nat Commun* (2015) 6:8424. doi: 10.1038/ncomms9424

49. Oherle K, Acker E, Bonfield M, Wang T, Gray J, Lang I. Insulin-like growth factor 1 supports a pulmonary niche that promotes type 3 innate lymphoid cell development in newborn lungs. *Immun* (2020) 52(2):275–294.e9. doi: 10.1016/j.immuni.2020.01.005

50. Harbour SN, DiToro DF, Witte SJ, Zindl CL, Gao M, Schoeb TR. TH17 cells require ongoing classic IL-6 receptor signaling to retain transcriptional and functional identity. *Sci Immunol* (2020) 5(49):eaaw2262. doi: 10.1126/sciimmunol.aaw2262

51. Jones GW, McLoughlin RM, Hammond VJ, Parker CR, Williams JD, Malhotra R. Loss of CD4+ T cell IL-6R expression during inflammation underlines a role for IL-6 trans signaling in the local maintenance of Th17 cells. *J Immunol Baltim Md 1950* (2010) 184(4):2130–9. doi: 10.4049/jimmunol.0901528

52. Sutton CE, Lalor SJ, Sweeney CM, Brereton CF, Lavelle EC, Mills KHG. Interleukin-1 and IL-23 induce innate IL-17 production from gammadelta T cells, amplifying Th17 responses and autoimmunity. *Immun* (2009) 31(2):331–41. doi: 10.1016/j.immuni.2009.08.001

53. Ivanov II, McKenzie BS, Zhou L, Tadokoro CE, Lepelley A, Lafaille JJ. The orphan nuclear receptor RORgammat directs the differentiation program of proinflammatory IL-17+ T helper cells. *Cell* (2006) 126(6):1121–33. doi: 10.1016/j.cell.2006.07.035

54. Yang XO, Pappu BP, Nurieva R, Akimzhanov A, Kang HS, Chung Y. T Helper 17 lineage differentiation is programmed by orphan nuclear receptors ROR alpha and ROR gamma. *Immun* (2008) 28(1):29–39. doi: 10.1016/j.immuni.2007.11.016

55. Kretschmer S, Dethlefsen I, Hagner-Benes S, Marsh LM, Garn H, König P. Visualization of intrapulmonary lymph vessels in healthy and inflamed murine lung using CD90/Thy-1 as a marker. *PloS One* (2013) 8(2):e55201. doi: 10.1371/journal.pone.0055201

frontiers | Frontiers in Immunology

TYPE Original Research
PUBLISHED 13 September 2022
DOI 10.3389/fimmu.2022.937331

OPEN ACCESS

EDITED BY
Bao-Hui Cheng,
Institute of ENT and Shenzhen Key Laboratory of Ear, Nose and Throat, China

REVIEWED BY
Guanghai Yan,
Yanbian University Medical College, China
Zhilong Jiang,
Fudan University, China
Yang Li,
Chinese Academy of Sciences (CAS), China
Detian Yuan,
Shandong University, China

*CORRESPONDENCE
Rongchang Chen
chenrc@vip.163.com
Shanze Chen
chenshanze@mail.sustech.edu.cn
Xiaohui Zhou
zhouxiaohui@fudan.edu.cn
Shun Li
lishun86@126.com

†These authors have contributed equally to this work

SPECIALTY SECTION
This article was submitted to Immunological Tolerance and Regulation, a section of the journal Frontiers in Immunology

RECEIVED 06 May 2022
ACCEPTED 22 August 2022
PUBLISHED 13 September 2022

CITATION
Yu L, Wang L, Hu G, Ren L, Qiu C, Li S, Zhou X, Chen S and Chen R (2022) Reprogramming alternative macrophage polarization by GATM-mediated endogenous creatine synthesis: a potential target for HDM-induced asthma treatment. *Front. Immunol.* 13:937331. doi: 10.3389/fimmu.2022.937331

Reprogramming alternative macrophage polarization by GATM-mediated endogenous creatine synthesis: A potential target for HDM-induced asthma treatment

Li Yu[1†], Lingwei Wang[1†], Guang Hu[1], Laibin Ren[1], Chen Qiu[1], Shun Li[2*], Xiaohui Zhou[2*], Shanze Chen[1*] and Rongchang Chen[1*]

[1]Department of Pulmonary and Critical Care Medicine, The First Affiliated Hospital (Shenzhen People's Hospital) and School of Medicine, Southern University of Science and Technology, Shenzhen, China, [2]Department of Animal Model, Shanghai Public Health Clinical Center, Fudan University, Shanghai, China

Cellular energy metabolism plays a crucial role in the regulation of macrophage polarization and in the execution of immune functions. A recent study showed that Slc6a8-mediated creatine uptake from exogenous supplementation modulates macrophage polarization, yet little is known about the role of the *de novo* creatine *de novo*biosynthesis pathway in macrophage polarization. Here, we observed that glycine amidinotransferase (GATM), the rate-limiting enzyme for creatine synthesis, was upregulated in alternative (M2) polarized macrophages, and was dependent on the transcriptional factor STAT6, whereas GATM expression was suppressed in the classical polarized (M1) macrophage. Next, we revealed that exogenous creatine supplementation enhanced IL-4-induced M2 polarization, confirming recent work. Furthermore, we revealed that genetic ablation of GATM did not affect expression of M1 marker genes (Nos2, IL1b, IL12b) or the production of nitric oxide in both peritoneal macrophages (PMs) and bone marrow-derived macrophages (BMDMs). By contrast, expression levels of M2 markers (Arg1, Mrc1, Ccl17 and Retnla) were lower following GATM deletion. Moreover, we found that deletion of GATM in resident alveolar macrophages (AMs) significantly blocked M2 polarization but with no obvious effect on the number of cells in knockout mice. Lastly, an upregulation of GATM was found in lung tissue and bronchoalveolar lavage fluid macrophages from HDM-induced asthmatic mice. Our study uncovers a previously

uncharacterized role for the *de novo* creatine biosynthesis enzyme GATM in M2 macrophage polarization, which may be involved in the pathogenesis of related inflammatory diseases such as an T helper 2 (Th2)-associated allergic asthma.

KEYWORDS

macrophage, polarization, creatine, glycine amidinotransferase (GATM), asthma

Introduction

Macrophages, which are professional phagocytes, are particularly plastic and dynamic during a variety of inflammatory responses (1). To adapt to complex environmental changes, macrophages can acquire distinct functionally polarized phenotypes regardless of the tissue of origin (2). Of note, upon stimulation by lipopolysaccharide (LPS) and/or interferon-γ (IFN-γ), macrophages polarize to the classically activated phenotypes (M1), which have anti-microbial properties *via* the production of effectors such as nitric oxide and defensins, and amplify pro-inflammatory responses *via* by releasing cytokines and chemokines such as tumor necrosis factor-a (TNF-α), IL-1b, IL-12, IL-6, CXCL1, CXCL2, CXCL9, CCL2, and CCL3 (3, 4). It is well documented that the essential transcription factors involved in regulating the expression of M1-related genes are nuclear factor kappa beta (NF-κB), signal transducer and activator of transcription 1/2 (STAT1/2), and interferon regulatory factor-1/3/5/7(IRF1/3/5/7) (5–9). In contrast, T helper 2 (Th2)-cell-associated cytokines such as interleukin-4/13 (IL-4/13) promote the alternative polarized macrophage phenotype (M2) (4), which is characterized by induction of the anti-inflammatory cytokine IL-10, transforming growth factor β (TGF-β), vascular endothelial growth factor (VEGF), arginase 1 (Arg1), resistin-like-α (Retnla) and macrophage mannose receptor1 (Mrc1). This allows M2 macrophages to execute functions that encourage tissue repair and resolve inflammation in addition to participating in Th2-associated chronic inflammatory disease progression (10, 11). M2 polarization is controlled by different transcription factors such as Krüppel-like factor 4 (KLF4), IRF4, STAT6, peroxisome proliferator-activated receptor γ (PPARγ), and C/EBPβ (12–14). Therefore, clarifying the regulatory molecular mechanism of macrophage polarization will be helpful for interpreting the pathogenesis of inflammatory diseases and finding potential drug intervention targets.

An accumulative body of evidence indicates that macrophage polarization is firmly coupled together with altered cellular energy metabolism (15, 16). Metabolic transitioning between glycolysis and oxidative phosphorylation (OXPHOS) is associated with M1 and M2 polarization processes, respectively (17). For example, during M1-polarization-related glycolysis under anaerobic conditions, glucose converts into pyruvate, and further converts to lactate, which is controlled by various glycolytic enzymes including hexokinase (HK), phosphoglucose isomerase (PGI), phosphofructokinase (PFK), aldolase, and pyruvate kinase. Notably, pharmacological inhibition of glycolysis with 2-deoxy-D-glucose (2-DG) blocks pro-inflammatory genes expression during M1 polarization (18). In contrast, M2 polarization is dependent on oxidative phosphorylation (OXPHOS), which is tightly coupled to the TCA cycle driven by acetyl coenzyme A (acetyl-CoA), pyruvate, fatty acids and α-ketoglutarate (αKG) reactions (19). Pu-Ste Liu et al. reported that the production of α-ketoglutarate (αKG) *via* glutaminolysis is important for alternative (M2) macrophage activation (20). Therefore, modulation of metabolic pathways are vital for macrophage polarization.

The arginine-creatine metabolic axis is thought to play a crucial role in macrophage polarization. Creatine is synthesized from glycine for the backbone, arginine for the amidine group, and S-adenosyl methionine (SAM) which supplies the methyl group. Its synthesis is catalyzed by amidinotransferase and methyltransferase. Creatine kinase catalyzes the transfer of sodium from ATP into the creatine molecule to form phosphocreatine reserves (21). Notably, L-arginine has various metabolic pathways available. For example, L-arginine is converted to NO by inducible nitric oxide synthase (iNOS) and is also utilized by arginase 1, two enzymes which are hallmarks of M1 and M2 polarized macrophages, respectively, and it is also converted to creatine by two enzymes, glycine amidinotransferase (GATM) and guanidinoacetate methyltransferase (GAMT) (22). Creatine, a widely used dietary supplement, was first described in 1835 by the French chemist Eugene Chevreau (23). Most endogenous creatine is produced naturally in the liver and kidneys. Creatine can be phosphorylated to creatine phosphate by creatine kinase, which serves as a phosphate donor in the conversion of ADP to ATP, and thus supplies energy necessary for cellular needs in an acute manner such as during muscle contraction (24). It has been reported that creatine impacts inflammatory responses. For example, Madan and Khanna observed in the late 1970s that creatine can ameliorate

carrageenan-induced inflammation of the foot pads in rats (25). Deminice et al. demonstrated that TNF-α and CRP levels were lower in individuals supplemented with creatine following acute exercise (26). Creatine can also be obtained from the food and taken up by Slc6a8-expressing cells. Recently, Ji et al. reported that macrophages express relatively high levels of Slca68, and specific deletion of Slc6a8 in macrophages significantly reduce the amount of macrophage creatine and increases the expression of the M1 markers iNOS and CXCL9, whilst decreasing expression of the M2 marker Arg1 (22). This demonstrates that Slc6a8-mediated exogenous creatine uptake plays an essential role in macrophage polarization. In previous work from our group, we used microarray and RNA-sequencing and surprisingly observed that macrophages expressed both creatine *de novo* synthesis enzymes, GATM and GAMT, which was dramatically induced polarization in M2 but suppressed it in M1, indicating that the mechanism underlying macrophage polarization is likely *via* metabolic reprogramming.

For the most part, research on creatine biology has focused on the brain, muscle and the liver (27). The function of creatine in the immune system still largely unknown. In present study, we investigated the role of the rate limiting enzyme GATM in macrophage polarization. We found that GATM is required for polarization of M2 but not M1. The expression of GATM was positively associated with M2 macrophages in the BALF of HDM-induced asthma model mice. The current study implicatesGATM-mediated endogenous creatine synthesis as a key player in macrophage metabolism and opens a new avenue for possible treatment targets in macrophage-related inflammatory diseases such as asthma.

Materials and methods

Animals and establishment of a mouse model with asthma

Balb/c mice (6–8 weeks; GemPharmatech Co., Ltd, China) were sensitized by injections (s.c.) of HDM extract (50 μg in 100 μL sterile saline; Greer Laboratories, lot XPB82D3A25) on days 0, 7, and 14, followed by daily intranasal (i.n.) rechallenges (50 μg in 20 μL sterile saline) on days 21, 22, K23, 24, and 25. Nonsensitized mice received sterile saline only (s.c and i.n). Analysis of lung function parameters and organ collection was performed 24 h after the last challenge. All measures were taken to keep animal suffering to a minimum.

The CRISPR/Cas9 design target was designed on exon3 of the transcript GATM-201, causing frame shift mutations to achieve the purpose of inactivating protein function (Figure S1A). GATM-sgRNA1 targeting CCAAAGATCATCTGAAGAAGG was used for microinjection. We used PCR to identify GATM mouse genotypes (Figure S1B). The GATM knockout F0 generation was obtained by embryo transfer and surrogate conception, and the F1 generation was bred to determine the GATM genotype using T7E1 and sequencing (Figure S1C). The pure heterozygotes were further determined using Sanger sequencing results. Mice were housed in a specific pathogen-free animal facility and maintained in isolated ventilated cages on a 12-h light/dark cycle with ad libitum access to food and water.

Lung histopathology

Tissue was taken from the left lung of each mouse and fixed in 4% paraformaldehyde overnight. The tissues were embedded in paraffin and then cut into 4-μm sections. Lung tissues were stained with H&E, periodic acid-Schiff (PAS), and Masson's trichrome to observe histological changes including inflammatory-cell infiltration into the peribronchial connective tissues, mucus secretion and fiber formation.

BALF analysis

After blood was taken, the lungs were lavaged *in situ* twice with 0.8 mL sterile saline (0.9% NaCl, prewarmed), and the recovered fluid was pooled. The total number of cells in BALF were counted, and a cytospin sample was prepared. The number of total blood cells, eosinophilic granulocytes, and lymphocytes in BALF were evaluated using a hemacytometer. The BALF was centrifuged at 3000 × rpm at 4°C for 15 min to collect the supernatant. Levels of IL-4 in cell-free BALF were determined using ELISA kits according to manufacturer instruction (ELM-IL-4-1, Raybio).

Measurement of serum IgE

Mice were sacrificed with an overdose of pentobarbital (100 mg/kg, i.p.) one day after the last airway challenge. Blood samples were taken from the retroorbital plexus/sinus, allowed to rest at room temperature for 1 hour, then centrifuged (3000 × rpm, 20 min), and supernatants were collected for detection of total IgE with an ELISA kit according to manufacturer instructions (ELM-IgE-1, Raybio).

Airway hyperresponsiveness measurement

AHR was measured using an animal pulmonary function instrument (Buxco Electronics, US). In brief, an ascending series of methacholine (6.26-50 mg/mL) was administrated into the trachea through the connected atomizer. The baseline airway resistance was evaluated using atomized PBS. The resistance

index (RI) of the total lung and airway was determined as per the protocols of the instrument.

Immunohistochemical staining

For GATM immunohistochemistry, deparaffinized lung sections were subjected to antigen retrieval, and then treated with H_2O_2 for 15 min to block endogenous peroxidase, and then incubated overnight at 4°C in recommended dilutions of anti-GATM antibodies. After washing with PBS, slices were incubated with a secondary antibody for 20 min at room temperature. Signals were visualized with DAB.

Immunofluorescence staining

The lung tissue was fixed in 4% paraformaldehyde for 1 hour at 4°C, blocked in 20% goat serum for 2 hours at 4°C, and incubated overnight with the antibodies against GATM (GB113430, Servicebio), CD68 (GB113109, Servicebio), and Arginase 1 (GB11285, Servicebio) at 4°C, and then with fluorescein isothiocyanate-labeled secondary antibody (GB22303, Servicebio), at room temperature for 1 hour. We then used a fluorescent triple staining kit (G1236-100T, Servicebio). In addition, DAPI (G1012, Servicebio) was used to stain the nuclei and anti-fluorescence quenching sealer (G1401, Servicebio). The staining was observed under an inverted fluorescence microscope (Servicebio).

Extraction and culture of alveolar macrophages, peritoneal macrophages and bone marrow-derived macrophages

Primary AMs were isolated by repeatedly flushing mouse lungs with 1 ml of PBS eight times at room temperature to obtain BAL. Cells were centrifuged at 1,500 rpm for 5 min, washed twice using DMEM complete medium, and then cells were incubated for 3 hours in 24-well plates at a density of 3 x 10^5 cells/well to allow cells to adhere. Next, the cells were washed twice with PBS to remove non-adherent cells for subsequent processing. To generating peritoneal macrophages, intraperitoneal injections of 3% thioglycolate broth were administered, and then cells were extracted and harvested for assays. To generate BMDMs, bone marrow cells were cultured in macrophage complete medium containing 20 ng/ml M-CSF (CB34, Novoprotein). After 6 days in culture, non-adherent cells were eliminated and adherent cells were harvested for assays. Next, the AMs, PMs and BMDMs were cultured in 1 μg/ml LPS (Sigma-Aldrich, St. Louis, MO, USA) and 20 ng/ml IFN-γ (C746, Novoprotein) for M1 polarization, or 20 ng/mL interleukin-4 (CK15, Novoprotein) for M2 polarization treatment for up to 24 hours. M1 and M2 macrophages were harvested for quantitative PCR and western blotting analysis.

RNA interference

For RNA interference experiments, primary cells were seeded in a 24-well plate in antibiotic-free growth medium. siRNA transfection was performed using Lipofectamine RNAi MAX reagent (13778150, Invitrogen) and Opti-MEM (Gibco, Germany) according to the manufacturer protocol. The sequences for siGATM (RIB-BIO; China) and siSTAT6 (RIB-BIO; China) were GGTCGAAGAGATGTGCAAT and GCTGATCATTGGCTTTATT, respectively; both used at a 50 nM concentration.

Purification of $CD4^+$ T cells from the mouse spleen

Primary BMDMs were incubated in 12-well plates (2 x 10^5 cells/well) for 48 h to allow siRNA to interfere with GATM. To purify $CD4^+$ T cells from the mouse spleen, spleens were dissected from healthy, female C57BL/6 mice (6–8 weeks old) under sterile conditions. A 100 μm cell strainer was placed in a sterile 10-cm dish and lymphocytes were isolated using a mouse lymphocyte separator (Dakewe, China) and $CD4^+$ lymphocyte subsets were enriched on T-cell columns (Miltenyi, Germany) by negative selection according to manufacturer instructions and red blood cells lysed with ACK lysis buffer.

Co-culture of macrophages with $CD4^+$ T cells

Mouse BMDMs and purified $CD4^+$ T cells were seeded into 12-well plates at a density of 2 × 10^5 cells/well in lower room and 2×10^6 cells/well and the upper room. Anti-mouse CD3 0.5 mg/l (eBioscience, America) and anti-mouse CD28 0.5 mg/l (eBioscience, America) antibodies were also added into the co-culture system to stimulate the proliferation of $CD4^+$T cells. After 72 hours of co-culture, T cells were collected, and quantitative PCR was used to detect T-bet and IL-10.

RNA isolation and quantitative PCR analysis

RNA isolation from AMs, PMs, BMDMs were performed *via* using the Total RNA extraction Kit (B511361-0100, BBI, China). Resulting total RNA was transcribed using *via* a HiScript® III RT SuperMix cDNA Synthesis kit (R223-01, Vazyme, China) according to the manufacturer instructions. Quantitative PCR

was performed using *via* ChamQ Universal SYBR quantitative PCR Master Mix (Q711-02, Vazyme, China) on a CFX Connect™ Real-Time System from BIO-RAD (BIO-RAD). β-actin was used as a reference gene. The sequences of primers used were as follows:

mouse β-actin-F TCCATCATGAAGTGTGACGT
mouse β-actin-R GAGCAATGATCTTGATCTTCAT
mouse Nos2 F CCTGTGAGACCTTTGATG
mouse Nos2 R CCTATATTGCTGTGGCTC
mouse TNF-α F CACCACGCTCTTCTGTCT
mouse TNF-α R GGCTACAGGCTTGTCACTC
mouse IL1b F CAACCAACAAGTGATATTCTCCATG
mouse IL1b R GATCCACACTCTCCAGCTGCA
mouse IL12b F GGAAGCACGGCAGCAGAATA
mouse IL12b R AACTTGAGGGAGAAGTAGGAATGG
mouse Arg1 F GGAACCCAGAGAGAGCATGA
mouse Arg1 R TTTTTCCAGCAGACCAGCTT
mouse Mrc1 F CATGAGGCTTCTCCTGCTTCT
mouse Mrc1 R TTGCCGTCTGAACTGAGATGG
mouse Ccl17 F TTGTGTTCGCCTGTAGTGCATA
mouse Ccl17 R CAGGAAGTTGGTGAGCTGGTATA
mouse Retnla F CGAGTAAGCACAGGCAGT
mouse Retnla R CCAGCTAACTATCCCTCCAC
mouse GATM-F TGAAGACAAGGCCACCCATC
mouse GATM-R GCATTTTCAGCTCTGCCCAC
mouse GAMT-F TTCCCTTGAAAGGCCTGTGG
mouse GAMT-R ACGTGAGGTTGCAGTAGGTG
mouse Slc6a8-F AGATCTCCGTTGCTCTGC
mouse Slc6a8-R TGGAAGACGTACATTCCACCATC
mouse Scd1-F GCTCTACACCTGCCTCTTCG
mouse Scd1-R GCCGTGCCTTGTAAGTTCTG
mouse T-bet-F TGTTCCCAGCCGTTTCTACC
mouse T-bet-R GCTCGGAACTCCGCTTCATA
mouse IL-10-F AGGCGCTGTCATCGATTTCT
mouse IL-10-R ATGGCCTTGTAGACACCTTGG
mouse IL-4-F ACGAGGTCACAGGAGAAGGGA
mouse IL-4-R AGCCCTACAGACGAGCTCACTC
mouse IL-5-F CTGGCCTCA AACTGGTAATGTAG
mouse IL-5-R ATGAGGGGGAGGGAGTATAACTC
mouse IL-13-F CCTCTGACCCTTAAGGAGCTTAT
mouse IL-13-R CGTTGCACAGGGGAGTCT

Western blotting assay

Total protein was extracted using a protein extraction kit (CST, USA). The protein concentration was determined by a BCA Protein Assay kit (Beyotime, China). Cells were lysed for 10 min at 95 °C and 20 μg of protein was loaded onto 10% SDS-PAGE gel, then the separated proteins were transferred to a PVDF membrane (Merck Millipore, Bedford, MA, USA) and incubated overnight at 4 °C with primary rabbit monoclonal antibodies against iNOS (1:1000; 13120, CST, USA), rabbit monoclonal antibodies against Arginase-1 (1:1000; 93668, CST, USA), rabbit polyclonal antibodies against GATM (1:1000, PA5-109756, Invitrogen, USA), rabbit monoclonal antibodies against STAT6 (1:1000; 5397, CST, USA), and β-actin-HRP(1:3000; AB2001, ABWays), followed by anti-rabbit-IgG horseradish peroxidase-conjugated secondary antibodies (CST, USA). Signals were detected by enhanced chemiluminescence (Merck Millipore, Bedford, MA, USA) and exposed using a ChemiDoc™ MP Imager (Bio-Rad, USA). The integral optical density of each sample was measured using Image J.

Quantification of nitric oxide

Nitric oxide was detected using the Griess Reagent System (Promega, USA).

Flow cytometry

Mouse lung tissues were ground into single cell suspensions using a Miltenyi automatic tissue grinder (Miltenyi, Germany). The flow cytometry antibodies used were CD11c (117309, Biolegend, USA) and Siglec F (155509, Biolegend, USA). Cell surface staining was performed at 4°C for 30–40 min in the dark. The purity of sorted populations was >99%, unless otherwise indicated. Data were obtained on a FACSCanto II clinical flow cytometry system (BD Biosciences) and analyzed using FlowJo software (FlowJo LLC, Ashland, Oregon).

Creatine assay

30 mg of lung tissue was lysed using CelLytic™ M (sigma, USA), centrifuged at 12000 rpm for 10 min, and the supernatant was collected for detecting 570 nm absorbance, according to the manufacturer instructions for Creatine colorimetric/fluorometric assay kit (BioVision, USA).

RNA-seq analysis

Total RNA was extracted from AMs and PMs from WT and GATM$^{-/-}$ mice using BBI reagent kits (BBI, China). High quality total RNA was used to construct an RNA-seq library. AMs and PMs were cultured in 12-well plates with 500,000 cells/well. PMs were stimulated with LPS and IFN-γ or IL-4 for 24 h. The integrity and total amount of RNA were assessed using the RNA Nano 6000 Assay Kit from the Bioanalyzer 2100 system (Agilent Technologies, CA, USA). RNA-seq library preparation (AMPure XP system) was performed at Novogene, where sequencing was performed on an Illumina NovaSeq 6000 machine.

Statistics and software

Data were analyzed using GraphPad Software (Prism 8.00, San Diego, CA, USA). Each experiment was performed independently in at least 3 times. Quantitative data are presented as mean ± S.D., according to the number of comparison groups, and Student's *t*-tests or one-way ANOVAs were performed as required. P <0.05 was considered statistically significant. *P <0.05; **P <0.01; ***P <0.001; ****P <0.0001.

Results

Creatine promotes IL-4 induced-M2 polarization *in vitro*

The creatine transporter protein Slc6a8 is known to activate M2 polarization by transporting exogenous creatine (22). However, the role of endogenous creatine synthesis (GATM) on macrophage polarization remains unknown. Here, to establish the macrophage polarization model, AMs, PMs and BMDMs were treated for 24 h either with LPS and IFN-γ to induce M1polarization or with IL-4 to induce M2 polarization. It is well known that DNA microarray technology is an established technique for profiling gene expression at the whole genomic level. To investigate potential polarization-relevant genes, we previously performed an Illumina microarray analysis of M1- and M2-polarized AMs (28). As expected, a great number of genes were found to be altered by polarization conditions; among these genes, we identified that GATM together with the M2 marker genes (Arg1, Mrc1, Ccl17 and Retnla) were clearly upregulated in M2-polarized AMs. In this study, we used RNA-sequence technology, which is well established for profiling gene expression of PMs at the whole transcription level, we found a decrease in GATM expression in M1 polarized macrophages. This indicates that M1 activation is negatively regulated by GATM, and is elevated in M2 polarized macrophages (Figure 1A and Table S1). Of the three genes associated with the synthesis and transport of creatine (GATM, GAMT, Slc6a8), quantitative PCR and western blotting analysis showed that only the expression levels of GATM were increased following M2 polarization, indicating that GATM is involved in M2 polarization (Figures 1B, C). To determine the effect of creatine on M2 polarization, we added creatine to PMs and quantitative PCR analysis showed elevated expression levels of Arg1, Retnla and Ccl17, whereas there was no change in GATM expression (Figure 1D). To further explore the regulatory factors in GATM expression, we used RNAi technology to knockdown STAT6, which a key transcription factor of M2 polarization, and we found that GATM mRNA and protein expression was reduced in IL-4 polarized macrophages (Figures 1E, F). Furthermore, we analyzed lipid-metabolism-related genes through transcriptome data and found that GATM knockout significantly reduced Scd1 expression (Figure 1G and Table S1). GATM knockdown also reduced Scd1 mRNA levels in M2 macrophages (Figure 1H). Taken together, we conclude that GATM acts as an endogenous proponent of M2 polarization and that GATM expression is regulated by STAT6. In addition, GATM knockdown inhibited lipid metabolism in M2 macrophages to some extent.

GATM promotes M2 polarization in BMDMs, but has only a small effect on M1 polarization

To specifically address the role of GATM in macrophage polarization, we generated mice with GATM ablation and obtained GATM$^{-/-}$ mice *via* CRISPR/Cas9-mediated gene editing. We found that GATM expressed in M2 polarization (Figure S2) and genetic ablation of GATM did not alter the level of nitric oxide (Figure 2A) and did not change transcript levels of Nos2, IL1b and IL12b (Figure 2B) or protein expression of iNOS (Figure 2D) in BMDMs. However, the expression of Arg1, Mrc1, Ccl17 and Retnla following IL-4-induced M2 polarization was reduced in GATM$^{-/-}$ mice (Figure 2C) and protein expression of GATM and Arg1 (Figure 2E) was also reduced. Therefore, the results indicate that GATM had only a small effect on M1 macrophages, however, it did promote M2 polarization.

AMs from GATM$^{-/-}$ mice have altered expression of genes involved in cell-cell adhesion, immune response, cytokines and cytokine-receptor interactions and inhibit M2 polarization

Creatine is a metabolite involved in cellular energy homeostasis, which facilitates the differentiation of muscle cells and neurons (29, 30). To explore the contribution of GATM in the differentiation and maturation of AMs, we used flow

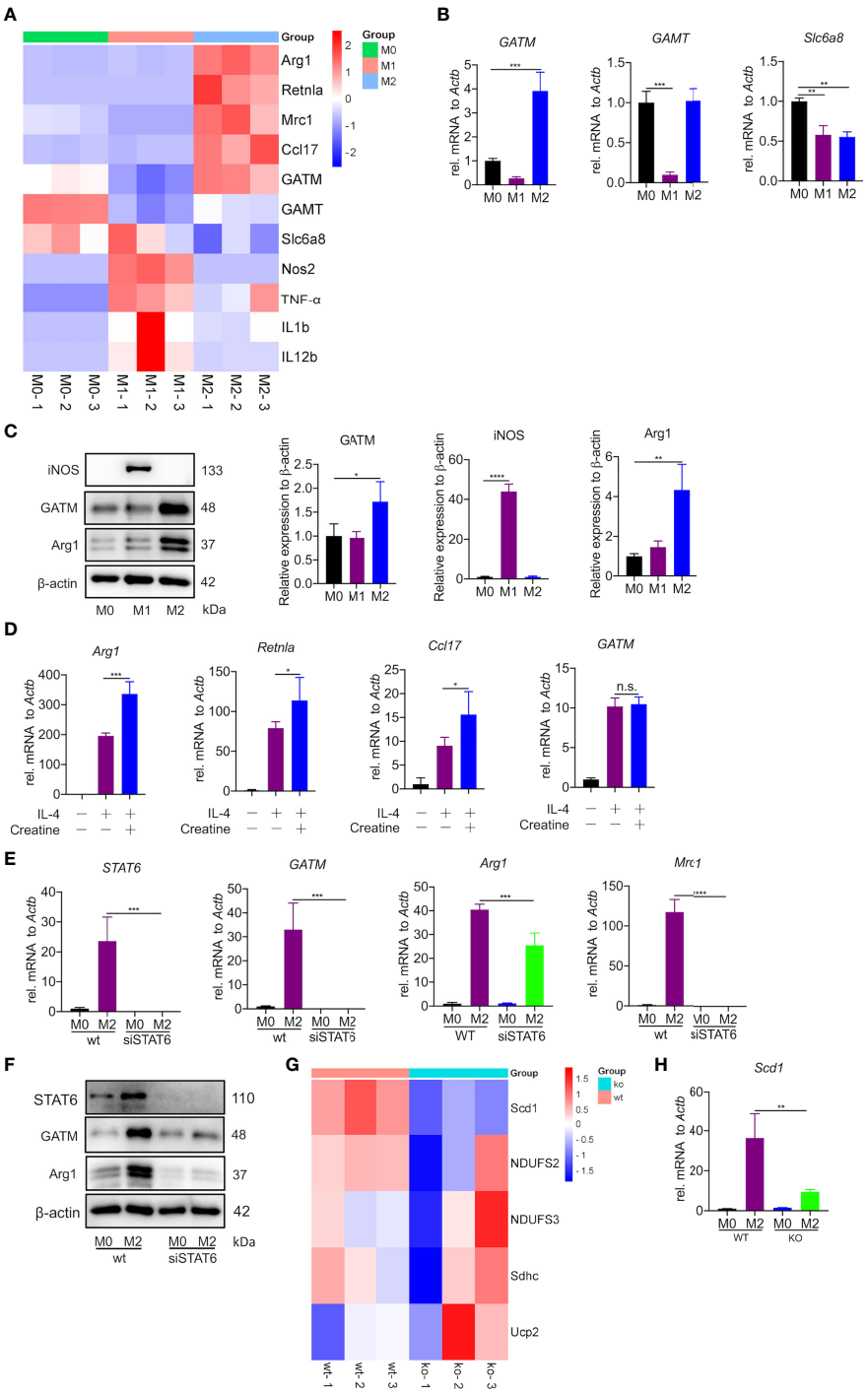

FIGURE 1
Creatine promotes IL-4 induced-M2 polarization *in vitro*. **(A)** Heatmap analysis of RNA-seq dataset of PMs showing subsets of genes in M1 and M2 macrophages relative to controls treated with LPS/IFN-γ or IL-4 for 24 hours. **(B)** Transcription levels of GATM, GAMT and Slc6a8 in BMDMs were detected by quantitative PCR (n=3). **(C)** Arg1 and GATM expression levels in BMDMs were detected using western blotting (n=3). **(D)** WT BMDMs were pretreated with creatine overnight and subsequently activated with IL-4 for 24 hours. Expression of Arg1, Retnla and Ccl17 mRNA were determined by quantitative PCR (n=4). **(E)** siRNA blocks STAT6 expression in IL-4 activated (24 hours) AMs. STAT6, GATM, Arg1 and Mrc1 expression was determined by quantitative PCR and **(F)**, western blotting. **(G)** Heatmap analysis of RNA-seq dataset of PMs showing subsets of genes in WT and GATM$^{-/-}$ (n=3). **(H)** Transcription levels of Scd1 in AMs were detected by quantitative PCR (n=3). Data are expressed as mean ± SEM. Statistical significance was determined by one-way ANOVAs with Tukey's multiple comparisons test; n.s., not significant *P<0.05, **P<0.01, ***P<0.001, ****P<0.0001.

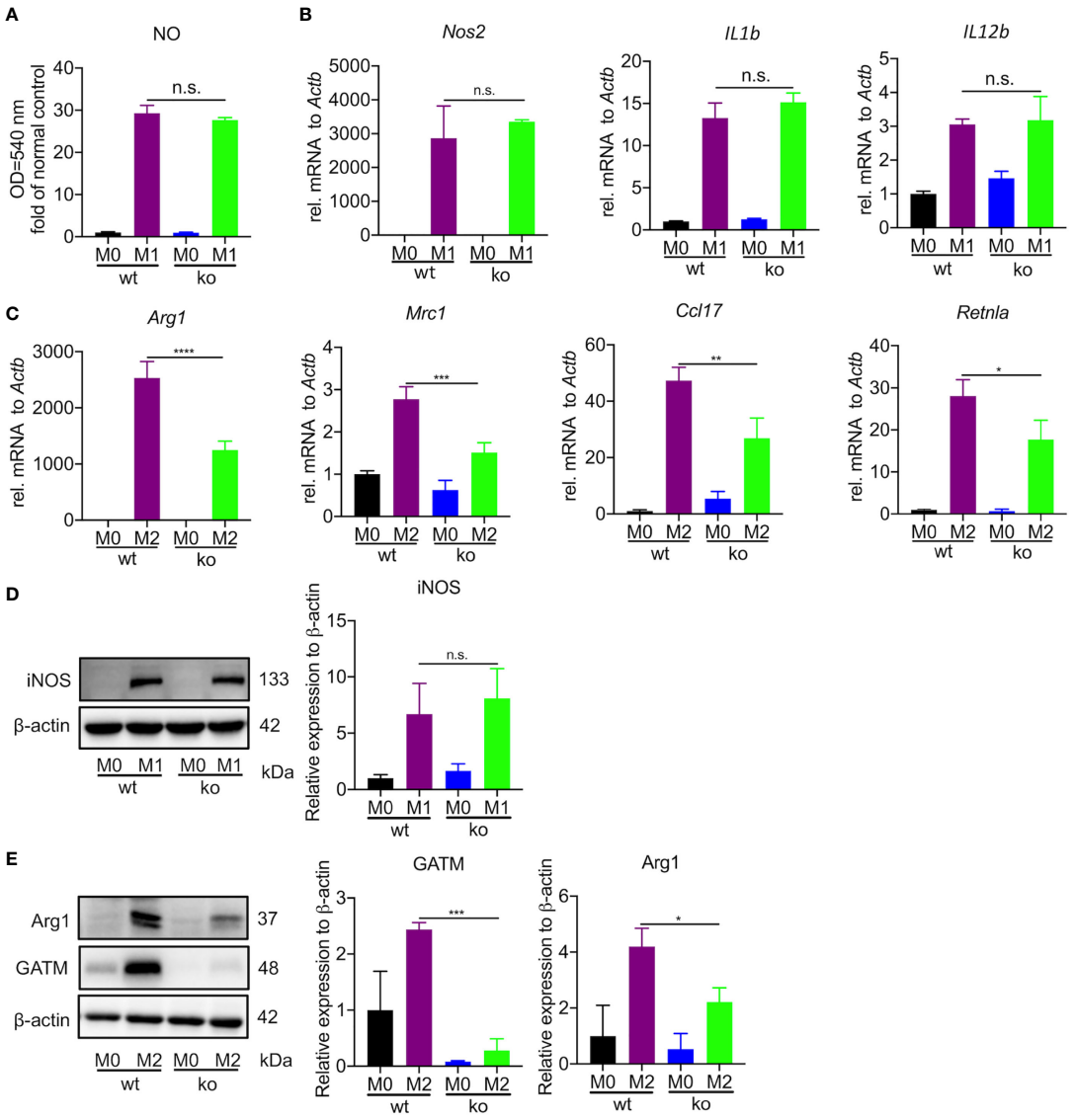

FIGURE 2
GATM promoted M2 polarization in BMDMs but had only a small effect on M1 polarization. **(A, B)**, GATM$^{-/-}$ BMDMs were activated with LPS and IFN-γ for 24 hours. Level of NO and Nos2, IL1b and IL12b mRNA expression was determined by quantitative PCR (n=3). **(C)** GATM$^{-/-}$ BMDMs were treated with IL-4 activation for 24 hours. Arg1, Mrc1, Ccl17 and Retnla mRNA expression was determined by quantitative PCR (n=3). **(D, E)**, GATM$^{-/-}$ AMs were treated with LPS and IFN-γ or IL-4 activation for 24 hours. iNOS and Arg1 protein expression was determined by western blotting (n=3). Data are expressed as mean ± SEM. Statistical significance was determined using one-way ANOVAs with Tukey's multiple comparisons test; n.s., not significant; *P<0.05, **P<0.01, ***P<0.001, ****P<0.0001.

cytometry to analyze the well-known AM markers CD11c and Siglec F. We observed a slight decrease in the number of AMs compared to wild type (Figure 3A). Furthermore, we used RNA-seq to compare the difference in transcriptomic analysis between wild type and GATM$^{-/-}$ AMs. In the comparative transcriptomic analysis, a total of 434 DEGs, including 349 up- and 85 down-regulated genes, were identified from comparing data between the WT and GATM$^{-/-}$ groups (Figure 3B and Table S2). We then used the DEGs for the bioinformatics analysis, which included Gene Ontology (GO) enrichment, Kyoto Encyclopedia of Genes and Genomes (KEGG) enrichment, and Ingenuity Pathway Analysis (IPA), to delineate the mechanism underlying the effect of GATM on macrophage polarization. In the comparison of WT and GATM$^{-/-}$ groups, the GO enrichment analysis showed that the GATM deletion altered multiple biological processes related to T-cell activation, regulation of cell-cell adhesion and activation of immune response, (Figure 3C; Table S3). The KEGG pathway analysis

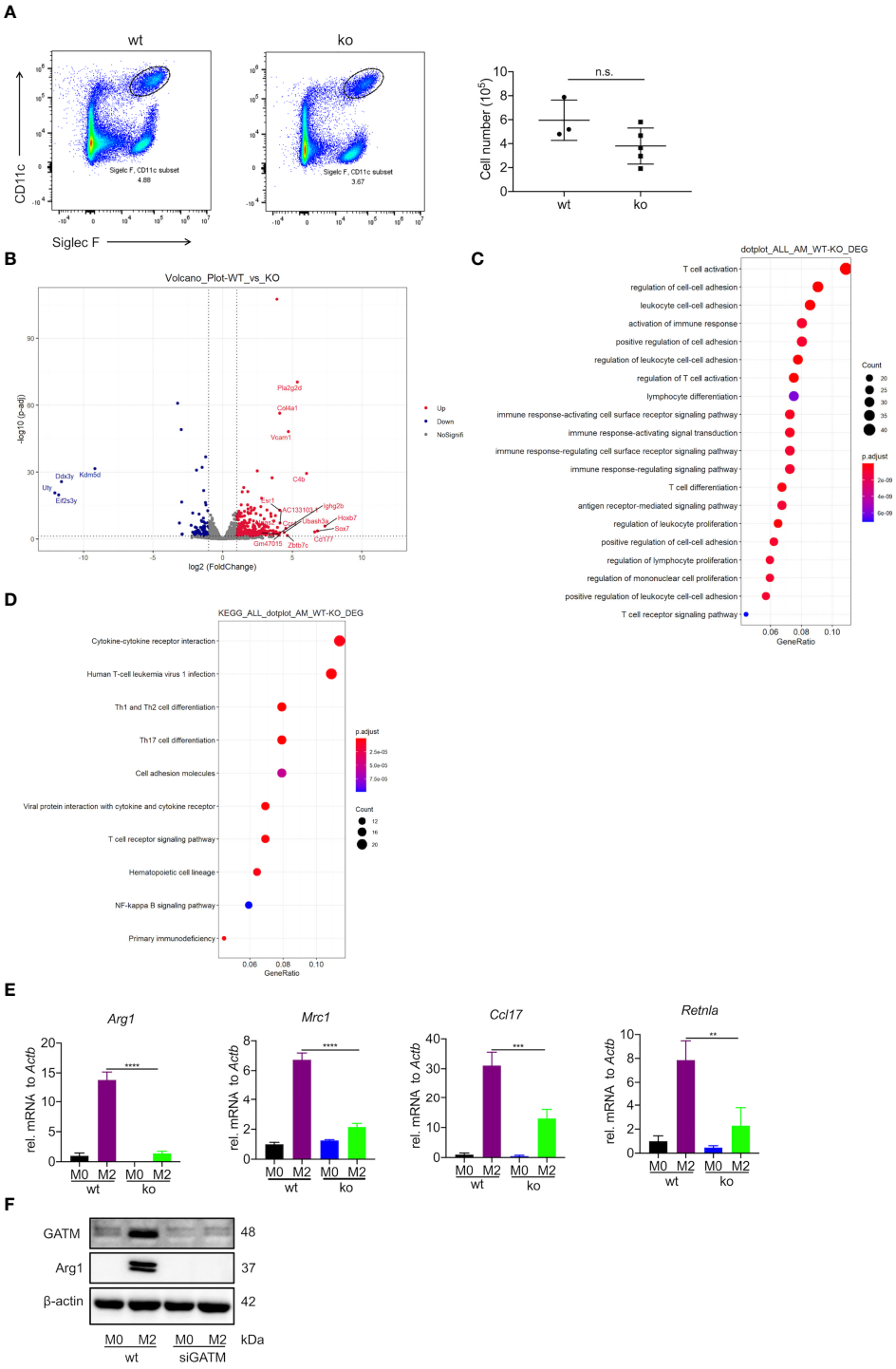

FIGURE 3
Deficiency of GATM inhibits M2 polarization in AMs. **(A)** AMs maturation was detected by flow cytometry (n=3–5). **(B)** Volcano plot depicting GATM knockdown upregulation of significantly upregulated genes. Red dots represent significant upregulation of expressed genes and blue dots represent significant downregulation of expressed genes ($GATM^{-/-}$ vs. control) **(C)** Biological processes and **(D)** cell-signaling pathways related to AMs. Rich factor represents the number of differential genes/the total number of genes in the enrichment term; the greater the Rich factor, the higher the degree of GO/KEGG enrichment. Dot size represents the number of differential genes and the color of the dots represents the p-value in the enrichment analysis. siRNA blocks GATM expression in IL-4 activated (24 hours) AMs, **(E)** GATM and Arg1 protein expression was determined using western blotting (n=3). Data are expressed as mean ± SEM. Statistical significance was determined using one-way ANOVAs with Tukey's multiple comparisons test; n.s., not significant $^{**}P<0.01$, $^{***}P<0.001$, $^{****}P<0.0001$. **(F)** and inhibit M2 polarization.

highlighted cytokine/cytokine-receptor interaction, T-cell differentiation and viral-protein interaction with cytokines and cytokine receptors (Figure 3D; Table S4). We therefore investigated whether macrophage-intrinsic GATM dampens pro-inflammatory T-cell responses using *in vitro* co-culture of BMDMs with splenocytes. After 3 days of co-culture, GATM knockdown in BMDMs distinctly promoted the expression of T-bet and IL-10 compared to $CD4^+$ T cells (Figure S3). IL-10 production by Treg cells is critical for the control of immune response and increases allergy-induced lung inflammation and hyperreactivity in $Il10^{flox/flox}$×$Foxp3^{YFP\text{-}Cre}$ mice (31). T-Bet expression acquisition by Tregs is necessary for the control of type 1 inflammation *in vivo* (32). Furthermore, we found that $GATM^{-/-}$ inhibited the expression of Arg1, Mrc1, Ccl17, Retnlain AMs (Figure 3E), and reduced the expression of Arg1 protein after GATM interference with AMs using RNAi technology (Figure 3F). Taken together, our results suggest that GATM promoted M2 polarization and altered clusters of functional genes involved in the immune response.

Pulmonary expression of GATM and creatine is elevated in a HDM-induced asthma model

Asthma is a typical Th2-associated inflammatory disease in which macrophages exhibit M2 polarization (33). To link GATM expression with disease condition, we generated an acute HDM-induced murine model of asthma as a proxy for the acute inflammatory phenotype found in humans (34) (Figure 4A). As expected, airway exposure to HDM induced increased airway hyperresponsiveness to methacholine (Figure 4B), the majority of serum IgE and BAL IL-4 raised (Figure 4C). Examination of lung tissue revealed epithelium injury and smooth muscle thickening of the airway, and peribranchial inflammation with copious amounts of eosinophil and macrophage infiltration in the airway lumen were evident (Figures 4D-F). BAL cells had eosinophils and lymphocytes and other factors consistent with other HDM-induced asthma models (Figure 4G), indicating that the characteristics of chronic airway inflammation and airway remodeling are well demonstrated in this model. In addition, we detected that the transcriptional level of IL-4, IL-5 and IL-13 were significantly expressed in the lung tissue of asthmatic mice (Figure 4H). Studies have reported that creatine aggravates the inflammatory response in asthma (35, 36). Our results showed that the concentration of creatine in the lung tissue of asthmatic mice was higher than in the control group, indicating that creatine may be involved in the development of asthma (Figure 4I). Western blotting and immunohistochemistry of GATM showed that there was relatively high expression in lung tissue, and it appeared that HDM sensitization and challenge altered GATM expression in the lungs (Figure 4J and Figure S4). Consistent with this, immunofluorescence revealed that HDM exposure raised GATM expression across the whole lung (Figure 4K). Therefore, GATM is involved to some extent in the development of asthma.

GATM is involved in the polarization of M2 type macrophages in asthma

To investigate whether the upregulated GATM in asthmatic lung tissue was related to macrophage polarization, we analyzed GATM colocalization with M1 (CD68, iNOS) and M2 (CD68, Arg1) markers in lung tissue using confocal microscopy, and found that GATM was upregulated in M2 macrophages but not M1 polarized macrophages (Figure 5A and S4A). Furthermore, we isolated AMs using BAL and cultured them for 3 hours to adhere to the well walls, then observed them under the microscope and found that that the majority of macrophages in the asthma group exhibited a shuttle-like shape, while the control group alveolar macrophages still retained a round shape (Figure 5B). We detected that mRNA expression of Arg1, Retnla and GATM was upregulated in AMs, but not in GAMT, Slc6a8, Nos2, IL1b, or IL12b (Figures 5C, D and Figure S4B). Moreover, western blotting verified the upregulation of GATM and Arg1 protein levels in these cells (Figure 5E). Overall, our present study suggests that GATM may contribute to the progression of asthma *via* modulation of M2 macrophage polarization.

Discussion

In this study, we uncovered a novel GATM function in alternative macrophage activation, which is dependent on the STAT6 pathway. RNAi- and CRISPR/Cas9-mediated deletion of GATM resulted in lower expression of M2 marker genes such as Arg1, Mrc1, Ccl17 and Retnla in polarized M2 AMs, PMs and BMDMs, suggesting a vital role of GATM in the regulation of innate immune function. Previous work reported that Slc6a8 regulated creatine uptake and synthesis in PMs, indicating that Slc6a8 mediated macrophage metabolism in the resting state (22). In contrast, we found that Slc6a8 expression was reduced in polarized macrophages. However, GATM expression was increased in polarized M2 macrophages, but not in polarized M1 macrophages, indicating that GATM regulates M2 polarization. In addition, GATM was differently expressed in M1 and M2 polarized macrophages, indicating that it is likely to be regulated by disparate mechanisms. Furthermore, we found that STAT6 regulated GATM expression but we did not find direct evidence in the TFBS database for STAT6 regulation of GATM expression, probably for STAT6 indirectly regulating GATM expression through regulating intermediate molecules. Previous studies have shown that the addition of exogenous creatine promotes the

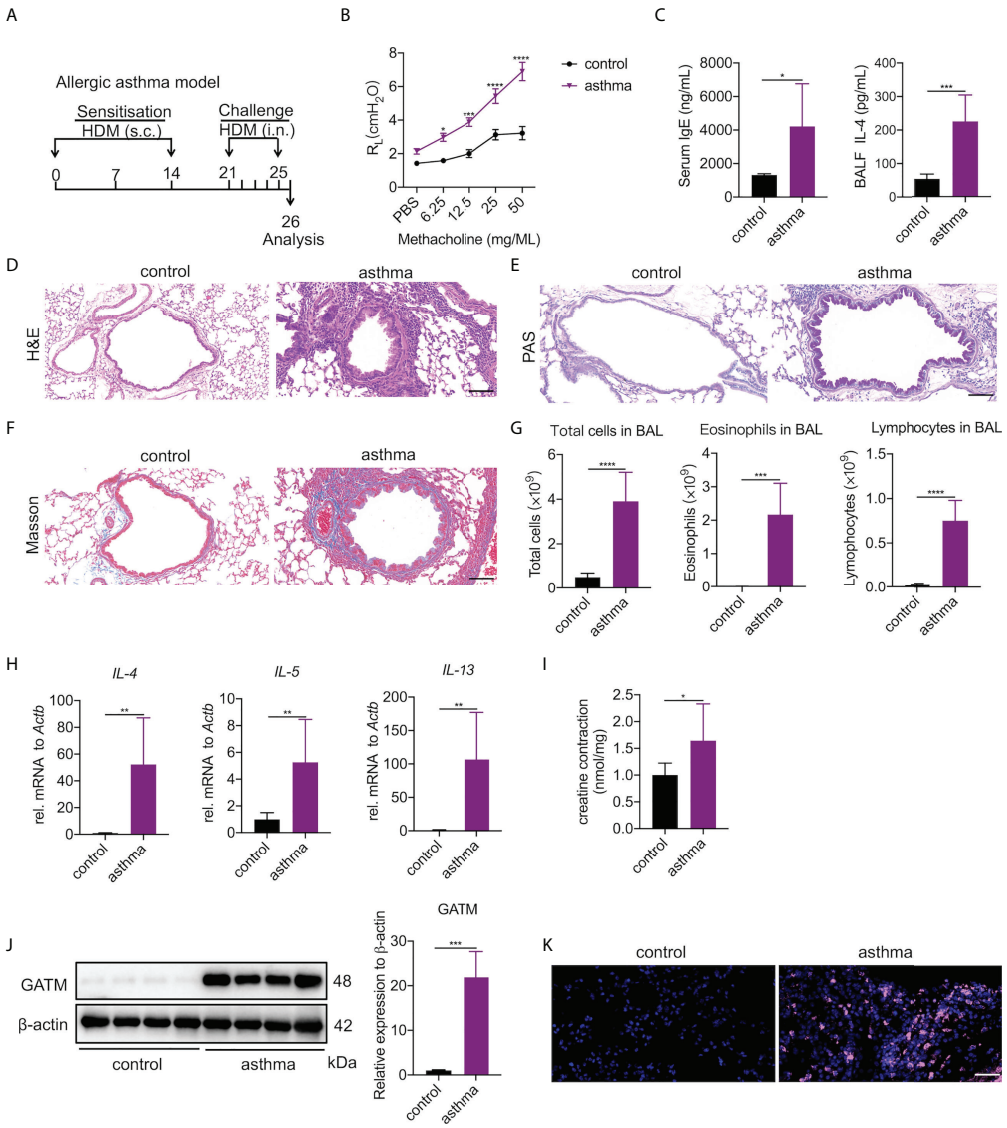

FIGURE 4
Pulmonary expression of GATM and creatine in HDM-induced asthma model. **(A)** Experimental timeline. **(B)** AHR as measured by lung resistance (R_L; n=7). **(C)** Serum level of IgE and BALF levels of IL-4 (n=6–8). **(D)** Representative H&E-stained lung sections showing different groups. Original magnification x 200 (n=6). Scale bar=100 uM. **(E)** Representative PAS-stained lung sections showing goblet cell metaplasia in different groups. Original magnification x 200 (n=4). Scale bar=100 uM. **(F)** Representative Masson-stained lung sections showing submucosal collagen deposition in different groups. Original magnification x 200 (n=4). Scale bar=100 uM. **(G)** Total cells, eosinophils and lymphocytes in BALF (n=6). **(H)** The expression of IL-4, IL-5, IL-13 in asthma. **(I)** Creatine concentration in asthma. **(J)** western blotting detection of GATM protein expression in the lung (n=4). **(K)** Immunofluorescence detection of GATM protein expression in the lung (n=4). Scale bar=20 uM. Data expressed as mean ± SEM. Statistical significance was determined using t-tests; *P<0.05, **P<0.01, ***P<0.001, ****P<0.0001.

expression of M2 markers (Arg1, Retnla) in PMs (22), and we also confirmed this result in BMDMs, suggesting that creatine promotes M2 polarization in macrophages of different origins using similar regulatory mechanisms. Moreover, we found that GATM$^{-/-}$ mice had inhibited expression of Scd1, suggesting that GATM promoted M2 macrophage polarization by affecting lipid metabolism. Typically, studies on macrophages have used PMs and BMDMs as models. We also utilized BMDMs as a model and showed that GATM does not affect M1 polarization and that endogenous creatine has little effect on M1 polarization. Endogenous creatine promotes cancer metabolism through activation of Smad2/3 (37). Nevertheless, a large number of studies have shown that exogenous creatine inhibits M1 polarization *via* JAK-STAT

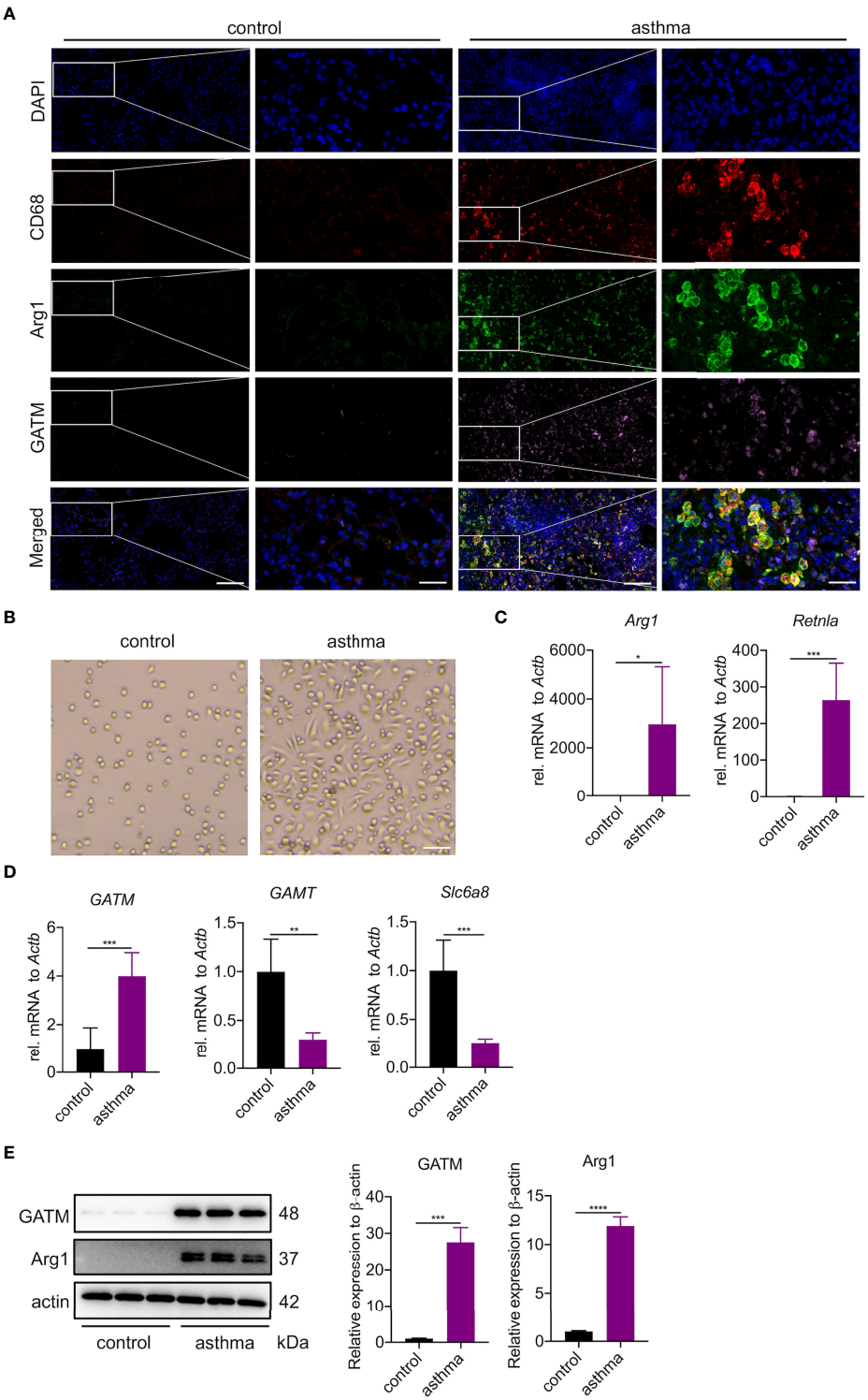

FIGURE 5
GATM is involved in the polarization of M2 type macrophages in asthma. **(A)** Immunofluorescence staining of CD68, Arg1 and GATM in lung tissue. Original magnifications x 200 *left* and x 630 *right* panel (n=4). Scale bar=20 uM. **(B)** Morphology of AMs under the microscope. Original magnification x 100 (n=5). Scale bar=200 uM. **(C)** Transcription levels of Arg1 and Retnla in AMs were detected by quantitative PCR (n=5). **(D)** Transcription levels of GATM, GAMT and Slc6a8 in AMs were detected by quantitative PCR (n=5). **(E)** Arg1 and GATM expression levels in AMs were detected by western blotting (n=4). Data are expressed as mean ± SEM. Statistical significance was determined using t-tests; **P*<0.05; ***P*<0.01, ****P*<0.001, *****P*<0.0001.

signaling (22, 38), but not *via* NF-κB signaling. It is known that endogenous creatine and exogenous creatine have distinct roles and regulatory mechanisms on M1 polarization in diverse diseases. Previous studies have shown that exogenous creatine promotes M2 polarization *via* the STAT6 pathway (22), and here we demonstrated that both exogenous and endogenous creatine promote M2 polarization *via* the STAT6 pathway, which complements the immunological effects of endogenous creatine found in previous research. In addition, we also list other transcription factors that may regulate GATM expression in Table S5. For example, one study found that monounsaturated fatty acids generated by Stearoyl-CoA desatSurase-1 (SCD1), an enzyme responsible for the desaturation of saturated fatty acids, reduced the surface abundance of the cholesterol efflux transporter ABCA1, which in turn promoted lipid accumulation and induced an inflammatory phagocyte phenotype (39). We found that GATM knockdown robustly decreased the mRNA expression of Scd1 but not of Scd2 isoforms in AMs, indicating GATM knockout blocked creatine synthesis and inhibited lipid metabolism, thereby inhibiting M2 polarization. In addition, complementing the immune mechanism of action of endogenous creatin.

Macrophages are the only cells that are present in every organ in the body. They mainly have roles in anti-inflammatory responses and tissue repair (40), which have received much attention. We previously found that GATM was significantly expressed in M2 polarization, but the effect of GATM deletion on macrophage polarization remained uncertain. Therefore, we generated GATM$^{-/-}$ transgenic mice using CRISPR/Cas9 technology and, despite decreasing the number of cells, did not affect the maturation of alveolar macrophages, likely because of the inconsistent number of mice, or because of individual differences. It may be that increasing the samples size would give different results in this instance. Macrophages and T cells activate and suppress each other and together regulate the environmental homeostasis of the organism (41). RNA-seq further analyzed GATM$^{-/-}$ in AMs and found enrichment of T-cell activation and immune-related pathways, demonstrating that GATM$^{-/-}$ may activate T-cell-mediated immune responses. In addition, GATM may be necessary for Tregs control of Th1 inflammation. The effect of GATM$^{-/-}$ on AMs was consistent across PMs and BMDMs (reduced Arg1, Mrc1, Ccl17, Retnla), suggesting that GATM possibly affects M2 polarization through the same mechanism in both AMs and PMs. It has been suggested that Mrc1 (42, 43), Retnla (44–46) and Ccl17 (47–49) mediate allergic sensitization and asthma or COPD. Accordingly, GATM may be a good target for the relief of allergic inflammation.

GATM is the key rate-limiting step that catalyzes endogenous creatine biosynthesis: the transfer of amino groups from arginine to glycine to form ornithine and guanidinoacetic acid directly promotes creatine biosynthesis, which is supplemented by cytoplasmic ATP *via* phosphocreatine shuttling while consuming mitochondrial ATP (37). In hereditary diseases where creatine synthesis is impaired, creatine has a disease-modifying capacity, including mental fatigue (50), sleep deprivation (51, 52), environmental hypoxia such as in mountain climbing and advanced age (53–55), but except people with kidney disease (56). Recent studies have found that exogenous creatine aggravates the inflammatory response in asthma (35), but the mechanism had not been elucidated. We found that GATM was significantly expressed in the mouse asthma model, but not GAMT and slc6a8. Therefore, we mainly explored the expression of GATM in macrophages. The expression of IL-4 was still significantly elevated in the HDM-induced asthma model. *In vitro*, we used IL-4 to stimulate M2 polarization. Based on this, we speculate that GATM expression increases in asthma may also be due to Th2-type immune-factor stimulation. However, due to homozygous infertility restrictions, our research did not adopt an acute HDM-induced GATM$^{-/-}$ murine model of asthma to study the effect of creatine on the inflammatory response of asthma, which is limitation of this study.

Data availability statement

The datasets presented in this study can be found in online repositories. The names of the repository/repositories and accession number(s) can be found in the article/Supplementary Material.

Ethics statement

The animal study was reviewed and approved by The Animal Subjects Committee of Shenzhen People's Hospital.

Author contributions

LY, SC, and RC conceptualized and designed the study. SL, XZ, SC, and RC carried out the experiments. LW, CQ, RC, and XZ analyzed the data. LY, SC, and RC drafted the manuscript. LY, SC, and RC edited the manuscript for language. SL, XZ, SC, and RC revised the manuscript. All authors contributed to the article and approved the submitted version.

Funding

This study was supported by grants from the National Natural Science Foundation of China (81803183, 82170042),

the Shenzhen Science and Technology Innovation Program (JCYJ20210324114400002), the Natural Science Foundation of Guangdong Province (2022A1515011966), the Key Project of Science and Technology Foundation of Sichuan Province (2019YFS0230) and the Project of Shanghai Municipal Health Commission (No.20204Y0335).

Conflict of interest

The reviewer ZJ declared a shared parent affiliation with the authors, WZ, SL, to the handling editor at the time of the review.

The remaining authors declare that the research was conducted in the absence of any commercial or financial relationships that could be construed as a potential conflict of interest.

Publisher's note

Supplementary material

The Supplementary Material for this article can be found online at: https://www.frontiersin.org/articles/10.3389/fimmu.2022.937331/full#supplementary-material

SUPPLEMENTARY FIGURE 1
GATM mouse construction protocol. (A) Analysis of conserved regions of mouse GATM gene structure and protein function. (B) GATM mouse genotyping PCR product. (C) Results of T7E1 analysis of GATM mouse genotyping.

SUPPLEMENTARY FIGURE 2
GATM expression in M2 polarized macrophages.

SUPPLEMENTARY FIGURE 3
The expression of T-bet and IL-10 was detected by quantitative PCR (n=3). Statistical significance was determined using one-way ANOVAs with Tukey's multiple comparisons test; $^{**}P<0.01$, $^{***}P<0.001$, $^{****}P<0.0001$.

SUPPLEMENTARY FIGURE 4
GATM expression in the HDM-induced asthma model using immunohistochemistry (n=4). Scale bar=50 uM.

SUPPLEMENTARY FIGURE 5
GATM is barely affected in M1 polarized macrophages in asthma. (A) Immunofluorescence staining of CD68, iNOS and GATM in lung tissue. Original magnifications x 200 *left* and 630 *right* panel (n=4). Scale bar=20 uM (B) The expression of Nos2, TNF-α, IL1b, IL12b was detected by quantitative PCR (n=5). Data are expressed as mean ± SEM. Statistical significance was determined using t-tests; $^{*}P<0.05$, $^{***}P<0.001$, $^{****}P<0.0001$.

References

1. Verschoor CP, Puchta A, Bowdish DM. The macrophage. *Methods Mol Biol* (2012) 844:139–56. doi: 10.1007/978-1-61779-527-5_10

2. Funes SC, Rios M, Escobar-Vera J, Kalergis AM. Implications of macrophage polarization in autoimmunity. *Immunology* (2018) 154:186–95. doi: 10.1111/imm.12910

3. Atri C, Guerfali FZ, Laouini D. Role of human macrophage polarization in inflammation during infectious diseases. *Int J Mol Sci* (2018) 19:1801. doi: 10.3390/ijms19061801

4. Sica A, Mantovani A. Macrophage plasticity and polarization: *in vivo* veritas. *J Clin Invest* (2012) 122:787–95. doi: 10.1172/jci59643

5. Wang L, Gong Z, Zhang X, Zhu F, Liu Y, Jin C, et al. Gut microbial bile acid metabolite skews macrophage polarization and contributes to high-fat diet-induced colonic inflammation. *Gut Microbes* (2020) 12:1–20. doi: 10.1080/19490976.2020.1819155

6. Nie Y, Wang Z, Chai G, Xiong Y, Li B, Zhang H, et al. Dehydrocostus lactone suppresses LPS-induced acute lung injury and macrophage activation through NF-κB signaling pathway mediated by p38 MAPK and akt. *Molecules* (2019) 24:1510. doi: 10.3390/molecules24081510

7. Lam E, Stein S, Falck-Pedersen E. Adenovirus detection by the cGAS/STING/TBK1 DNA sensing cascade. *J Virol* (2014) 88:974–81. doi: 10.1128/jvi.02702-13

8. Zhu X, Guo Q, Zou J, Wang B, Zhang Z, Wei R, et al. MiR-19a-3p suppresses M1 macrophage polarization by inhibiting STAT1/IRF1 pathway. *Front Pharmacol* (2021) 12:614044. doi: 10.3389/fphar.2021.614044

9. Krausgruber T, Blazek K, Smallie T, Alzabin S, Lockstone H, Sahgal N, et al. IRF5 promotes inflammatory macrophage polarization and TH1-TH17 responses. *Nat Immunol* (2011) 12:231–8. doi: 10.1038/ni.1990

10. Elzayat MA, Bayoumi AMA, Abdel-Bakky MS, Mansour AM, Kamel M, Abo-Saif A, et al. Ameliorative effect of 2-methoxyestradiol on radiation-induced lung injury. *Life Sci* (2020) 255:117743. doi: 10.1016/j.lfs.2020.117743

11. Hasita H, Komohara Y, Okabe H, Masuda T, Ohnishi K, Lei XF, et al. Significance of alternatively activated macrophages in patients with intrahepatic cholangiocarcinoma. *Cancer Sci* (2010) 101:1913–9. doi: 10.1111/j.1349-7006.2010.01614.x

12. Liao X, Sharma N, Kapadia F, Zhou G, Lu Y, Hong H, et al. Krüppel-like factor 4 regulates macrophage polarization. *J Clin Invest* (2011) 121:2736–49. doi: 10.1172/jci45444

13. Satoh T, Takeuchi O, Vandenbon A, Yasuda K, Tanaka Y, Kumagai Y, et al. The Jmjd3-Irf4 axis regulates M2 macrophage polarization and host responses against helminth infection. *Nat Immunol* (2010) 11:936–44. doi: 10.1038/ni.1920

14. Yu T, Gan S, Zhu Q, Dai D, Li N, Wang H, et al. Modulation of M2 macrophage polarization by the crosstalk between Stat6 and Trim24. *Nat Commun* (2019) 10:4353. doi: 10.1038/s41467-019-12384-2

15. Viola A, Munari F, Sánchez-Rodríguez R, Scolaro T, Castegna A. The metabolic signature of macrophage responses. *Front Immunol* (2019) 10:1462. doi: 10.3389/fimmu.2019.01462

16. Yan J, Horng T. Lipid metabolism in regulation of macrophage functions. *Trends Cell Biol* (2020) 30:979–89. doi: 10.1016/j.tcb.2020.09.006

17. Puleston DJ, Buck MD, Klein Geltink RI, Kyle RL, Caputa G, O'Sullivan D, et al. Polyamines and eIF5A hypusination modulate mitochondrial respiration and macrophage activation. *Cell Metab* (2019) 30:352–63.e8. doi: 10.1016/j.cmet.2019.05.003

18. Orihuela R, McPherson CA, Harry GJ. Microglial M1/M2 polarization and metabolic states. *Br J Pharmacol* (2016) 173:649–65. doi: 10.1111/bph.13139

19. Liu Y, Xu R, Gu H, Zhang E, Qu J, Cao W, et al. Metabolic reprogramming in macrophage responses. *biomark Res* (2021) 9:1. doi: 10.1186/s40364-020-00251-y

20. Liu PS, Wang H, Li X, Chao T, Teav T, Christen S, et al. α-ketoglutarate orchestrates macrophage activation through metabolic and epigenetic reprogramming. *Nat Immunol* (2017) 18:985–94. doi: 10.1038/ni.3796

21. Curt MJ-C, Voicu P-M, Fontaine M, Dessein A-F, Porchet N, Mention-Mulliez K, et al. Creatine biosynthesis and transport in health and disease. *Biochimie* (2015) 119:146–65. doi: 10.1016/j.biochi.2015.10.022

22. Ji L, Zhao X, Zhang B, Kang L, Song W, Zhao B, et al. Slc6a8-mediated creatine uptake and accumulation reprogram macrophage polarization *via* regulating cytokine responses. *Immunity* (2019) 51:272–84.e7. doi: 10.1016/j.immuni.2019.06.007

23. Mesa JL, Ruiz JR, González-Gross MM, Gutiérrez Sáinz A, Castillo Garzón MJ. Oral creatine supplementation and skeletal muscle metabolism in physical exercise. *Sports Med* (2002) 32:903–44. doi: 10.2165/00007256-200232140-00003

24. Kazak L, Cohen P. Creatine metabolism: energy homeostasis, immunity and cancer biology. *Nat Rev Endocrinol* (2020) 16:421–36. doi: 10.1038/s41574-020-0365-5

25. Khanna NK, Madan BR. Studies on the anti-inflammatory activity of creatine. *Arch Int Pharmacodyn Ther* (1978) 231:340–50.

26. Deminice R, Rosa FT, Franco GS, Jordao AA, de Freitas EC. Effects of creatine supplementation on oxidative stress and inflammatory markers after repeated-sprint exercise in humans. *Nutrition* (2013) 29:1127–32. doi: 10.1016/j.nut.2013.03.003

27. Horn M, Frantz S, Remkes H, Laser A, Urban B, Mettenleiter A, et al. Effects of chronic dietary creatine feeding on cardiac energy metabolism and on creatine content in heart, skeletal muscle, brain, liver and kidney. *J Mol Cell Cardiol* (1998) 30:277–84. doi: 10.1006/jmcc.1997.0590

28. Chen S, Kammerl IE, Vosyka O, Baumann T, Yu Y, Wu Y, et al. Immunoproteasome dysfunction augments alternative polarization of alveolar macrophages. *Cell Death Differ* (2016) 23:1026–37. doi: 10.1038/cdd.2016.3

29. Ellery SJ, Murthi P, Davies-Tuck ML, Della Gatta PA, May AK, Kowalski GM, et al. Placental creatine metabolism in cases of placental insufficiency and reduced fetal growth. *Mol Hum Reprod* (2019) 25:495–505. doi: 10.1093/molehr/gaz039

30. Balestrino M, Adriano E. Beyond sports: Efficacy and safety of creatine supplementation in pathological or paraphysiological conditions of brain and muscle. *Med Res Rev* (2019) 39:2427–59. doi: 10.1002/med.21590

31. Rubtsov YP, Rasmussen JP, Chi EY, Fontenot J, Castelli L, Ye X, et al. Regulatory T cell-derived interleukin-10 limits inflammation at environmental interfaces. *Immunity* (2008) 28:546–58. doi: 10.1016/j.immuni.2008.02.017

32. Kitz A, Dominguez-Villar M. Molecular mechanisms underlying Th1-like treg generation and function. *Cell Mol Life Sci* (2017) 74:4059–75. doi: 10.1007/s00018-017-2569-y

33. Fricker M, Gibson PG. Macrophage dysfunction in the pathogenesis and treatment of asthma. *Eur Respir J* (2017) 50:1700196. doi: 10.1183/13993003.00196-2017

34. Lu K, Lai KP, Stoeger T, Ji S, Lin Z, Lin X, et al. Detrimental effects of microplastic exposure on normal and asthmatic pulmonary physiology. *J Hazard Mater* (2021) 416:126069. doi: 10.1016/j.jhazmat.2021.126069

35. Garcia M, Santos-Dias A, Bachi ALL, Oliveira-Junior MC, Andrade-Souza AS, Ferreira SC, et al. Creatine supplementation impairs airway inflammation in an experimental model of asthma involving P2 × 7 receptor. *Eur J Immunol* (2019) 49:928–39. doi: 10.1002/eji.201847657

36. Vieira RP, Duarte AC, Claudino RC, Perini A, Santos AB, Moriya HT, et al. Creatine supplementation exacerbates allergic lung inflammation and airway remodeling in mice. *Am J Respir Cell Mol Biol* (2007) 37:660–7. doi: 10.1165/rcmb.2007-0108OC

37. Zhang L, Zhu Z, Yan H, Wang W, Wu Z, Zhang F, et al. Creatine promotes cancer metastasis through activation of Smad2/3. *Cell Metab* (2021) 33:1111–23.e4. doi: 10.1016/j.cmet.2021.03.009

38. Li Y, Jin X, Yang X, Zhang L, Qi Z. Creatine promotes the repair of peripheral nerve injury by affecting macrophage polarization. *Biochem Biophys Res Commun* (2022) 604:116–22. doi: 10.1016/j.bbrc.2022.03.047

39. Bogie JFJ, Grajchen E, Wouters E, Corrales AG, Dierckx T, Vanherle S, et al. Stearoyl-CoA desaturase-1 impairs the reparative properties of macrophages and microglia in the brain. *J Exp Med* (2020) 217:e20191660. doi: 10.1084/jem.20191660

40. Ginhoux F, Guilliams M. Tissue-resident macrophage ontogeny and homeostasis. *Immunity* (2016) 44:439–49. doi: 10.1016/j.immuni.2016.02.024

41. Zhu X, Cui J, Yi L, Qin J, Tulake W, Teng F, et al. The role of T cells and macrophages in asthma pathogenesis: A new perspective on mutual crosstalk. *Mediators Inflammation* (2020) 2020:7835284. doi: 10.1155/2020/7835284

42. Zhou Y, Do DC, Ishmael FT, Squadrito ML, Tang HM, Tang HL, et al. Mannose receptor modulates macrophage polarization and allergic inflammation through miR-511-3p. *J Allergy Clin Immunol* (2018) 141:350–64.e8. doi: 10.1016/j.jaci.2017.04.049

43. Hattori T, Konno S, Hizawa N, Isada A, Takahashi A, Shimizu K, et al. Genetic variants in the mannose receptor gene (MRC1) are associated with asthma in two independent populations. *Immunogenetics* (2009) 61:731–8. doi: 10.1007/s00251-009-0403-x

44. Zhao J, Jiao X, Wu J, Wang J, Gong W, Liu F, et al. FIZZ1 promotes airway remodeling in asthma through the PTEN signaling pathway. *Inflammation* (2015) 38:1464–72. doi: 10.1007/s10753-015-0121-5

45. Dong L, Wang SJ, Camoretti-Mercado B, Li HJ, Chen M, Bi WX. FIZZ1 plays a crucial role in early stage airway remodeling of OVA-induced asthma. *J Asthma* (2008) 45:648–53. doi: 10.1080/02770900802126941

46. Lin C, Chen L, Huang Z, Wu Y, Liu S. Effect of cigarette smoke extraction on the expression of found in inflammatory zone 1 in rat lung epithelial L2 cells. *Chin Med J (Engl)* (2014) 127:2363–7. doi: 10.3760/j:issn:0254-5101.2002.02.043

47. Ait Yahia S, Azzaoui I, Everaere L, Vorng H, Chenivesse C, Marquillies P, et al. CCL17 production by dendritic cells is required for NOD1-mediated exacerbation of allergic asthma. *Am J Respir Crit Care Med* (2014) 189:899–908. doi: 10.1164/rccm.201310-1827OC

48. Girkin J. Is CC chemokine ligand 17 (TARC) driving disease progression in chronic obstructive pulmonary disease? *Am J Respir Cell Mol Biol* (2022) 66:358–60. doi: 10.1165/rcmb.2021-0518ED

49. Machida H, Inoue S, Shibata Y, Kimura T, Sato K, Abe K, et al. Thymus and activation-regulated chemokine (TARC/CCL17) predicts decline of pulmonary function in patients with chronic obstructive pulmonary disease. *Allergol Int* (2021) 70:81–8. doi: 10.1016/j.alit.2020.04.004

50. Whittingham TS, Lipton P. Cerebral synaptic transmission during anoxia is protected by creatine. *J Neurochem* (1981) 37:1618–21. doi: 10.1111/j.1471-4159.1981.tb06337.x

51. Goel N, Basner M, Rao H, Dinges DF. Circadian rhythms, sleep deprivation, and human performance. *Prog Mol Biol Transl Sci* (2013) 119:155–90. doi: 10.1016/b978-0-12-396971-2.00007-5

52. Cook CJ, Crewther BT, Kilduff LP, Drawer S, Gaviglio CM. Skill execution and sleep deprivation: effects of acute caffeine or creatine supplementation - a randomized placebo-controlled trial. *J Int Soc Sports Nutr* (2011) 8:2. doi: 10.1186/1550-2783-8-2

53. Candow DG, Chilibeck PD, Forbes SC. Creatine supplementation and aging musculoskeletal health. *Endocrine* (2014) 45:354–61. doi: 10.1007/s12020-013-0070-4

54. Gualano B, Rawson ES, Candow DG, Chilibeck PD. Creatine supplementation in the aging population: effects on skeletal muscle, bone and brain. *Amino Acids* (2016) 48:1793–805. doi: 10.1007/s00726-016-2239-7

55. Turner CE, Byblow WD, Gant N. Creatine supplementation enhances corticomotor excitability and cognitive performance during oxygen deprivation. *J Neurosci* (2015) 35:1773–80. doi: 10.1523/JNEUROSCI.3113-14.2015

56. Gualano B, Painelli V, Roschel H, Lugaresi R, Dorea E, Artioli GG, et al. Creatine supplementation does not impair kidney function in type 2 diabetic patients: a randomized, double-blind, placebo-controlled, clinical trial. *Eur J Appl Physiol* (2011) 111:749–56. doi: 10.1007/s00421-010-1676-3

frontiers | Frontiers in Immunology

TYPE Review
PUBLISHED 06 December 2022
DOI 10.3389/fimmu.2022.983852

OPEN ACCESS

EDITED BY
Bao-Hui Cheng,
Longgang ENT Hospital, Institute of ENT and Shenzhen Key Laboratory of ENT, China

REVIEWED BY
Paola Parronchi,
University of Florence, Italy
Arzu Didem Yalcin,
Academia Sinica, Taiwan

*CORRESPONDENCE
Maciej Kupczyk
maciej.kupczyk@umed.lodz.pl

SPECIALTY SECTION
This article was submitted to Immunological Tolerance and Regulation, a section of the journal Frontiers in Immunology

RECEIVED 01 July 2022
ACCEPTED 31 October 2022
PUBLISHED 06 December 2022

CITATION
Kardas G, Panek M, Kuna P, Damiański P and Kupczyk M (2022) Monoclonal antibodies in the management of asthma: Dead ends, current status and future perspectives. *Front. Immunol.* 13:983852. doi: 10.3389/fimmu.2022.983852

Monoclonal antibodies in the management of asthma: Dead ends, current status and future perspectives

Grzegorz Kardas, Michał Panek, Piotr Kuna, Piotr Damiański and Maciej Kupczyk*

Clinic of Internal Medicine, Asthma and Allergy, Medical University of Lodz, Łódź, Poland

Patients with moderate-to-severe asthma may now be treated using a variety of monoclonal antibodies that target key inflammatory cytokines involved in disease pathogenesis. Existing clinical data on anti-IgE, anti-IL-5 and other immunological pathways indicate these therapies to offer reduced exacerbation rates, improved lung function, greater asthma control and better quality of life. However, as several patients still do not achieve satisfactory clinical response with the antibodies available, many more biologics, aiming different immunological pathways, are under evaluation. This review summarizes recent data on existing and potential monoclonal antibodies in asthma. Recent advances have resulted in the registration of a new antibody targeting TSLP (tezepelumab), with others being under development. Some of the researched monoclonal antibodies (e.g. anti-IL-13 tralokinumab and lebrikizumab or anti-IL-17A secukinumab) have shown optimistic results in preliminary research; however, these have been discontinued in asthma clinical research. In addition, as available monoclonal antibody treatments have shown little benefit among patients with T_2-low asthma, research continues in this area, with several antibodies in development. This article summarizes the available pre-clinical and clinical data on new and emerging drugs for treating severe asthma, discusses discontinued treatments and outlines future directions in this area.

KEYWORDS

asthma, severe asthma, monoclonal antibodies, tezepelumab, dupilumab, benralizumab, mepolizumab, omalizumab

Abbreviations: ACQ, Asthma Control Questionnaire; AQLQ, Asthma Quality-of-Life Questionnaire; EMA, European Medicines Agency; FDA, U.S. Food and Drug Administration; FeNO, Fractional exhaled Nitric Oxide; GINA, Global Initiative for Asthma; ICS, Inhalable Corticosteroids; LABA, Long-acting Beta-agonists; LAMA, Long-acting Muscarinic Antagonists; NA, None available; PEF, Peak Expiratory Flow; RCT, Randomized Control Trial; SABA, Short-acting Beta-agonists; TSLP, Thymic Stromal Lymphopoetin.

Introduction

Asthma is a chronic, heterogeneous and inflammatory respiratory condition characterized by shortness of breath, cough, wheezing, and chest tightness. It belongs to the group of obstructive diseases characterized by variable airflow limitation (1). Asthma occurs in several phenotypes that vary in their pathogenesis, and the intensity and frequency of symptoms and exacerbations (2). Currently, its prevalence is estimated to reach 1-18% depending on the country studied (1, 3, 4). The disease affects all age groups, with new cases diagnosed predominantly in children aged 0-9 [early-onset asthma, usually atopic (5)] and in adults aged 40-49 [late-onset asthma, often eosinophilic phenotype (6)]. It is important to note that, as is the case for other allergic diseases, its global prevalence is increasing (4, 7, 8), which has been attributed to various factors such as air pollution, antibiotic misuse, viral infections and a high-hygiene lifestyle (9, 10).

The term *asthma* is currently considered an umbrella term that encompasses several clinical and pathophysiological variants. The main axis of division refers to the type of inflammation, i.e. type 2 inflammation and non-type 2 inflammation. Furthermore, asthma phenotypes are considered as either eosinophilic or non-eosinophilic, with blood eosinophil count considered a major, yet controversial, phenotype-distinguishing biomarker (11). Most patients present a T_h2-predominant allergic phenotype asthma, which develops on basis of atopy triggered by inhaled allergens, e.g. house dust mite, grass pollens, trees or pets (6). Apart from the classical, early-onset allergic asthma, late-onset eosinophilic asthma is also under intensive study (12), as are other various asthma phenotypes, including obesity-associated asthma, neutrophilic asthma and very-late onset asthma. Asthma pathogenesis is strongly influenced by a number of mediators of inflammation, such as IgE, IL-3, IL-4, IL-5, IL-9, IL-13, IL-33 and TSLP, with many more being discovered (13).

Current clinical options for the treatment of severe asthma

In clinical practice, three levels of asthma severity are distinguished (mild, moderate and severe), with treatment being based on the five Global Initiative for Asthma (GINA) steps (1). The most severe cases, in which asthma control is not reached despite using high doses of inhaled corticosteroids, may be qualified for GINA step 5 biological treatment with monoclonal antibodies that are targeting key asthma mediators.

According to current epidemiological data, 3.6-10.0% of asthma patients are believed to demonstrate severe disease (14–16), which corresponds to four million patients globally. Although much less prevalent than mild and moderate asthma, severe asthma contributes to about 60% of costs associated with the disease, mainly due to higher costs of drugs and hospital care, as well as various indirect costs (17, 18). Current research efforts in the field are strongly oriented towards learning more of the pathomechanisms of severe asthma and concurrent developing of new biological therapies and identifying groups of patients best responding to a certain therapy (19). The ground-breaking change in asthma was achieved in 2003 with the first biological treatment of severe asthma: the anti-IgE monoclonal antibody omalizumab. This discovery was followed by more biological agents targeting key inflammatory nodes in the chronic inflammation underlying asthma, such as IL-5, IL-5R, IL-13 and IL-4R. Each of these drugs targets a certain immunological pathway that triggers and controls airway inflammation. Currently, omalizumab, mepolizumab, benralizumab, reslizumab, dupilumab and tezepelumab are those approved by the FDA for the treatment of severe asthma (20). With the variety of monoclonal antibodies currently available for treating asthma, clinicians may now personalize therapy according to asthma phenotype

Omalizumab is a humanized IgG1/κ monoclonal antibody that binds to the IgE immunoglobulin Fc fragment (21). Thus, it inhibits the main mediator of the type I reaction pathway. By binding free IgE molecules in the circulation, it inhibits the activation of mast cells and basophils. As a result, the number of IgE receptors on the surface of these cells declines over time, which is considered to be a critical component of the drug's clinical efficacy. Omalizumab also inhibits binding of IgE to the low-affinity IgE receptor (FcεRI) (22),. Launched in 2003, omalizumab has been used in severe allergic asthma and, since 2014, in chronic urticaria. In 2004, omalizumab was the very first monoclonal antibody to be included in Step 5 of the GINA recommendations as an addition to standard therapy with *inter alia* high doses of inhaled steroids or β2-agonists. Since then, clinical and observational studies have found its use in improving asthma control, relieving symptoms, reducing exacerbation risk and improving lung function (23–25). The drug is known to be safe for long-term use regarding oncological safety and can be safely used during pregnancy (26–28) and by children (29).

Another biological drug in severe asthma is mepolizumab, which was registered in 2015. This antibody binds IL-5, thus preventing it from binding to the IL-5R α subunit on eosinophils. This IL-5 signal blockade reduces the eosinophil population in patients with eosinophilic asthma, leading to clinical improvement (30). Clinical and observational studies confirm that mepolizumab improves asthma control, reduces the number of exacerbations and steroid doses and improves lung function in severe eosinophilic asthma (31, 32). Importantly, both mepolizumab and omalizumab exhibit a comparable safety profile (33).

Benralizumab – registered in the US in 2017 – is a monoclonal antibody targeting IL-5R α subunit (20). Randomised clinical studies have shown the drug's efficacy

and safety in patients with severe asthma and elevated eosinophils (34, 35). It was shown to be effective in lowering exacerbation rates, symptom burden, and oral glucocorticoid use, together with improvements in lung function (36, 37). This was also confirmed in real-world studies, including 2- and 3-year-long observations (38, 39)

Another anti-IL-5 antibody is reslizumab, which was registered in the US in 2016. (anti-IL-5 antibody, US registration in 2016)

Dupilumab is a monoclonal antibody inhibiting IL-4 and IL-13 signaling. It was registered in the US in 2017) and (20, 40).

The newest drug, tezepelumab, was registered by the FDA in December 2021. It is a human, IgG2 monoclonal antibody blocking thymic stromal lymphoprotein (TSLP). This makes it a first-in-class candidate for a new group of antibodies targeting alarmins – key epithelial inflammatory cytokines involved in asthma pathogenesis (TSLP, IL-25 and IL-33). The drug has been intensively studied in recent years and promising results of phase II and III trials have been recently published (41).

The clinical efficacy of tezepelumab has been demonstrated in the following pivotal clinical studies carried out in the period 2017-2020: PATHWAY (Phase IIb), NAVIGATOR (Phase III), SOURCE (Phase III) and CASCADE3 (Phase II). Their results, published in 2021, confirm that tezepelumab is effective in a very wide population of patients with severe asthma. This has been attributed to its ability to inhibit TSLP - the mediator at the top of the inflammatory cascade.

The results of PATHWAY were published in 2017. This study was the first to examine the efficacy of tezepelumab in patients aged 18-75 with uncontrolled asthma receiving long-acting beta-agonists and medium-to-high doses of inhaled glicocorticosteroids. The drug was administered subcutaneously at three doses, *viz.* 70mg, 210mg or 280 mg, every four weeks and compared to placebo. The patients were also characterized by blood eosinophil count (<250 or ≥250), FeNO (<24 or ≥24) and Th2 status (low or high). The annualized asthma exacerbation rates at week 52 were 0.27 (70 mg), 0.20 (210mg) and 0.23 (280 mg), compared with 0.72 in the placebo group. In addition, prebronchodilator FEV1 changed by 0.12 liters, 0.13 liters and 0.15 liters at week 52 compared to baseline and was higher than in the placebo group in the three respective study groups (42). Moreover, the drug was reported to be effective in improving patient-reported quality-of-life and symptom severity compared to placebo (43). A *post hoc* analysis of the study results found that the 210mg dose reduced exacerbation rates by 64-82% across all four seasons, with the greatest reduction in summer and lowest in winter (44).

The NAVIGATOR study of tezepelumab included 1,061 patients with severe asthma. Although the study entry criteria did not include peripheral blood eosinophil counts, approximately 50% of patients were estimated to have ≥300 cells/μL. The annual rate of exacerbations in the entire study population decreased by 56% and hospitalization by 85% during tezepelumab treatment. A 70% reduction of exacerbations was noted in the population with eosinophilia ≥300 cells/μl, and 41% in the group with <300 cells/μl. Patients treated with tezepelumab achieved a 130 ml increase in FEV1 over the study, which was statistically significant. A statistically significant improvement in quality of life was also reported: the tezepelumab group demonstrated a 0.33 point better ACQ-6 score and 0.34 point better AQLQ score. In addition, the patients with eosinophilia above 300 cells/μl also demonstrated greater improvement in FEV1 and ACQ-6 and AQLQ questionnaire scores (45).

Another phase III study on tezepelumab was the SOURCE study, which aimed to assess its effectiveness in reducing the dose of oral steroids in the course of steroid-dependent asthma among 150 patients. Although no statistically significant differences were found between the study drug and placebo among patients in general, tezepelumab treatment enabled a reduction of the oral steroid dose in the population of patients with > 150 cells/μl peripheral eosinophilia (46).

A continuation of the NAVIGATOR and SOURCE studies is the ongoing DESTINATION study, in which patients will continue treatment with tezepelumab for another year or, if they were taking placebo, will be re-randomized in a 1: 1 ratio. The aim of the study is a long-term evaluation of the tolerability, safety and efficacy of tezepelumab in a cumulative two-year follow-up. The results of this study will be known soon: the planned completion date is May 2022 (47).

Tezepelumab has been recently registered by the FDA (December 2021), and European registration by the EMA was authorized in September 2022. Information on the monoclonal antibodies currently registered in severe asthma treatment may be found in Table 1.

Dead ends in severe asthma research - promising, yet unsuccessful drugs in recent years

Despite the development of groundbreaking new therapies for severe asthma over the last two decades, certain groups of patients still do not respond to available therapies and hence, there still remains a substantial need for further therapeutic options. This is particularly the case among those who cannot be clearly categorized to a certain severe asthma phenotype and fail to meet the selection criteria for a particular monoclonal antibody. Moreover, even those who present as candidates for good response to a certain therapy may never be completely certain of success. Current research is also focused on search for biomarkers of possible response to available biological therapies (48).

Hence, many potential alternatives to current therapeutic strategies have recently been investigated. Some of these, discussed below, are at a late stage of research; however, they

TABLE 1 Current clinical options with monoclonal antibodies in severe asthma.

DRUG	FORM	TARGET	WAY OF TREATMENT, TIME INTERVAL AND DOSE	BIOLOGICAL EFFECTS	CLINICAL EFFECTS	OTHER FDA-APPROVED INDICATIONS
Omalizumab	Humanized IgG1/κ, monoclonal antibody	IgE	s.c. 2 or 4 weeks interval from 75 to 600 mg depending on patient's weight and initial total IgE	↓ circulating total IgE Down-regulation of FcεRI receptors on basophils, mast cells, and dendritic cells	Improvement of lung function (FEV1) Improvement of quality of life (AQLQ) Improvement of asthma control (ACT) ↓ oral and inhaled corticosteroid use Reduction in exacerbation and hospitalization frequency	Chronic idiopathic urticaria
Mepolizumab	Humanized IgG1/κ, monoclonal antibody	IL-5	s.c. 4 weeks interval 100 mg	Blockage of IL-5/IL-5R binding on eosinophils ↓ blood eosinophils ↓ sputum eosinophils	Reduction in exacerbation frequency *vs* placebo Improvement in AQLQ *vs* placebo No significant effect on FEV1, PEF, PC_{20}	NA
Benralizumab	Humanized IgG1/κ, monoclonal antibody	IL-5 Receptor alpha subunit (IL-5Rα)	s.c. 4 weeks interval (first 3 doses), then 8 weeks interval 30 mg	↓ eosinophils and basophils *via* antibody dependent cell mediated cytotoxicity (ADCC)	Reduction in exacerbation frequency No significant effect on FEV1 Mixed data on quality of life and asthma symptom scores	NA
Dupilumab	human IgG4 monoclonal antibody	IL-4 Receptor alpha subunit (IL-4Rα)	s.c. 2 weeks interval 600 mg – 1st dose, then 300 mg (in adults) In children 6-11-years-old doses from 100 mg to 300 mg depending on weight and treatment interval (2 or 4 weeks)	Blockage of IL-4/IL-4Rα binding Blockage of IL-13/IL-4Rα binding	Reduced rate of severe asthma exacerbations and improved lung function (FEV1), asthma control and quality of life	Atopic dermatitis, moderate-to-severe atopic dermatitis in adolescents Chronic rhinosinusitis with nasal polyps
Reslizumab	humanized IgG4/κ mAb	IL-5	i.v. 4 weeks interval From 100 to 575 mg depending on patient's weight	Blockage of IL-5/IL-5R binding ↓ circulating eosinophils ↓ sputum eosinophils	Reduced exacerbations, improved FEV1, forced vital capacity, the 7-item Asthma Control Questionnaire	NA
Tezepelumab	human, IgG2 monoclonal antibody	TSLP	s.c. 4 weeks interval 210 mg	Blockage of TSLP/TSLP-receptor binding	Inhibition of late allergen-induced asthmatic response (FEV1) Reduction of annualized asthma exacerbation rate	NA

NA, none available.
?, Downregulates or lowers.

10.3389/fimmu.2022.983852

have not yet reached the assumed clinical endpoints in RCTs, and therefore have not received approval in the treatment of severe asthma. In this section we summarize the available information on drugs that were considered and studied in the area of severe asthma, yet were eventually discontinued in this indication.

Tralokinumab

Tralokinumab is a human IgG4 monoclonal antibody targeting IL-13. The drug was studied in several clinical studies and reached phase III in STRATOS 1, STRATOS 2 and TROPOS studies. STRATOS 1 study was aimed to identify a biomarker-specific sub-group that would potentially benefit most from 300mg tralokinumab and that was further studied in STRATOS 2. The group comprised patients with baseline FeNO 37 ppb or higher, who demonstrated a reduced asthma exacerbation rate in STRATOS 1, but not in STRATOS 2 (49). The results of the TROPOS study indicate that tralokinumab use does not allow any reduction of oral corticosteroid use by patients with OCS-dependent asthma (50–52).

The phase II MESOS study examined whether tralokinumab would inhibit the release of eosinophil chemotactic factors in the lungs, resulting in decreased eosinophil lung population, despite increasing the overall eosinophil population possibly due to inhibition of eosinophil–endothelial adhesion, as observed in previous studies (53–55). The findings indicate that tralokinumab does not affect eosinophilic inflammation in bronchial submucosa, blood or sputum compared to placebo, although it did reduce FeNO and IgE concentrations (56).

A meta-analysis of six available RCTs of tralokinumab, i.e. those mentioned above with additional two phase II studies (53, 54), found that the drug improved FEV1 and FVC in patients with moderate-to-severe asthma; however, it did not improve asthma-related quality of life, nor reduce asthma exacerbations in unselected patients. Treatment has nevertheless resulted in improvements in asthma exacerbation rates in patients with high FeNO (57). Tralokinumab has been shown to be well-tolerated with a low risk of adverse events and low likelihood of immunogenicity (58).

Hence, tralokinumab treatment does not appear to be an effective strategy for severe uncontrolled asthma (59). Research has shifted from asthma to treating skin conditions, and the drug has shown promising results in atopic dermatitis (60)

Lebrikizumab

Lebrikizumab is another humanized IgG4 monoclonal antibody targeting IL-13 that has been intensively studied in moderate-to-severe asthma. It has been evaluated in several phase II and phase III studies. In phase II studies it has demonstrated reduced exacerbation rates and improved FEV1 in patients with uncontrolled asthma, particularly among those with high periostin concentration or blood eosinophil count (61).

Replicate phase III studies - LAVOLTA1 and LAVOLTA2 - have analyzed the effects of subcutaneous lebrikizumab treatment, 37.5 mg and 125 mg once every four weeks, compared to placebo; the patients have been divided into biomarker-high (periostin, blood eosinophils) and biomarker-low subgroups. However, the results remain inconsistent, as the primary endpoint, i.e. a significant (greater than 30%) reduction of exacerbation rate, was reached in LAVOLTA1, but not in LAVOLTA2. The drug indeed improved FEV1 in the biomarker-high patients, but did not improve secondary outcomes, *viz.* AQLQ(S) and ACQ-5 scores, in either group (62).

Another pair of replicate phase III studies were LUTE and VERSE. They were primarily designed as phase III trials, but were converted to phase IIb due to the discovery of a host-cell impurity in the study drug material. Thus, the findings only included the placebo-controlled period of variable duration, and were pooled across both studies. Changes in exacerbation rate were far more pronounced in the periostin-high group (60% reduction) than in the periostin-low group (5% reduction); these two groups also demonstrated 9.1% (high group) and 2.6% changes (low group) in FEV1 (63).

Recent reports indicate that research into lebrikizumab has been moved from asthma to atopic dermatitis and chronic spontaneous urticaria. However, it may be further investigated in sub-populations of asthma patients with high blood eosinophil count and high FeNO (64).

A meta-analysis of lebrikizumab and tralokinumab studies found that although IL-13 inhibitors showed some benefits in clinical studies, a more promising approach would be the combined blocking of IL-13 and IL-4, which demonstrate overlapping pathophysiological roles (65).

Secukinumab

Secukinumab is a human IgG1κ monoclonal antibody targeting IL-17A. It is currently registered for the treatment of plaque psoriasis, psoriatic arthritis and ankylosing spondylitis. Although the safety, tolerability and efficacy of the drug in patients with uncontrolled asthma was investigated in a Phase II study, no improvements in ACQ were found and the investigation was discontinued by the producer. This is the only available clinical study of secukinumab in severe asthma (66).

Previously, secukinumab had been evaluated in the ozone-induced airway neutrophilic inflammation model in healthy volunteers. Following ozone stimulation, study subjects were randomized to receive secukinumab (10 mg/kg), placebo or a single-dose oral corticosteroid treatment. No significant differences in airway neutrophilia compared to baseline were

observed between study groups, including the secukinumab group (67). These findings suggest that the drug would probably not bring any clinical improvement in neutrophilic asthma.

Brodalumab

Brodalumab is a human, IgG2 monoclonal antibody targeting IL-17RA, which is currently registered for the treatment of psoriasis vulgaris, psoriatic arthritis, pustular psoriasis and psoriatic erythroderma. The drug was studied in a randomized, double-blind phase II study with 315 participants in four groups: placebo, brodalumab 140 mg, brodalumab 210 mg and brodalumab 280 mg. No clinically significant differences were observed between the groups in terms of ACQ score, FEV1, morning PEF, SABA use, daily and nighttime symptom scores or symptom-free days. A predefined subgroup analysis found that only the high bronchodilator reversibility subgroup demonstrated clinically significant benefits (68).

Another phase II study of brodalumab with 421 patients was initiated but later terminated; however, this was due to lack of observed efficacy, not safety concerns. The results are not publicly available (69).

Fevipiprant

Another mediator pivotal to orchestrating immunological and inflammatory mechanisms in asthma is prostaglandin D_2 (PGD_2), an eicosanoid which is released by degranulating mast cells. Fevipiprant, an oral, nonsteroidal, highly-selective, reversible antagonist of the DP2 receptor showed promising results in three phase II studies. Although it is not a monoclonal antibody, due to its advanced stage of development, we decided to include it in this review to broaden the context of current advances in asthma.

Early-phase trials have confirmed its safety and demonstrated its potential efficacy in patients with asthma, specifically, improvement in FEV1 and eosinophilic airway inflammation (70, 71). Despite these results, the subsequent phase III trials did not yield satisfactory clinical conclusions.

In two placebo-controlled replicate phase III studies named ZEAL-1 and ZEAL-2, patients received 150 mg fevipirant (or placebo) plus standard-of-care asthma therapy (medium- or high-dose ICS, low-dose ICS plus either LABA or LTRA, or medium-dose ICS plus LABA for at least three months prior to screening). Neither study met its primary endpoint, defined as change from baseline in pre-dose pre-bronchodilator FEV1 at the end of the 12-week treatment period. Nor did it meet its secondary endpoints: change from baseline in daytime asthma symptom score and total dailySABA use over 12 weeks of treatment, and change from baseline in AQLQ +12 score at week 12 (72).

Another two replicate phase 3 studies of fevipirant (LUSTER-1 and LUSTER-2) examined the effects of fevipiprant on moderate to severe asthma exacerbation annualized rate in patients aged 12 or older receiving GINA step 4 or 5 treatment. Patients were randomised to receive 150 or 450 mg of fevipirant or placebo throughout a 52-week observation period. Neither of the studies demonstrated a significant reduction in asthma exacerbation annualized rates (73). Due to this observed overall lack of clinical efficacy, the manufacturer has discontinued its research in asthma.

Anakinra

Anakinra is a human IL-1 receptor antagonist produced by recombinant DNA technology in an *E. coli* expression system. As the IL-1-regulated pathway is believed to play a significant role in asthma pathogenesis in both Th2/Th17-high and –low phenotypes, it has become an attractive therapeutic target (74). However, two recent clinical trials that were designed to assess the effectiveness of anakinra as a rescue treatment for airway inflammation in allergic asthma, either through early- or late-phase administration after allergen challenge, were withdrawn due to the COVID-19 pandemic and the risks associated with allergen exposure and anakinra treatment (75, 76). Another study of the drug has been suspended (77).

Other potential treatments for severe asthma have unfortunately failed to demonstrate satisfactory results and thus are not being continuously studied. Such examples include:

- Cendakimab (formerly known as RPC4046), a monoclonal antibody targeting IL-13, which was only reported in a Phase I study in asthmatic patients (78). The drug is being further developed in eosinophilic esophagitis (79)
- GSK 679586 – another monoclonal antibody targeting IL-13 reported to reach phase II. The drug did not demonstrate any clinically-relevant improvements in asthma control, pulmonary function or exacerbations in patients with severe asthma (80).
- Daclizumab - a monoclonal antibody that binds the IL-2R α chain (CD25), which in turn inhibits lymphocyte activation. The available literature only includes one RCT for the drug: A 2008 study by Busse et al. examined its effects on FEV1 changes in 115 patients with moderate to severe uncontrolled asthma. An improvement was observed in the 88-patient daclizumab group ($4.4 \pm 1.80\%$ *vs* $1.5 \pm 2.39\%$; $p = 0.05$), daytime asthma symptoms were reduced ($p = 0.018$), and the time to exacerbation was prolonged ($p = 0.024$). An absolute increase of FEV1 was observed in the treated group, i.e. from 2.34 ± 0.07 in baseline to 2.4 ± 0.08 at Day 84, the patients receiving placebo had a

decrease in FEV1 (from 2.25 ± 0.1 to 2.2 ± 0.1 L), and an increase in serious adverse events was reported in the treatment arm (5 *vs* 1) (81). Although it was discussed at the time as a potential asthma therapy, the drug was not further studied in asthma (82). Daclizumab is now registered and indicated in multiple sclerosis (83)

- Enokizumab/Medi-528 - an antibody targeting IL-9: an inflammatory cytokine that regulates the development of airway inflammation, mucus production, airway hyperresponsiveness, and airway fibrosis by increasing mast cell numbers and activity (84). Enokizumab showed an acceptable safety profile in phase I studies (85). The drug reached Phase II clinical trials in 2011 (86). However, at this stage, the drug administration (dosed subcutaneously at three dosages – 30, 100 and 300 mg every 2 weeks for 24 weeks in addition to concurrent asthma medication) did not yield any improvements in ACQ-6 scores, asthma exacerbation rates or FEV1 values (87).
- Canakimumab – a monoclonal antibody targeted at IL-1β. The drug was tested in one small study in 16 asthmatics with positive results, with attenuation of the late asthmatic response after inhalative allergen challenge and a >90% decrease of IL-1β level (88). The drug is currently registered in Periodic Fever Syndrome, Cryopyrin-Associated Periodic Syndromes, Tumor Necrosis Factor Receptor-Associated Periodic Syndrome, hyperimmunoglobulin D syndrome and several other rheumatoid diseases.
- Risankizumab - a monoclonal antibody targeting the p19 subunit of IL-23: a cytokine mostly affecting Th17 cells and thus decreasing antigen-induced Th2 cytokine production (89). Only one phase IIa study on this drug has been published to date. The results indicate that treatment failed to reduce the annualized asthma exacerbation rate compared to placebo, with the risankizumab group demonstrating shorter time to first asthma worsening (90). Therefore, research in this area is discontinued, with potential other applications (e.g. psoriasis) being currently researched (91).
- VR942 - a dry-powder formulation containing CDP7766, a high-affinity anti-human-IL-13 antigen-binding antibody fragment. Only one phase I study has examined the safety and pharmacodynamics of the drug. Although the concept of direct inhalable administration of monoclonal antibodies to the target tissue seems promising, this study remains one of few such reports in humans (92). A 2012 study by Hacha et al. examined the concept of nebulized anti-IL-13 antibody treatment in a murine model of asthma with promising results; however, the idea was not continued (93). Even so, other studies have evaluated the potential of similar drug delivery methods in other respiratory conditions (94).

A summary on the above-mentioned discontinued drugs in severe asthma is presented in Table 2.

Other approaches for treating severe asthma and potential new targets

Research on monoclonal antibodies in severe asthma has made significant progress in recent years. With the six monoclonal antibodies currently available (omalizumab, mepolizumab, benralizumab, reslizumab dupilumab and tezepelumab), patients with severe asthma have a fairly wide range of possible treatments. However, although these are highly-advanced drugs that target specific pathophysiological pathways of asthma, a large group of patients still fails to respond to treatment (100). Consequently, the terms 'non-responders', 'responders' and 'super-responders' have emerged to categorize those who do or do not reach improvements with biologics. This problem may be partially explained by the fact that the target molecule is a part of a causal network of many other inflammatory mediators rather than an element of a linear cause and effect relation (101). Many efforts have been made to identify biomarkers of response to biological treatment, yet no dichotomous factor has been found to date (101–104).

As such, research has turned to new antibodies aimed at other cytokines. This section summarizes the current findings concerning molecular targets in severe asthma obtained in clinical and pre-clinical research.

Tocilizumab (also called 'atlizumab')

Tocilizumab is a humanized IgG1 antibody targeting IL-6R – the receptor for IL-6, that is an interleukin recently attributed to contribute to asthma pathogenesis and which may represent a pathophysiological target (105). This drug is registered for the treatment of rheumatological conditions such as rheumatoid arthritis. More recently, it has been intensively studied and registered as a drug in SARS-COV-2 infection (106). However, as of May 2022, there have been no clinical studies of tocilizumab in severe asthma, and very limited data exists on the use of the drug in asthma.

In May 2019 Esty et al. reported two pediatric cases of severe persistent, non-atopic asthma treated with tocilizumab. Both patients demonstrated good clinical (FEV1 increase, reduction of oral corticosteroids) and immunological (reduced IL-4 and IL-17 production) responses to the therapy and no adverse events (107).

A proof-of-concept study by Revez et al. published in June 2019 studied the effects of tocilizumab on asthma patients with high sIL-6R levels following two allergen inhalation challenge tests. The study included 11 patients: six who received tocilizumab and five placebo. No significant differences in the primary endpoint was observed between study arms: late asthmatic response, maximum percentage fall in FEV1 and AUC of the percent fall in FEV1 (108).

10.3389/fimmu.2022.983852

TABLE 2 Drugs discontinued in severe asthma research.

DRUG	FORM	TARGET	LAST PHASE OF STUDY	LAST PHASE OF STUDY YEAR	OTHER FDA-APPROVED INDICATIONS
Tralokinumab	Human IgG4 monoclonal antibody	IL-13	Phase III	2019 (51)	Atopic dermatitis
Lebrikizumab	Humanized IgG4 monoclonal antibody	IL-13	Phase III	2016 (62)	NA, possibly atopic dermatitis
Secukinumab	Human IgG1κ monoclonal antibody	IL-17A	Phase II	2015 (66)	Plaque psoriasis, Psoriatic arthritis, Ankylosing spondylitis
Brodalumab	Human, IgG2 monoclonal antibody	IL-17RA	Phase II	2013 (95)	Plaque psoriasis
Fevipirant	Non-steroidal selective receptor inhibitor	CRTH2	Phase III	2021 (72)	NA
Anakinra	Protein	IL-1R	Phase I/Phase II		Rheumatoid arthritis, COVID-19, Periodic fever syndrome, Cryopyrin-associated periodic syndromes, Familial Mediterranean Fever, Adult-onset Still's disease
Cendakimab	Monoclonal antibody	IL-13	Phase I	2017 (78)	NA
GSK 679586	Monoclonal antibody	IL-13	Phase II	2014 (80)	NA
Daclizumab	Humanized IgG1 Monoclonal antibody	IL-2Rα	Phase II	2008 (81)	Multiple sclerosis
Enokizumab/ Medi-528	Humanized IgG1κ monoclonal antibody	IL-9	Phase II	2013 (87)	NA
Canakimumab	Humanized IgG1κ monoclonal antibody	IL-1β	Phase I/Phase II	2006 (88)	Relapsing fever syndrome, Cryopyrin-Associated Periodic Syndromes, Tumor Necrosis Factor Receptor-Associated Periodic Syndrome, hyperimmunoglobulin D syndrome and several other rheumathoid diseases
Risankizumab	Human IgG1 monoclonal antibody	IL-23	Phase IIa	2021 (90)	Plaque psoriasis Psoriatic arthritis
VR942	Inhalable fragment of antibody	IL-13	Phase I	2018 (92)	NA
Itepekimab (REGN-3500)	Human IgG4P monoclonal antibody	IL-33	Phase II	2021 (96)	NA
Etokimab	Monoclonal antibody	IL-33	Phase IIa	2019 (97)	NA
Melrilimab	Monoclonal antibody	IL-33	Phase II	2020 (98)	NA
LY3375880	Monoclonal antibody	IL-33	Preliminary	2020 (99)	NA

NA, none available.

Anti-IL-33: Itepekimab, etokimab, melrilimab, LY3375880, MEDI3506

Itepekimab, found in the literature under the aliases REGN-3500 or SAR440340, is an anti-IL33 antibody that has recently been studied or treating asthma. Although research on this antibody has reached phase II, the results are insufficient to continue it further. A recent study by Weschler et al. compared the efficacy of itepekimab with three other treatments: dupilumab, itepekimab+dupilumab and placebo. The groups were randomized in a 1:1:1:1 ratio and the primary endpoint was the occurrence of an event indicating loss of asthma control. By week 12, such an event occurred in 22% of patients in the itepekimab group, 27% in the combination group, and 19% in the dupilumab group, as compared to 41% in the placebo group (96). As a consequence of these results, the drug was discontinued for asthma research in February 2021; however, its potential against COPD remains under study (109).

Etokimab is another anti-IL-33 monoclonal antibody which has been recently studied as a possible asthma treatment. Currently, no peer-reviewed reports are available; however, it has been speculated that the drug might be studied against asthma, pending results of failing studies in eczema and atopic dermatitis (99).

Other anti-IL-33/IL-33R drugs reported are melrilimab by GSK, LY3375880 by Lilly and MEDI3506 by AstraZeneca. Only the latter is currently being studied in an on-going phase II clinical trial, the FRONTIER-3 trial, with an estimated completion date in August 2022 (110).

Bispecific antibodies

An interesting approach, although still only in the initial research phase and without any significant progress regarding severe asthma biological therapy, is based on the concept of bispecific antibodies, i.e. such that one particle can target two immunological targets at the same time. Compared with hypothetical combination therapy including two monospecific antibodies, bispecific antibody treatment may incur lower costs of development and clinical trials. Such examples include:

- BITS7201A (a monoclonal antibody that binds both IL-13 and IL-17) which to date has only been studied in a single phase I study; it showed good drug tolerance, but a high incidence of anti-drug antibodies (111)
- a monoclonal antibody simultaneously targeting IL-4Rα and IL-5 in a murine model of asthma (112)
- bispecific anti-TSLP/IL13 antibodies called Zweimabs (monovalent bispecific) and Doppelmabs (bivalent bispecific) (113)

Selected other particles with signaled or ongoing research in severe asthma are presented in Table 3. The summary on available, currently researched and discontinued agents in severe asthma is shown in Figure 1. Also, a brief graphic summary on future perspectives of research in the field of severe asthma may be found in Figure 2.

Challenges and future perspectives in the biological therapy of severe asthma

Clearly, research of new drugs for severe asthma remains intense, with many potential pathways under investigation. Parallel to the development of new drugs, attempts are being made to optimize the use of existing therapies and to better understand their mechanisms. One promising direction involves

TABLE 3 Monoclonal antibodies and drugs in current clinical trials or suggested as potential agents in severe asthma.

DRUG	FORM	TARGET	CURRENT STUDY STAGE	OTHER FDA-APPROVED INDICATIONS
Tocizilumab	Humanised IgG1 monoclonal antibody	IL-6R	Casuistic	Rheumatoid arthritis COVID-19 Juvenile idiopathic arthritis Cytokine release syndrome
Clazakizumab	Humanized monoclonal IgG1 antibody	IL-6	Phase 2 (114)	NA
CSJ117	Antibody fragment in powder for delivery to the lungs *via dry powder in*haler	TSLP	Phase 2 (115)	NA
FB825	Humanised IgG1 monoclonal antibody	CεmX domain on human B lymphocytic cells expressing membrane-bound IgE (mIgE).	Phase 2 (116)	NA
CM310	Monoclonal antibody	IL-4Rα	Phase 2 (117)	NA
610	Monoclonal antibody	IL-5	Phase 1 (118)	NA
FB704A	Human antibody	IL-6	Phase 2 (119)	NA
MEDI3506	Monoclonal antibody	IL-33	Phase 2 (120)	NA

NA, none available.

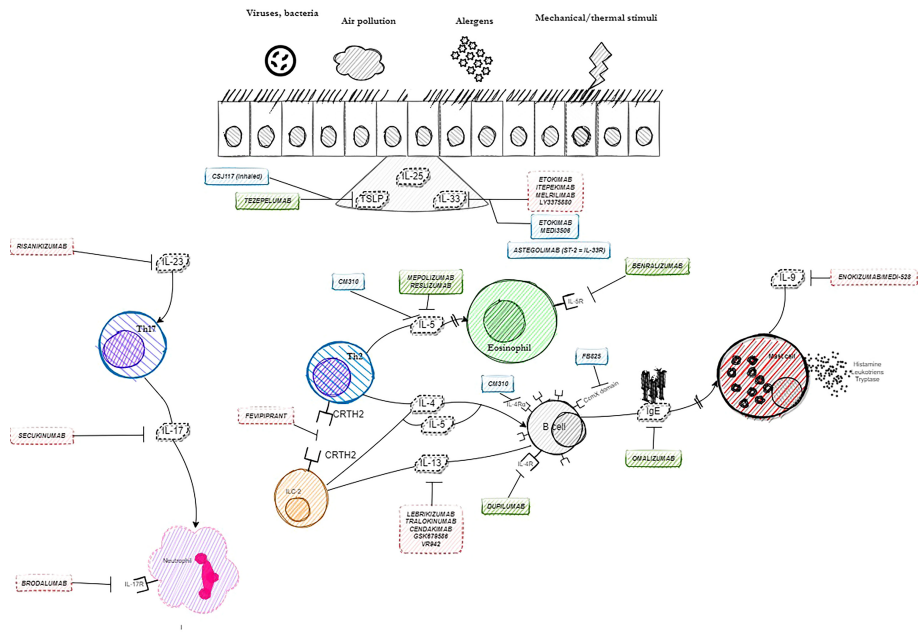

FIGURE 1
Summary on available, continued and discontinued agents in severe asthma.

identifying the biomarkers of response to a specific monoclonal antibody, an important aspect of personalizing treatment, while another concerns improving the phenotyping of asthma, and thus the selection of a drug compatible with the immune background. For example, many patients qualify for both omalizumab (high IgE) and anti-IL-5 therapies (high blood eosinophilia), forcing a difficult decision in the choice of a drug (121), which may be suboptimal (122).

However, as few studies have compared individual molecules under real-life and head-to-head conditions, there is often inadequate data to conclusively state that a given drug is better than another. As such, the choice of treatment remains a clinical challenge, not only due to the differentiation of the disease, but also to the variety of potential treatment options (123). Although some ongoing head-to-head studies cover this issue, such as PREDICTUMAB, a head-to-head study of omalizumab and mepolizumab (124), or Choosebetweenmab (125), they are few in number. Notably, no direct head-to-head comparisons between anti-IL-5 antibodies in asthma have been made, although one head-to-head study comparing benralizumab and mepolizumab in Eosinophilic Granulomatosis With Polyangiitis is ongoing (MANDARA) (126). Therefore, no clear advantage can be found for any of these treatments (127, 128).

Another important aspect of research into severe asthma and implementation of new drugs concerns their effect on airway remodeling: an important aspect of research, with great efforts being aimed at determining whether new, or existing, drugs reverse this process. For example, the effect of tezepelumab on bronchial remodeling was already verified in phase II studies (129), unlike the majority of previously registered drugs (130).

Finally, no matter how successful the new and future biologics may be at treating severe asthma, research is still needed into the selection of an appropriate treatment depending on the individual characteristics of the patient's disease. There is a clear need for updating state-of-art algorithms biologics selection to allow them to reflect nuances in asthma phenotype and treatment response. Some progress in this field has been made recently with algorithms proposed by Papadopoulos (131), Viswanathan (123) or Buhl (132).

Summary

Monoclonal antibodies targeting specific inflammatory cytokines are undoubtedly revolutionary drugs in many fields of medicine and have begun a new chapter in the treatment of severe and complex cases of immunological diseases. This is also the case in severe asthma, where we have moved from demanding and aggravating oral steroid therapy to a targeted and personalized immunological approach. In asthma, the use of monoclonal antibodies has given many patients the chance to control their disease and significantly improve their quality of life. However, there is still a need to develop new therapies that will be effective in more complex and unusual cases, or where existing treatment has not been successful.

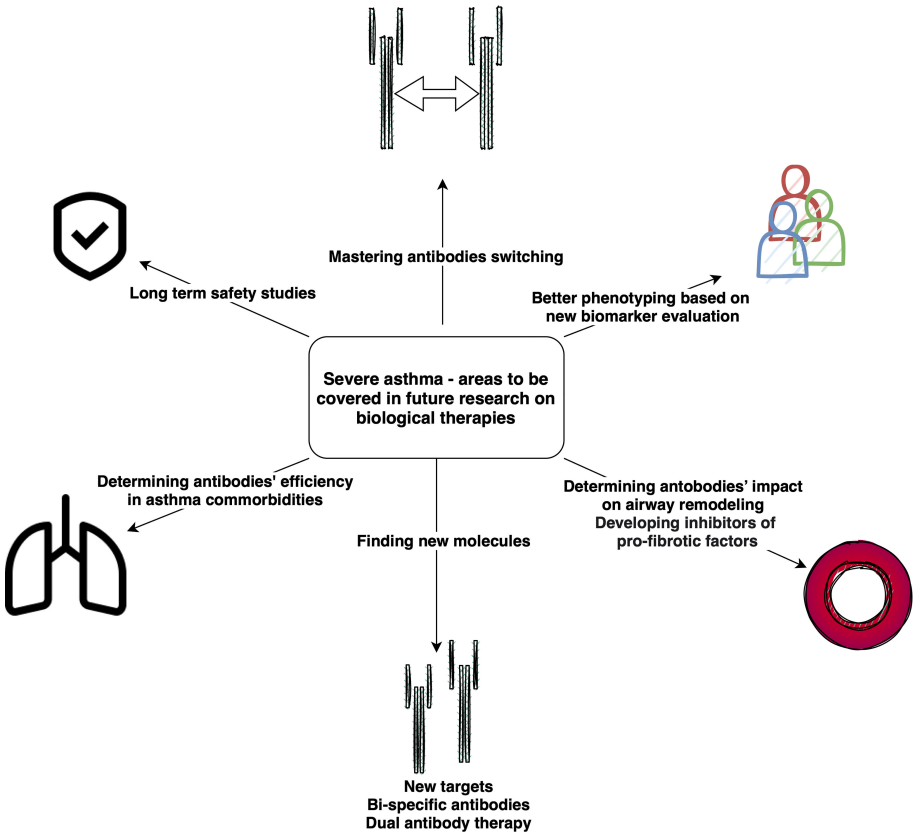

FIGURE 2
Summary on future perspectives in severe asthma research.

Research on new monoclonal antibodies in asthma does not always bear fruit. The immunological complexity of the disease, with its considerable variation in phenotypes and endotypes, greatly hinders the identification of new therapeutical solutions. The bench-to-bed process of drug development is always a challenge which continually demands greater efforts and many of the promising concepts are not confirmed in clinical trials; however, while this may appear as failure, these findings allow future research in a given area to be narrowed or redirected to other areas of medicine.

Author contributions

GK, PD, MP and MK created the concept of the paper. GK conducted the literature research and wrote the initial version of the manuscript. PK, MP and MK revised the paper. All authors contributed to the article and approved the submitted version.

Funding

The article was partially funded by Polish National Science Centre grant no. UMO-2021/41/N/NZ5/03162.

Conflict of interest

MP reports personal fees from AstraZeneca, Allergopharma, Sanofi Aventis, PPD Poland, Stallergenes and Quintiles outside the submitted work. PK reports personal fees from Adamed, AstraZeneca, Berlin Chemie Menarini, FAES, Glenmark, Novartis, Polpharma, Boehringer Ingelheim, Teva and Zentiva outside the submitted work. MK reports personal fees from Abbvie, Adamed, Alvogen, AstraZeneca, Berlin Chemie, Celon Pharma, Chiesi, Emma, GlaxoSmithKline, Lekam, Novartis, Polpharma, Sanofi Aventis, Teva, and Zentiva outside the submitted work.

The remaining authors declare that the research was conducted in the absence of any commercial or financial relationships that could be construed as a potential conflict of interest.

Publisher's note

References

1. GINA. *GLOBAL STRATEGY FOR ASTHMA MANAGEMENT AND PREVENTION* (2020) (Accessed April 7, 2020).

2. Wenzel SE. Asthma phenotypes: The evolution from clinical to molecular approaches. *Nat Med* (2012) 18:716–25. doi: 10.1038/nm.2678

3. Liebhart J, Dobek R, Małolepszy J, Wojtyniak B, Pisiewicz K, Płusa T, et al. The prevalence of allergic diseases in Poland-the results of the PMSEAD study in relation to gender differences. *Adv Clin Exp Med* (2014) 23:757–62. doi: 10.17219/acem/37238

4. Samoliński B, Raciborski F, Lipiec A, Tomaszewska A, Krzych-Fałta E, Samel-Kowalik P, et al. Epidemiologia chorób alergicznych w polsce (ECAP) epidemiology of allergic diseases in Poland. *Otolaryngol Pol* (2014) 1:10–8. doi: 10.1016/j.alergo.2014.03.008

5. Schatz M, Rosenwasser L. The allergic asthma phenotype. *J Allergy Clin Immunol Pract* (2014) 2:645–8. doi: 10.1016/j.jaip.2014.09.004

6. Hirano T, Matsunaga K. Late-onset asthma: Current perspectives. *J Asthma Allergy* (2018) 11:19–27. doi: 10.2147/JAA.S125948

7. Lundbäck B, Backman H, Lötvall J, Rönmark E. Is asthma prevalence still increasing? *Expert Rev Respir Med* (2016) 10:39–51. doi: 10.1586/17476348.2016.1114417

8. Akinbami LJ, Moorman JE, Bailey C, Zahran HS, King M, Johnson CA, et al. Trends in asthma prevalence, health care use, and mortality in the united states, 2001-2010. *NCHS Data Brief* (2012) (94):1–8.

9. Strannegard O, Strannegard I-L. The causes of the increasing prevalence of allergy: is atopy a microbial deprivation disorder? *Allergy* (2001) 56:91–102. doi: 10.1034/j.1398-9995.2001.056002091.x

10. Burbank AJ, Sood AK, Kesic MJ, Peden DB, Hernandez ML. Environmental determinants of allergy and asthma in early life. *J Allergy Clin Immunol* (2017) 140:1–12. doi: 10.1016/j.jaci.2017.05.010

11. Carr TF, Zeki AA, Kraft M. Eosinophilic and noneosinophilic asthma. *Am J Respir Crit Care Med* (2018) 197:22–37. doi: 10.1164/rccm.201611-2232PP

12. De Groot JC, Brinke AT, Bel EHD. Management of the patient with eosinophilic asthma: A new era begins. *ERJ Open Res* (2015) 1(1):00024–2015. doi: 10.1183/23120541.00024-2015

13. Fahy JV. Type 2 inflammation in asthma–present in most, absent in many. *Nat Rev Immunol* (2015) 15:57–65. doi: 10.1038/nri3786

14. Hekking PPW, Wener RR, Amelink M, Zwinderman AH, Bouvy ML, Bel EH. The prevalence of severe refractory asthma. *J Allergy Clin Immunol* (2015) 135:896–902. doi: 10.1016/j.jaci.2014.08.042

15. Larsson K, Ställberg B, Lisspers K, Telg G, Johansson G, Thuresson M, et al. Prevalence and management of severe asthma in primary care: an observational cohort study in Sweden (PACEHR). *Respir Res* (2018) 19:12. doi: 10.1186/s12931-018-0719-x

16. Backman H, Jansson S, Stridsman C, Eriksson B, Hedman L, Eklund B, et al. Severe asthma–a population study perspective. *Clin Exp Allergy* (2019) 49:819–28. doi: 10.1111/cea.13378

17. Nunes C, Pereira AM, Morais-Almeida M. Asthma costs and social impact. *Asthma Res Pract* (2017) 3:1–11. doi: 10.1186/s40733-016-0029-3

18. Sadatsafavi M, Lynd L, Marra Pharmd C, Carleton Phd B, Mb WCT, Phd SS, et al. Direct health care costs associated with asthma in British Columbia. *Can Respir J* (2010) 17(2):74–80. doi: 10.1155/2010/361071

19. Israel E, Reddel HK. Severe and difficult-to-treat asthma in adults. *N Engl J Med* (2017) 377:965–76. doi: 10.1056/NEJMra1608969

20. Koski RR, Grzegorczyk KM. Comparison of monoclonal antibodies for treatment of uncontrolled eosinophilic asthma. *J Pharm Pract* (2019) 33(4):513–22. doi: 10.1177/0897190019840597

21. Schulman ES. Development of a monoclonal anti-immunoglobulin e antibody (Omalizumab) for the treatment of allergic respiratory disorders. *Am J Respir Crit Care Med* (2001) 164:S6–S11. doi: 10.1164/ajrccm.164.supplement_1.2103025

22. Kawakami T, Blank U. From IgE to omalizumab. *J Immunol* (2016) 197:4187–92. doi: 10.4049/jimmunol.1601476

23. Pelaia C, Calabrese C, Terracciano R, de Blasio F, Vatrella A, Pelaia G. Omalizumab, the first available antibody for biological treatment of severe asthma: more than a decade of real-life effectiveness. *Ther Adv Respir Dis* (2018) 12:1753466618810192. doi: 10.1177/1753466618810192

24. Alhossan A, Lee CS, MacDonald K, Abraham I. Real-life" effectiveness studies of omalizumab in adult patients with severe allergic asthma: Meta-analysis. *J Allergy Clin Immunol Pract* (2017) 5:1362–1370.e2. doi: 10.1016/j.jaip.2017.02.002

25. Esquivel A, Busse WW, Calatroni A, Togias AG, Grindle KG, Bochkov YA, et al. Effects of omalizumab on rhinovirus infections, illnesses, and exacerbations of asthma. *Am J Respir Crit Care Med* (2017) 196:985–92. doi: 10.1164/rccm.201701-0120OC

26. Long A, Rahmaoui A, Rothman KJ, Guinan E, Eisner M, Bradley MS, et al. Incidence of malignancy in patients with moderate-to-severe asthma treated with or without omalizumab. *J Allergy Clin Immunol* (2014) 134:560–67. doi: 10.1016/j.jaci.2014.02.007

27. Namazy J, Cabana MD, Scheuerle AE, Thorp JM, Chen H, Carrigan G, et al. The xolair pregnancy registry (EXPECT): The safety of omalizumab use during pregnancy. *J Allergy Clin Immunol* (2015) 135:407–12. doi: 10.1016/j.jaci.2014.08.025

28. Adachi M, Kozawa M, Yoshisue H, Lee Milligan K, Nagasaki M, Sasajima T, et al. Real-world safety and efficacy of omalizumab in patients with severe allergic asthma: A long-term post-marketing study in Japan. *Respir Med* (2018) 141:56–63. doi: 10.1016/j.rmed.2018.06.021

29. Busse WW, Morgan WJ, Gergen PJ, Mitchell HE, Gern JE, Liu AH, et al. Randomized trial of omalizumab (Anti-IgE) for asthma in inner-city children. *N Engl J Med* (2011) 364:1005–15. doi: 10.1056/NEJMoa1009705

30. Fala L. Nucala (Mepolizumab): First IL-5 antagonist monoclonal antibody FDA approved for maintenance treatment of patients with severe asthma, in: *Am heal drug benefits* (2016). Available at: http://www.ncbi.nlm.nih.gov/ (Accessed November 15, 2019).

31. Ortega HG, Liu MC, Pavord ID, Brusselle GG, FitzGerald JM, Chetta A, et al. Mepolizumab treatment in patients with severe eosinophilic asthma. *N Engl J Med* (2014) 371:1198–207. doi: 10.1056/NEJMoa1403290

32. Bel EH, Wenzel SE, Thompson PJ, Prazma CM, Keene ON, Yancey SW, et al. Oral glucocorticoid-sparing effect of mepolizumab in eosinophilic asthma. *N Engl J Med* (2014) 371:1189–97. doi: 10.1056/NEJMoa1403291

33. Cockle SM, Stynes G, Gunsoy NB, Parks D, Alfonso-Cristancho R, Wex J, et al. Comparative effectiveness of mepolizumab and omalizumab in severe asthma: An indirect treatment comparison. *Respir Med* (2017) 123:140–8. doi: 10.1016/j.rmed.2016.12.009

34. FitzGerald JM, Bleecker ER, Nair P, Korn S, Ohta K, Lommatzsch M, et al. Benralizumab, an anti-interleukin-5 receptor α monoclonal antibody, as add-on treatment for patients with severe, uncontrolled, eosinophilic asthma (CALIMA): a randomised, double-blind, placebo-controlled phase 3 trial. *Lancet (London England)* (2016) 388:2128–41. doi: 10.1016/S0140-6736(16)31322-8

35. Bleecker ER, FitzGerald JM, Chanez P, Papi A, Weinstein SF, Barker P, et al. Efficacy and safety of benralizumab for patients with severe asthma uncontrolled with high-dosage inhaled corticosteroids and long-acting β2-agonists (SIROCCO): a randomised, multicentre, placebo-controlled phase 3 trial. *Lancet (London England)* (2016) 388:2115–27. doi: 10.1016/S0140-6736(16)31324-1

36. Cushen B, Menzies-Gow A. Benralizumab: an updated treatment of eosinophilic asthma. *Expert Rev Respir Med* (2020) 14:435–44. doi: 10.1080/17476348.2020.1739526

37. Nair P, Wenzel S, Rabe KF, Bourdin A, Lugogo NL, Kuna P, et al. Oral glucocorticoid–sparing effect of benralizumab in severe asthma. *N Engl J Med* (2017) 376:2448–58. doi: 10.1056/NEJMoa1703501

38. Busse WW, Bleecker ER, FitzGerald JM, Ferguson GT, Barker P, Sproule S, et al. Long-term safety and efficacy of benralizumab in patients with severe, uncontrolled asthma: 1-year results from the BORA phase 3 extension trial. *Lancet Respir Med* (2019) 7:46–59. doi: 10.1016/S2213-2600(18)30406-5

39. Busse WW, Bleecker ER, FitzGerald JM, Ferguson GT, Barker P, Brooks L, et al. Benralizumab for adolescent patients with severe, eosinophilic asthma: Safety and efficacy after 3 years of treatment. *J Allergy Clin Immunol* (2021) 148:266–71.e2. doi: 10.1016/J.JACI.2021.02.009

40. Patel SS, Casale TB, Cardet JC. Biological therapies for eosinophilic asthma. *Expert Opin Biol Ther* (2018) 18:747–54. doi: 10.1080/14712598.2018.1492540

41. Dorey-Stein ZL, Shenoy KV. Tezepelumab as an emerging therapeutic option for the treatment of severe asthma: Evidence to date. *Drug Des Devel Ther* (2021) 15:331–8. doi: 10.2147/DDDT.S250825

42. Corren J, Parnes JR, Wang L, Mo M, Roseti SL, Griffiths JM, et al. Tezepelumab in adults with uncontrolled asthma. *N Engl J Med* (2017) 377:936–46. doi: 10.1056/NEJMoa1704064

43. Corren J, Garcia Gil E, Griffiths JM, Parnes JR, van der Merwe R, Sałapa K, et al. Tezepelumab improves patient-reported outcomes in patients with severe, uncontrolled asthma in PATHWAY. *Ann Allergy Asthma Immunol* (2021) 126:187–93. doi: 10.1016/J.ANAI.2020.10.008

44. Corren J, Karpefors M, Hellqvist Å, Parnes JR, Colice G. Tezepelumab reduces exacerbations across all seasons in patients with severe, uncontrolled asthma: A *post hoc* analysis of the pathway phase 2b study. *J Asthma Allergy* (2021) 14:1–11. doi: 10.2147/JAA.S286036

45. Menzies-Gow A, Corren J, Bourdin A, Chupp G, Israel E, Wechsler ME, et al. Tezepelumab in adults and adolescents with severe, uncontrolled asthma. *N Engl J Med* (2021) 384:1800–9. doi: 10.1056/NEJMOA2034975

46. Wechsler ME, Menzies-Gow A, Brightling CE, Kuna P, Korn S, Welte T, et al. Evaluation of the oral corticosteroid-sparing effect of tezepelumab in adults with oral corticosteroid-dependent asthma (SOURCE): a randomised, placebo-controlled, phase 3 study. *Lancet Respir Med* (2022) 10(7):650–60. doi: 10.1016/S2213-2600(21)00537-3

47. Menzies-Gow A, Colice G, Griffiths JM, Almqvist G, Ponnarambil S, Kaur P, et al. NAVIGATOR: a phase 3 multicentre, randomized, double-blind, placebo-controlled, parallel-group trial to evaluate the efficacy and safety of tezepelumab in adults and adolescents with severe, uncontrolled asthma. *Respir Res* (2020) 21 (1):266. doi: 10.1186/s12931-020-01526-6

48. Abe Y, Suga Y, Fukushima K, Ohata H, Niitsu T, Nabeshima H, et al. Advances and challenges of antibody therapeutics for severe bronchial asthma. *Int J Mol Sci* (2021) 23(1):83. doi: 10.3390/IJMS23010083

49. Panettieri RA, Sjöbring U, Péterffy AM, Wessman P, Bowen K, Piper E, et al. Tralokinumab for severe, uncontrolled asthma (STRATOS 1 and STRATOS 2): two randomised, double-blind, placebo-controlled, phase 3 clinical trials. *Lancet Respir Med* (2018) 6:511–25. doi: 10.1016/S2213-2600(18)30184-X

50. Panettieri RA, Wang M, Braddock M, Bowen K, Colice G. Tralokinumab for the treatment of severe, uncontrolled asthma: The ATMOSPHERE clinical development program. *Immunotherapy* (2018) 10:473–90. doi: 10.2217/imt-2017-0191

51. Busse WW, Brusselle GG, Korn S, Kuna P, Magnan A, Cohen D, et al. Tralokinumab did not demonstrate oral corticosteroid-sparing effects in severe asthma. *Eur Respir J* (2019) 53(2):1800948. doi: 10.1183/13993003.00948-2018

52. Available at: https://clinicaltrials.gov/ct2/show/results/NCT02281357. (Accessed July 01, 2022)

53. Brightling CE, Chanez P, Leigh R, O'Byrne PM, Korn S, She D, et al. Efficacy and safety of tralokinumab in patients with severe uncontrolled asthma: A randomised, double-blind, placebo-controlled, phase 2b trial. *Lancet Respir Med* (2015) 3:692–701. doi: 10.1016/S2213-2600(15)00197-6

54. Piper E, Brightling C, Niven R, Oh C, Faggioni R, Poon K, et al. A phase II placebo-controlled study of tralokinumab in moderate-to-severe asthma. *Eur Respir J* (2013) 41:330–8. doi: 10.1183/09031936.00223411

55. George L, Brightling CE. Eosinophilic airway inflammation: Role in asthma and chronic obstructive pulmonary disease. *Ther Adv Chronic Dis* (2016) 7:34–51. doi: 10.1177/2040622315609251

56. Russell RJ, Chachi L, FitzGerald JM, Backer V, Olivenstein R, Titlestad IL, et al. Effect of tralokinumab, an interleukin-13 neutralising monoclonal antibody, on eosinophilic airway inflammation in uncontrolled moderate-to-severe asthma (MESOS): a multicentre, double-blind, randomised, placebo-controlled phase 2 trial. *Lancet Respir Med* (2018) 6:499–510. doi: 10.1016/S2213-2600(18)30201-7

57. Zhang Y, Cheng J, Li Y, He R, Pan P, Su X, et al. The safety and efficacy of anti–IL-13 treatment with tralokinumab (CAT-354) in moderate to severe asthma: A systematic review and meta-analysis. *J Allergy Clin Immunol Pract* (2019) 7:2661–71.e3. doi: 10.1016/j.jaip.2019.05.030

58. Carlsson M, Braddock M, Li Y, Wang J, Xu W, White N, et al. Evaluation of antibody properties and clinically relevant immunogenicity, anaphylaxis, and hypersensitivity reactions in two phase III trials of tralokinumab in severe, uncontrolled asthma. *Drug Saf* (2019) 42:769–84. doi: 10.1007/s40264-018-00788-w

59. Chung KF. Tralokinumab unsuccessful for management of severe, uncontrolled asthma. *Lancet Respir Med* (2018) 6:480–1. doi: 10.1016/S2213-2600(18)30194-2

60. Wollenberg A, Blauvelt A, Guttman-Yassky E, Worm M, Lynde C, Lacour JP, et al. Tralokinumab for moderate-to-severe atopic dermatitis: results from two 52-week, randomized, double-blind, multicentre, placebo-controlled phase III trials (ECZTRA 1 and ECZTRA 2). *Br J Dermatol* (2021) 184(3):437–49. doi: 10.1111/bjd.19574

61. Corren J, Lemanske RF, Hanania NA, Korenblat PE, Parsey MV, Arron JR, et al. Lebrikizumab treatment in adults with asthma. *N Engl J Med* (2011) 365:1088–98. doi: 10.1056/NEJMoa1106469

62. Hanania NA, Korenblat P, Chapman KR, Bateman ED, Kopecky P, Paggiaro P, et al. Efficacy and safety of lebrikizumab in patients with uncontrolled asthma (LAVOLTA I and LAVOLTA II): replicate, phase 3, randomised, double-blind, placebo-controlled trials. *Lancet Respir Med* (2016) 4:781–96. doi: 10.1016/S2213-2600(16)30265-X

63. Hanania NA, Noonan M, Corren J, Korenblat P, Zheng Y, Fischer SK, et al. Lebrikizumab in moderate-to-severe asthma: Pooled data from two randomised placebo-controlled studies. *Thorax* (2015) 70:748–56. doi: 10.1136/thoraxjnl-2014-206719

64. Available at: https://www.medpagetoday.com/meetingcoverage/aaaai/97409. (Accessed July 01, 2022)

65. Li H, Wang K, Huang H, Cheng W, Liu X. A meta-analysis of anti-interleukin-13 monoclonal antibodies for uncontrolled asthma. *PLoS One* (2019) 14(1):e0211790. doi: 10.1371/journal.pone.0211790

66. Available at: https://www.clinicaltrials.gov/ct2/show/NCT01478360. (Accessed July 01, 2022)

67. Kirsten A, Watz H, Pedersen F, Holz O, Smith R, Bruin G, et al. The anti-IL-17A antibody secukinumab does not attenuate ozone-induced airway neutrophilia in healthy volunteers. *Eur Respir J* (2013) 41:239–41. doi: 10.1183/09031936.00123612

68. Busse WW, Holgate S, Kerwin E, Chon Y, Feng J, Lin J, et al. Randomized, double-blind, placebo-controlled study of brodalumab, a human anti–IL-17 receptor monoclonal antibody, in moderate to severe asthma. *Am J Respir Crit Care Med* (2013) 188:1294–302. doi: 10.1164/rccm.201212-2318OC

69. Available at: https://clinicaltrials.gov/ct2/show/NCT01902290. (Accessed July 01, 2022)

70. Erpenbeck VJ, Popov TA, Miller D, Weinstein SF, Spector S, Magnusson B, et al. The oral CRTh2 antagonist QAW039 (fevipiprant): A phase II study in uncontrolled allergic asthma. *Pulm Pharmacol Ther* (2016) 39:54–63. doi: 10.1016/J.PUPT.2016.06.005

71. Bateman ED, Guerreros AG, Brockhaus F, Holzhauer B, Pethe A, Kay RA, et al. Fevipiprant, an oral prostaglandin DP2 receptor (CRTh2) antagonist, in allergic asthma uncontrolled on low-dose inhaled corticosteroids. *Eur Respir J* (2017) 50:1700670. doi: 10.1183/13993003.00670-2017

72. Castro M, Kerwin E, Miller D, Pedinoff A, Sher L, Cardenas P, et al. Efficacy and safety of fevipiprant in patients with uncontrolled asthma: Two replicate, phase 3, randomised, double-blind, placebo-controlled trials (ZEAL-1 and ZEAL-2). *EClinicalMedicine* (2021) 35:100847. doi: 10.1016/J.ECLINM.2021.100847/ATTACHMENT/E71115DE-4BD9-44FB-8109-AA38D50E7266/MMC1.PDF

73. Brightling CE, Gaga M, Inoue H, Li J, Maspero J, Wenzel S, et al. Effectiveness of fevipiprant in reducing exacerbations in patients with severe asthma (LUSTER-1 and LUSTER-2): two phase 3 randomised controlled trials. *Lancet Respir Med* (2021) 9:43–56. doi: 10.1016/S2213-2600(20)30412-4

74. Osei ET, Brandsma CA, Timens W, Heijink IH, Hackett TL. Current perspectives on the role of interleukin-1 signalling in the pathogenesis of asthma and COPD. *Eur Respir J* (2020) 55(2):1900563. doi: 10.1183/13993003.00563-2019

75. Available at: https://clinicaltrials.gov/ct2/show/NCT03513471?term=anakinra&cond=Asthma&draw=2&rank=2. (Accessed July 01, 2022)

76. Available at: https://clinicaltrials.gov/ct2/show/NCT03513458?term=anakinra&cond=Asthma&draw=2&rank=1. (Accessed July 01, 2022)

77. Available at: https://clinicaltrials.gov/ct2/show/NCT04035109?term=anakinra&cond=Asthma&draw=2&rank=3. (Accessed July 01, 2022)

78. Tripp CS, Cuff C, Campbell AL, Hendrickson BA, Voss J, Melim T, et al. RPC4046, a novel anti-interleukin-13 antibody, blocks IL-13 binding to IL-13 α1 and α2 receptors: A randomized, double-blind, placebo-controlled, dose-escalation first-in-Human study. *Adv Ther* (2017) 34:1364–81. doi: 10.1007/S12325-017-0525-8

79. Dellon ES, Collins MH, Rothenberg ME, Assouline-Dayan Y, Evans L, Gupta S, et al. Long-term efficacy and tolerability of RPC4046 in an open-label extension trial of patients with eosinophilic esophagitis. *Clin Gastroenterol Hepatol* (2021) 19:473–83.e17. doi: 10.1016/J.CGH.2020.03.036

80. De Boever EH, Ashman C, Cahn AP, Locantore NW, Overend P, Pouliquen IJ, et al. Efficacy and safety of an anti-IL-13 mAb in patients with severe asthma: a randomized trial. *J Allergy Clin Immunol* (2014) 133:989–96. doi: 10.1016/J.JACI.2014.01.002

81. Busse WW, Israel E, Nelson HS, Baker JW, Charous BL, Young DY, et al. Daclizumab improves asthma control in patients with moderate to severe persistent asthma: a randomized, controlled trial. *Am J Respir Crit Care Med* (2008) 178:1002–8. doi: 10.1164/RCCM.200708-1200OC

82. Antoniu S A. Daclizumab: a potential asthma therapy? *Recent Pat Inflammation Allergy Drug Discovery* (2010) 4:214–21. doi: 10.2174/187221310793564254

83. Bielekova B. Daclizumab therapy for multiple sclerosis. *Cold Spring Harb Perspect Med* (2019) 9(5):a034470. doi: 10.1101/CSHPERSPECT.A034470

84. Méndez-Enríquez E, Hallgren J. Mast cells and their progenitors in allergic asthma. *Front Immunol* (2019) 10:821. doi: 10.3389/FIMMU.2019.00821

85. White B, Leon F, White W, Robbie G. Two first-in-human, open-label, phase I dose-escalation safety trials of MEDI-528, a monoclonal antibody against interleukin-9, in healthy adult volunteers. *Clin Ther* (2009) 31:728–40. doi: 10.1016/J.CLINTHERA.2009.04.019

86. Parker JM, Oh CK, LaForce C, Miller SD, Pearlman DS, Le C, et al. Safety profile and clinical activity of multiple subcutaneous doses of MEDI-528, a humanized anti-interleukin-9 monoclonal antibody, in two randomized phase 2a studies in subjects with asthma. *BMC Pulm Med* (2011) 11:14. doi: 10.1186/1471-2466-11-14

87. Oh CK, Leigh R, McLaurin KK, Kim K, Hultquist M, Molfino NA. A randomized, controlled trial to evaluate the effect of an anti-interleukin-9 monoclonal antibody in adults with uncontrolled asthma. *Respir Res* (2013) 14:93. doi: 10.1186/1465-9921-14-93

88. *A monoclonal antibody to IL-1B attenuates the late asthmatic response to antigen challenge in patients with mild asthma*. Available at: https://www.ers-education.org/lr/show-details/?idP=5730 (Accessed May 9, 2022).

89. Nakajima H, Hirose K. Role of IL-23 and Th17 cells in airway inflammation in asthma. *Immune Netw* (2010) 10:1. doi: 10.4110/IN.2010.10.1.1

90. Brightling CE, Nair P, Cousins DJ, Louis R, Singh D. Risankizumab in severe asthma — a phase 2a, placebo-controlled trial. *N Engl J Med* (2021) 385:1669–79. doi: 10.1056/NEJMOA2030880/SUPPL_FILE/NEJMOA2030880_DATA-SHARING.PDF

91. Gu C, Yang J. Risankizumab for the treatment of psoriasis. *Expert Rev Clin Pharmacol* (2019) 12:851–7. doi: 10.1080/17512433.2019.1657829

92. Burgess G, Boyce M, Jones M, Larsson L, Main MJ, Morgan F, et al. Randomized study of the safety and pharmacodynamics of inhaled interleukin-13 monoclonal antibody fragment VR942. *EBioMedicine* (2018) 35:67–75. doi: 10.1016/J.EBIOM.2018.07.035

93. Hacha J, Tomlinson K, Maertens L, Paulissen G, Rocks N, Foidart JM, et al. Nebulized anti-IL-13 monoclonal antibody fab' fragment reduces allergen-induced asthma. *Am J Respir Cell Mol Biol* (2012) 47:709–17. doi: 10.1165/RCMB.2012-0031OC

94. Parray HA, Shukla S, Perween R, Khatri R, Shrivastava T, Singh V, et al. Inhalation monoclonal antibody therapy: a new way to treat and manage respiratory infections. *Appl Microbiol Biotechnol* (2021) 105:6315. doi: 10.1007/S00253-021-11488-4

95. Busse WW, Holgate S, Kerwin E, Chon Y, Feng J, Lin J, et al. Study of brodalumab , a human anti – IL-17 receptor monoclonal antibody , in moderate to severe asthma. *Am J Respir Crit Care Med* (2013) 188:1294–302. doi: 10.1164/rccm.201212-2318OC

96. Wechsler ME, Ruddy MK, Pavord ID, Israel E, Rabe KF, Ford LB, et al. Efficacy and safety of itepekimab in patients with moderate-to-Severe asthma. *N Engl J Med* (2021) 385:1656–68. doi: 10.1056/NEJMOA2024257

97. Available at: https://ir.anaptysbio.com/news-releases/news-release-details/anaptysbio-presents-updated-data-etokimab-phase-2a-proof-concept/. (Accessed July 01, 2022)

98. Available at: https://clinicaltrials.gov/ct2/show/study/NCT03207243. (Accessed July 01, 2022)

99. Available at: https://www.evaluate.com/vantage/articles/news/snippets/glaxos-latest-asthma-cull-puts-astra-spotlight. (Accessed July 01, 2022)

100. *Monoclonal antibody therapy for severe asthma - national asthma council Australia*. Available at: https://www.nationalasthma.org.au/living-with-asthma/resources/health-professionals/information-paper/monoclonal-antibody-therapy-for-severe-asthma (Accessed May 30, 2022).

101. Hyland ME, Masoli M, Lanario JW, Jones RC. *A possible explanation for non-responders, responders and super-responders to biologics in severe asthma* (2019). Available at: http://www.xiahepublishing.com/.

102. Hamada K, Oishi K, Murata Y, Hirano T, Matsunaga K. Feasibility of discontinuing biologics in severe asthma: An algorithmic approach. *J Asthma Allergy* (2021) 14:1463. doi: 10.2147/JAA.S340684

103. Upchurch K, Wiest M, Cardenas J, Skinner J, Nattami D, Lanier B, et al. Whole blood transcriptional variations between responders and non-responders in asthma patients receiving omalizumab. *Clin Exp Allergy* (2020) 50:1017–34. doi: 10.1111/CEA.13671

104. Eger K, Kroes JA, ten Brinke A, Bel EH. Long-term therapy response to anti-IL-5 biologics in severe asthma-a real-life evaluation. *J Allergy Clin Immunol Pract* (2021) 9:1194–200. doi: 10.1016/J.JAIP.2020.10.010

105. Lin YL, Chen SH, Wang JY. Critical role of IL-6 in dendritic cell-induced allergic inflammation of asthma. *J Mol Med* (2016) 94:51–9. doi: 10.1007/s00109-015-1325-8

106. Khan FA, Stewart I, Fabbri L, Moss S, Robinson K, Smyth AR, et al. Systematic review and meta-analysis of anakinra, sarilumab, siltuximab and tocilizumab for COVID-19. *Thorax* (2021) 76(9):907–19. doi: 10.1136/thoraxjnl-2020-215266

107. Esty B, Harb H, Bartnikas LM, Charbonnier LM, Massoud AH, Leon-Astudillo C, et al. Treatment of severe persistent asthma with IL-6 receptor blockade. *J Allergy Clin Immunol Pract* (2019) 7:1639–42.e4. doi: 10.1016/j.jaip.2019.02.043

108. Revez JA, Bain LM, Watson RM, Towers M, Collins T, Killian KJ, et al. Effects of interleukin-6 receptor blockade on allergen-induced airway responses in mild asthmatics. *Clin Transl Immunol* (2019) 8(6):e1044. doi: 10.1002/cti2.1044

109. Available at: https://clinicaltrials.gov/ct2/results?recrs=&cond=asthma&term=REGN-3500&cntry=&state=&city=&dist. (Accessed July 01, 2022)

110. Available at: https://clinicaltrials.gov/ct2/show/NCT04570657?term=MEDI3506&draw=2&rank=1. (Accessed July 01, 2022)

111. Staton TL, Peng K, Owen R, Choy DF, Cabanski CR, Fong A, et al. A phase I, randomized, observer-blinded, single and multiple ascending-dose study to investigate the safety, pharmacokinetics, and immunogenicity of BITS7201A, a bispecific antibody targeting IL-13 and IL-17, in healthy volunteers. *BMC Pulm Med* (2019) 19(1):5. doi: 10.1186/S12890-018-0763-9

112. Godar M, Deswarte K, Vergote K, Saunders M, de Haard H, Hammad H, et al. A bispecific antibody strategy to target multiple type 2 cytokines in asthma. *J Allergy Clin Immunol* (2018) 142:1185–93.e4. doi: 10.1016/J.JACI.2018.06.002

113. Venkataramani S, Low S, Weigle B, Dutcher D, Jerath K, Menzenski M, et al. Design and characterization of zweimab and doppelmab, high affinity dual antagonistic anti-TSLP/IL13 bispecific antibodies. *Biochem Biophys Res Commun* (2018) 504:19–24. doi: 10.1016/J.BBRC.2018.08.064

114. Available at: https://clinicaltrials.gov/ct2/show/NCT04129931?term=antibody&recrs=a&cond=severe+asthma&draw=4&rank=28. (Accessed July 01, 2022)

115. Available at: https://clinicaltrials.gov/ct2/show/NCT04946318?term=antibody&recrs=a&cond=severe+asthma&d (Accessed July 01, 2022)raw=4.

116. Available at: https://clinicaltrials.gov/ct2/show/NCT05008965?term=FB825&draw=2&rank=3. (Accessed July 01, 2022)

117. Available at: https://clinicaltrials.gov/ct2/show/NCT05186909?term=antibody&recrs=a&cond=severe+asthma&draw=2&rank=7. (Accessed July 01, 2022)

118. Available at: https://clinicaltrials.gov/ct2/show/NCT04445038?term=antibody&recrs=a&cond=severe+asthma&draw=4&rank=21. (Accessed July 01, 2022)

119. Available at: https://clinicaltrials.gov/ct2/show/NCT05018299?term=antibody&recrs=a&cond=severe+asthma&draw=2&rank=5. (Accessed July 01, 2022)

120. Available at: https://clinicaltrials.gov/ct2/show/NCT04570657. (Accessed July 01, 2022)

121. Bakakos A, Loukides S, Usmani OS, Bakakos P. Biologics in severe asthma: the overlap endotype - opportunities and challenges. *Expert Opin Biol Ther* (2020) 20:1427–34. doi: 10.1080/14712598.2020.1809651

122. Papaioannou AI, Fouka E, Papakosta D, Papiris S, Loukides S. Switching between biologics in severe asthma patients. when the first choice is not proven to be the best. *Clin Exp Allergy* (2021) 51:221–7. doi: 10.1111/CEA.13809

123. Viswanathan RK, Busse WW. How to compare the efficacy of biologic agents in asthma. *Ann Allergy Asthma Immunol* (2020) 125:137–49. doi: 10.1016/J.ANAI.2020.04.031

124. Available at: https://clinicaltrials.gov/ct2/show/NCT03476109. (Accessed July 01, 2022)

125. Available at: https://clinicaltrials.gov/ct2/show/NCT04585997?term=antibody&recrs=a&cond=severe+asthma&draw=3&rank=11. (Accessed July 01, 2022)

126. *Efficacy and safety of benralizumab in EGPA compared to mepolizumab. - full text view*. Available at: https://clinicaltrials.gov/ct2/show/NCT04157348 (Accessed October 25, 2022).

127. Rogliani P, Calzetta L, Matera MG, Laitano R, Ritondo BL, Hanania NA, et al. Severe asthma and biological therapy: When, which, and for whom. *Pulm Ther* (2020) 6:47. doi: 10.1007/S41030-019-00109-1

128. Busse W, Chupp G, Nagase H, Albers FC, Doyle S, Shen Q, et al. Anti–IL-5 treatments in patients with severe asthma by blood eosinophil thresholds: Indirect treatment comparison. *J Allergy Clin Immunol* (2019) 143:190–200.e20. doi: 10.1016/J.JACI.2018.08.031

129. Diver S, Khalfaoui L, Emson C, Wenzel SE, Menzies-Gow A, Wechsler ME, et al. Effect of tezepelumab on airway inflammatory cells, remodelling,

and?hyperresponsiveness in patients with moderate-to-severe uncontrolled asthma (CASCADE): a double-blind, randomised, placebo-controlled, phase 2?trial. *Lancet Respir Med* (2021) 9:1299–312. doi: 10.1016/S2213-2600(21)00226-5

130. Kardas G, Kuna P, Panek M. Biological therapies of severe asthma and their possible effects on airway remodeling. *Front Immunol* (2020) 11:1134. doi: 10.3389/FIMMU.2020.01134

131. Papadopoulos NG, Barnes P, Canonica GW, Gaga M, Heaney L, Menzies-Gow A, et al. The evolving algorithm of biological selection in severe asthma. *Allergy* (2020) 75:1555–63. doi: 10.1111/ALL.14256

132. Buhl R, Bel E, Bourdin A, Dávila I, Douglass JA, FitzGerald JM, et al. Effective management of severe asthma with biologic medications in adult patients: A literature review and international expert opinion. *J Allergy Clin Immunol Pract* (2022) 10:422–32. doi: 10.1016/J.JAIP.2021.10.059

Frontiers in Immunology

Explores novel approaches and diagnoses to treat immune disorders.

The official journal of the International Union of Immunological Societies (IUIS) and the most cited in its field, leading the way for research across basic, translational and clinical immunology.

Discover the latest Research Topics

See more →

Frontiers

Avenue du Tribunal-Fédéral 34
1005 Lausanne, Switzerland
frontiersin.org

Contact us

+41 (0)21 510 17 00
frontiersin.org/about/contact